Modeling, Design, Fabrication, and Characterization of a Highly Sensitive Fluorescence-based Detection Platform for Point-of-Care Applications

by

Uwadiae Obahiagbon

A Dissertation Presented in Partial Fulfillment
of the Requirements for the Degree
Doctor of Philosophy

Approved November 2018 by the
Graduate Supervisory Committee:

Jennifer M. Blain Christen, Chair
Karen S. Anderson
Michael Goryll
Barbara S. Smith

ARIZONA STATE UNIVERSITY

December 2018

ABSTRACT

Over the past several decades, there has been a growing interest in the use of fluorescent probes in low-cost diagnostic devices for resource-limited environments. This dissertation details the design, development, and deployment of an inexpensive, multiplexed, and quantitative, fluorescence-based lateral flow immunoassay platform, in light of the specific constraints associated with resource-limited settings.

This effort grew out of the need to develop a highly sensitive, field-deployable platform to be used as a primary screening and early detection tool for serologic biomarkers for the high-risk human papillomavirus (hrHPV) infection. A hrHPV infection is a precursor for developing high-grade cervical intraepithelial neoplasia (CIN 2/3+). Early detection requires high sensitivity and a low limit-of-detection (LOD). To this end, the developed platform (DxArray) takes advantage of the specificity of immunoassays and the selectivity of fluorescence for early disease detection. The long term goal is to improve the quality of life for several hundred million women globally, at risk of being infected with hrHPV.

The developed platform uses fluorescent labels over the gold-standard colorimetric labels in a compact, high-sensitivity lateral flow assay configuration. It is also compatible with POC settings as it substitutes expensive and bulky light sources for LEDs, low-light CMOS cameras, and photomultiplier tubes for photodiodes, in a transillumination architecture, and eliminates the need for expensive focusing/transfer optics. The platform uses high-quality interference filters at less than $1 each, enabling a rugged and robust design suitable for field use.

The limit of detection (LOD) of the developed platform is within an order of magnitude of centralized laboratory diagnostic instruments. It enhances the LOD of absorbance or reflectometric and visual readout lateral flow assays by 2 - 3 orders of magnitude. This system could be applied toward any chemical or bioanalytical pro-

cedure that requires a high performance at low-cost. The knowledge and techniques developed in this effort is relevant to the community of researchers and industry developers looking to deploy inexpensive, quantitative, and highly sensitive diagnostic devices to resource-limited settings.

This dissertation is dedicated to the Almighty God, my source and my strength, without whom I am nothing; and to all who relentlessly continue to pursue their dreams.

ACKNOWLEDGMENTS

First and foremost, thanks to God for life, strength, and soundness of my mind and body to be able to complete this work and for His grace that has kept me going.

A heart-felt gratitude to Dr. Jennifer M. Blain Christen for giving me the opportunity to work and conduct research under your guidance. Thanks for her guidance, advice, suggestions, questions, and direction she provided through each step of this research work and for being a great source of encouragement even through my program. Your patience, care, friendship, and concern is unparalleled. Thanks for not letting me settle for less, I am indeed very grateful that you constantly inspired me to do more and to aim higher. I am also very grateful to Dr. Karen S. Anderson for your kindness and insightful conversations about science and life in general. Your professionalism and consistency has been a great source of inspiration. Thanks for all that you do towards making the world a better place. Many thanks to Dr. Barbara S. Smith, it has been a great joy knowing and interacting with you. Thanks for all your professional counsel, recommendations, and for your patience in answering my many questions about work and life. Your positive and optimistic approach to life has given me reason to see the impossible as mere challenges and obstacles to be overcome. Thanks to Dr. Michael Goryll, you have been an invaluable resource for the past 4 years. I have learned a lot from you, thanks for being such a great resource and for letting me borrow and use your equipment without any hindrances, for the interactions, questions, and constructive suggestions throughout this work. You are a true mentor and role model, and I hope to be as knowledgeable in breadth and depth as you are someday.

Finally, thanks to all my friends at Arizona State University, to all members of the Bioelectrical Systems Technology Lab (BEST), past and present, under the

direction of Dr. Blain Christen and to all staff and students of the School of Electrical, Computer and Electrical Engineering, the IRA A. Fulton School of Engineering, the Graduate College and the Biodesign Institute, all members of the Karen Anderson Lab under the Center for Personalized Diagnostics (CPD), especially to Ching-wen Hou, Meilin Zhu, Hany Arafa, Dixie Kullmann, Radwa Ewaisha, Benjamin A. Katchman, and Joseph T. Smith.

Thanks to my family, to my wife, Alzetta Clay Obahiagbon, for your love, care, patience and understanding through the years, for your encouragement, for urging me to go on, push through and for being everything to me. I love you very much Alzetta! To my parents, Rev (Prof.) and Dr. (Mrs) F. I. Obahiagbon for being true parents indeed, my spiritual support and to my sibblings, Dr. Ikponmwonsa Obahiagbon, Dr. Osarobo Obahiagbon and Oy Obahiagbon, your love, support, and prayers have kept me going. Thanks to Dr. Micheal A. Awaah and Dr. Isibhakhomen Awaah for their support and advice and for helping me begin this journey and being with me through it all. Many thanks to Dr. and Mrs. Temitope and Folashade Sabitu for being there for me all the way and in every way, for being true friends to me and my family, and last and by no means the least, to Dr. and Mrs. C. Ope for being a great spiritual support and for their true and sincere counsel.

Thanks to everyone who has helped me along the way, for your constructive criticisms and suggestions, kind and harsh comments and for the doubt, faith and hope expressed.

Thanks to the National Science Foundation (NSF) and the National Cancer Institute (NCI) for providing funding for this research. This work was supported in part by the National Science Foundation Smart and Connected Health [grant number IIS-1521904] SCH: INT: “Disposable high sensitivity point-of-care immunosensor for multiple disease and pathogen detection” and the National Cancer Institute Cancer

Detection, Diagnosis, and Treatment Technologies for Global Health [grant number CA211415]: "Rapid Point-of-Care Detection of HPV-associated Malignancies".

This has by no means been an individual effort. The highly interdisciplinary and collaborative nature of this work has been very fulfilling and engaging. Thanks to everyone with whom I have been privileged to work with on this project. Generally, the writer's contributions consisted of developing and investigating several material platforms for microfluidic implementations in a fluorescence-based detection platform (not discussed in this dissertation), as well as the design of several experiments leading to routine protocols in the day-to-day assay development, testing, and troubleshooting, characterization tools, material selection, evaluation, and optimization of the developed assays and fluorescence detection device. Chapter 3 is adapted from a previously published paper by Obahiagbon *et al.* (2016). Chapter 4 is adapted from previously published papers by Katchman *et al.* (2016b); Smith *et al.* (2016a); Obahiagbon *et al.* (2019) and a book chapter by Obahiagbon *et al.* (2019) in review. Chapter 5 is adapted from a previously published paper by Obahiagbon *et al.* (2018) Jennifer M. Blain Christen (Ph.D.) and Karen S. Anderson (M.D., Ph.D.) supervised the work, revised, and edited all publications related to this work.

Specifically, the list below summarizes the writers overall contributions:

- Modeled an inexpensive fluorescence detection platform and devised a method to predict a given systems performance *a priori*. This work and its potential applications, was published and presented at the IEEE-NIH HIPOCT conference in Cancun, 2016 and won the first place award for the best student paper presentation.

- Developed a single-site fluorescence-based detection system based on charge integration and interference filters. Also developed a data extraction and analysis

macro, ramp time, and detection time, slope, and derivative analysis. The system is capable of clinical detection sensitivity. This unit was used to generate and analyze all data that led to the Nature Scientific Reports Journal and JDT publications. The single-site device is still in operation and used routinely for assay development.

- Developed a filter assembly and encapsulation process for small size filters (3x3 mm) for low-cost fluorescence detection applications.

- Developed optomechanical isolation structures that eliminated crosstalk even at undiluted microsphere concentrations at adjacent site. These led to a journal publication in Biosensors and Bioelectronics Journal.

- Adapted novel glass-based HPV-assay to a NC format, increasing detection limit and providing a path toward semi-autonomous assay processing for LMIC application.

- Performed a complete analysis of microsphere size and flow rate effects in fluorescence-based LFA. For the first time, this provides useful information for other fluorescence LFA researchers and developers.

- Designed an automated multiplexed/multi-site detection platform for multi-analyte analysis in HPV (2x2, 4x2, and 4x4 site systems).

- Developed a normalized fluorescence intensity (NFI) algorithm, specifically for fluorescence-based LFA, where a lot of the norms and axioms from visual or instrumented colorometry-based LFAs do not directly translate.

- Design and fabricated a coplanar fluorescence detection configuration.

- Overall, the developed fluorescence detection device has LOD and sensitivity, comparable to Standard central laboratory analytical devices (e.g., microplate reader and microarray scanner), however significant improvements to the assay performance (covalent protein immobilization, reduced non-specific binding, and low-optical noise floor) will improve the overall performance of the platform.

TABLE OF CONTENTS

CHAPTER Page

CHAPTER Page

CHAPTER Page

CHAPTER Page

CHAPTER Page

CHAPTER Page

LIST OF TABLES

LIST OF FIGURES

Figure Page

Figure Page

Figure Page

Chapter 1

INTRODUCTION

An effective approach to combat infectious diseases, monitor disease outbreak, and vaccine coverage campaigns is to deploy hand-held devices at the point-of-care (POC) for screening or self-monitoring applications. In the past decade, major disease outbreaks including Ebola, Zika, and Dengue obviate the need for very sensitive, low-cost, and quantitative field-deployable diagnostic devices. The development of ideal low-cost biorecognition technologies that satisfy the ASSURED (affordable, sensitive, specific, user-friendly, rapid and robust, equipment-free and deliverable to end users) criteria put forth by the World Health Organization (WHO) Mabey *et al.* (2004); Wu and Zaman (2012), is of renewed importance. Many simple rapid diagnostic tests take advantage of the almost 40 years of development in lateral flow assays (LFA) and the existing manufacturing infrastructure. While the emergence of microfabrication and soft lithography has accelerated the growth of microfluidic devices for many bioanalytical applications, most of these devices are yet to make it to the field due the infrastructure requirements for their operation, high cost, poor stability in harsh environments, and relatively poor performance compared to laboratory-based tests.

This dissertation effort grew out of the need to develop a field-deployable platform that will have a high impact for screening and early detection of serologic markers for cervical cancer linked to human papilloma virus (HPV). Aside from being the most common cancer cause of death in the developing countries, cervical cancer is the fifth most common cancer in humans, and the second most common cancer in women worldwide, accounting for over 270,000 deaths annually Ferlay *et al.* (2015); Ewaisha *et al.* (2017). It is caused by HPV especially the high-risk serotypes HPV-

16 and 18, which contribute over 70% of all cervical cancer cases. Currently, there are no low-cost, inexpensive, quantitative and multiplexed platforms for serologic testing for HPV. Current diagnostic procedures are subjective, require centralized clinics, and highly trained professionals. Additionally, commercially available central laboratory diagnostic equipment is expensive to install and maintain, limiting access to much needed healthcare in resource-limited settings. This work delivers high-quality diagnostic information at the point-of-use representing a paradigm shift from a centralized approach to a more patient centered approach, especially in regions of the world where access to healthcare resources are limited Chin *et al.* (2007). The demand for a compact, quantitative, inexpensive, reliable, rugged, and robust platform is imperative.

The relatively lower performance of lateral flow assays (LFAs) compared to central laboratory assay techniques is a major factor limiting the widespread implementation of fluorescent LFAs in hand-held diagnostic devices (Tang *et al.*, 2016). Other issues include the cost and bulkiness of optical and electronic components. The development of low-cost, compact, and disposable devices, most notably those intended for use in point-of-care (POC) settings have received a lot of attention in the last 2 decades (Lee *et al.*, 2013; Hu *et al.*, 2014; Kumar *et al.*, 2015). Several groups have attempted to develop portable and sensitive platforms aimed at improving the sensitivity and limit of detection (LOD) for POC diagnostic devices. However, many high performance fluorescence systems rely on bulky optical components and expensive detectors including cooled charged coupled devices (CCD), complementary metal-oxide semiconductor (CMOS) cameras, or photomultiplier tubes (PMTs). Previous attempts to adapt such fluorescent systems for POC applications still use bulky laser light sources, expensive interference filters, and bulky optics such as lenses and mirrors (Lee *et al.*, 2013), which require very precise alignment. High-Q filters with

sharp transition edges and high transmission are critical for high-sensitivity fluorescence applications (Dandin *et al.*, 2007); however, these high performance filters are prohibitively expensive.

Many LFA-based devices rely on colorimetric detection usually using an enzyme as in an enzyme-linked immunosorbent assay (ELISA) or colored labels such as latex microspheres, incorporating several signal enhancement or amplification strategies including colloidal gold, silver enhanced gold, cellulose nanobeads, and carbon black nanoparticles (Hu *et al.*, 2013; O'Farrell, 2015a). The use of fluorescent labels toward improving the sensitivity of LFAs has also been investigated and well-reported in the literature (Banerjee *et al.*, 2010a; O'Farrell, 2015a). In particular, several groups have investigated the use of fluorescent labels for signal enhancement in compact microfluidic detection platforms (Lee *et al.*, 2013; Yetisen *et al.*, 2013a). The relatively low sensitivity reported in many systems (Li *et al.*, 2010; Khreich *et al.*, 2010; Lee *et al.*, 2013; Williams *et al.*, 2014), is mostly due to the difficulty in deploying low-cost and efficient filters, which significantly impacts the signal-to-noise (SNR) ratio (Dandin *et al.*, 2007; Yetisen *et al.*, 2013a). In the past decade, several studies have reported the use of gel filters (Venkatraman and Steckl, 2015a), absorption filters (Lefevre *et al.*, 2015; Ryu *et al.*, 2011a), and cross polarizers (Banerjee *et al.*, 2010a). The aforementioned systems show low performance in terms of analytical sensitivity and limit of detection. Others are expensive or very difficult to fabricate, and thus not suitable for low-cost, high-volume applications requiring high sensitivity or for applications in resource-poor settings.

Herein, we explore the development of a novel fluorescence-based detection platform suitable for resource-limited settings. The optoelectronic detection platform is based on interference filters and charge-integration readout electronics that enables clinical-level sensitivity at the POC (at home, clinical, or non-clinical settings). The

platform advances the state of the art, implementing a high-sensitivity optoelectronic and optomechanic setup using fluorescent labels over the gold-standard colorimetric labels. The platform is compatible with POC settings as it substitutes expensive and bulky light sources for LEDs, low-light CMOS cameras and photomultiplier tubes for photodiodes in a sandwiched configuration, eliminating the need for expensive focusing optics. The developed compact, rugged, and robust platform is engineered to function effectively in remote settings, in a van or in mobile clinics.

Overall, this Ph.D. work addresses the hypothesis that the combination of low-cost biorecognition in a fluorescence lateral flow immunoassay (LFIA) format with inexpensive fluorescence detection optoelectronics is capable of delivering clinically significant detection sensitivity and limit-of-detection required for early diagnosis and screening in low and medium income countries (LMICs). The results of this work identify pathways toward the development of inexpensive optoelectronic platforms capable of detecting low light emissions from excited fluorescent probes. Compared to an instantaneous measurement, the charge-integration technique used in this work, trades time for accuracy producing a quantitative concentration-dependent voltage readout as a function of time, thereby increasing the signal-to-noise ratio (SNR). Compared to standard colorimetric techniques, the platform improves the LOD by 2-3 orders of magnitude and is well within an order of magnitude of typical central laboratory analytical instruments. Furthermore, this dissertation presents optomechanical design techniques for eliminating crosstalk in an array configuration, interference filter cost reduction, interference filter assembly, and encapsulation procedures. Additionally algorithms for signal interpretation in a lateral flow assay have been developed. This work enables a fundamental and comprehensive understanding of the design constraints for low-cost fluorescence-based lateral flow devices, integration of on-board fluid storage, efficient blood filtration mechanism, and minimization of

assay-bias (inter- and intra-assay variations) for low-cost POC applications. This research endeavor is interdisciplinary, drawing on knowledge in several areas including: immunology, biochemistry, surface chemistry, microfluidics, optics, mechanical, and electrical engineering.

1.1 Hypotheses and Specific Aims

Fundamental hypothesis: Low-cost biorecognition in a fluorescence lateral flow immunoassay (LFIA) format combined with inexpensive fluorescence detection optoelectronics is capable of clinically significant detection sensitivity and limit-of-detection (LOD) required for early disease diagnosis and screening in low and middle-income countries (LMIC).

Hypothesis (1): The development of an inexpensive fluorescence detection system using low-cost optoelectronics will enable a field-deployable fluorescence platform with high-sensitivity.

Specific Aim (1): Model, design, fabricate, and characterize fluorescence detection system based on low-cost, portable excitation sources, detector, filters, and electronic readout. The system will be engineered without the use of transfer/focusing optics. Chapter 3 presents the optical design, modeling, and architecture of an inexpensive detection platform suitable for fluorescence applications in the near ultraviolet, visible, and near infrared (IR) spectrum as well as being field-deployable in resource-limited settings.

Hypothesis (2): The use of organic light emitting diodes (OLED) as an excitation source in fluorescence applications will enable high-density and low-cost biorecognition arrays. The platform will require the adaptation of a laboratory-based (microarray, well plate) HPV biorecognition to a microscope slide format.

Specific Aim (2): Demonstrate the detection of serologic biomarkers for HPV by im-

mobilizing capture antigens on a glass slide and use OLEDs as an excitation source in detector electronics. This research is discussed in Chapter 4 which presents a review of the diagnostic applications of organic light emitting diodes (OLED) adapted from flexible display technology. In addition, the specifics for the case study presented in this work related to the detection of HPV are presented.

Hypothesis (3): Inexpensive, high-quality decentralized interference filters will enable a low-cost multiplexed detector array. High-sensitivity and zero cross-talk will provide useful information for multianalyte analysis.

Specific Aim (3): Determine pathways for increasing array density using low-cost interference filters, determine the effect of reduced filter dimensions on performance, and benchmark the performance of the array platform against central laboratory scale detection equipment. Chapter 5 details the design, fabrication, and characterization of a multiplexed array platform using inexpensive high-performance interference filters.

Hypothesis (4): Detector platform performance is affected by optical architecture/configuration.

Specific Aim (4): Effect of system architecture on sensitivity, comparing two architecture: transillumination mode (T-mode) and coplanar mode (C-mode). Investigate the use of the same platform for applications in fluorescence and colorimetry. This effort is discussed in Chapter 6.

Hypotheis (5): Translation of microscope slide-based biorecognition to lateral flow assay format will enhance the performance of immunoassays. The development of high density (4x4) fluorescence detection array will enable the development of a HPV specific IgG biomarker panel.

Specific Aim (5): Develop a 4x2 and 4x4 fluorescence detection array integrated with a nitrocellulose-based solid support, evaluate solid support effects in terms of

surface area to volume ratio, background and non-specific binding (NSB), intrinsic autofluorescence, opacity, flow rate, particle size effects, and single strip multiplexing. Chapters 7 reports the development of 4x2 and 4x4 high sensitivity arrays, adaptation of glass-based HPV assay to a novel nitrocellulose-based format, a comparative analysis of fluorescent microsphere and membrane pore size effects, and considerations for single-strip multiplexed lateral flow assays. It also details sources of interference, background, and non-specific binding effects in lateral flow assay microfluidics. Chapter 8 summarizes the main findings in this dissertation.

Prior to discussing the specific aims listed above, this dissertation begins with a brief introduction of some background concepts related to absorbance and fluorescence, fluorescence detection techniques, and lateral flow immunometric assays, fluorophore characteristics, labels, device performance characteristics and figures of merit (FOM), lateral flow assay formats, and laboratory scale bioanalytical detection devices. This is the focus of chapter 2.

Chapter 2

FLUOROPHORES, DETECTION TECHNIQUES, AND LATERAL FLOW ASSAY FUNDAMENTALS

Fluorescence detection has emerged as one of the most popular optical sensing modes. Other sensing modes for the detection of analytes include: absorbance, chemiluminescence, fluorescence lifetime, waveguides, surface enhanced Raman, and surface plasmon resonance Cunningham (1998). Fluorescent detection, however, is a well-established analytical technique, proven to be an effective method for clinical and environmental sensing applications Guilbault (1990); Lakowicz (2006). Fluorescent detection schemes offer several attractive attributes including increased sensitivity, specificity, and a wide dynamic range Guilbault (1990); Yetisen *et al.* (2013a). Filter-based fluorescence detection in particular, continues to be investigated and commercialized for biochemical applications O'Farrell (2015a). To gain a better understanding of fluorescence for low-cost applications, we must first briefly review the basic principles of absorbance, fluorescence, diagnostics, and lateral flow assays.

2.1 Absorbance and Optical Density

The instantaneous (10^{-15} s), non-radiative absorption process that occurs in an absorbing medium upon exposure to radiant energy is embodied by the Beer-Lambert law Swinehart (1962) as stated in Equation 2.1:

$$I = I_0 \exp(-\epsilon l c), \tag{2.1}$$

where, I, is the transmitted light intensity; I_0, is the excitation light intensity; ϵ, is the extinction coefficient or molar absorptivity ($M^{-1}\ cm^{-1}$) of the absorbing

species (chromophore); c (M), is the molar concentration; l (cm), is the optical path length through the sample. Absorbance is related to transmission as presented in Equation 2.2:

$$A = log\left[\frac{1}{T}\right] = log\left[\frac{I_0}{I}\right] = \epsilon lc = optical \quad density \quad (OD), \tag{2.2}$$

where T is transmission, the ratio of the transmitted light to the excitation light intensity. The absorbance of a material is equal to the optical density (OD) in the absence of turbidity.

Absorbance spectroscopy involves the measurement of light transmission through a sample. The transmitted light, being at the same wavelength as the excitation light, poses a serious challenge for most measurement setups as the goal is the measurement of transmitted light over a high background. Modern absorbance spectrophotometry applies monochromators and interference filters with sharp cutoff to minimize the excitation light so as not to saturate the detector.

2.2 Fluorescence Fundamentals

Fluorescence is a photoluminescence phenomenon that occurs in three stages. Photon energy $(h\upsilon_{EX})$ supplied from an external source is absorbed by an electronic singlet ground state (S_0) which gets promoted to a singlet excited state (S_1 or S_2). A schematic of the electronic-state diagram (Jablonski diagram) is shown in Figure 1. The electrons return to the singlet ground state with photon emissions $(h\upsilon_{FEM})$ after undergoing some energy abstraction. This loss in energy ensures that the emitted photon energy is less than the absorbed energy. The corresponding emitted photons (fluorescence) is characterized by a decrease in frequency or longer wavelength shift called a Stokes shift Valeur (2002); Guilbault (1990); Lakowicz (2006).

The lifetime of the excited state in typical fluorescent molecules (generally polyaro-

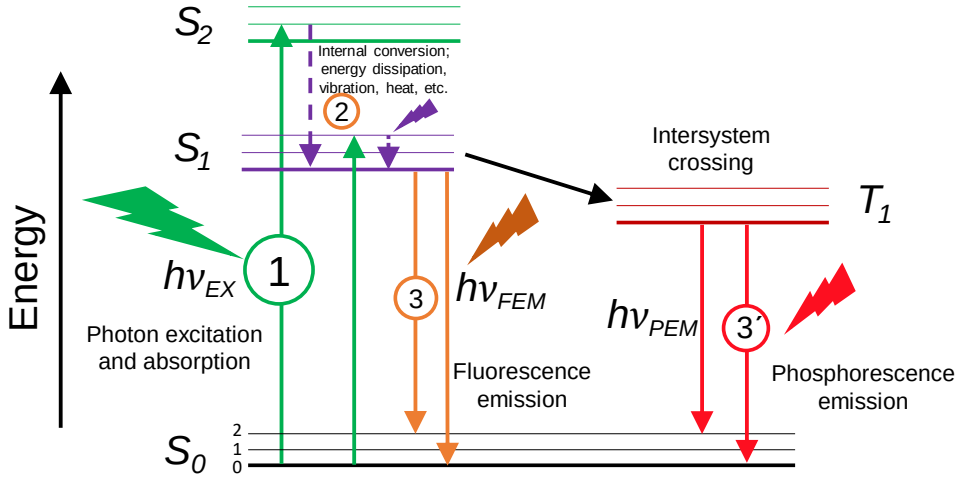

Figure 1: Energy (Jablonski) Diagram Illustrating the Fluorescence Process.

matic hydrocarbons) is short, ranging from $10^{-8} - 10^{-9}$ s. Phosphorescent molecules undergo a similar process to fluorescence but have an extended lifetime ($10^{-3} - 100$ s) and longer wavelength shift (relative to fluorescence), through a triplet state (T_1). Quantum dots also have a relatively longer lifetime in the μs range. Together, fluorescence and phosphorescence belong to a family of processes called photoluminescence. This is distinguished from chemiluminescence or electroluminescence where the excited state is populated by a chemical reaction or by the application of a voltage, respectively Roda (2011); Mueller (2000).

2.2.1 Fluorophore Characteristics

The Stokes shift is illustrated in Figure 2; the absorption/excitation spectrum and the emission spectrum are characteristic of a particular fluorophore. The Stokes shift is a very important process for fluorescence detection as it allows the fluorescence emissions to be measured at a different wavelength than the excitation wavelength.

Hence, with the use of dispersive optics, the relatively low intensity fluorescence emissions can be measured against a low background by suppressing the excitation light. A unique property of fluorescence spectra is the dependence of fluorescence emission intensity on the excitation light intensity. Also for most fluorophores used in practice, the emission spectra is independent of the excitation wavelength Lakowicz (2006). The cyclic fluorescence process ensures that continuous absorption and the subsequent fluorescence emissions can be measured over time, as long as the excitation source does not cause permanent excited state damage (photobleaching), which is a function of the excitation intensity and duration. High resistance to photobleaching is a desirable property for fluorophore selection.

Fluorescence Equation In the case of fluorescence (unlike absorbance), the fluorescence emission intensity I_F, is directly related to the quantum yield (QY) of the

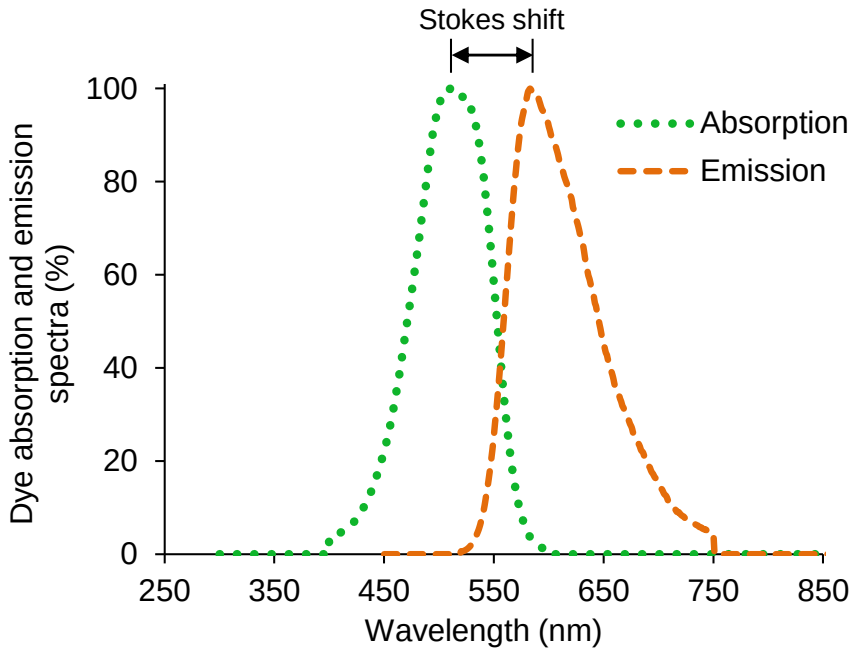

Figure 2: Representative Fluorescent Dye Absorption/Excitation and Emission Intensity Spectra.

fluorophore and the excitation intensity as shown in Equation 2.3:

$$I_F = KI_0QY[1 - exp(-\epsilon lc)], \tag{2.3}$$

where, ϵ is the extinction coefficient or molar absorptivity of the fluorophore; c, is the molar concentration; l, is the optical path length through the sample; I_0, is the excitation source intensity; K, is a system dependent proportionality constant (see Chapter 3 for more detailed treatment of system collection efficiency).

For moderately low concentrations (weakly absorbing) and uniformly distributed solute in a solvent, the fluorescence emission intensity due to absorption of radiant energy is also described by the Beer-Lambert law and Equation 2.3 could be approximated using a Taylor series expansion to yield:

$$I_F = 2.303KI_0QY(\epsilon lc). \tag{2.4}$$

Deviations from this linear relationship may be due to a high optical density/high absorption/self-absorption, aggregation of absorbing species in solution (agglomeration), or instrumental artifacts. Other effects from interferants, contaminants, and scattered or stray light could bias the interpretation of the fluorescence signal Lakowicz (2006).

2.2.2 Fluorescent Probes

A variety of fluorophores are commercially available at different wavelengths, widely varying spectra, Stokes shift, quantum yield, and extinction coefficients. These labels could be fluorescent molecular/organic dyes/fluorochrome, fluorescent microspheres, fluorescent proteins (protenacious fluorochromes), and longer lifetime and wider stokes shift labels (quantum dots, europium). A few examples are presented in

Table 1 Life Technologies (2010); O'Farrell (2013); Thermo Fisher Scientific (2009). Despite the vast array of options, care must be taken during the design process to ensure that the fluorophore choice satisfies a significant number of requirements, including: matching with the excitation source, filters, flow characteristics, brightness, stability and photobleaching, etc. A detailed treatment of the design choices in the fluorophores selection process is presented in Chapters 3 and 4. Fluorescent microspheres, quantum dots, and europium microspheres have received significant interest in lateral flow assay development because of the inherent amplification (brightness), flow properties, stoke shift, and time-gated detection which contribute toward background reduction (see Section 2.7).

2.3 Elements of a Fluorescence Detection System

Any fluorescence system at a minimum requires a radiant/excitation source (mercury-arc lamp, xenon-arc lamp, tungsten-halogen lamp, laser sources from UV to red, or LED) to excite the fluorophores; filters to selectively discriminate between the excitation source photons and the photons from the fluorophore emission; and a detector (Charge-coupled logic camera, CCD; complementary metal oxide semiconductor camera, CMOS; a photomultiplier tube, PMT, a photodiode, PD; or an avalanche photodiode, APD) that converts photons to a measurable parameter, usually a current or voltage. The fluorophore is typically bound to a substrate/carrier (well plate, microscope slide, plastic slides, microfluidic channel, or paper-based membrane) as a result of a biorecognition event. All the elements mentioned above play a significant role in the overall performance of the system and care must be taken in the design process to satisfy the design constraints. The specific design constraints for inexpensive, field-deployable, and highly sensitive systems suitable for LMIC applications is the focus of the rest of this dissertation.

Table 1: Common Commercially Available Fluorescent Labels Used in Immunoassays, Excitation (EX) and Emission (EM) Maxima, Stokes Shift, Quantum Yield (QY), and Extinction Coefficient (ϵ).

Label	EX/EM^*	Stokes shift	QY	ϵ^{**}
F1-Y	555/568	-	-	150,000
DyLight® 549	555/575	20	-	150,000
Cy®3	555/568	13	0.15	136,000
Cy®5	646/662	16	0.30	250,000
Fluorescein	494/522	28	0.90	75,000
Rhodamine 6G	525/555	30	-	-
Nile red microspheres	535/575	40	0.21	37,859
Alexa Fluor® 488	495/519	24	-	73,000
Alexa Fluor® 555	555/565	10	-	155,000
Alexa Fluor® 647	650/668	18	-	270,000
Europium (FluoSpheres™)	365/610	-	-	-
Qdot™ 605	350/605	-	0.79	>2,000,000

*(+/− 4 nm) in phosphate buffered saline (PBS) or methanol
**Molar extinction coefficient ($M^{-1}\ cm^{-1}$) at the absorption maximum

2.4 Central Laboratory Absorbance and Fluorescence Instrumentation

Routine operations in a central laboratory include the use of instruments that employ an optical detection technique. These include: luminometers, spectrofluorometers, spectrophotometers (microplate readers), flat-bed scanners (microarray scanners, gel, blot, and chromatogram scanners), fluorescence microscopes, flow cy-

tometers, DNA sequencers, surface plasmon resonance, etc. These instruments provide information about the bulk properties of a fluid under test or provide fluorescence or absorbance information as a function of spatial coordinates in 2D or 3D. Details of the operation of such devices are presented elsewhere Guilbault (1990); Lakowicz (2006), however, a brief summary of common components for these instruments follows. Typically, laboratory-based chemical and biochemical analytical instruments are built to accommodate a wide range of applications and automate the experiment/measurement operation at a high throughput. Fluorescence and absorbance based instruments (e.g. spectrophotometers and spectrofluorimeters) can be fairly complicated devices with numerous optical and electronic components (combinations of lenses, beam splitters, mirrors, laser sources, PMTs, holographic notch filters, bandpass and cut-off filter wheels, monochromators, cooled CCD, and/or CMOS camera technologies) ensuring high performance. A common feature worth mentioning is the adaptive gain usually obtained by varying a PMT voltage automatically or manually adjusting its response to different intensity levels. However, such a high performance comes at a high cost, both monetary and complexity. This dissertation focuses on developing an inexpensive fluorescence and absorbance platform that draws inspiration from central laboratory instruments for applications in resource-limited settings.

2.5 Units, Figures of Merit, and Quantitation

2.5.1 Units for Fluorescence Intensity

The measured fluorescence intensity from a sample is dependent on the system used for the measurement (system collection efficiency) and the molecular environment of the fluorophore. Fluorescence emission intensity is typically reported in relative light units (RLU), relative fluorescence units (RFU), arbitrary units (a.u.),

or qualitatively as "bright" or "dim", etc. Attempts to standardize fluorescence measurements have not gained wide acceptance in many circles. Notable among these efforts is the development of the Mean Equivalent Soluble Fluorochrome (MESF) unit of fluorescence intensity Schwartz *et al.* (2004); Wang *et al.* (2002); Schwartz *et al.* (2002); Gaigalas *et al.* (2005) when working with molecular fluorochromes, and the Equivalent Number of Reference Fluorophores (ERF) Wang and Hoffman (2017), when working with microsphere encapsulated dyes. Both units have been defined and developed at the National Institute of Standards and Technology (NIST) over the the past 3 decades. The MESF and ERF unit has been used extensively in flow cytometry. The MESF unit provides a internationally standardized approach toward comparing quantitative fluorescence intensity across platforms and, over time, eliminating instrumental bias. Under the formalization of the MESF unit, a fundamental fluorophore solution property is defined (the Fluorescence Yield) as the product of the sample concentration and the molecular quantum yield such that the fluorescence yield from a standard solution and an unknown sample can be compared (MESF). The use of a standard enables sensitivity specification that is independent of the platform on which the measurement is made. The measured fluorescence intensity response of a system is given in Equation 2.5 as:

$$I_F = [g(CE)\epsilon(QY)\int R(\lambda)E(\lambda)T(\lambda)d\lambda]c, \tag{2.5}$$

where, g is the system/detector gain; CE, is the collection efficiency; $R(\lambda)$, is the spectral response of the detector at λ; $E(\lambda)$, is the normalized emission spectrum at λ; and $T(\lambda)$, filter characteristics at λ (see Chapter 3 for modeling our in-house developed inexpensive fluorescence system). The standard and the unknown solution must be measured on the same system and with the same settings to eliminate system dependent parameters such as the collection efficiency (CE) or gain (g). Furthermore,

the excitation and emission spectrum of the standards must match that of the unknown and must be in the same molecular environment for an accurate fluorescence yield comparison. Provided the conditions above are satisfied, we could eliminate and collect system dependent parameters into a factor, K:

$$K = [\epsilon \int R(\lambda)E(\lambda)T(\lambda)d\lambda]. \tag{2.6}$$

and thus the measured fluorescence intensity could be written as:

$$I_F = K(QY)c. \tag{2.7}$$

Since the quantum yield, excitation, and emission characteristics of the standard and the unknown sample is the same, then the factor K is the same for the two samples. The term $(QY)c$ is the fluorescence yield, (FY), which can be compared for the standard and the unknown sample, since (FY) is directly proportional to the measured fluorescence intensity, I_F). We can therefore write that the concentration of the unknown sample, c_u is related to the standard as:

$$c_u = \frac{I_{Fu}}{I_{Fs}} c_s, \tag{2.8}$$

where, I_{Fu}, is the measured fluorescence intensity of the unknown sample; c_s, is the concentration of the standard; I_{Fs}, is the measured intensity of the standard. This comparison although limited by the practical difficulty in maintaining the same molecular environment in both the standard/calibrator and the unknown samples, is extremely important for calibration and quantitation in low-cost POC screening programs which include the use of multiple reader devices DeRose *et al.* (2007); Wang and Hoffman (2017).

2.5.2 Sensitivity (SEN)

Instrument Sensitivity

The focus of this section is to briefly define a few measures of performance associated with analytical instruments. Usually, the performance parameters are determined using data obtained from the measurement of a standard/calibrator, a titration (for fluorophores or chromogenic probes) to obtain a calibration curve, or from a population study. Linear and non-linear (sigmoidal) relationships between the instrument response and concentration is frequently encountered in bioanalytical processes Cunningham (1998). The sensitivity of absorbance measuring instruments, for example, a UV-VIS spectrophotometer, can be easily standardized because it is based on an absolute unit of measurement/material property, the optical density (OD). As is the case with most samples, the OD in the absence of turbidity/cloudiness of the sample is equal to the absorbance. In photoluminescence (fluorescence, phosphorescence) or chemiluminescence applications, however, there is no fixed unit or universally acceptable standard unit. For this reason, it is difficult to specify the sensitivity of a system in comparison to others. Some instruments include a stable reference standard within the instrument for reference and normalization of the measured sample, or for initial instrument calibration. Such internal standards are now making their way into compact fluorescence readers like the cPOC from LRE Medical. Although these standards are stable, they need to be replaced over time or their degradation needs to be monitored and compensated for.

Analytical Sensitivity

Calibration curves of known samples enable the identification of unknown samples based on the measured responses. A representative response as a function of concen-

tration for a fluorescence measurement is shown in Figure 3. Typically the analytical sensitivity (SEN) refers to the slope of the the linear region of the response. It is the smallest measurable change in response for a unit change in concentration, (dr/dc).

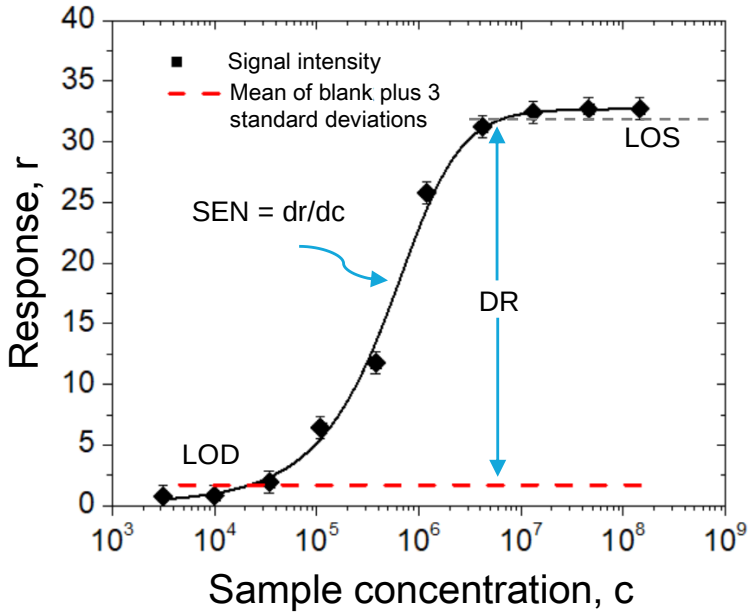

Figure 3: Representative Sensor Response as a Function of Concentration.

For optical sensors, the response, r, is usually in relative light units and the concentration, $\log_{10}$(c), expressed in mass concentration g/L, molar concentration, M, or in number of microspheres/particles.

Clinical Sensitivity

In the context of a patient population or clinical test Lalkhen and McCluskey (2008), the sensitivity of a test or diagnostic device is defined as the true positive rate. It measures how well the test or sensor is able to correctly identify positive samples. Given a sample population test, the number of true positives (TP), false positives (FP), true negatives (TN), and false negatives (FN), the sensitivity is calculated in

Equation 2.9 as:

$$SEN = \frac{TP}{TP + FN}. \tag{2.9}$$

2.5.3 Specificity (SPC)

The specificity of a test is defined as the true negative rate. It measures how well the test is able to correctly identify negative samples or controls. Specificity is calculated as shown in Equation 2.10,

$$SPC = \frac{TN}{TN + FP}. \tag{2.10}$$

Other measures of performance associated with clinical studies or patient trials include: efficiency, positive predictive value (PPV), negative predictive value (NPV), likelihood ratio, accuracy (ACC), and efficiency Wong and Tse (2009); Motulsky (2017). An understanding of these parameters through the test and detector design stage is necessary to minimize issues with false positive and false negatives.

2.5.4 Dynamic Range (DR)

The dynamic range is the linear range of the system response in the calibration curve as illustrated in Figure 3. The S-shaped sigmoidal response is very frequently encountered in immunoassays and optical detection technologies. Above and below the linear dynamic range, there is a plateau indicating no discrimination in the system response. Responses in the asymptotic sections of the test response, lead to inaccurate results for quantitative tests. Complex clinical laboratory instruments would typically have an adaptive dynamic range using sensitive detectors and advanced electronic processing methods.

2.5.5 Limit of Detection (LOD), Limit of Saturation (LOS), and Limit of Quantitation (LOQ)

There are several methods of estimating the limit of detection (LOD). The most commonly used, and least accurate method, is by conducting a visual inspection of a calibration curve. In the case of non-instrumented technologies like visual readout lateral flow assays, a color chart of known concentrations could be used as a reference in setting the minimum detectable analyte concentration. This technique is subjective and suitable for qualitative measures. According to the International Union of Pure and Applied Chemistry (IUPAC), the LOD is the concentration that corresponds to the mean of the response (μ_i) of the blank samples or controls plus k standard deviations (kσ), where k (usually = 3) is chosen based on the desired confidence level. The number of standard deviations could be increased for a higher level of certainty. If c_L is the analyte concentration (LOD), then the corresponding response, r_L, is:

$$r_L = \mu_i + k\sigma_i, \tag{2.11}$$

where μ_i, is the mean of the blank measures, σ_i, is the standard deviation of the blank measures McNaught and Wilkinson (1997); Armbruster and Pry (2008).

Other methods to calculate LOD have been used widely in literature Cunningham (1998). Particularly, the LOD is calculated based on the standard deviation and slope of the response as $LOD = k\sigma/SEN$, where the sensitivity, $SEN = dr/dc$, k has a value of 3 or 6 and σ_i is the standard deviation. Because the slope changes across a typical sigmoidal response, the determination of the LOD based on this technique is dependent on the region of the curve chosen. The LOD could also be estimated from the signal-to-noise (SNR) ratio . Generally, the ratio of the response from the test sample to a well-defined blank or control at low analyte concentrations is

frequently used to determine the LOD. With the use of SNR, an SNR between 3 or 2:1 is considered acceptable ICH Harmonised Tripartite Guideline (2005). The limit of quantitation (LOQ) is computed in a similar manner, using the same techniques described above, except that $k = 10$ and an SNR of 10:1 is a generally acceptable rule of thumb ICH Harmonised Tripartite Guideline (2005).

2.5.6 Selectivity (SEL)

Selectivity (SEL) refers to the ability of a system or test to distinguish between components of a sample (the measurand and interferants) under analysis. The ideal sensor should give a response solely from the measurand. In the context of fluorescence-based, lateral flow assays, the use of interference filters (discussed in Chapter 3) selectively isolates other emissions and scattered light, such that the detector measures only specific light emissions from the fluorophore in a narrow band. The selectivity of biomarkers in a complex matrix like blood is also a very important parameter to consider in assay design.

2.5.7 Sample-to-answer Time/Response Time

The sample-to-answer (STA) time refers to the time it takes to get a test result after the sample input is provided. It is desirable for point-of-care assays to have a short, sample-to-answer time, less than 30 min Peeling and Mabey (2010). This should include the time for the test to run and for the results to be presented to the user or communicated to a care provider. Short STA time minimizes patient revisits and expedites patient diagnosis and care. This has an impact on survival rate, lowers healthcare costs, and improves quality of care and quality of life. The response time, from an instrumental perspective, is the time taken for an instrument or device to analyze the samples under test.

2.5.8 *Inter and Intra-assay Variability and Coefficient of Variation*

The reproducibility of a test is critical to performance. A robust test will have acceptable variations over time, across multiple runs and between users, benches, and laboratories. The coefficient of variation (%CV) for the response obtainable from LFAs using a conjugate pad is reported to be between 15 to 30% O'Farrell (2013). The CV can be used to determine or set an acceptable level of precision for a test. Responses to changing altitude, vibrations, humidity, and temperature should be understood and suitably controlled or accounted for.

2.5.9 *Qualitative, Semi-quantitative, and Quantitative Tests*

Qualitative, semi-quantitative, and quantitative tests are used routinely to determine or express the quantity of analyte in a specimen/sample, depending on the application. Qualitative tests have been used extensively in lateral flow assays, especially for rapid diagnostic tests based on color/visual interpretation. Nitrocellulose membranes have been traditionally dyed white for this reason, to provide a high contrast, although several color labels have been used (most commonly blue, black, and red). The availability of multi-colored labels enables multiplexed testing and easy visual interpretation where only a minimum threshold/cutoff is required. For qualitative tests, if the measured response is equal to or greater than a clinically pre-defined cutoff value (CO), the sample is considered positive. A response value below the CO means the sample does not contain enough analyte to be considered positive by the test in question, hence the test is declared clinically negative. Visual read tests are subject to the individual operators' perception of color, the time the assay is inspected (reading too early or too late), and lighting conditions Wong and Tse (2009), hence the need for instrumented readout for improved accuracy.

Semi-quantitative tests usually have a descriptive interpretation of the results beyond the interpretation of "positive" or "negative" as is the case with qualitative tests. An example of this application is found in the digital ovulation kit or the weeks-estimator pregnancy test from ClearBlue®. In the ovulation test kit, the luteinizing hormone (LH) concentration (a biomarker for ovulation) is reported as "low fertility", "high fertility", and "peak fertility". Here, the absolute concentration of the LH is not reported.

Quantitative tests report numerical values associated with the sample, e.g. a biomarker concentration in g/L, M, or a numeric particle concentration. The reported concentration is traceable to a standard assay (calibrator), calibration curve, or a universal reference assay. This makes the development of truly quantitative assays very challenging, especially for biomarkers where no standards exist. The demand for quantitative tests is a major factor driving the advancement of lateral flow tests from a simple home use pregnancy test to a versatile tool with applications in different fields Wong and Tse (2009). Quantitative tests are useful for early detection of diseases, monitoring treatment, drug response, and for the development of reliable diagnostic tests especially for resource-limited settings where there is no access to complex clinical laboratory diagnostic tools. Additionally, quantitative tests are useful for applications where the rapid changes in biomarker levels are directly related to the disease progression and/or treatment. To meet this demand, the need for higher sensitivity and a wider dynamic range is imperative, hence the development of lateral flow assays using fluorescent labels (see Section 2.7). Quantitative tests require a calibration curve and a strict quality control and assurance (QC, QA). The response profile could be generated by a titration experiment and fitted with multiple regression models including quadratic, 4 or 5-parameter (4-PL or 5-PL), logistic models, log or linear model, and others. Quantitative lateral flow tests, however, are limited

by the relatively poor reproducibility and repeatability (test-to-test variability issues) compared to standard lab protocols.

2.6 Lateral Flow Assays

Lateral flow assays (LFAs) have been identified as a suitable tool to detect and diagnose diseases especially in resource-limited settings Ngom *et al.* (2010). This is due to their relatively simple operation compared to laboratory tests, minimal sample preparation requirements, rapid results, low manufacturing cost, stability especially with lyophilized reagents, fast sample-to-answer time, and use by unskilled or minimally trained workers Sajid *et al.* (2015); Linares *et al.* (2012). This is reflected in the number of HIV, malaria and other rapid diagnostic tests (RDTs) now prequalified by the WHO World Health Organization (2018a) and the vast array of tests currently being developed. Since the invention and commercialization of the first compact lateral flow test home pregnancy test in 1980s by Unilever under the brand name, Clearblue® van Amerongen *et al.* (2018); Chard (1992), lateral flow assays have become a versatile tool, with applications in numerous fields/sectors including veterinary medicine, water testing, food safety, drug testing, pathogens, hormones, antibody testing, and others Wong and Tse (2009); Ngom *et al.* (2010). It is worth noting that clinical and veterinary applications occupy the largest share in sales revenue (89% and 8% respectively O'Farrell (2013)) estimated to be over $4.5 billion in 2015. Lateral flow assays have been deployed mostly for qualitative and semiquantitative tests and in a few cases for quantitative analysis of target analyte Posthuma-Trumpie *et al.* (2009). Significant challenges with developing quantitative tests in a LFA format include %CV and reproducibility van Amerongen *et al.* (2018). Overall, some of the limitations of LFA include the poor analytical sensitivity relative to gold standard procedures (ELISA, NAT), lack of quantitative output, multiplexing chal-

lenges Li and Macdonald (2016b); Hu *et al.* (2017), high tendency for cross-reactivity and non-specific binding, fluid control using valves may be necessary, which increases the device complexity Tang *et al.* (2016); Sajid *et al.* (2015); Posthuma-Trumpie *et al.* (2009); Swanson and D'Andrea (2013), test reproducibility, challenges with integration, and the use of small sample volumes usually below 1 μL. Advancements in manufacturing technology (stable labels, quantitative dispensing technologies, automated processing and assembly technologies, high quality membranes and materials), and relatively newer approaches in 2D and 3D paper networks are targeted toward resolving some of the limitations of lateral flow assays Fu *et al.* (2011); Jaione Tirapu-Azpiroz (2018); Natoli *et al.* (2018); Yetisen *et al.* (2013b); Osborn *et al.* (2010).

2.6.1 Visual/Reflectometric and Absorbance-based Probes/Chromogenic Probes

Absorbance-based signal transduction is by far the most frequently used technique in lateral flow assays, especially for visual-based readout. Some of the most commonly used chromogenic labels for colorimetric immunoassays and lateral flow assays in general include enzyme-substrate pairs like horseradish peroxidase - 3,3',5,5'-Tetramethylbenzidine (HRP-TMB)or HRP-3,3'-Diaminobenzidine (HRP-DAB), colored latex microspheres, colloidal gold nanoparticles (AuNP), silver enhanced AgNP, carbon nanoparticles, cellulose nanobeads, silica nanoparticles, etc., each one having its own unique merits and weaknesses Linares *et al.* (2012); van Amerongen *et al.* (2018). Other labels reported included: magnetic particles, selenium nanoparticles, textile dyes, and liposomes. Enzyme-substrate pairs and molecular dyes are rarely used in LFAs. Colloidal gold, however, has been used extensively in lateral flow assays with significant success Huang *et al.* (2016); Mak *et al.* (2016) and is now the gold standard for visual LFA and used in about 75% of all lateral flow tests manufactured Ngom *et al.* (2010). Typically the size of the particles used are in the 20 to 40

nm range to achieve a stable suspension of the particles in a solvent and ensure flow and uniform release from a conjugate pad O'Farrell (2013); Posthuma-Trumpie *et al.* (2009). Labels should be detectable at low concentration, stable over time, proper flow characteristics, and easily functionalized and conjugated to biomolecules. Overall, visual signal interpretation is subjective, depending on the individual and upon lighting conditions. Quantitative results are therefore not accurate because of the difficulty in discriminating concentrations by the naked eye. Instrumented technologies, however, do not suffer from this deficiency. However, assays based on colored labels, even with absorbance/reflectometric instrumented technologies have a smaller dynamic range and sensitivity compared to fluorescence techniques.

2.6.2 Lateral Flow Immunoassay Formats - Biorecognition

There are striking similarities in the format of standard laboratory protocols, e.g., enzyme-linked immunosorbent assay (ELISA) and the lateral flow immunoassay, or between nucleic acid tests and the nucleic acid lateral flow test format. Immunoassays take advantage or the high affinity between antigen and antibodies for immunometric detection. In a microplate ELISA, capture agents are bound to the walls of the μL volume wells in the microplate. Through a series of incubation steps with the analyte containing sample and wash steps, the analyte can be detected using an enzyme-substrate pair with a stop reagent or with fluorescent-detector conjugates, gold nanoparticles, or chemiluminescent detectors. The setup is not much different in lateral flow assays as shown in Figure 4 (a) - (c).

2.6.3 Lateral Flow Assembly and Manufacturing

The basic design and assembly of a lateral flow strip includes a linear arrangement of overlapping membranes/pads (stationary solid phase) through which a mobile liq-

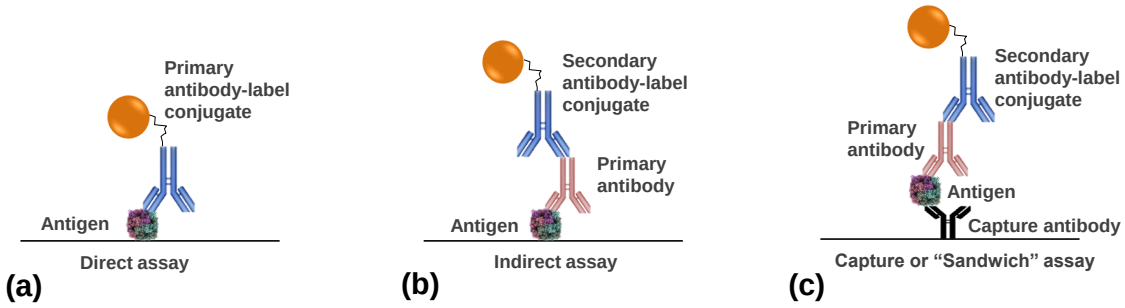

Figure 4: Immunoassay Formats on a Solid-phase/Matrix/Solid Support Showing Different Antigen-Antibody-Label Configurations. (a) Direct Assay (b) Indirect Assay (c) Capture Assay.

uid phase flows by capillary action. A lateral flow test strip typically includes the following components Yetisen *et al.* (2013b) as depicted in Figure 5.

Sample Pad

The sample matrix (whole blood, serum, plasma, urine, saliva) is typically introduced into the lateral flow assay through the sample pad is located upstream (left) as shown in Figure 5. The sample pad could serve multiple functions including whole blood filtration. The sample pad selection process is critical to the assay performance and issues with sample loss due to retention in the membrane should be carefully considered. Some commercially available sample pads include EMD Millipore CFSP223000 (C083), Standard 14 and Standard 17 from GE Healthcare. Most of these pads could be used as conjugate and absorbent pads depending on the assay.

Conjugate Pad

Usually used to hold/store the dried/lyophilized detector-label conjugate (e.g. colloidal gold- or microsphere conjugated antibodies specific for the target or assayed

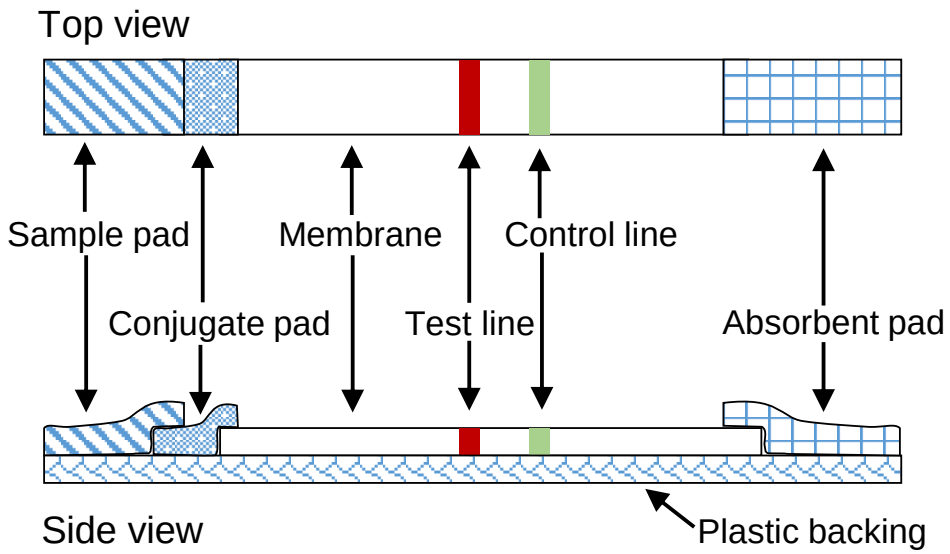

Figure 5: Schematic of a Lateral Flow Assay Pad and Membrane Assembly.

analyte). Reagent storage in a dried form typically eliminates the need for refrigeration or cold transport, as well as an extended shelf-life. For multi-step assays where undesirable to have the unrelated entities in the sample matrix interact with the conjugate, the use of the conjugate pad is omitted. This, however, necessitates the design of other reagent and conjugate release mechanisms to execute the assay.

Analytical Membrane

The gold standard analytical membrane for LFAs is nitrocellulose (NC) Holstein *et al.* (2016). Nitrocellulose membranes form the solid support to immobilize capture agents and a medium through which samples containing the target flows. The immobilization process is usually accomplished by passive adsorption via a combination of intermolecular forces (hydrophobic, van der Waals, and electrostatic interactions) Kim and Herr (2013). However, the exact mechanism is not well-understood Tonkinson (2002); EMD Millipore (2013); Fridley *et al.* (2013). There are not many easy and straight-

forward strategies at the moment for covalent immobilization or chemical activation required at the molecular level for binding capture reagents on nitrocellulose Fridley *et al.* (2013); Ahmad *et al.* (2012); Tovey and Baldo (1989); Tan *et al.* (2008); Nargang *et al.* (2016); Nakamura *et al.* (1989); Pelton (2009). It is important to determine and eliminate the factors that might cause the capture agent to lift-off/desorb and migrate downstream the membrane. Reports indicate the formation of a test line and the subsequent disappearance due to lift-off as the assay progresses EMD Millipore (2013). The presence of a surfactant EMD Millipore (2013) or salt Fridley *et al.* (2013) can affect protein adsorption by masking the membrane surface area or acting as potential stripping agents. Furthermore, because of the porous and composite nature of the nitrocellulose membranes, techniques to accurately estimate the amount of protein immobilize or the immobilization efficiency over the membrane cross-section could be complicated Wang *et al.* (2006); Tan *et al.* (2008). Intensity measurements Ahmad *et al.* (2012); Nakamura *et al.* (1989) based on absorbance (OD) may not give accurate depth information with respect to the thickness/Brunauer-Emmett-Teller (BET) surface area (which describes/determines the pore size and total available specific surface area in m^2/g in a porous membrane Tylkowski and Tsibranska (2015)). Immobilization efficiency may also be dependent on molecular length, size Tonkinson (2002), and pH which alters protein properties EMD Millipore (2013). The molecular structure/compactness/effective diameter also determines the loading capacity of the protein in a membrane. Typical membranes used in lateral flow assays have an IgG loading capacity of 50 - 200 $\mu g/cm^2$ Yetisen *et al.* (2013b); EMD Millipore (2013). The binding capacity for a test strip with 1 mm wide test lines and strip width of 5 mm, is between 2.5 and 10 μg. The capture agents are typically dispensed/striped perpendicular to the flow direction in the membrane. This presents a uniform pressure front to the flow of reagents through the membrane. Other dispensing formats

have been investigated including LFA microarrays Reck *et al.* (2008), symbolics, and 7-segment display lateral flow tests Li and Macdonald (2016a) in which an array of capture reagents are dispensed as circular dots/spots. The capture line(s) is usually co-printed with a control line spaced 3 to 4 mm apart. The line thickness is typically between 1 - 2 mm EMD Millipore (2013). Depending on the dispense pressure, thickness, and porosity of the membrane, the capture agent penetration is a function the protein concentration dispensed Wang *et al.* (2006). The capillary flow properties and immunochromatographic reaction in nitrocellulose Li *et al.* (2012) eliminates and simplifies the movement of fluid without external equipment (including syringe pumps and other vacuum or pressure sources) commonly used in microfluidic channels/devices based on other polymer types (PDMS, PMMA, Topas, PC, etc). The high protein binding affinity of nitrocellulose and its protein binding capacity make it a preferred membrane over other potential membrane candidates including glass fiber or cellulose acetate. The success of nitrocellulose is mostly due to the low cost associated with paper production (10 cents/m^2) Tobjörk and Österbacka (2011); Pelton (2009), tuneable porosity and pore size (that determine the flow rate), as well as the binding capacity due to its high surface area-to-volume ratio (SAVR). Although an imperfect membrane, NC has become the gold standard. Some of the challenges with using NC include handling, protein immobilization by passive adsorption, and the membrane opacity. Efforts to replace nitrocellulose have not gained significant acceptance by industry or researchers. Among the most significant efforts, the development of FUSION5 provided an alternative to nitrocellulose with the goal of manufacturing a single continuous membrane to was capable of handling all the functions of the various parts of the lateral flow strip assembly Wong and Tse (2009). Commercial suppliers of nitrocellulose for lateral flow assays include: EMD Millipore, GE Healthcare, Sartorious, and Pall. Fluid flow in a porous membrane is determined by the

membrane and fluid characteristics: pore size and distribution, porosity, fluid viscosity, surface tension, and contact angle. The composite mesh structure of porous nitrocellulose suggests that the path of a particle is not equivalent to flow through a straight channel, however, it is sufficient to approximate the path as a straight line for most treatments Fridley *et al.* (2013). The entire membrane cross-section is therefore treated as a collection of straight channels in parallel. Hence the observed laminar flow dynamics driven by capillary action in porous membranes is governed by the Washburn equation Washburn (1921) and Darcy's law Brown (2002); Yetisen *et al.* (2013b); Osborn *et al.* (2010), representing initial "wet-out" flow and fully wetted flow regimes in a porous solid phase. For a membrane of uniform cross-section, and an infinite fluid supply reservoir, the wet-out regime describes the fluid flow through a dry porous membrane. It is expressed in the Washburn equation as:

$$L^2 = \frac{\gamma d_p cos(\theta) t}{4\mu}, \tag{2.12}$$

where L is the length of the fluid column or the distance covered by the fluid front in the porous material, d_p is the average pore diameter, γ is the effective fluid surface tension, θ is the contact angle, t is the transport or flow time of the fluid front, and μ is the dynamic fluid viscosity. Equation 2.12 demonstrates that the fluid front migrating into the dry parts of the membrane (downstream) is affected by the viscous resistance of the fluid in the wet area (upstream), such that the resistance increases with the length of the fluid column.

Once the membrane is fully wetted, the porous membrane is saturated with a fluid, the flow is characterized by Darcy's law expressed in Equation 2.13 as:

$$Q = -\frac{\kappa A \Delta P}{\mu l}, \tag{2.13}$$

where Q is the volumetric flow rate, κ is the intrinsic permeability of the membrane, A is the cross-sectional area of the membrane, ΔP is the pressure drop/difference over the length of the membrane, l and the term $[(\mu l)/(\kappa A)]$ is the hydraulic resistance of the membrane, R_{hyd}. Darcy's law is the fluid analogue of Ohm's law in electricity.

Wick/Absorbent Pad

The wicking pad located downstream acts as a sink, pulling the fluid out of the membrane and serving as a waste collection point EMD Millipore (2013); Wong and Tse (2009). Some commercially available wicking pads with high capacity include: CF7 and CF5 from GE Healthcare.

Plastic Backing

A plastic backing material (white PVC or polystyrene) on which a pressure sensitive adhesive (e.g. GL-187 from Lohmann) is applied in order to hold all the other parts together using a pressure-based lamination process. The plastic backing also provides rigidity and support for handling in the manufacturing process as well as supports capillary flow through the device. This dissertation focuses on the use of low-cost optoelectronics in a transillumination architecture, requiring that the backing material be transparent. Although white backing materials are the industry standard and readily available off-the-shelf, we are able to obtain an optically clear backing material from Lohmann Inc. Details of the optical effects of the backing material, opacity, and scattering effects of paper-based membranes are presented in Chapters 4, 7, and 8.

2.6.4 Other Lateral Flow Assay Readout Technologies

Several readout/transduction approaches have been investigated by researchers including: optical, electrochemical, magnetic beads Jacinto *et al.* (2018); Cardoso *et al.*

(2017); Connolly and Kennedy (2017); Barnett *et al.* (2014), thermal signatures Qin *et al.* (2012), and label free methods Gubala *et al.* (2012).

2.7 Fluorescence-based Lateral Flow Assays

Although the potential improvements in sensitivity and dynamic range Lee *et al.* (2013) through the use of chemiluminescent and fluorescent reporter particles in lateral flow assays have been well identified O'Farrell (2015b), these labels are not yet used extensively, compared to the existing chromogenic probes (AuNP and colored polystyrene microspheres). This partly due to the instrumentation requirements for fluorescence, issues with stabilizing the fluorescence particles and conjugates O'Farrell (2015b), coupled with the relative ease of visual readout in test protocols Mak *et al.* (2016). Although researchers have continued to investigate improvements using existing colorimetric labels Morbioli *et al.* (2017) and developing fluorescence lateral flow assays with enhanced performance Huang *et al.* (2016); Foubert *et al.* (2017); Juntunen *et al.* (2012); O'Farrell (2013); Qu *et al.* (2016), a manufacturing price point of $0.38 Bangs Laboratories (2013) for many visual rapid tests is hard to beat with any additional instrumentation. The use upconverting phosphors (UCNP) Song and Knotts (2008) in a time-resolved luminescence configuration for detecting C-reactive protein (CRP), quantum dots for CRP and human heart fatty acid binding protein (hFHFP) Wu *et al.* (2018); Savin *et al.* (2018), europium(III) chelate Eu(III) and fluorescent microspheres, and fluorescence resonance energy transfer (FRET) Wang *et al.* (2018) in LFAs have been reported. Currently, there are not many commercially available or field-deployable fluorescence lateral flow assays Huang *et al.* (2016)for resource-constrained environments. Although absorbance measurements are suitable for applications that do not require very high sensitivity, many early detection applications require high enough sensitivity to detect the onset of an infection or disease

condition Juntunen *et al.* (2012). Some of the challenges with this development are explored in the chapters that follow.

2.8 Compact Fluorescence Reader Technologies

A small number of reader technologies have emerged with significant adoption by the LFA development community. These readers include those manufactured and sold by Qiagen ESE Quant, Lake Constance, LRE cPOC (Esterline), Alere (Now Abbott), Axxin Inc, DCN fluorescent assay visualizer, Optricon, Novarum (uses a camera on smartphone), Magna Biosciences, and Holomic. The signal detection system in these readers operates either by scanning or static imaging. In the scanning approach, the entire length of the strip is scanned by moving the test strip over a stationary emitted-detector assembly fixed or vice versa. Repeated scanning ensures that the test line is covered. The scanning approach offers more flexibility and is easily adapted to read multiple cassette configurations. In the static imaging approach, a CMOS/CCD camera is used to image the entire test line. It is critical that the strips are accurately aligned as a small deviation in position could significantly impact the intensity reading. The optoelectronic configuration in most portable readers resemble an epi-fluorescence microscope in which the sample is illuminated from the top. Wherein, the LFA membrane test lines are illuminated from the top (nitrocellulose side) of the strip using excitation and emission bandpass filters and a dichroic mirror, with the detector arranged perpendicular to the excitation light source. This configuration helps to reduce the excitation light reaching the detector and thus improves the SNR. Other configurations include the off-axis and the v-optics configuration. The aforementioned configurations necessitate the use of optical components that require consistent alignment and contribute significantly to the total cost of the reader (also see patent filing Fleming *et al.* (2014)). The rest of this dissertation explores the

transillumination (typically used in gel imagers and light tables) and co-planar architectures without the use of focusing optics. The elimination of focusing optics results in reduced cost and improved ruggedness and robustness required for field-deployable devices.

2.8.1 Cellphone-based Reader Technologies

Smartphone-based analysis takes advantage of the compact CMOS camera and sometimes, the torchlight LEDs behind the phone. Applications for colored and fluorescent labels have been explored Roda *et al.* (2016); Oncescu *et al.* (2013). In all cases, a phone attachment is required, typically including a lens for focusing and sometimes, transfer optics to implement several functions, including microscopy Roda *et al.* (2016) and spectrometry Scheeline (2016). However, the rapid development and advances in smartphones requires that manufacturers stock-up on a particular series to maintain supply and development that may not port from one platform to another or from one series to another. The differences between smartphones necessitate a calibration for both the camera and the LED. Additionally, differences in firmware and cross-platform compatibility presents significant challenges. Since smartphones have become ubiquitous, resolving the issues with smartphone readers may truly lead to a powerful diagnostic tool in the hands and pockets of over a third of the world population.

2.9 Commercial Available Tests for High-risk HPV Types

A list of some commercially available HPV virological technologies (HPV DNA) are presented in Table 2 World Health Organization (2018b); Cepheid (2017); Roche Molecular Systems, Inc. (2015); Atila Biosystems (2018). The performance characteristics of some of the commercially available (FDA approved) HPV DNA tests and

systems are indicated. The WHO prequalification list for *in vitro* diagnostics has been dominated by products for Malaria and HIV diagnosis. For the first time, a test for HPV was prequalified this year for applications in low-resource environments. This is a significant development World Health Organization (2018b,a). The *care*HPV^{TM} Test manufactured by QIAGEN GmBH is classified under HPV virological technologies. The *care*HPV^{TM} Test is capable of qualitative detection of 14 high-risk HPV (hrHPV) types (16, 18, 31, 33, 35, 39, 45, 51, 52, 56, 58, 59, 66, and 68) using a nucleic acid hybridization assay with signal amplification in a microplate chemiluminescence assay. At the time of this writing, there is no prequalified or commercially available serologic test for identifying high-risk HPV types. Our group is developing a test to detect HPV-specific IgG antibodies. More details are presented and discussed in the later chapters of this dissertation. The current clinical practice for diagnosis is the Pap test (cytology) followed by high-risk HPV DNA testing for a referral to colposcopy or biopsy if necessary.

Table 2: Commercially Available HPV DNA Tests and Instruments

	careHPV^{TM} Test	Xpert® HPV	Cobas® HPV Test	Onclarity	Atila MHPVF-100
Manufacturer	QIAGEN	Cepheid	Roche	Becton Dickinson	Atila Biosystems
Sample type	Cervical specimen	Cervical specimen	Cervical specimen	Cervical specimen	Cervical specimen
sample volume (μl)	50	1000	3000	-	25
Detection method	NAH(HC2)† Chemiluminescence	NAAT‡ Fluorescence	NAAT and NAH Fluorescence	NAH (HC2) Fluorescence	Isothermal NAAT real-time fluorescence
hrHPV detected*	16, 18, 31, 33, 35, 39, 45, 51, 52, 56, 52, 58, 59, 66, 68	16, 18/45, 31, 33, 35, 39, 51, 52, 56, 58, 59, 66, 68	16, 18; pooled, 31, 33, 35, 39, 45, 51, 52, 56, 58, 59, 66, 68	6, 18, 31, 45, 51, 52; pooled 14 hrHPV types	16, 18, 31, 33, 35, 39, 45, 51, 52, 53, 56, 58, 59, 66, 68
Duration	2h30min	60 min	3h30min	2h	1h30min
SEN/SPC/LOD**	74.42/97.45/1x10^6	90.8/42.6/2903	90.0/70.5/-	-	-
Tests/run(result)	90(qualitative)	(qualitative)	96(qualitative)	30(qualitative)	(qualitative)
Shelf life (months)	12	-	-	-	-
Certification	CE	CE	FDA	-	-

* High-risk HPV (hrHPV) types singly detected, or pooled (any type); ** Sensitivity (SEN) and specificity (SPC) in percentage and limit of detection (LOD) in IU/L; † Nucleic acid hybridization (NAH), using Hybrid Capture2 assay (HC2®); ‡ Nucleic acid amplified test (NAAT)

2.10 Requirements for POC/Field-deployable Applications - Ideal Assay and Reader Devices

The ASSURED criteria as outlined by the WHO Peeling and Mabey (2010) best captures the requirements for field-deployable technologies, especially in resource-limited areas. Any lateral flow, microfluidic, reader or assay technologies developed for LMICs is best benchmarked against the ASSURED criteria Wu and Zaman (2012). The ASSURED framework is described briefly:

Affordable - The test should be inexpensive for the target market, a fraction of the daily income is recommended. With visual read lateral flow tests manufacturable at ∼$0.38, tests that cost less than $1 are desirable, especially considering that a significant percentage of those who need low-cost tests live under $1.9 per day. A good model for an instrumented, high-sensitivity, and quantitative test that can meet this price point is a reusable reader unit with low-cost biorecognition consumables. For example, a lateral flow assay cassette manufactured for a fraction of a dollar, combined with a reusable and ultimately disposable inexpensive reader platform could significantly reduce diagnostic costs. This is the focus of subsequent chapters in this dissertation.

Sensitive - It is preferred that the diagnostic system and assay be not only capable of detecting low analyte concentrations but that the system can reliably provide clinically useful diagnostic information. The number of false negatives should be minimal.

Specific - The system should be able to reliably identify the target analyte with minimal false positives due to interferants.

User-friendly - Should be easily operated by a minimally trained worker and must be operated in a few steps

Rapid and robust - should provide same-day diagnosis, preferable a sample-to-answer time less than 30 min for timely clinical decisions, minimize hospital re-visits and poor follow-up that leads to complications. The system must function correctly under harsh environmental conditions, a shelf life of 6 months to 1 year at room temperature.

Equipment-free - Simple protocols and assay processes at the point-of-need, no cold chain storage/shipping required, minimal equipment (can be solar powered)

Deliverable to end users - Should be portable, hand-held, and easily transported to remote locations. The quality of healthcare delivery could be improved using modern technology such as Bluetooth, wireless communication, ubiquity of smart-phones, cloud-server connectivity to enable rapid and reliable diagnosis even when highly-skilled healthcare professionals are not on-site at the remote locations.

Another useful criterion for POC diagnostic devices is the Clinical Laboratory Improvement Amendments (CLIA) of 1998 Department of Health and Human Services (1998), that regulates all facilities that conduct testing on human specimens or devices created for home use for diagnosis, prevention, or disease treatment in the United States. As part of the requirements, low-risk tests could be waived but they must be simple to use, with instructions that are simple to follow, in order to minimize erroneous results.

2.11 Summary

In this chapter, a quick review of basic fluorescence, absorbance, and lateral flow immunoassays has been presented. Fluorescence detection enables higher sensitivity and a wider dynamic range for detection of analytes. However, there are significant challenges in developing high-performance fluorescence-based assay platforms for resource-limited settings. Having covered the background information with a lit-

erature review on fluorescence-based lateral flow immunoassays presented, the rest of this dissertation will focus on addressing the hypotheses put forth in Chapter 1, with a view to tackling most of the challenges highlighted in this chapter.

Chapter 3

OPTICAL DESIGN, MODELING, AND CHARACTERIZATION OF A HIGHLY SENSITIVE FLUORESCENCE DETECTION SYSTEM FOR POINT-OF-CARE APPLICATIONS

3.1 Introduction

Fluorescence detection is a well-established analytical technique, proven to be an effective method for chemical and biochemical sensing applications Guilbault (1990); Lakowicz (2006). Fluorescence detection offer several attractive attributes including increased sensitivity, specificity, and a wide dynamic range Guilbault (1990); Yetisen *et al.* (2013a). Filter-based fluorescence detection in particular, continues to be investigated and commercialized. This chapter presents the optical design, modeling, and architecture of an inexpensive detection platform suitable for fluorescence applications across the ultraviolet and visible (UV-VIS) spectrum. The system is intended for use with a Lateral Flow Immunoassay (LFIA) Wild (2005) that is field-deployable in resource-limited settings and will be applied towards disease diagnosis in a portable microfluidic point-of-care (POC) format.

Additionally, the performance characterization of the developed fluorescence detection system is reported. The detection device leverages time integration to improve the signal-to-noise ratio (SNR) compared to an instantaneous measurement and does not use complicated focusing optics and electronics typically found in bulky and expensive laboratory-scale devices. The system was characterized by measuring the fluorescence (voltage-time) response to a logarithmically scaled dilution series of 1 μm Nile red fluorescent microspheres immobilized on microscope slides. This approach

eliminates assay dependencies and elucidates the actual system performance.

Optimizing fluorescence systems and fluorophores requires a detailed model and estimation of the system response based on the specific individual components of the system. This goes a step beyond the visual spectra viewers used for a rough inspection of fluorophores, sources, and filters, offered by commercial fluorophore vendors. A few of such online spectra viewers include: Fluorescence SpectraViewer^{TM} by ThermoFisher Scientific ThermoFisher Scientific (2018), Spectra Viewer^{TM} by Novus Biologicals Novus Biologicals (2018), and Curvomatic by Omega Optical. There is a need to not only inspect the fluorophore characteristics independently, but that the composite choice of fluorophore, filters, sources, detector, housing, the sample matrix will determine the system performance. The degree of matching between optical components is a viable tool or metric for predicting the performance of low-cost fluorescence detection systems.

In this chapter, a theoretical model that predicts the time-integrated output voltage profile of a inexpensive and highly sensitive fluorescence sensor is presented. Such a prediction is useful for evaluating any lens-free fluorescent system based on a set of filters, fluorophores, excitation source LED, and photodiode detector. By relating the fluorophore concentration, system design parameters and the output voltage, the model matches well with the empirical data. The limit of detection (LOD) for 1 μm diameter Nile red microspheres is estimated as $\sim$ 20-200 microspheres on a microscope glass slide solid support. This system provides a sensitive and potentially low-cost device for fluorescent diagnosis in an integrated and compact/miniaturized POC device, lab-on-chip device or a portable reader. Finally, this chapter also details the application of the proposed detection technique for the detection of fluorescent labels in the near ultraviolet (UV), visible (VIS), and near infrared (NIR)/red regions of the electromagnetic spectrum.

3.2 Optomechanical and Optoelectronic Assembly

The fluorescence detector reported in this chapter achieves high sensitivity by trading time for accuracy using a photodiode-based integrator/capacitive transimpedance amplifier (CTIA) and high-quality interference filters. While the CTIA and interference filters do not represent new technologies themselves, the application is novel and the system exploits a simple and elegant detection technique. It takes advantage of a time-integrated readout which averages out the noise, in comparison to an instantaneous measurement. The system draws on inspiration from standard fluorescence detection systems (discussed in Chapter 2), with significant trade-off targeted towards cost-reduction, robustness, and size while striving to maintain performance. Light emitting diodes (LEDs) are used as the excitation source as opposed to laser sources, flash lamps, etc; focusing and transfer optics are eliminated with the exception of interference filters, adopting a "sandwiched" transillumination architecture with separation distances between source-sample and sample-detection on the order of a few millimeters; charge coupled device (CCD), complementary metal oxide semiconductor (CMOS) camera, or photomultiplier tube (PMT) are replaced with a photodiode (PD). Fluorescent recognition samples are excited by LEDs and the emissions are detected with photodiodes connected in a transimpedance amplifier configuration. The current generated is converted to a concentration-dependent output voltage yielding a quantitative readout in a voltage-time space. The resulting system assembly is shown in Figure 6.

The schematic configuration of the interference filter-based fluorescent detection system shown in figure 6 forms the basis for the detection platform analyzed in this chapter. Modifications to the optoelectronic and optomechanical design are presented in subsequent chapters.

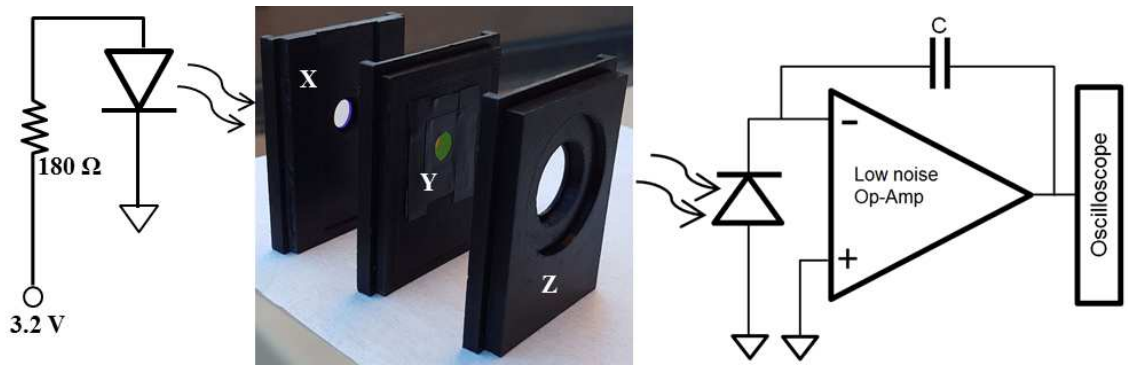

Figure 6: Schematic of Experimental Setup Showing (a) Green LED Excitation Source With 180 Ω Current Limiting Resistor; (b) 3D Printed ABS Opaque Assembly, Housing Green Excitation Filters and Microscope Slide (X), Orange Emission Filter (Y) and Photodiode and Integrator Aperture (Z); (c) Charge Integration Amplifier Circuit ($C = 100$ pF). The Output Voltage of the Capacitive Transimpedance Amplifier (CTIA)/Charge Integrator Circuit is Monitored Using an Oscilloscope.

3.3 Optical Design and Analysis

Modeling the response of the fluorescence detection platform is important in the design process and is useful in excitation source, fluorophore, filter, and detector selection, to determine the optoelectronic performance of the system *a priori*. Such a model is also useful in optimizing performance and predicting the sensor's response when modifications or desired outcomes are conceived. Figure 7, shows the normalized intensity and transmission spectra for the optical assembly of the system including: excitation source (LED) spectrum, excitation and emission spectra of the dye (Nile red microspheres), and the transmission spectra for the emission and excitation filters and photodiode responsivity.

A good model should take into account the above mentioned parameters as well as the influence of system factors including geometric effects, background fluorescence, and other noise contributions. The system design and model analysis detailed here

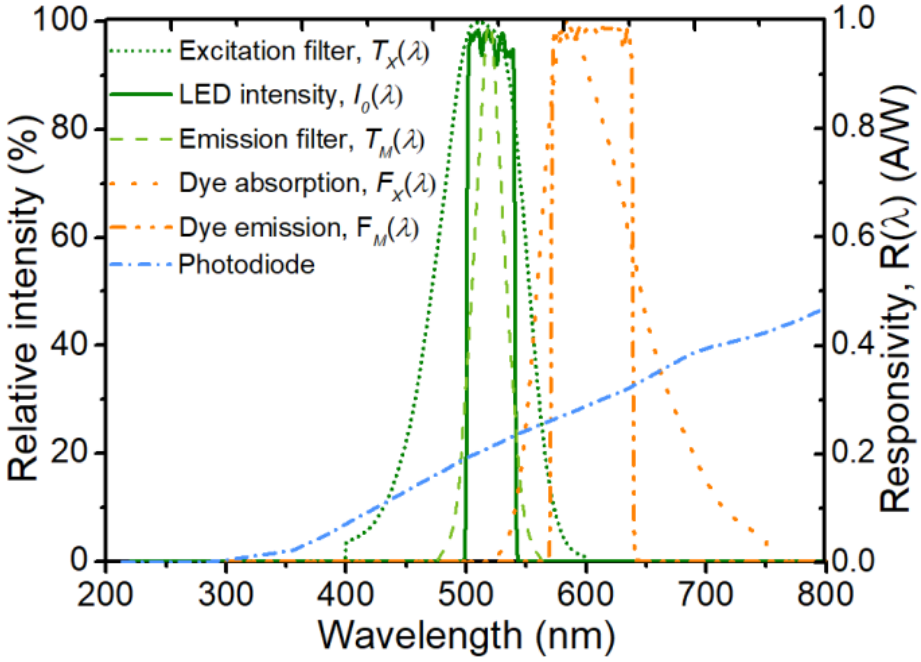

Figure 7: LED Electroluminescence (E.L.) Intensity, Fluorophore/dye Emission and Excitation Spectra, Excitation and Emission Filter Transmission, and Photodiode Responsivity (Secondary Axis). The Filters Were Chosen to Match the Excitation Light Source, Peak of the Excitation and Emission Spectrum of the Fluorophore, the Fluorophore was Chosen to Match the LED Peak Emission.

takes into account the influence of the system factors and parameters like excitation source spectrum and intensity, fluorophore properties, geometry, filter transmission and photodiode responsivity. Herein, a theoretical model that predicts the output voltage of the system as a function of time is discussed.

3.3.1 Light Emitting Diode (LED) Characteristics

The optical power emitted or external quantum efficiency of an LED can be expressed as Sze (2007):

$$\eta_{LED} = \frac{n_p h\upsilon}{nqV}, \tag{3.1}$$

where, n_p, is the number of photons emitted externally; $h\upsilon$, is the photon energy; n, is the number of carriers passing the junction; q, is the elementary charge; and V is the applied voltage bias. The LED intensity ($W/Area$) or brightness must be sufficient to generate an excited state in the fluorophores. LEDs used in this work have luminous intensity >1000 mcd. The specific fabrication techniques, material selection, and characterization of LEDs is presented elsewhere Sze (2007). Multicolor LEDs are now available across the UV-VIS spectrum providing a low-cost excitation source or illumination source for several application. A shift in excitation wavelength away from the absorption or excitation maxima yields a corresponding decrease in emission intensity Lakowicz (2006); Life Technologies (2010). Also, at a fixed wavelength, the emission intensity decreases with excitation intensity.

3.3.2 Photodetector/Photodiode Response

The current output of the detector (primary photocurrent), I_{PD}, is proportional to the fluorescence power/intensity reaching the photodiode, (P_D), (generating electron-hole pairs) Sze (2007) and is given by:

$$I_{PD} = q\left(\eta\frac{P_D}{h\upsilon}\right) = R(\lambda)P_D, \tag{3.2}$$

where, η, is the photodiode quantum efficiency which is the ratio of the number of electrons output by the photodiode to the number of photons incident; $R(\lambda)$, is the wavelength dependent photodiode responsivity which is the ratio of the current generated by the photodiode to the power incident on the photodiode in Amperes/Watt (A/W). The current generated in the a photodiode increases with area, but so does

the dark current and capacitance. Photodiodes could be tuned to maximize response for a specific wavelength.

3.3.3 Bandpass Filter Transfer Characteristics

The fluorescence power, P_{DF}, that gets transmitted through the filters is determined by the emission filter transmission/transfer function and the fluorophore emission spectra $E(\lambda)$ Thrush (2004):

$$P_{DF} = \frac{\int T_X(\lambda) T_M(\lambda) E(\lambda) d\lambda}{E(\lambda) d\lambda}, \tag{3.3}$$

where, $T_X(\lambda)$ and $T_M(\lambda)$, are the excitation and emission filter transmission respectively, which determines how many fluorophore emission photons are passed and excitation light rejected. Ideally, the emission filter has a 100% transmission at the emission wavelength of the fluorophore. Additionally, an ideal filter should have a vertical edge transition with zero edge width and zero transmission in the stop bands and a ripple-free pass band. These characteristics are not obtainable in practice and there is therefore some trade-off with filter selection.

3.3.4 Fluorescence Intensity and Light Generated Current

From Beer-Lambert law, the current output of the photodiode detector I_{PD}, is proportional to the fluorescence intensity reaching the photodiode Guilbault (1990); Lakowicz (2006); Banerjee *et al.* (2010a); Dandin *et al.* (2007); Sze (2007); Life Technologies (2010); Thrush (2004). The photodiode current due to fluorescence emissions could thus be written as:

$$I_{PD} = R(\lambda) \eta_{LCE} T_X(\lambda) T_M(\lambda) QY(\lambda) I_0 [1 - exp(-\epsilon(\lambda) lc)], \tag{3.4}$$

So that we can write,

$$I_{PD} = KI_0(\lambda)[1 - exp(-\epsilon(\lambda)lc)], \tag{3.5}$$

and,

$$K = R(\lambda)\eta_{LCE}T_X(\lambda)T_M(\lambda)QY(\lambda), \tag{3.6}$$

where, ϵ is the extinction coefficient or molar absorptivity of the fluorophore; c, is the molar concentration; l, is the path length through the sample; I_0, is the excitation source intensity (which is proportional to the current generated by the photodiode); K, is a proportionality constant that depends on the photodiode responsivity, collection efficiency of the system, filter transmission, and fluorophore quantum yield (QY). The components of K was used as a fitting parameter in our model. The wavelength dependent extinction coefficient ϵ is obtained by measuring the absorption spectrum of the fluorophore of known concentrations in a cuvette, from which ϵ can be calculated across the scanned wavelength. For the narrow bandpass application described here, ϵ can be assumed constant. Hence the ϵ at absorption maximum was used.

In practice however, it is worth noting that the total current measured includes the fluorescence signal and other noise sources. There is a non-zero background current detected in the device even in the absence of a fluorophore. This background current is mostly due to the photodiode dark current, I_{dark}; leakage light, I_{leak} reaching the detector from the excitation source Banerjee *et al.* (2010a); background fluorescence of optomechanical parts and system housing, optical effects from glass/solid-support/microfluidics as well as reagents used in sample preparation, I_{noise}. Excitation source light reaching the photodiode is a result of imperfection in filters Dandin *et al.* (2007). The dark current is independent of the excitation source Sze (2007) and is estimated to be a few pA.

Therefore, the total current generated by the photodiode is more accurately writ-

ten as:

$$I = I_{PD} + I_B, \tag{3.7}$$

where, I_B is the total background current:

$$I_B = I_{dark} + I_{leak} + I_{noise}. \tag{3.8}$$

The current generated by the photodiode is then input to the inverting terminal of the op-amp. The output voltage of the charge-integrator circuit is given as:

$$V_{out} = \frac{1}{C}\int_0^T Idt, \tag{3.9}$$

where C, is the feedback capacitance and T is the maximum integration time which ranges from 30 to 60 s. Equation 3.9 could be re-written to give an expression for the fluorophore-concentration-dependent output voltage of the op-amp based integrator circuit. Hence, the output voltage could be expressed as:

$$V_{out} = \frac{1}{C}\int_0^T [R(\lambda)\eta_{LCE}T_X(\lambda)T_M(\lambda)QY_(\lambda)I_0((1 - exp(-\epsilon lc)) + I_B]dt \tag{3.10}$$

$$V_{out} = \frac{1}{C}\int_0^T [KI_0((1 - exp(-\epsilon lc)) + I_B]dt \tag{3.11}$$

Equation 3.11 completely describes the detector output voltage as a function of system parameters, photodiode output current and time. This equation is useful in predicting the output voltage profile over time and for determining system performance during the design stage. As discussed below in Section 3.5.2, a script written in MATLAB was used to implement Equation 3.11. The MATLAB calculation results were compared to empirical results and detailed below.

3.4 Experimental Procedure

A 2 mm^2 green LED was used as the excitation light source, peak emission λ = 520/35 nm (SunLED, XZM2DG45S). The LED is operated at 3.2 V with a forward current of 17 mA using a 180 Ω limiting resistor as shown in Figure 6. The broadband spectrum of the LED is filtered by a 520/40 nm excitation filter (Chroma Technology Corp., ID IN048394, lot no. 283392, Bellows Falls, VT, USA). Nile red fluorescent microspheres (product no. F-8819, lot no. 1154194 specified absorption/emission wavelength 535/575 nm, molar absorption coefficient, ϵ, 37859 M^{-1} cm^{-1}, relative quantum yield, QY_{fl}, 0.19, purchased from Life Technologies, CA, USA). The microspheres were diluted in 1X phosphate buffered saline (PBS), immobilized and dried on microscope slides (VWR Microscope slides, 76 mm x 26 mm x 1 mm) by pipetting 2 μL five times to obtain a total volume of 10 μL, by drying between each pipetting steps. The logarithmic dilution series ranged from 1:10 to 1:100,000,000 for the Nile red microspheres. A representative image of the reference and test spots is shown in Figure 8.

A 605 nm/70 nm Chroma filter (ID IN048400, lot no. 283395) was combined with a Lee 105 orange gel filter and used as the emission filter to further reduce leakage light reaching the detector. The capacitive transimpedance amplifier (CTIA) comprises

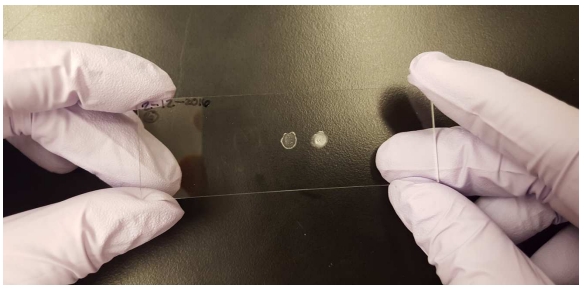

Figure 8: Representative Image of 10 μL 1X PBS Reference Spot (Left) and 10 μL Nile Red (Undiluted) Test Spot (Right).

an op-amp used to detect the fluorophore emissions. The op-amp (LMC6041IN, National Semiconductor) fitted with a photodiode (PDB-C139, responsivity, R(λ) of $\sim$0.2 to 0.3 A/W from 550 to 650 nm and a 59° viewing angle, was purchased from Advanced Photonix Incorporated, Camarillo, CA, USA). The short-circuit current for the photodiode is 67 μA. The amplifier and LED circuit was powered by a 9 V battery supply and a 3.2 V regulated supply, respectively. A digital oscilloscope (Tektronix TDS 2004B, 60 GS/s) was used to monitor and record the integrated output voltage from the sensor. The output signal was measured and allowed to ramp until the signal output railed at the power supply voltage. Table 3 shows an estimation of the number of microspheres in the dilution series. Furthermore, for a fixed sample volume, the ability to distinguish between lower concentrations is dependent on the number of fluorophores present; this number decreases with volume and dilution.

3.5 Results and Discussion

3.5.1 Fluorophore Concentration Measurement and Analysis

A representative plot of the system voltage output as a function of time is shown in Figure 9. A high concentration corresponds to a steepest slope and a shorter time-to-rail (TTR) compared to lower concentrations with lower slope and thus a longer TTR. However, the TTR metric was not correlated with detected fluorophore concentration; instead, the ramp-time (RT) which was chosen as the time difference (Δt) from 1 to 8 V as shown in Figure 9. The RT is used to minimize the effect of small voltage (millivolt) variations in the battery supply over several measurements as well as up to 2 second variations in manually turning on the detector at the start of the measurement. While the RT is inversely correlated with concentration, the detection time is directly correlated with concentration. We define the detection time as the

Table 3: Estimated Number of Microspheres in 10 μL of Fluorophore Pipetted on a Glass Slides. 50 μL of Fluorophore was First Diluted in 500 μL of 1X PBS and Subsequent Dilutions Made Serially. The Stock Concentration is 3.6 x 10^{10} Microspheres/mL.

S/N	Dilution	Microspheres in 550 μL	Microspheres in 100 μL	Microspheres in 10 μL
1	1:1	36,000,000,000	3,600,000,000	360,000,000
2	1:10	1,800,000,000	327,000,000	32,700,000
3	1:100	164,000,000	29,800,000	2,980,000
4	1:1,000	14,900,000	2,704,733	270,473
5	1:10,000	1,352,367	245,885	24,588
6	1:100,000	122,942	22,353	2,235
7	1:1,000,000	11,177	2,032	203
8	1:10,000,000	1,016	185	18
9	1:100,000,000	92	17	2
10	1:1,000,000,000	8	2	<1
11	1:10,000,000,000	<1	<1	<1

difference between the RT for a pipetted dilution compared to a reference. Extracting the difference in this manner eliminates errors due to slight optical variations in blank microscope slides as well as background due to PBS. The system output as a function of Nile red fluorophore concentration was measured and the result shown in Figure 10. The total background noise (dark current and leakage current) is lumped in the measurement with a blank slide with PBS.

To evaluate the system response to a titration of fluorophores, a test and reference spot was defined on a blank microscope slide (5 mm diameter and 9 mm pitch). The Nile red microspheres were immobilized on the first spot while 10 μL of 1X PBS immobilized on a second spot on each blank slide. The PBS spot was used as a control/reference. The measured output signal (with a reference slide inserted in the detection chamber) composed of several components and is broadly regarded as a background signal. This is the system output when no fluorophore is present. The greatest contribution to the background signal is the leakage of excitation light (off-axis) reaching the photodiode due to imperfection in the filters. Also, the dark current of the photodiode (current signal measured with the photodiode in the dark) is a function of the photodiode design, material properties, composition, and tempera-

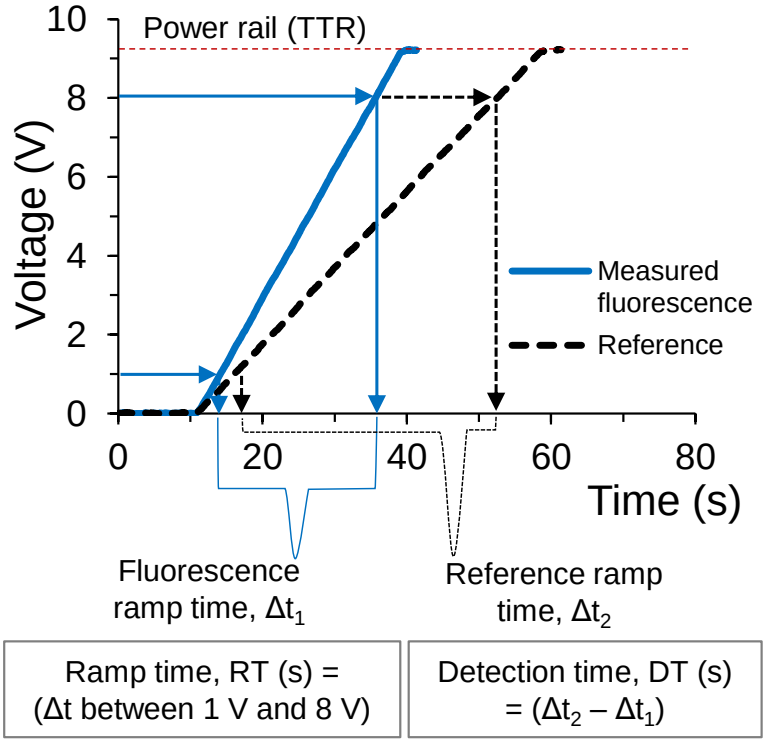

Figure 9: System Output Voltage of Nile Red Microspheres Integrated Over Time. A Steeper Slope is Indicative of a Higher Concentration and Hence a Shorter Δt.

ture. Other contributing optical effects could include scattering, reflection, refraction, diffraction, leakage through interfaces of the walls of the 3D printed structure and, ambient light leakage through the external housing. The device was well encapsulated and rigidly fixed, minimizing stray slight and ensuring repeatability. We estimated the the LOD to be between 20 - 200 Nile red microspheres with a diameter of 1 μm from Figure 10. Error due to pipetting is ± 1 s and variations in readout electronics are less than a second as estimated from repeated runs and indicated by the standard deviation, σ (ms). At lower concentrations, although it becomes increasingly difficult to quantitatively discriminate the system response, the response is in agreement with Beer-Lambert Law which could be approximated as a linear equation in a Taylor series expansion at moderately low concentrations Bruus (2008); Pais *et al.* (2008a). The transparency of glass as a solid support material leads to a high performance in the spot test described above. However, these result are dependent on the solid support used. Further analysis on solid support effects is presented in Chapters 5, 6, and 7. The Nile red microspheres were observed to be very stable with no significant bleaching even at higher light intensity Finger *et al.* (2009) and as observed over repeated measurements of the same sample under test.

3.5.2 Theoretical Model Predictions and LOD

The Beer-Lambert Law and Equation 3.11 were used to develop a predictive model for the output voltage profile for Nile red microspheres. Equation 3.11 was applied to obtain the output voltage profile as a function of concentration and compared to the empirical data. A MATLAB script was developed to generate the system output voltage as a function of time from which the RT shown in Figure 11 was calculated. The measured and calculated responses show an inherent nonlinear response. The lumped constant K was used as a fitting parameter. For the Nile red microspheres

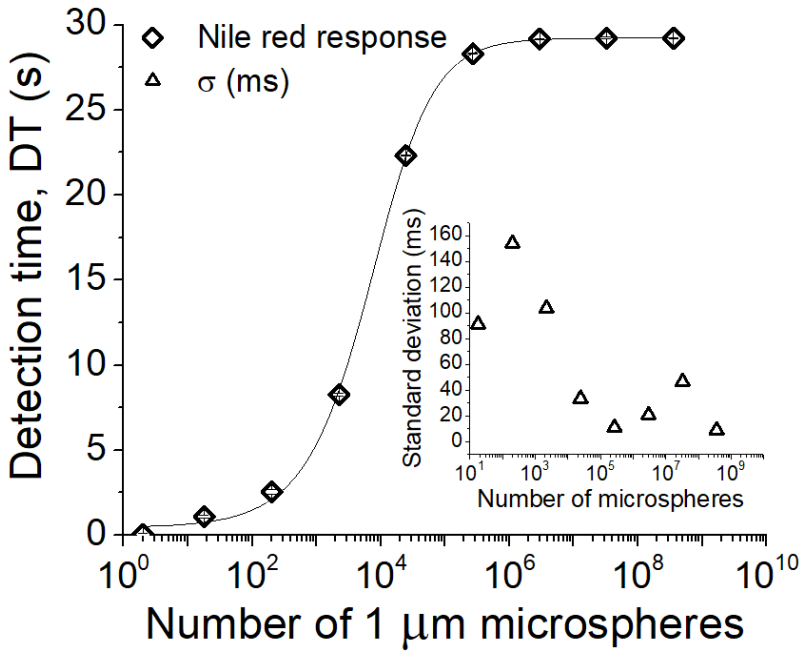

Figure 10: Detection Time for Nile Red Microspheres Extracted From the Voltage-time Output Profile. Detection Time is Shown as a Function of Number of Microspheres in 1X PBS. The Inset Shows the Standard Deviation in ms for N=5 at Each Concentration. Errors Due to Pipetting are Estimated to be ±1 s.

(relative $QY_{fl} = 0.19$, $\epsilon = 37859\ M^{-1}\ cm^{-1}$), $l = 50\text{x}10^{-4}$ cm, $I_B = 4.804\text{x}10^{-12}$ A, KI_0 ((A/W)*W) = 150 A , $C = 100$ pF.

$$V_{out} = 2.68 \times 10^{12}[1 - exp(-189.29c)] + 0.0445t \tag{3.12}$$

The goal is to maximize K, and minimize I_B, for example, by using effective optomechanical designs with apertures to increase the collection efficiency of the system, and minimize or eliminate ambient light and stray (off-axis) light within the system.

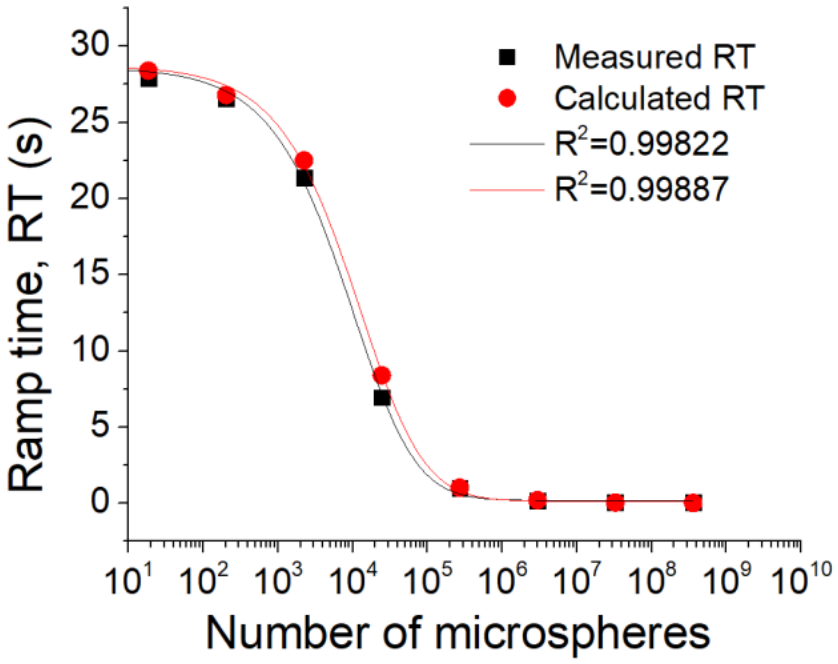

Figure 11: Ramp-Time (RT) as a Function Nile Red Fluorophore Concentration, Showing Agreement Between Empirical (Squares) and Calculated (Circles) Values. The Model Agrees Well With the Measured Data.

3.5.3 Multi-spectral Applications

This section presents the application of the developed fluorescence platform for the detection of red wavelength fluorophores (Alexa Fluor 647) and UV-excite labels - europium (III) chelate and Qdot. To evaluate the performance of the interference-based charge-integration configuration at different wavelength ranges, we obtained long wavelength premium filters (excitation filter: 635QM30, XF1419, ; emission filter: 710QM80, XF3414, Omega Optical, USA) and UV and long wavelength bandpass filters (ZET365/20x nm and emission filter: 605/70 nm, Chroma Technology Corp., USA). Red excite fluorophore (Alexa Fluor 647, 651/672 nm, 270,000 $M^{-1}cm^{-1}$, Cat. No. A20006, ThermoFisher Scientific, CA, USA), Europium luminescent microspheres (0.2 μm, 365/610 nm, decay $>$ 500 μs, 0.5% solids Eu^{3+} Cat. No. F20881,

Molecular Probes Inc., OR, USA), and Qdot (0.2 μm, 605 nm, 73% quantum yield, Cat. No. Q11201MP, Molecular Probes Inc., OR, USA). In addition and following the techniques used to develop the green-excite system reported previously in this chapter, two reader systems were configured for UV and red-excite, respectively, using commercially available premium filters. The optoelectronic characteristics of both systems is illustrated in Figure 12 (a), (c), and (e). UV LED (LTPL-C034UVH365, 365 nm center, 500 mA, 3.8 V, 665 mW radiant power, Mouser Electronic, USA) and Red LED (LTPL-C034UVH365, 624 nm center, 50 mA, 2.1 V, 700 mcd luminous intensity, Mouser Electronic, USA) was used as the excitation source in the UV-excite and red-excite systems, respectively. Figure 12 depicts the excitation, emission, spectra, and photodiode responsivity (PDB-C139) on the secondary axis of (a), (c), and (e). A logarithmic dilution series was prepared, spotted as described in Section 3.4, however on nitrocellulose membranes (N=3) rather than glass microscope slides. The optoelectronic configuration for the red excite system and the fluorescence response to a logarithmic dilution series of the Alexa Fluor 647 dye is shown in the Figure 12 (e) and (f). The optoelectronic configuration for the wide Stokes shift (Europium and Qdot) UV excite system and the fluorescence response to a logarithmic dilution series of the Qdot and EU^{3+} is shown in the Figure 12 (a) - (d). one advantage of the UV-excite fluorophores is the wide separation of the excitation peak ($\sim$365 nm) from the emission peak ($\sim$610 nm), allowing for better selectivity of the emitted fluorescence using appropriate filter combinations. Figure 12 (b), (d), and (e) shows the fluorescence response as a function of concentration for the Qdot, Europium and Alexa Fluor 647 dyes respectively. (d) also shows the fluorescence response from a typical green-excite fluorophore (F1-Y050, Merck, France) used in this dissertation and plotted for comparison.

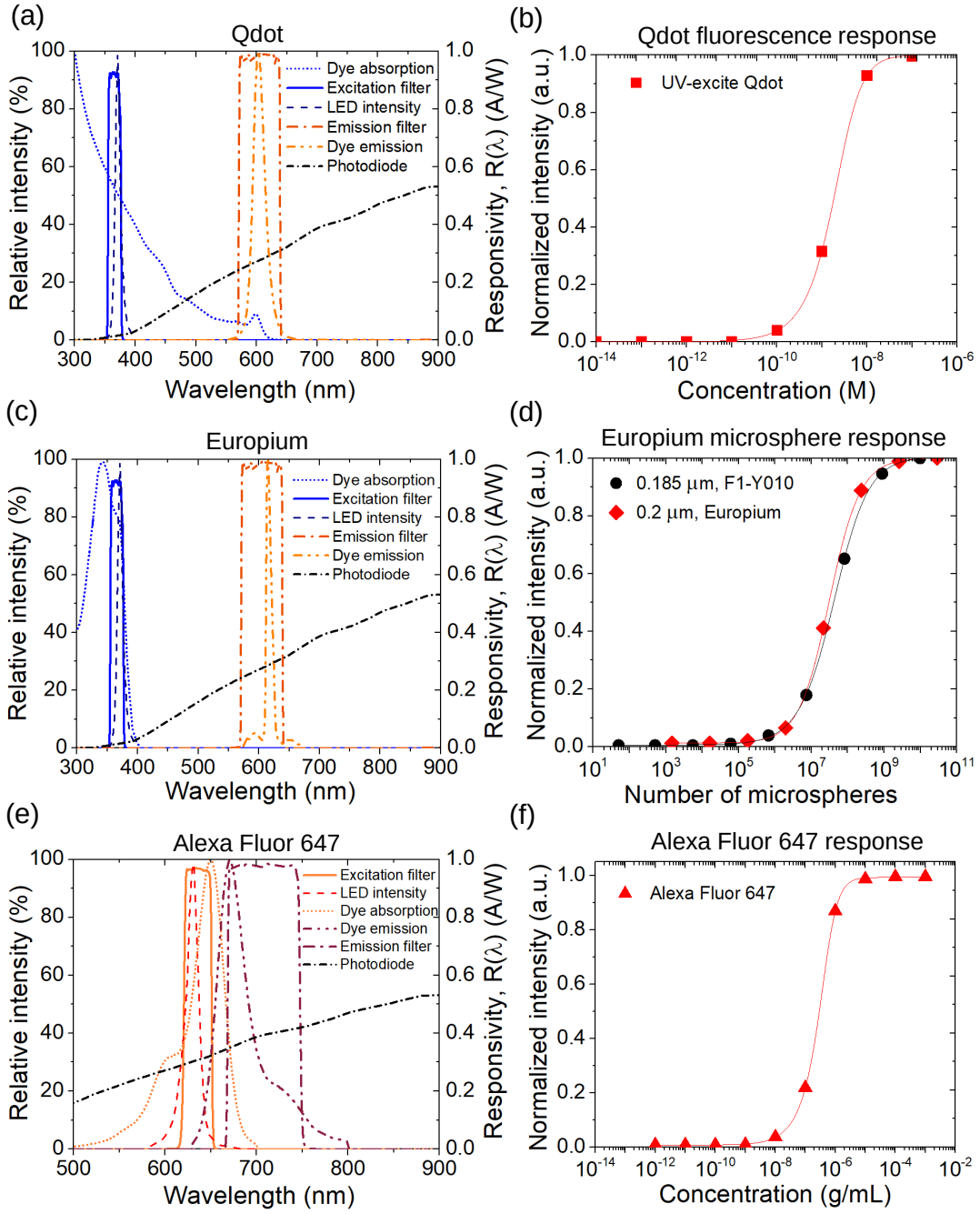

Figure 12: Application of Interference Filter-based Low-cost Fluorescence Detection System Across the Ultraviolet and Visible Spectrum. (a) UV-excite System with Qdot Labels (b) Qdot Response (c) UV-excite System With Europium Microspheres (d) Europium Response Compared to Green-excite Microspheres. (e) Red-excite System with Alexa Fluor 647 (f) Alexa Fluor 647 Response.

It has been widely reported that autofluorescence (intrinsic fluorescence) of many materials decreases with increasing wavelength excitation, and is maximum in the blue and near UV regions. Assuming all other conditions are constant (equivalent filter performance, equal efficiency of excitation, fluorophore quantum yield, stability, neutral density absorption, etc.), comparing a green excite to red excite wavelength system, one may get at most an order of magnitude improvement in overall system performance. This perceived improvement may be masked and other system factors such as filter performance, fluorophore flow in a nitrocellulose membrane, non-specific binding (NSB), light absorption in solid support, etc.

It is worth noting that the human eye is not sensitive to light at wavelengths beyond 650 nm, so that the emission of the Alexa Fluor 647 dye cannot be inspected under a typical epi-fluorescence microscope. Additionally, extra precaution should be taken with respect to safety in low-cost fluorescence detection development involving the use of high power UV light emitting diodes.

3.6 Conclusion

The design, fabrication, modeling and characterization of a very sensitive and compact fluorescence detector for POC applications was presented. A LOD of ∼200 microspheres with 1 μm diameter has been demonstrated with samples spotted on a microscope slide. The work gives insight into how the system could be optimized. The spot test used to characterize the systems developed in this chapter are useful to verify functionality during development and benchmark performance against central laboratory instruments ignoring assay dependencies. The reported characterization technique is also useful in lateral flow assay development (Chapter 7) to determine the optimal label concentration that can be infused into a lateral flow strip, providing enough label reagents for the test without causing significant non-specific binding

which limits SNR. This chapter also presented a theoretical predictive model based on system design parameters that determine the sensitivity and LOD. The optoelectronic model uses fluorophore characteristics, filter transmission, collection efficiency and photodiode response to predict the output voltage of a charge integration amplifier-based fluorescence detection systems. The output voltage profile of the model matches the empirical data, thus validating our model. This low-cost detector setup has potential applications in integrated microfluidic lab-on-chip, miniaturized POC and over-the-counter (OTC) diagnostic test strip readout. The application of the proposed low-cost fluorescence detection technology for labels across the UV, VIS, and NIR regions of the electromagnetic spectrum has also been demonstrated. The platform was adapted to different wavelength ranges by substituting the excitation source (LED) and interference filters, to match the fluorophore under test.

Chapter 4

LOW-COST FLUORESCENCE-BASED BIORECOGNITION USING ORGANIC LIGHT EMITTING DIODES

4.1 Introduction

4.1.1 Application of Flexible Displays for Biochemical Analysis

The basic unit of organic flat panel/flexible displays is the organic light emitting diode (OLED), a single pixel. Compared to inorganic light emitting diodes (ILED), OLEDs have physical and optoelectronic characteristics that make them suitable for sensor design. Typically, ILEDs are fabricated from III-V semiconductor materials, which are not easily deposited over large areas. Notably, the feasibility of fabricating OLEDs on different substrates (glass, plastic, polyimide, metal, etc.) has led to several applications. Particularly, the fabrication of flexible displays is enabled by the unique properties of the organic materials used, in that their conformal characteristics allow for deposition on flexible substrates over a large area. Flexible display technology has opened numerous avenues for miniaturization and integration of technologies for biochemical analysis. Microarrays, which are on the order of the size of a pixel could deliver high throughput analysis for biological and chemical applications. The attractive characteristic of OLEDs including lower production cost, also make them suitable for POC applications, especially for resource-poor settings. Owing to their flexibility, emission properties, ultra-thin profile (<1 μm excluding substrate), light weight, transparency, full color capabilities, and cost-effective fabrication (large area, solution processed, Pierre and Arias (2016); Shu *et al.* (2017) or roll-to-roll manufacturing on polyethylene terephthalate (PET) films Crawford (2005)), OLEDs

have proven to be the material of choice for flexible flat panel display technology and increasingly used in sensor development Nikam *et al.* (2012); Deshpande *et al.* (2017).

4.1.2 Organic Light Emitting Diodes and Organic Photodiodes as Optical Excitation Sources and Detectors

Optical transduction systems typically require an excitation light source that probes a sample in order to measure a concentration dependent parameter, e.g., absorbance, reflection, transmission, or light emissions from a fluorescent dye. A photodetector is used to convert the concentration dependent optical parameter to an electric current, which can be amplified, processed, analyzed, and displayed. Standard light sources (including xenon, mercury, lasers) are not easily integrated with miniaturized sensors or at best lead to bulky analytical instruments. Although the inorganic light emitting and laser diodes are gradually becoming the dominant light source for many analytical applications Yeh *et al.* (2017); Bui and Hauser (2015), OLEDs are viable excitation sources for optical detection systems Williams *et al.* (2014); Liu *et al.* (2011); Smith *et al.* (2016b). With advances in technology, significant progress has been made toward manufacturing OLEDs with sufficient brightness and stability necessary to function as excitation sources especially in disposable POC sensors. From a practical standpoint, OLEDs could be operated at low voltages (5V) or at higher voltages in pulsed-mode to obtain higher brightness while maintaining stability. OLEDs also have a wide viewing angle (suitable for bending and folding applications) with devices fabricated across the visible range (red, green and blue emitters) combined with active matrix (TFT technology) making a crisp, full color display. Figure 13 shows normalized electroluminescence spectra for blue, green, and red OLEDs manufactured at the Flexible Electronics and Display Center (FEDC) at Arizona State University (ASU). These can be used to excite fluorophores or measure

absorption across a broad spectrum of applications. Furthermore, UV and IR OLEDs have also been reported Krujatz *et al.* (2016).

One of the challenges associated with miniaturizing central laboratory optical detection devices is the form factor and geometries of various components used in their design, including standard photodetectors such as photomultiplier tubes (PMT), avalanche photodiodes (APD), charge-coupled device (CCD), or complementary metal oxide semiconductor (CMOS) detectors. Inorganic photodiodes based on Si have been used extensively as photodetectors in many applications. However, organic photodiodes (OPD) are relatively easily fabricated with processes that are compatible with organic flat panel display fabrication, enhancing the ease with which miniaturized and compact devices could be fabricated Manna *et al.* (2015). Several integrated sensor configurations using OLEDs and OPDs have been studied Krujatz *et al.* (2016).

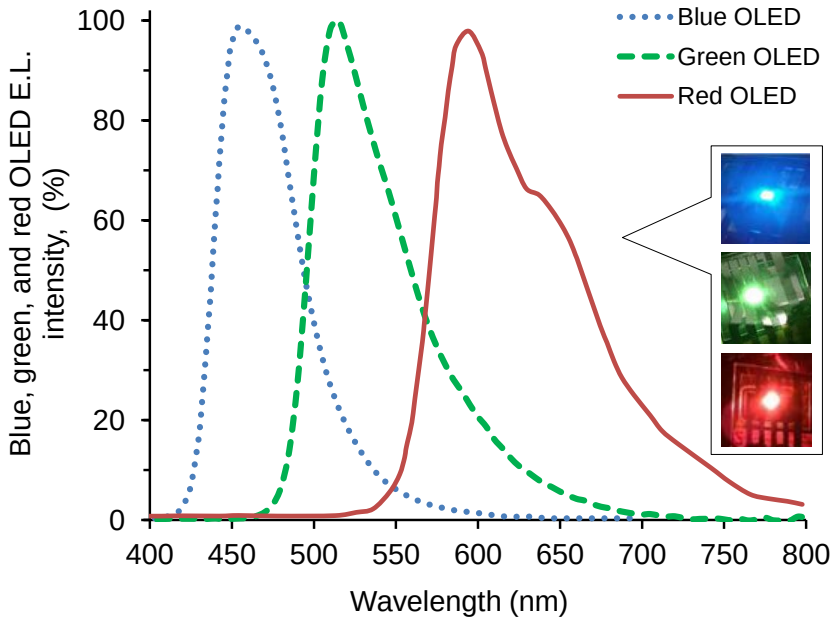

Figure 13: Emission Spectra of Blue, Green, and Red OLEDs Fabricated at the ASU Flexible Electronics and Display Center. Inset Shows Images of the OLEDs Under Operation.

It is easier to implement the "front detection" (transmission or transillumination) configuration, where the bio-affinity compound/sensing element/microfluidic channel is sandwiched between the OLED excitation source and a photodetector (PD). In the "back detection" (reflection/coplanar) configuration, the OLED and the PD are next to each other on the same plane. For example, in fluorescence applications, the OLED is patterned to allow detection of the emitted fluorescence through the spaces or over the entire backside in the case of transparent OLEDs. There are a few applications that are better suited to reflection and absorption configurations Venkatraman and Steckl (2015b); Prabowo *et al.* (2014). The configuration choice depends on the design.

An added advantage of using OLEDs and OPDs in place of traditional/standard sources and detectors is that the emission wavelength and responsivity of OLEDs and OPDs can be relatively easily tuned (mostly based on material selection), to maximize sensitivity at a particular wavelength. Furthermore, OLEDs and organic photodiodes (OPD) are ideal candidates for disposable applications due to their simple planar polymer microfabrication and low-cost. Additionally, in sensing applications, OLEDs are either operated in DC mode or in pulsed mode. With advances in signal processing and miniaturized integrated circuits, there is a realistic potential to take advantage of pulsed mode excitation for noise reduction, minimizing re-calibration and enhance dye stability in compact devices. A major challenge with optical detection systems, in general, is the need to suppress or minimize the excitation light intensity reaching the detector. This intensity increases (inverse square law) as the distance between the excitation source and detector decreases. In fluorescence applications, usually, the excitation light reaching the detector can be several orders of magnitude higher than the emitted fluorescence of interest Kraker *et al.* (2008). Technologies and techniques to minimize this effect are discussed in this dissertation. The broad electroluminescence

(EL) spectrum and tails of OLED sources are detrimental to the system sensitivity (spectral crosstalk). For applications requiring high sensitivity, a potent way to minimize this effect is the use of interference filters. Realizing miniaturized optoelectronic diagnostic devices for biological, environmental, drug, and food safety applications have generated a lot of interest over the years. This trend has been enabled by the vast research, development and significant progress in the area of flexible OLEDs and integrated LOC devices. Particularly, the detection of chemical and biologically relevant species has been the focus of several research groups Katchman *et al.* (2016c); Pais *et al.* (2008b); Venkatraman and Steckl (2015b); Williams *et al.* (2014); Shinar and Shinar (2008); Shu *et al.* (2017); Camou *et al.* (2003); Eeshita *et al.* (2015).

4.1.3 Device Integration

Integration of optical transduction systems with standard light sources and detectors is either not possible due to geometric constraints or logistically not feasible. Although inorganic LEDs (ILED) could be integrated with LOC or microfluidic channels, there are significant limitations in the array density and complexity of the design. For example, Cho et al., Cho and Bright (2001) physically machined $\sim$500 μm deep wells on the top of discrete ILEDs to create reaction wells into which recognition elements were immobilized for oxygen detection. This negates the benefit of large area surface emission, which is an attractive quality of flexible display technology. Perhaps for direct immobilization on an emitter surface, flat panel technology combined with microarray printing will not only yield a simpler process, but also a more robust and flexible configuration. Flexible display technology not only provides a path for direct integration of the sensing element as part of the fabrication process, but also the planar and relatively simple fabrication procedure allows for the integration of optical components (e.g. interference filters) and other technologies (LOC, microfluidics and

flexible electronics, e.g. organic thin film transistors OTFTs). Standard light sources are not easily integrated with sensing platforms due to form factor constraints or cost. Furthermore, the heat generated from most of these sources could damage the sensor or analyte of interest. Device integration for flexible display technology with LOC and microfluidic protein printing technologies does not have these limitations. Negligible joule heating of the sensing element and components occurs when OLEDs are used as an excitation source, even when the sensing element is in contact with the OLEDs Choudhury *et al.* (2004). Also advantageous is the fact that the planar and flexible form factor allows for patterning and assembly. Monolithic Tam *et al.* (2015), structural, or modular Koetse *et al.* (2008) integration of organic optoelectronics - OLEDs and OPD, with microfluidics, planar optics, and LOC is simple because of the planar and flexible configuration. The ease of fabrication and processing (low temperature, sequential/layer-by-layer deposition, solution processing, screen printing) makes it possible to develop organic optoelectronics on several substrates. The processing steps involved are suitable for mass production. Ultimately this leads to compact and miniaturized devices, making these technologies attractive for integrated systems. Integrated optical excitation sources, detectors, and sensing elements are useful for the development of miniaturized high throughput sensor arrays and for wearable applications.

4.2 Flexible Display Technology for Multi-analyte Sensor Array Platforms

4.2.1 Integrated Lab-on-a-chip and Flexible Display Devices

Central to the concept of LOC systems is the development of integrated micro-analytical platforms. The goal is to miniaturize central laboratory processes, reduce sample volume and processing time, at low manufacturing cost. This concept ulti-

mately yields disposable inexpensive tests, especially for POC diagnostic applications. Organic electronics are particularly suited for miniaturization since they are deposited on planar/flexible substrates at low temperature. Additionally, they can be patterned, and fabricated by processes that are compatible with mass manufacturing. The low-temperature processing of flexible displays enables fabrication of emissive devices on plastic, glass, fabrics, polyimide, and a host of other flexible substrates. Hence, organic optoelectronic devices could be integrated with microfluidics for LOC applications, especially for optical detection Hofmann *et al.* (2008); Pais *et al.* (2008b); Hofmann *et al.* (2005). Flexible organic optoelectronics can be deposited directly on polymers used in microfluidics (e.g PDMS) or on substrates that can easily be bonded directly to microfluidics and LOC devices Williams *et al.* (2014). The overall flexibility and robustness of organic display technology makes it suitable for integration with LOC devices for a wide array of applications in healthcare and medicine. Integration is enabled by advancement in research and commercialization of these respective technologies. For example, the pixel size in flexible display technology is on the order of the size of a typical microfluidic channel. Hence, there are significant benefits in applying the concepts and designs in microfluidics, LOC, and flexible display technology, toward the development of integrated devices. One such benefit is the development of multi-analyte sensors and multiplexed high-throughput analytical platforms, for applications in personal health monitoring, infectious disease, and vaccine screening.

4.2.2 Multiplexed Sensor Platforms

The inherent design and characteristics of flexible display technology (including OLEDs and TFTs) are suitable and meet the requirements for multiplex biomarker detection; a 2D array of pixels can be patterned and individually addressed, tar-

geting/probing different detection sites or a group of sites, for low sample volume and high throughput applications. This chapter explores the potential of combining high density protein microarray printing, developed at the Virginia G. Piper Center for Personalized Diagnostics (CPD), with flexible display technology developed at the Flexible Electronics and Display Center (FEDC), both at Arizona State University (ASU). The concept is that each element in the array consists of pitch-matched OLED-photodiode pairs in a sandwiched transmission-mode configuration, yielding a compact and highly sensitive device. This approach eliminates the need for transfer/focusing optics (lenses, fiber, beam splitters), motorized stages, or expensive low-light detectors and emitters. The goal is to achieve high sensitivity and low LOD using OLEDs as the excitation source to probe fluorescent markers for biochemical and diagnostic applications. An added benefit of a fluorescence-based assay is a clear path to developing a quantitative readout, which aids clinicians in making a diagnosis. Miniaturized fluorescence detection platforms using OLEDs for multiplexed detection of infectious diseases, is not yet commercially available. With heightened interest in this area by academia and industry, it is not hard to imagine that such devices may become available in the near future. There have been several efforts to develop multi-analyte sensors using OLEDs over the years. Notably, Shinar et al. reported extensively on the detection of oxygen and used the same principles in the development of an enzyme-based multi-analyte array (Cai *et al.* (2008); Shinar and Shinar (2008)) for detection of glucose, lactate, and ethanol by PL intensity quenching or decay time decrease of an oxygen sensitive dye.

4.3 Point-of-care Disease Diagnosis and Pathogen Detection Using Flexible Display Optoelectronics

Flexible OLED POC immunosensors are devices that incorporate a biological sensing element usually an antigen (Ag) or antibody(Ab), a detector agent (usually colorimetric or fluorescent), an OLED excitation source, a photodetector (photodiode), and readout electronics, converting the biological parameters of a sample to an interpretable output. Central laboratory techniques and biosensors that operate based on optical transduction mechanisms have become commonplace in disease diagnosis, vaccine screening, and drug treatment monitoring applications. Although there are other transduction mechanisms (electrochemical, mechanical, thermal, and electromagnetic), optical transduction offers a number of advantages which include: a wide electromagnetic spectral range, multiple measurement modalities (intensity, frequency, polarization, phase) Cunningham (1998), multianalyte arrays fabrication feasibility, and finally, high sensitivity and selectivity, e.g. fluorescence. Particularly, combining optical detection schemes with immunometric assays has been very successful at central laboratories yielding high sensitivity and low limit-of-detection (LOD) for most analytical procedures (e.g. the gold standard enzyme-linked immunosorbent assay, ELISA). Immunosensors take advantage of the high affinity and specificity of Ag-Ab interactions toward the detection of species in an analyte. Antibodies and Ags are also used as biomarkers required to make a clinical diagnosis. In some fluorescence applications, an Ab-conjugated fluorophore is used as the detector label, such that the fluorescence emissions (due to bound labels) is directly correlated to the concentration of the target species in a sample/analyte. Fluorescence has been widely used for several biological and chemical analytical procedures including: proteomic analysis, DNA sequencing, cell studies, environmental monitoring, and food and water analysis.

Some challenges associated with deploying central laboratory analytical tools at the POC include the high infrastructure and logistic cost, as well as the bulky form factor due to the expensive and complicated optoelectronic and automated optomechanical components required for high performance. Furthermore, very often these systems require frequent calibration and alignment of the optics. Miniaturization of laboratory scale platforms is a potent approach to improve patient access and reduce diagnostic cost. Flexible display emitters are particularly suited for deployment in systems that rely on optical detection. Many groups have reported attempts to integrate optical detection schemes with paper-based, and PDMS/PMMA/glass microfluidics, using OLEDs as the excitation source and inorganic or organic photodiodes (OPD) as detectors Pais *et al.* (2008b); Banerjee *et al.* (2010b); Krujatz *et al.* (2016); Katchman *et al.* (2016c); Venkatraman and Steckl (2015b, 2017); Marcello *et al.* (2013); Manzano *et al.* (2015); Hofmann *et al.* (2005); Ryu *et al.* (2011b); Lefèvre *et al.* (2015); Shu *et al.* (2017)

Early reports on integrated OLEDs for fluorescence sensing includes the work reported by Hofmann et al. in 2005 Hofmann *et al.* (2005). The authors reported the development of a disposable PDMS microchannel, integrated with a yellow OLED excitation source for the detection of urinary human serum albumin (HSA) as a marker for renal disease (microalbuminuria, MAU). The authors adopted a filter-less discrimination by using an orthogonal detection geometry, where the fluorescence emissions were captured using a fiber optic spectrometer, oriented orthogonally to the OLED excitation. Although this system demonstrated proof-of-concept toward a fully integrated device, the authors report an LOD of 10 mg/L and a linear range between 10 and 100 mg/L HSA. The linear range for the detection of HSA was clinically relevant (clinical cut-off levels: 15 - 10 mg/L). Later work by the same group Ryu *et al.* (2011b) reported an injection molded (polystyrene) 2-channel microfluidic LOC

fluorescence detection system for cardiac markers myoglobin and creatine kinase-muscle/brain (CK-MB). An LOD of 1.5 ng/mL for both myoglobin and CK-MB was reported using a combination of absorption filters, linear and reflective polarizers, an ILED (InGaN) as excitation source, and an OPD and Si PD as the detector.

Pais and Banergee et al., detailed the development of a disposable LOC device with integrated thin-film green OLED as an excitation source and an OPD as a detector for fluorescence detection Pais *et al.* (2008b). The system was designed with crossed polarizers. The excitation source was polarized with the first polarizer (polarizer 1) and the emitted fluorescence was collected through a second polarizer (polarizer 2) oriented perpendicularly to the first. The goal was to suppress the excitation source intensity reaching the detector. The authors reported that the crossed polarizer scheme reduced the excitation light leakage by 25 dB while reducing the fluorescence emission by approximately only 3 dB. Rhodamine 6G and fluorescein were used as model dyes to test the system and a LOD of 100 nM and 10 nM for rhodamine 6G and fluorescein, respectively. This represents one of the first reports that demonstrated the potential toward fully integrated monolithic LOC system comprising polarization filters, an OLED excitation source, and a detector using an organic photodiode excluding standard detectors (PMT, CCD, CMOS). By improving the design of the OPD (10x responsivity increase), the authors demonstrated an improvement from 100 nM to 1 nM for rhodamine 6G (although with the use of an AC lock-in amplifier detection setup to reduce the noise and therefore increase the SNR) Yun Shuai *et al.* (2008).

Sensor applications for early detection, however, require higher sensitivity and a lower LOD, especially for detecting markers that are minimally expressed. Hence, it is desirable that fluorescence detection devices perform at the level of clinical or central laboratory analytical devices to be useful for early detection at the POC.

Additionally, many platforms under development still rely on external sources of pressure (e.g. syringe pumps, pipettes) to drive the reagents/reactants involved in the assay. In this dissertation, the use of paper-based capillary pressure to route reagents is explored. Chapter 7 details the integration of a nitrocellulose based microfluidic platform with a high sensitivity fluorescence detection system for infectious disease applications.

A significant problem with many LOC systems is the difficulty in deploying a standalone system for field application. As such, many innovative systems eventually end-up on the shelves or in cabinets in laboratories; at most, they are restricted to laboratory use. The architecture reported by Katchmann et al. enables a field-deployable platform for disease diagnosis, vaccine screening campaigns, and drug treatment monitoring. Combining flexible display and protein microarray technology, the utility of this platform for the detection of IgG antibodies to multiple viral antigens in patient sera is investigated. The goal is to develop a low-cost, multiplexed, and disposable diagnostic platform, enabled by the monolithic integration of our filter design with flexible display technology platform, protein microarray printing, and microfluidic technologies.

Recently, Shu et al. reported the first integrated fluorescence sensing system fabricated fully by solution processing Shu *et al.* (2017). Such vacuum-free techniques have the potential to reduce the OLED fabrication cost. A blue OLED, OPD, and sensor integrated on a glass chip (with a glass channel) was developed for potential applications in fluorescence sensing. The system was tested with a model dye (fluorescein amidite, FAM) using linear (crossed) polarization filters to suppress the excitation light reaching the detector and isolate fluorescence emissions. The advantage of using crossed polarizers is that they could be used for the detection of multiple fluorophores at different excitation and emission wavelengths. Thus, compared to interference or

absorption filter-based systems, the cross polarizer-based detection system could be used with any fluorophore in the UV-VIS or near IR regions of the electromagnetic spectrum without making any change to the filter. Interference filter-based systems, however, require dictated bandpass filters hence the use of monochromators and filter wheels in advanced instrumentation. However, with the crossed polarizer-based system reported by Shu et al., a 1 μM ($\sim$0.33 mg/mL) LOD was reported. However, the superior performance of interference filters still make it the component of choice in modern day spectroscopy.

Venkatraman et al. reported the development of an integrated OLED-lateral flow immunoassay (OLED-LFIA) with a nitrocellulose membrane Venkatraman and Steckl (2015b). The authors used a color plastic filter (absorption filter) bonded to an OLED (fabricated on PET substrate) and an emission filter, positioned on top of the LFIA strips. They investigated the use of quantum dots (QD) for improved sensitivity in a model immunoreaction assay; mouse (anti-flu) and (donkey) anti-mouse conjugate. The performance (visual sensitivity) of the QD-LFIA was compared to the conventional gold nanoparticles (AuNP). However, both assays were designed for visual observation-based qualitative LFIA, upon excitation with an OLED. Ambient light photographs of the test lines formed on the strips were analyzed using Image J software. An LOD of 3 nM and 21 nM using the QD-LFIA and Au-LFIA labels, respectively, was reported, representing a 7X improvement using the QD over AuNP. The same group Venkatraman and Steckl (2017) recently, reported improvements to their previous work by integrating OLEDs with a LFIA and an OPD. However this time, the application was the development of a quantitative colorimetry (AuNP) transmission mode detection configuration (through the paper-based membrane). The intensity of the test line is measured over time as the analyte reaches and binds to the test line. In other words, the development of the test line takes $\sim$20 to 30 min and the

signal intensity is monitored during this time. With the transmission mode configuration, the intensity decreased over time as expected. The current reaching the OPD, decreases as the concentration of the AuNP bound on the test line increased over time, scattering more light away from the detector. Although not standalone-operational, the authors also presented a concept in which the OLED and OPD (fabricated on a flexible substrate) would be integrated with commercially available rotavirus test kits (LFIA test for rotavirus in a cassette). The issues with required signal control, processing, and readout electronics need to be resolved with the rotavirus detection system. Using OLEDs and OPDs, enhanced sensitivity will be required for clinical level performance.

The reported LOD and sensitivity in the literature could be further improved by adopting effective design strategies, such as those presented here and in Chapter 5 and Chapter 7. In this chapter, we explore the design, fabrication, and characterization of an OLED-based fluorescence detection platform using a silicon photodiode and interference filters. An application toward the detection of serologic biomarkers for human papillomavirus is presented. By adapting central laboratory protein microarray, protein expression, purification, and immobilization techniques, the developed system is capable of detecting clinically significant biomarker concentrations in patient plasma with required sensitivity and specificity. The result indicates that the system is capable of detecting 100 fM ($\sim$10 pg/mL) of DyLight$^{\text{TM}}$ 549. The high performance of this system is directly linked to the use of bright OLEDs, high-quality interference filters, and charge-integration readout electronics. Here we substitute the typical bulky light sources with a thin film flexible OLED excitation; transfer optics by adopting a "face-to-face" transmission/transillumination architecture; and switch out the standard PMTs, CMOS, and CCDs with a photodiode. Compared to the work reported by Pais et al., we substituted the complicated bulky readout electron-

ics (preamplifiers and lock-in amplifiers) with a simple and efficient charge-integration readout. The constant current generated, due to the fluorescence emissions reaching the photodiode is stored as charge on a capacitor (current or charge-to-voltage converter). This readout technique averages out the noise and trades time for accuracy such that the system yields a concentration dependent output voltage that can be monitored and processed by a simple and inexpensive microcontroller.

4.4 Experimental Procedure

4.4.1 OLED Fabrication, Operation, and Characterization

The green organic light emitting diodes (OLEDs) used in this work were fabricated by the ASU Flexible Electronics and Display Center (FEDC). The details of the fabrication process have been reported elsewhere O' Brien *et al.* (2013); Raupp *et al.* (2007). However, briefly, the planar bottom-emission thin-film multilayer device is deposited by vacuum thermal evaporation on an Indium-tin oxide (ITO) patterned flexible substrate, temporarily bonded to an alumina carrier. Electroluminescence occurs by hole and electron recombination in the green phosphorescent emissive layer (EML) when a potential difference is applied across the reflective aluminum (or MgAg) cathode and transparent ITO anode. The EML is sandwiched between hole and electron injection (HIL and EIL), hole and electron transport (HTL and ETL), and hole blocking (HBL) layers as shown in the inset of Figure 14. The thin layer (<1 μm thick) stack is encapsulated with a thin-film barrier material to protect the device from ambient oxygen exposure. The OLED was characterized by a standard exponential current density-voltage curve, radiance, and electroluminescence (E.L.). Figure 14 shows the luminance and optical power output obtained under ambient conditions and a pulsed (6 Hz) forward voltage to minimize device degradation at high voltage.

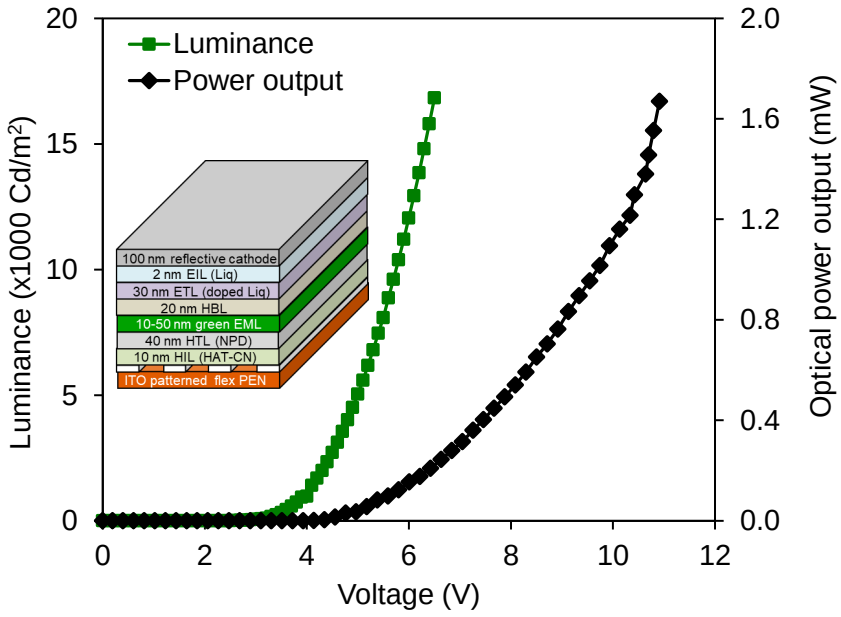

Figure 14: Luminance and Optical Power Output of a Green OLED. Inset Shows Flexible Bottom Emitting ASU Green OLED Device Test Structure Schematic; Layer Composition and Thicknesses Indicated.

4.4.2 System (FlexDx) Test-bench Setup and Compact Configuration

The Al cathode of the OLEDs used in this dissertation, was bonded to a thin metal foil heat sink and pulsed at 10 Hz to obtain a high optical power output while minimizing the degradation in the organic layers that occurs due to the application of a continuous DC voltage across OLEDs. The optoelectronic setup used is similar to the one described in Chapter 3 and shown here in Figure 15.

Radiant energy from the OLED is filtered using a 520 nm/40 bandpass excitation interference filter and used to interrogate fluorescent samples. The fluorophores are specifically bound to capture agents in a biorecognition event on a glass slide. The fluorescence photon emissions from the sample are collected using a bandpass emission filter (605 nm/70). Both bandpass filters are needed to obtain a high extinction

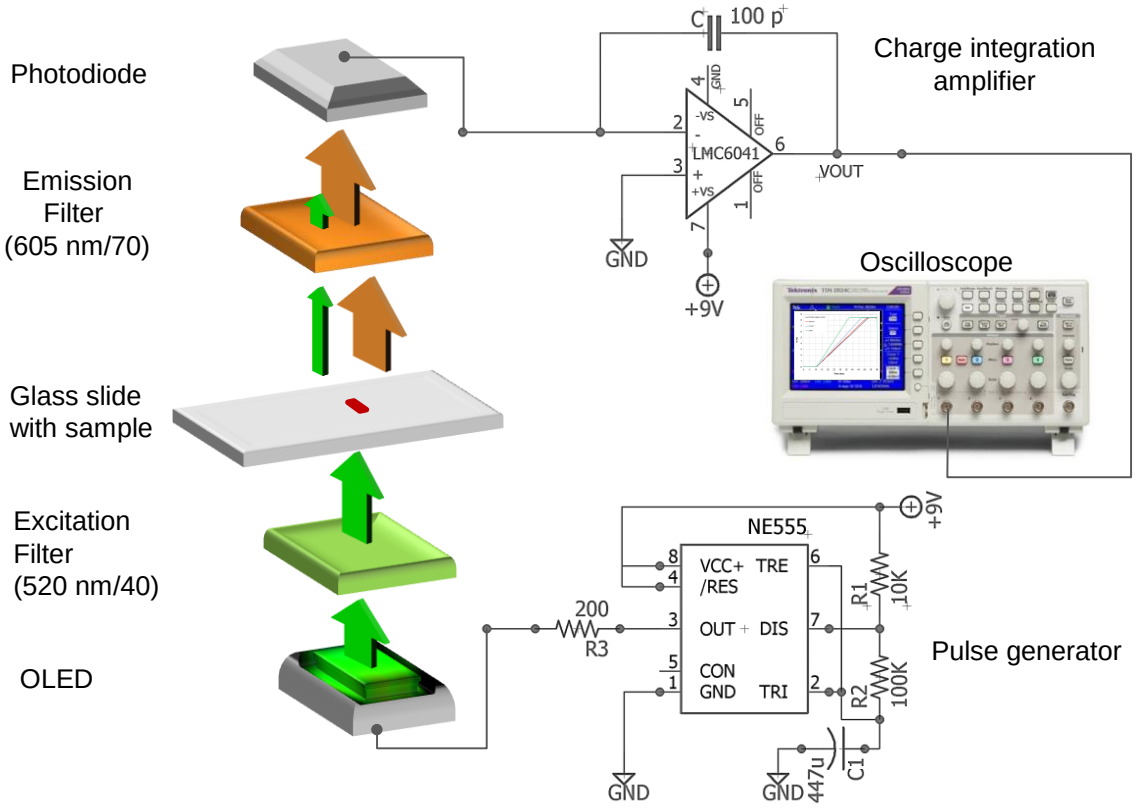

Figure 15: Circuit Schematic of the Test-bench Setup.

ratio (See Section 4.5.2). The emitted fluorescence is detected by a photodiode connected in a capacitive transimpedance amplifier configuration (charge-integrator) as discussed previously (Chapter 3). The evaluation of the viability of using OLEDs as an excitation source for immunometric applications, led to the design of a compact reader system shown in Figure 16. Here, the oscilloscope shown in Figure 15 is replaced by a low-cost embedded system platform (Arduino mini®). A 9 V battery was used to provide the power required by the pulse generator circuit and the charge integration amplifier.

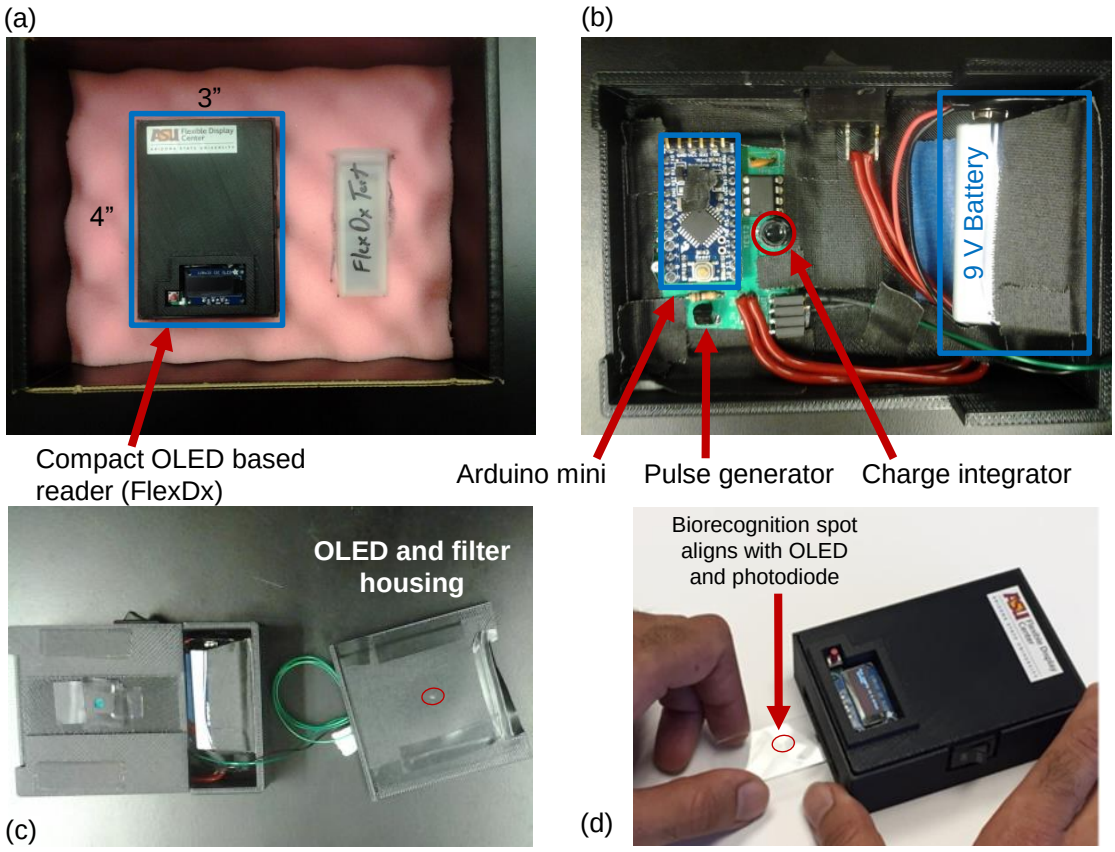

Figure 16: Assembly of OLED-based Fluorescence Detector System (a) Assembled Unit, (4x3 inches) (b) Internal Wiring Showing Microcontroller, Integrator and OLED Driver (c) 3D Printed Optomechanical Assembly (d) Glass-based Assay Insert.

4.4.3 Protein Microarray Technology

Advances and development in organic electronics, microfluidics, fluorescence detection, and protein microarray technology provide a path toward the development of low-cost diagnostic devices for LMICs. Interestingly, these technologies have become mainstream over the past 30 years. Microarrays are useful as a highly sensitive tool for biomedical research analyzing tissues, proteins, and nucleic acids. A typical peptide microarray has hundreds to thousands of μm sized spots on a solid support (usually glass or plastic) in a spatially discrete pattern. The Nucleic Acid Programmable

Protein Array (NAPPA) developed at ASU Ewaisha *et al.* (2016), for example, comprises 2000 spots (<1 μm diameter and pitch) on a 3 x 1 inch microscope slide. Protein/peptide microarray technology provides a high-throughput screening tool for disease biomarker discovery, profiling proteins, enzymes, cells, and drug development and discovery Meng *et al.* (2018); Cretich *et al.* (2013). This technology has been successfully applied toward the mapping and characterization of diseases Ewaisha *et al.* (2017); Gallerano *et al.* (2015) which is useful for diagnosis, antibody response/drug treatment monitoring, and vaccine trials. Some technical limitations associated with the practical implementation of protein microarrays include: the difficulty in optimizing a single solid support substrate for a variety of applications, finding efficient blocking strategies for each application, high cost of peptide libraries, limited intramolecular interactions for short chain peptides making passive adsorption inefficient for peptide immobilization. Some strategies for efficiency improvements in protein microarrays could be achieved by covalent immobilization ensuring proper peptide orientation, surface modification of the solid support to increase the available binding surface area, and strategic design and selection of peptides using advanced tools Meng *et al.* (2018).

4.4.4 Adapting Fluorescence-based Protein Microarray Technology for POC Diagnostics

The development of self-assembling high-density NAPPA arrays has been extensively reported in the literature Ramachandran *et al.* (2004, 2008b,a). The NAPPA arrays have a high-throughput and reproducibility and have been adapted for numerous applications at the Center for Personalized Diagnostics (CPD) at the ASU Biodesign Institute. These arrays have been applied extensively in the study of autoantibodies (AAb) as biomarkers for ovarian cancer, breast cancer, and serum immune profiling

for antibodies (Ab) to other HPV associated cancers Anderson *et al.* (2015a); Katchman *et al.* (2016a); Ewaisha *et al.* (2016); Anderson *et al.* (2011a,b, 2015b,c, 2008, 2010). At the CPD, protein microarrays are typically analyzed by fluorescence imaging, where fluorophores bound to a detection agent are used to indicate the presence of a target analyte. The spatially patterned microarrays are scanned using a high resolution (2 μm) fluorescence microarray scanner, Tecan PowerScanner^{TM} (Tecan Trading AG, Switzerland). The scanner is fitted with dual lasers (20 mW at 532 nm and 25 mW at 635 nm to 638 nm), dual PMT setup with automated gain, fine xyz motion, dynamic focusing, a 676/37 nm and 579/42 nm emission filter wheel, making it compatible with Cy3^{TM}or DyLight^{TM} 549, AlexaFluor® 555, Cy5^{TM}or AlexaFluor® 647, or similar fluorophores or microspheres, e.g. Nile red and F1-Y050 (see fluorophores characteristics in Table 1). To evaluate the use of green OLEDs (515 nm) toward the fluorescence-based detection of HPV-specific IgG antibodies, HPV protein microarray technology Ewaisha *et al.* (2016) is adapted to a POC format by immobilizing purified HPV proteins on a glass slide. DyLight 549 (Jackson ImmunoResearch Laboratories, Inc., PA) and AlexaFluor® 555 (Life Technologies, OR, USA) were chosen as fluorescent probes to match the green OLED as much as possible and enable the same slides to be read by laboratory-based equipment (scanner and microplate reader). Integrating planar capture protein arrays with planar organic optoelectronics for multiplexed detection of target analytes, presents a viable path toward low-cost, high-throughput biochemical analysis, especially for disease diagnosis in LMICs. The development of microcavity OLEDs Williams *et al.* (2014); Liu *et al.* (2011, 2013) lends itself well to such an application.

4.4.5 System Response - Fluorophore Standard Curve

To evaluate the detection system (FlexDx) response, a logarithmic dilution series of 1 μm Nile red microspheres (Life Technologies, CA, USA), DyLight^{TM} 550 (Thermo Scientific, IL, USA), and DyLight^{TM} 549 (Jackson ImmunoResearch Laboratories, Inc., PA) ranging from 1:10 to 1:1,000,000 for Nile red, and 1 mg/ml to 10 pg/mL for DyLight^{TM} 550 and DyLight^{TM} 549, was prepared in 1X phosphate buffered saline (PBS). The Nile red microspheres were sonicated for 5 min, before use to prevent agglomeration. The diluted fluorophores were pipetted by hand on an (3-Aminopropyl)triethoxysilane (APTES) coated glass slide. To control the diameter of the spot, 1 μL was pipetted and allowed to dry. The process was repeated 9 times to get a total volume of 10 μL for each spot (N = 3). The slides were dried for 10 min at ambient temperature. The fluorescent samples were measured by sequentially inserting the slides into the FlexDx reader and recording the fluorescence intensity. The performance of the FlexDx system was benchmarked against a standard clinical laboratory microplate reader (EnVision^{TM} 2104-0010 Multilabel Reader, Perkin Elmer, MA, USA).

4.4.6 Fluorescence-based Detection of IgG Antibodies

To simulate antibody-antigen binding reaction and quantify the LOD of the FlexDx platform, an initial evaluation with the direct binding of whole human IgG and anti-human IgG-fluorophore conjugate (typically used as positive control) was performed. Microscope slides, 75 x 25 x 1 mm (VWR International, Radnor, PA, USA) were coated with 2% APTES (Sigma Aldrich, USA), e.g., 12 mL of APTES (ThermoFisher Scientific, TX, USA) in 600 mL of acetone (Sigma Aldrich, MO, USA) by submerging the slides arranged vertically on a metal carrier in a glass washing dish 2% APTES

and rocking for 15 min. The slides were rinsed by dunking 5X in 100% acetone and then rinsed 5X with deionized (DI) water (Millipore, USA). The slides were blow dried with filtered compressed air. Two experiments were conducted in this effort. First, the whole human IgG immobilized on a glass slide was held at a fixed concentration (25 μg/mL) and the anti-human IgG concentration was varied from 13 μg/mL to 130 pg/mL, diluted in 5% milk-PBST. Second, whole human IgG was diluted and logarithmically scaled from 1 mg/mL to 1 fg/mL (25 μg/mL) in DI water. In both experiments, bovine serum albumin (BSA) was used as the negative control and spotted at 25 μg/mL. All proteins were manually spotted on APTES coated slides in 1 μL steps and repeated 4X for a total volume of 5 μL per spot (N = 2), allowing the protein to dry at room temperature after each 1 μL volume spotted. The hydrophobic surface characteristics of the glass slide ensured that the 1 μL spots were confined to $\sim$2 mm diameter. This ensured that the spot size was completely in the field-of-view of the FlexDx system optoelectronics, as the spots were pitch-matched to the OLED and photodiode. The separation between the photodiode and sample spot ($\sim$5 mm) ensured a complete coverage of the spot under test. The slides were incubated at 4°C overnight for 16 to 18 hours. DyLight^{TM} 549 AffiniPure Goat Anti-Human IgG, F(ab')$_2$ fragment specific (2° antibody-fluorophore conjugate) diluted 1:50 in 5% milk-PBST (0.2% tween in 1X PBS) was used to probe the protein on the glass slides, incubating and rocking for 1 hour. The slides were measured using the FlexDx system and the Tecan PowerScanner. Figure 17 depicts the assay steps and shows the whole human IgG-anti-human-fluorophore conjugate system. This assay is used as a positive control for all assays in this dissertation.

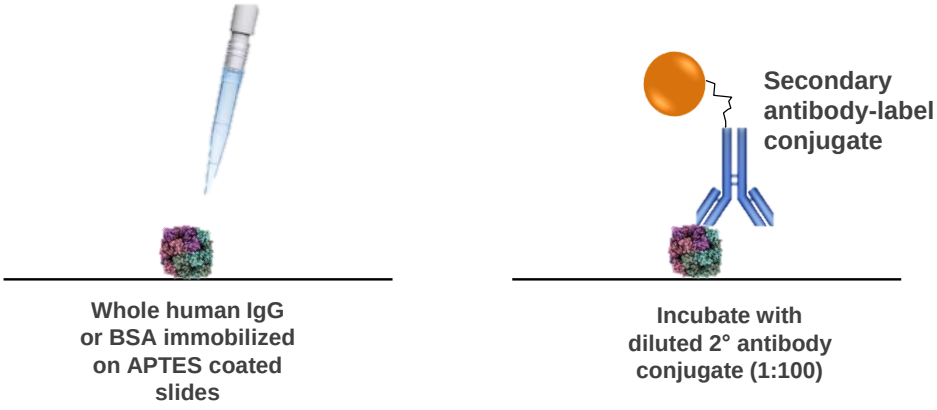

Figure 17: Recombinant Whole Human IgG Protein Assay on Aminosilane Coated Glass Slides.

4.4.7 Adapting Rapid Antigenic Protein InSitu Display (RAPID) ELISA for POC Applications

Protein Expression and Purification

The HPV proteins were separated and purified using a GST-tag (Glutathione S-transferase) system which was used to separate the GST-fusion protein. Details of the protein expression and purification technique developed by Dr. Karen S. Anderson has been reported elsewhere Anderson *et al.* (2011b), as well as methods to quantitate the protein (C-terminal fragment-CE2, E6, and E7) yield and purity. The Rapid Antigenic Protein *In Situ* Display (RAPID) ELISA developed by Dr. Karen S. Anderson et al. Ramachandran *et al.* (2008a); Anderson *et al.* (2010) is a programmable ELISA assay developed for 96-well microplates. HPV antigens are expressed and captured to the individual wells using anti-tag antibodies, similar to the NAPPA approach that uses a lysate for *in vitro* transcription/translation (IVTT). This obviates the need for protein purification. Diluted plasma samples (typically, 1:100) are added to the

wells (coated with CE2, E6, E7), incubated, and detected with HRP-conjugated goat anti-human secondary IgG antibody, to which a chemiluminescent substrate and stop solution is added. Luminescence is read with a microplate reader. RAPID ELISA is a highly sensitive central laboratory-type assay, that requires typical infrastructure, highly trained personnel, and expensive equipment. These factors limit the application in resource-constrained settings (RCS). By drawing inspiration from microarray spotting and RAPID ELISA techniques, we adapt these systems to a relatively inexpensive assay format on glass slides, by immobilizing recombinant purified HPV proteins on APTES coated slides, and detecting anti-HPV IgG antibodies in human plasma by probing with a fluorescent labeled secondary anti-human IgG conjugate. In theory, a high density detection array using OLEDs could be pitch-matched to each detection site in an array, providing a high-throughput detection and pre-screening tool in RCS.

4.4.8 Detection of HPV16 E7 IgG Antibodies in Human Plasma

The POC assay protocol for the detection of HPV16 IgG specific antibodies in plasma is illustrated in Figure 18 and detailed in Table 4.

The plasma samples (HPV+ and healthy controls) used in this work were tested for HPV16 E7 DNA by PCR in a previous study, the Human Oral Papillomavirus Transmission in Partners over Time (HOTSPOT) study Anderson *et al.* (2015c). The study design, enrollment, and serologic responses to HPV16 has been previously detailed and reported D'Souza *et al.* (2014). (Clinical Trials number: NCT01342978). Written informed consent was obtained from all subjects in accordance with Arizona State University institutional review board approval. All experimental protocols were approved and were carried out in accordance with the relevant guidelines under the Arizona State University institutional review board. All of the methods involving

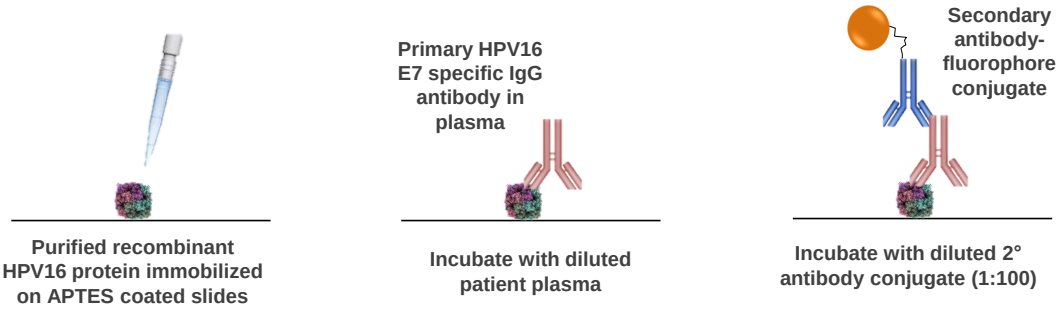

Figure 18: Assay Protocol Using Recombinant HPV16 Protein Immobilized on Aminosilane Coated Glass Slides and Used to Detect HPV16 Specific IgG Antibodies in Plasma From HPV16+ Cases and Healthy Controls. Purified Recombinant Human IgG Protein was Used as Positive Control and BSA as Negative Control.

human subjects were carried out in accordance with the relevant guidelines previously stated in Anderson *et al.* (2015c). Figure 18 depicts the assay steps for HPV detection in a POC, low-cost format and shows the secondary antibody-fluorophore, HPV16 specific IgG antibodies captured from plasma using purified recombinant protein immobilized on a microscope slide.

Table 4: HPV16 E7 Microscope Slide-based Assay Protocol for POC Applications.

Assay step	Conditions	Comments
Coat 75 x 25 mm microscope slides with 2% APTES	15 min, room temperature (RT) Set dish on a rocker at RT Rinse slides 5X with pure anhydrous acetone Rinse slides 5X in DI Blow dry slides with filtered compressed air	Use a slide tray (metal) to ensure uniform coating. Note that slides are hydrophobic after coating Dried slides can be stored at RT. Carefully lay down the first spot, it determines the diameter. Automated spotter will reduce CV vs. manual
Spot 5 μL of purified recombinant HPV16 protein, negative control (BSA or GST), and positive control (IgG or EBNA) protein on APTES coated slides	Diluted protein concentration to 50 μg/mL at room temperature Spot 1 μL at a time (5X) Incubate at 4°C overnight	Dilute protein in DI or PBS No significant difference at higher temperature. Spotting smaller volumes repeatedly improves protein adhesion. 16 - 18 hours, low RH helps
Rinse 1X in DI and block in 5% milk-PBST	Block for 1 hour RT Set on a rocker at RT	Blocking with Milk-PBST (5% milk in 0.2% tween in 1X PBS). Blocking strategy is not as effective as desired on glass slides. Aspirate fluids with a pipette or decant off glass slide safely
Incubate with case and control plasma samples	Dilute plasma in 5% milk-PBST Add 300 μL of diluted plasma Incubate for 1 hour on rocker at RT Plasma dilutions (1:1, 1:10, 1:100) Wash 3X in PBST in a slide holder	Cover samples throughout the assay to limit evaporation and unfiltered light effects. The use of a staining tray is recommended. Find a suitable SNR titrating plasma in a population study. Ensure spots are completely covered
Incubate with anti-human IgG DyLight 549 conjugate	Dilute secondary conjugate in 5% milk-PBST. Incubate Secondary dilution (1:50) for 1 hour on a rocker at RT	Could be diluted in DI or other non-protein blockers. Suitable dilution is found by titration experiment
Rinse in PBST and DI	Wash slides 3X in PBST Wash slides 3X in DI	Submerge slide in PBST in a sealed holder. Vigorous shaking helps wash off non-specifically bound fluorophores

4.4.9 Multiplexed Detection of HPV16 E2, E6 and E7 Antibodies in Human Plasma

POC HPV16 Array, Assay Protocol, and Cross-talk Evaluation

To demonstrate the utility of FlexDx of multiplexed detection of biomarkers, the crosstalk fluorescence intensity between sites was used as a metric to determine the optimal pitch for the protein spots on the glass slides. Cross-talk originates from the unintended excitation of neighboring sites or the collection of fluorescent photon emissions from off-target sites. The detector aperture and the optomechanical design of the isolation structures within the reader directly affect the crosstalk intensity. See Chapter 5 for a more in-depth discussion of low-cost optical isolation and crosstalk elimination for multiplex detection. However, for the single-site FlexDx system, the optical path was designed with a ∼7 mm diameter aperture. Cross-talk was observed to increase significantly when the array pitch was decreased below 6 mm as depicted in Figure 19 (a).

A concentration dependent cross-talk is observed and decreases with array pitch for a fixed aperture size. At working fluorophore concentrations, 6 mm pitch was selected for HPV16 protein linear array on a microscope slide. Micro OLEDs will enable a higher density array with a smaller pitch, limited by practical considerations in the microfluidics. Multiplexed detection of CE2, E6, and E7 was demonstrated using a linear array of protein spots on a glass slide. Figure 19 (b), depicts the layout of the spots on a microscope slide. The slide was mechanically pushed into the reader and pulled out to predefined markers/stops to bring each site into alignment with the single-site reader optoelectronics in the POC system (FlexDx). The BSA and IgG sites were used as negative and positive controls, respectively. The assay protocol used for the multiplexed detection of HPV16 CE2, E6, and E7 antibodies is similar

to the one described in Section 4.4.8 and detailed in Table 4.

4.5 Results and Discussion

4.5.1 Fluorescence Intensity and OLED Optical Power Output

In a fluorescence detection system, the source of radiant energy must be capable of inducing an excited state in the fluorophores under test (see Section 2.2). To explore the use of OLEDs for low-cost applications and understand the excitation power requirements to induce fluorescence in typical fluorophores, an experiment using neutral density (ND) filters was conducted. Neutral density filters, ND 1, 2 4, 8, 16, and 32, corresponding to 100, 50, 25, 12.5, 6.25, and 3.125% transmission,

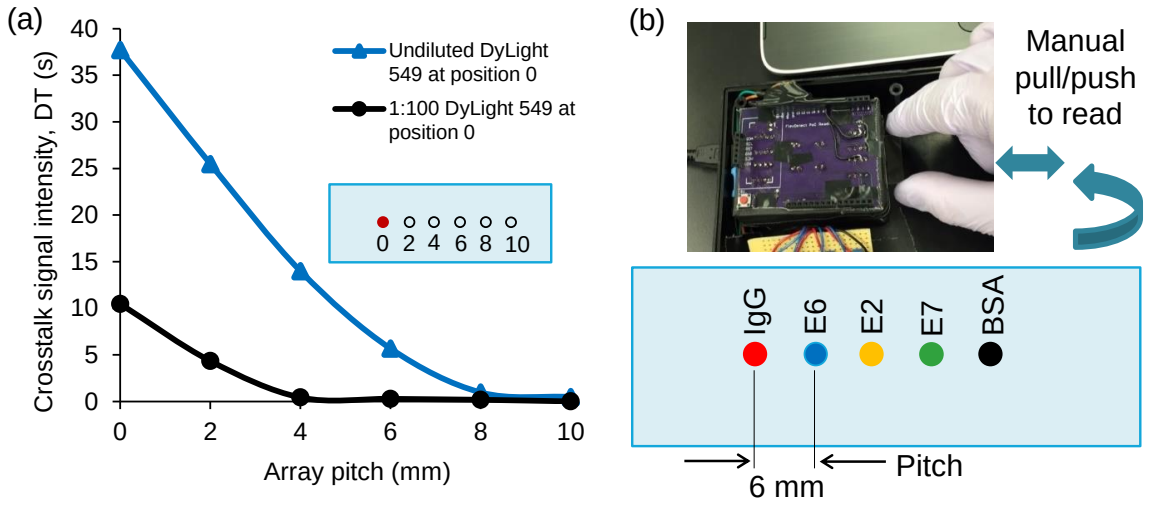

Figure 19: (a) Crosstalk Fluorescence Intensity at Different Positions of a Microscope Slide: 2, 4, 6, 8, and 10 mm From Position 0 Which has Extremely Bright Fluorophore Spotted (Triangles). The Crosstalk Due to Recommended Fluorophore Dilutions, e.g. 1:100 for DyLight 549 (Supplied at 1 mg/mL) is Also Shown (circles). A 6 mm Pitch was Chosen to Ensure Zero Crosstalk Between Antibody Recognition Sites Under Assay Conditions.

respectively, was used to vary the light intensity from a mercury lamp. The fluorescence response was measured using an Ocean Optics QE Pro-FL (Ocean Optics, FL, USA) high sensitivity fiber optic fluorescence spectrometer, mounted on a Nikon LV-100 fluorescence microscope (Nikon Instruments Incorporated, NY, USA). The OLED optical power output of 0.8 mW (shown previously in Figure 14) is obtained under operating conditions, 8.8 V and 10 Hz pulse (50% duty cycle). Figure 20 (a) depicts the OLED optical power output which corresponds to ∼62% transmission. Figure 20 (b) shows the fluorescence response from a fixed fluorophore concentration while varying the optical power. Matched sodium azide sample was used as a reference for the fluorescence spectra. The design of low-cost fluorescence systems as detailed in Chapter 3 and fluorescence system design principles in general posit that higher intensity implies more fluorescence signal. From a practical standpoint, higher excitation intensity may not be beneficial for the overall system stability and SNR. Intensity increase is limited by fluorophore stability and increased leakage light intensity especially in the configurations discussed in this dissertation.

4.5.2 System (FlexDx) Performance Characteristics

The green phosphorescent OLEDs used in this work has 5X higher luminous intensity and 125X higher optical power output at an operating voltage (8 V) compared to those used by Pais et al. Pais *et al.* (2008b); Banerjee *et al.* (2010b). Table 5 compares the parameters and performance of the system used by Pais et al. with the system reported in this Chapter. The intensity of the excitation source significantly affects the overall system performance since the fluorescence emission intensity is directly proportional to the excitation intensity (see Equation 3.4).

The optical power measured from a logarithmically scaled dilution series of 1 μm

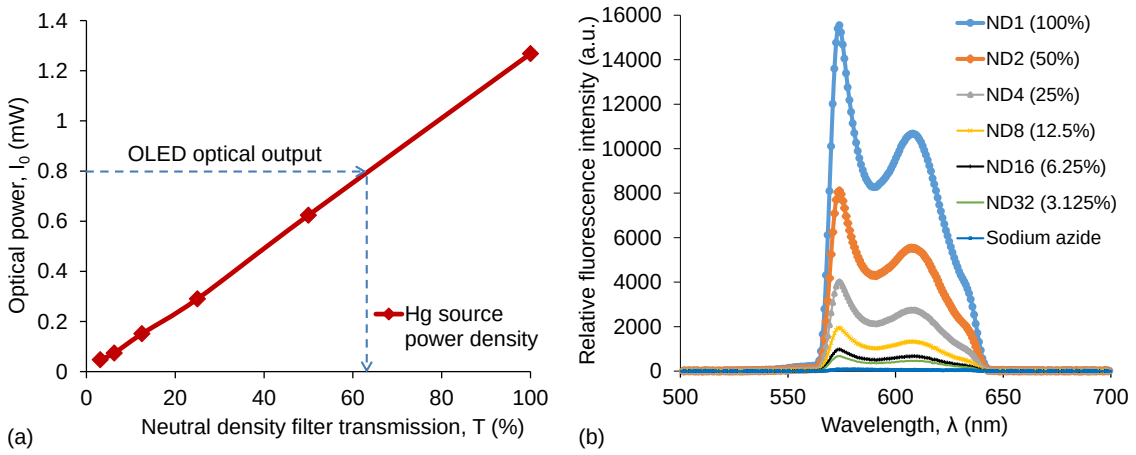

Figure 20: (a) Fluorescence Response as a Function of Excitation Source Power Density Using Neutral Density Filters (ND). (b) Power Density for Mercury (Hg) Source as a Function of Filter Transmission.

Nile red fluorescent microspheres is shown in Figure 21. The optical power was measured with a Newport 1830 C optical power meter, fitted with an 818-SL calibrated VIS photodiode (Newport, CA, USA). No attenuator was used in this measurement, as the expected optical power is in the nW range, thus maximizing the SNR.

The noise floor reported by Pais et al. (77 nW) using cross-polarizers limits the system performance. Using interference filters, we obtained 3 orders of magnitude relative reduction in the noise floor, with an extinction ratio of 70 dB using excitation and emission filters. The performance of a fluorescence-based detection system is directly linked to the degree of rejection of the excitation source, reducing the noise reaching the detector.

4.5.3 POC Platform Performance Characteristics - Response to Spotted Nile Red, DyLight^{TM} 550, and DyLight^{TM} 549

Figure 22 depicts the spectral characteristics of the system input: the normalized absorption spectrum of Dylight 549, the excitation filter, and the electroluminescence

Table 5: OLED Optical Power and Extinction Ratio Using Cross-polarizers and Interference Filters.

Parameter	Pais et al.*	FlexDx**
Luminous intensity (Cd/m^2)†	1000	5000
OLED optical power (W)†	4 x 10^{-6}	0.5 x 10^{-3}
Noise floor (W)	77 x 10^{-9}	60 x 10^{-12}
Extinction ratio (dB)	20	70
LOD (Nile red)‡	5 x 10^{6}	2 x 10^{3}
Electronic readout	Lock-in amplifier	Charge-integration
Microfluidics	PDMS	Glass

* Pais *et al.* (2008b) used cross polarizers
**FlexDx developed in this dissertation used interference filters
†Luminous intensity and optical power output measured at 8 V for both systems
‡Limit of detection (LOD) for 1 μm Nile red fluorescent microspheres

spectrum of the OLED compared to a green inorganic LED (iLED). Clearly, the OLED has a broader spectrum that the ILED, with band tails extending into the red spectrum at low intensity. The use of a bandpass filter with a sharp cutoff was therefore required to reject the excitation light reaching the detector. Both the OLED and ILED excite the fluorophore at about 50% of the absorption. A 523 nm green laser also excited the DyLight 549 at the same level, due to the wide vibrionic peak to the left of the main peak of the fluorophore.

There is usually a trade-off(s) to be made in the design of fluorescence systems and the choice of fluorophores. Here, a major trade-off is an acceptable level of mismatch for the use of off-the-shelf fluorophores for preliminary evaluation of our already existing flexible display platform. In theory, the spectral characteristics of a fluorophore, or OLED could be optimized to maximize the overlap. For fluorophores in the visible

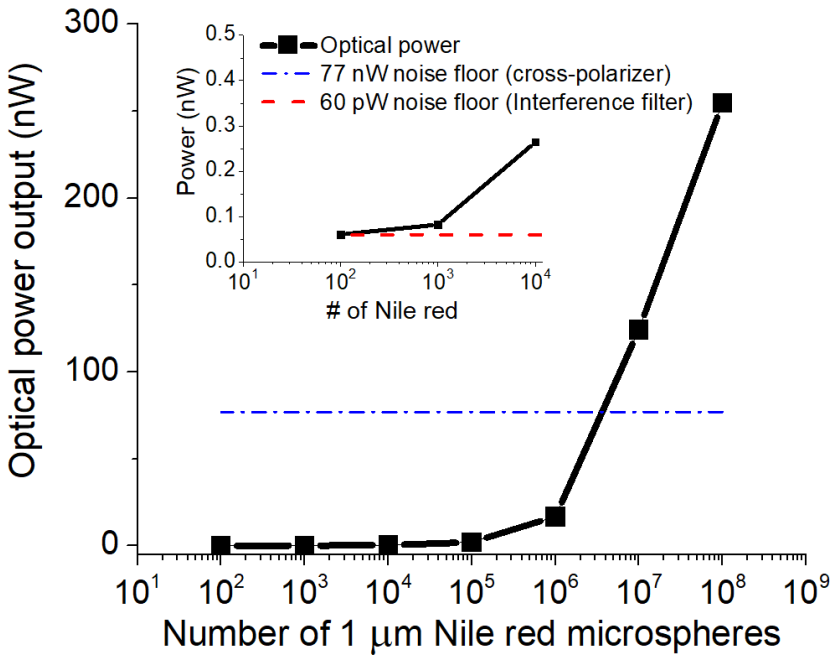

Figure 21: Optical Power as a Function of 1 μm Nile Red Fluorescent Microsphere Concentration. Inset Shows a Zoom Plot Indicating a 3 orders of Magnitude Lower Noise Floor Using Interference Filters Compared to Cross-polarizers.

spectrum, better matching of the excitation source and fluorophore could be obtained by setting the source wavelength in monochromator-based spectrofluorometers, where a wide and relatively flat radiant energy source (e.g. xenon lamp) is used with an array of filters on a wheel. See Figure 7 in Chapter 3 for Nile red, ILED, and excitation filter spectra. The effect of spectral mismatch is explored further in Chapter 6.

Signal Interpretation - Ramp Time, Detection Time, and Signal-to-noise Ratio

The concentration dependent voltage response (see Equation 3.11) that characterizes the fluorescent sample under test, could be represented by the following metrics:

1. Ramp time , RT (s) or Δt: inversely correlated with fluorescence intensity

(presented in Chapter 3)

2. Detection time, DT (s): directly correlated with fluorescence intensity (presented in Chapter 3)

3. Ramp rate or slope, S (V/s) and derivative analysis: directly correlated to fluorescence intensity (used in this and subsequent chapters)

4. Signal-to-reference: directly correlated to fluorescence intensity (used in this and subsequent chapters, useful for lateral flow assays)

5. Normalized fluorescence intensity, NFI (a.u.): directly correlated to fluorescence intensity (presented in Chapter 7, useful for lateral flow assays).

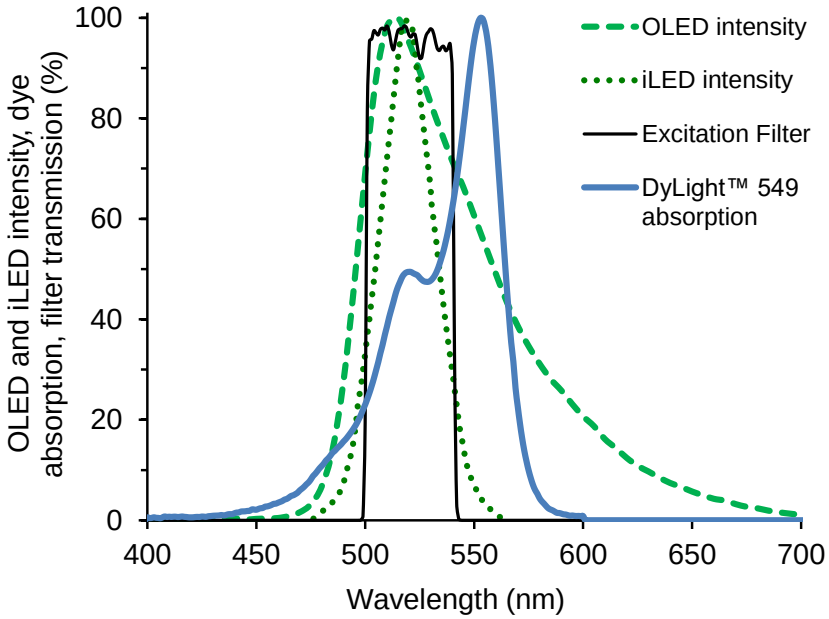

Figure 22: Green OLED and ILED Intensity Compared and 520/40 nm Excitation Filter Used to Isolate Excitation Source and Cut Off the Band Tails in the OLED Spectrum. Dylight 549 was Used as Fluorescent Tag for Most of the Data Shown Toward the Detection of hrHPV Biomarkers.

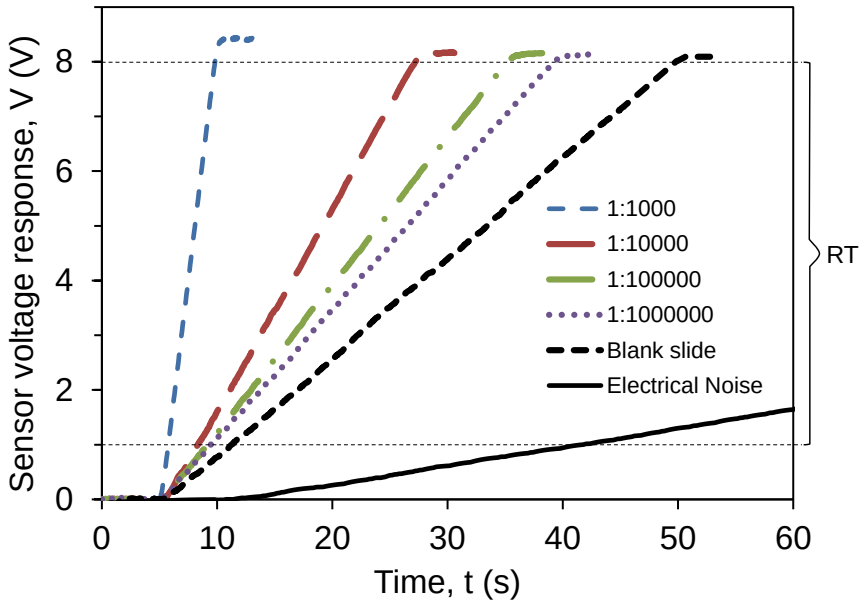

Figure 23: Representative System (FlexDx) Response to a Logarithmically Scaled Dilution Series of 1 μm Nile Red Microspheres. The Blank Slide (No Fluorophore) Level Represents the Electrical and Optical Noise Floor Combined. The Electrical Noise Floor Shown is the Ramp at the Output of the System when the OLED and the Integrator Only is Turned On.

Different metrics enable interpretation of the developed fluorescence system response in a variety of ways suitable for specific applications. The data presented in this section illustrates the used of these metrics except the NFI, presented in Chapter 7.

Figure 23 shows the system response to a dilution series prepared from 1 μm Nile red microspheres, with a stock particle concentration of 3.6 x 10^{10} microspheres/mL. The concentration was logarithmically varied from 3.27 x 10^{7} to 200 microspheres (higher concentrations not shown) and directly spotted on a glass slide (10 μL per spot, per dilution, N = 2).

Figure 24 depicts the signal-to-reference level as a function of the number of fluorophores in the corresponding dilutions (See Table 3). Herein, the reference level

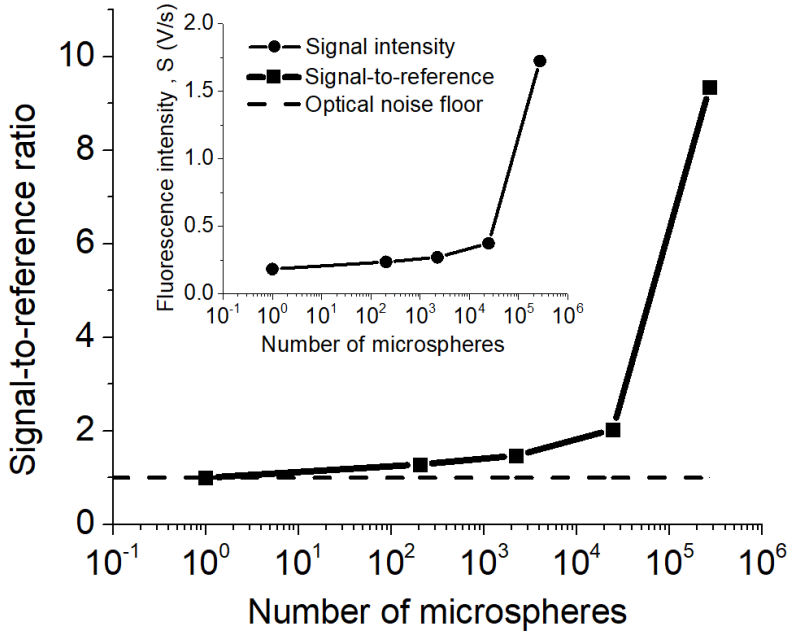

Figure 24: Signal-to-reference Calculated as the Ratio of the Nile Red Fluorescent Sample to the Blank Slide Reference Intensity. Blank Slide Level = 1. Inset: The Raw Fluorescence Intensity or Ramp Rate.

is represented by the system output with a blank microscope slide (no fluorophores spotted) shown in Figure 23. This signal level comprises negligible electrical noise and optical noise. The electrical noise is mostly due to negligible dark current as the photodiode is connected in photovoltaic mode, ambient leakage light, and ambient noise. The blank slide level when the excitation source is turned on is mostly due to leakage light reaching the detector. The leakage light arises as a result of filter imperfections, oblique incidence resulting from scattered and reflected light within the system housing, autofluorescence of the materials used in the design.

The inset shows the fluorescence intensity, S (V/s) which is the ramp rate or slope of the concentration dependent voltage-time output profile. As presented in Chapter 3, a lower (1 V) and upper (8 V) voltage threshold level are used to extract the ramp time (inversely correlated with the fluorescence intensity). The detection

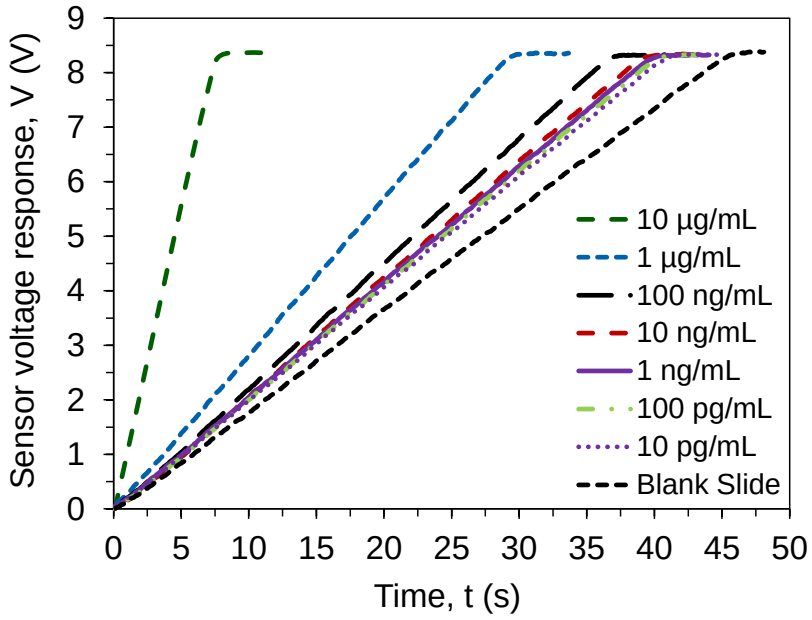

Figure 25: Representative System (FlexDx) Response to a Logarithmically Scaled Dilution Series of DyLight 550 (Molecular Dye).

time metric (ramp time difference between sample and reference), as well as the ramp rate, is directly proportional to the fluorescence intensity reaching the detector. With the OLED turned off, the noise floor reaches 1 V after 40 s and takes 254 s to reach 8 V, corresponding to ramp rate of 0.033 V/s. The ramp rate for a blank slide is 0.184 V/s as shown in the inset.

Figure 25 shows a representative system response to a dilution series prepared from 1 mg/mL DyLight® 550 (molecular/organic dye, EX_{max} = 562±4 nm, EM_{max} = 576±4 nm, in PBS). The concentration was logarithmically varied from 1 mg/mL to 10 pg/mL (higher concentrations not shown) and directly spotted on a glass slide (10 μL per spot, per dilution, N = 3). As the fluorophore concentration is decreased, it becomes increasingly difficult to distinguish concentrations.

The sharp drop in signal intensity or signal-to-reference shown in the Figure 26 at concentrations lower that 10 μg/mL suggests that the molecular dye should be used

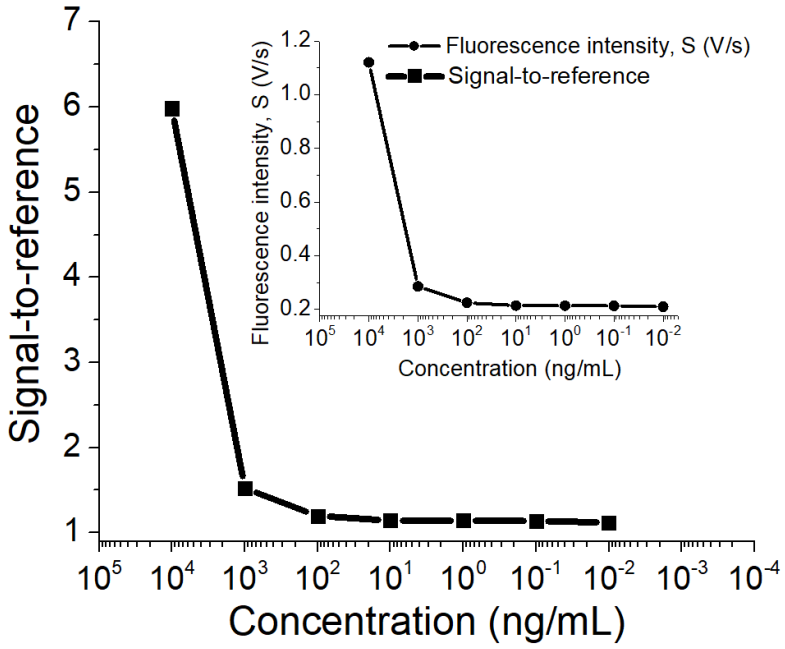

Figure 26: Signal-to-reference Calculated as the Ratio of the DyLight 550 Fluorescent Sample to the Blank Slide Reference Intensity. Blank Slide Level = 1. Inset: the Raw Fluorescence Intensity or Ramp Rate.

in assays at concentrations between 200 μg/mL and 2 μg/mL which corresponds to a 1:50 to 1:500 dilution of a 1 mg/mL stock.

Figure 27 shows a representative system response (detection time) to a dilution series prepared from 1 mg/mL stock DyLight® 549-TFP ester (molecular/organic dye, EX_{max} = 555, EM_{max} = 568). The concentration was logarithmically varied from 1 mg/mL to 10 pg/mL (higher concentrations not shown) and directly spotted on a glass slide (10 μL per spot, per dilution, N = 3). As the fluorophore concentration is decreased, it becomes increasingly difficult to distinguish concentrations. DyLight® 549-TFP ester gave a slightly higher response compared to DyLight® 550. This may be due to slight differences in the spectra with respect to the absorption and emission maxima. The inset shows the signal-to-reference and a sharp drop in signal intensity or signal-to-reference at concentrations lower than 10 μg/mL. Manufacturer

recommended concentration for most applications is between 1:100 to 1:800.

The performance of the OLED-based configuration was benchmarked against a standard central laboratory fluorescence microplate reader as shown in Figure 28. The OLED-based platform (FlexDx) and the microplate reader show a similar response profile detecting between 2000 and 10000 microspheres, indicating that OLEDs are a viable excitation source, for low-cost fluorescence system design. It is worth noting that the well-plate reader sample volume per well was 100 μL, compared to 10 μL spotted on the microscope slide in the FlexDx system. Note the scale on the secondary axis. However, as observed during the course of this dissertation research and presented in later chapters, microplate assay systems perform well under laboratory condition since the protocol typically involves significantly long incubation times, vigorous washing steps to reduce non-specific binding, and effective blocking

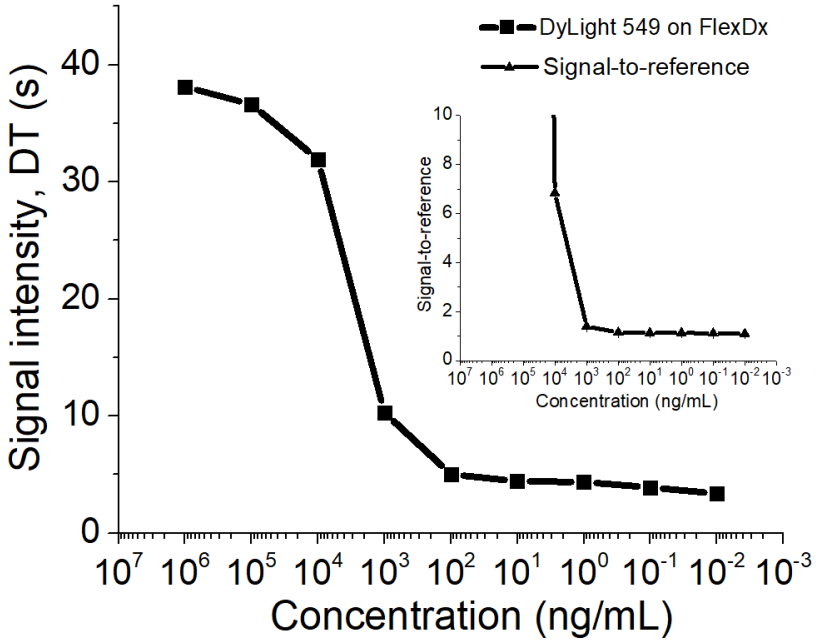

Figure 27: Representative System (FlexDx) Response to a Logarithmically Scaled Dilution Series of DyLight 549 (Molecular Dye).

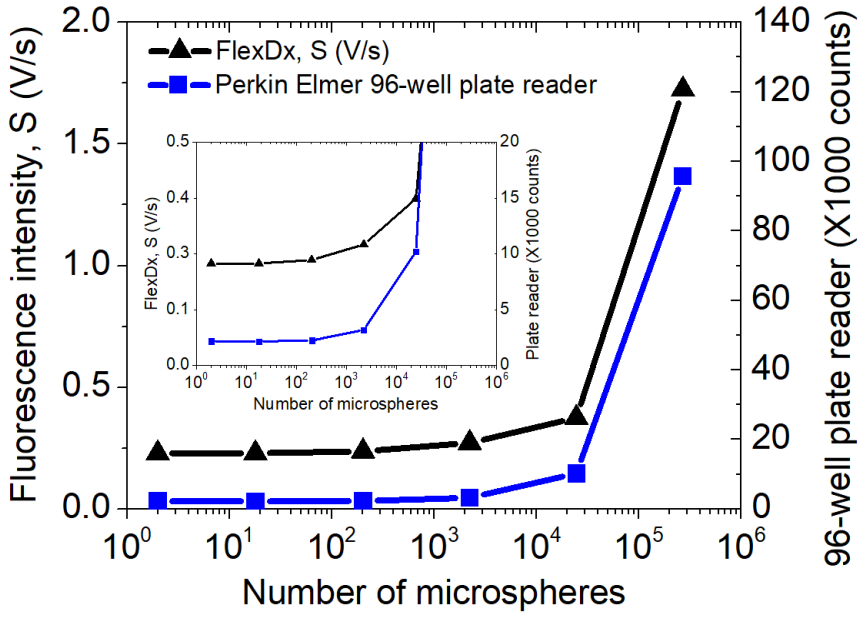

Figure 28: Response Comparison Between OLED-based Low-cost System (FlexDx) and a Standard Central Laboratory Microplate Reader (EnVision™ 2104-0010 Multilabel Reader, Perkin-Elmer).

steps/strategies. These conditions are not is easily implemented in low-cost POC platforms involving the use of low-cost paper-based microfluidics, or tests developed for resource-constrained settings where significant design constraints include a short sample to answer time under 30 min, easy/limited assay steps, and low cost.

4.5.4 Preliminary Demonstration of Direct Fluorescence Detection of Human IgG (Positive Control Assay)

Figure 29 depicts the signal intensity as a function of spotted whole human IgG concentration and anti-human IgG at a constant whole human IgG protein concentration immobilized on a glass slide and measured using the OLED-based fluorescence detection system. The signal output for the dilutions is expressed the detection time,

which is the ramp time difference between the test and control.

The OLED-based system was benchmarked against a microarray scanner (Tecan PowerScanner^{TM}). The raw intensity counts and the corresponding dilution is shown on the bottom of Figure 29. The scanner images were converted to intensity using ImageJ (NIH), normalized to BSA control. For the whole human IgG experiment shown, both instruments begin to saturate at low concentrations and are capable of detection in the pg/mL range. The OLED-based system demonstrates the detection of anti-human IgG concentration down to the pg/mL levels. This is a clinically significant detection range, indicating that the OLED-based system (FlexDx) is suitable for early detection and screening applications.

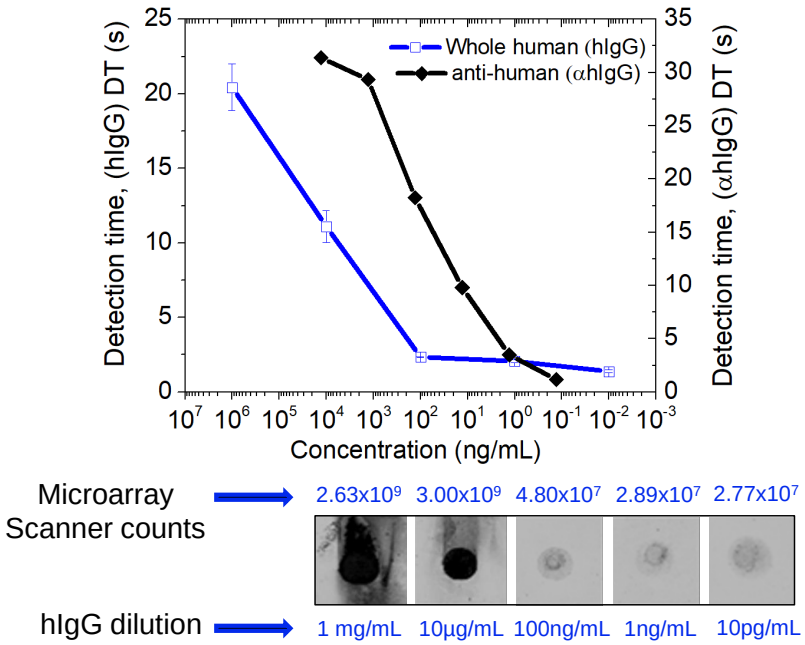

Figure 29: Representative Fluorescence Intensity From Direct IgG-anti-human IgG Assay, Showing Detection Limit Down in the pg/mL Levels. Here the Fluorescence Intensity is Denoted as a Detection Time. The Intensity is Normalized to the BSA Negative Control Site.

4.5.5 Preliminary Demonstration of Fluorescence Immunoassay for the Detection of HPV16 E7 Antibodies on Glass

This section details the detection of HPV16 E7 specific IgG antibodies in human plasma. To demonstrate the viability of a low-cost approach for the detection of HPV antibodies, a low-cost HPV assay was developed as described in Section 4.4.8 and Table 4. The samples were measured using the FlexDx system with OLEDs as an excitation source, combining a low-cost assay with a low-cost reader platform. In practice, a reusable and ultimately disposable reader will be combined with a disposable cartridge. This offers a cost-effective approach toward early diagnosis and pre-screening in RCS. Figure 30 (a) and (b) depicts the specific detection of HPV16 E7 IgG antibodies as indicated by the sensor voltage response. Known positive patient samples and healthy controls were diluted (1:1, 1:10, and 1:100) and incubated with the pre-printed HPV16 E7 protein immobilized on a glass slide. HPV16 E7 specific IgG antibodies were detected using a goat anti-human IgG-DyLight 549 conjugate. Clearly, the HPV16 E7+ (positive samples) ramp at a faster rate compared to the HPV16 E7- (healthy controls or negative samples). The non-specific binding or off-target signal levels observed in the healthy controls as shown in Figure 30 (b) and (c) demonstrates the significance of an effective blocking strategy to minimize non-specific interactions with other entities present in a plasma or whole blood, which is quite a complex matrix. Significant effort has been expended by Dr. Karen Anderson's laboratory, toward identifying and minimizing protein cross-reactivity. The signal-to-noise ratio is shown in Figure 30 (d), is calculated as the ratio of the signal intensity of the E7 site to a BSA site used as negative control. A more accurate reference negative control is the use of GST as the immobilized HPV antigens are GST tagged.

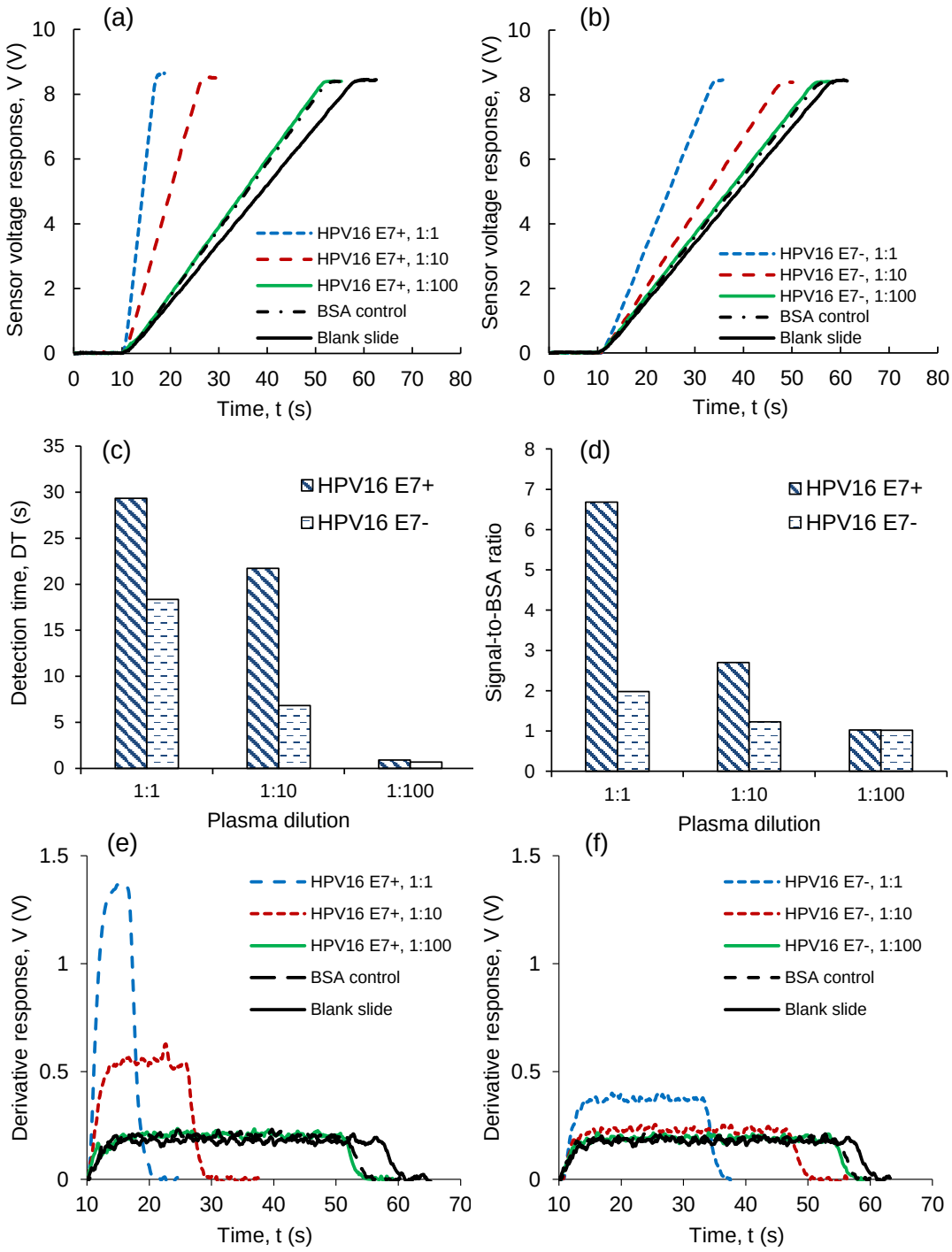

Figure 30: (a) and (b) Shows Voltage-time Responses From Serum Dilution (1:1 to 1:100) of Known Positive (HPV16 E7+) and Negative (HPV16 E7-) Patient Plasma Respectively. (c) and (d) Shows Detection Time Variations with Plasma Dilution. (e) and (f) Show Respective Derivative Responses.

A useful metric to characterize the system response is the derivative of the voltage output response of the system, this analysis is shown in Figure 30 (e) and (f). Significant information could be extracted from this plot. The ramp start and stop time could be determined from the inflection points. The distinct maxima at different concentrations, even at the early stages of integration (the rising edge) is correlated to the measured fluorescence intensity such that further integration may be unnecessary, saving time. This is useful for a multiplexed array where reading multiple sites may take several minutes. The measured fluorescence intensity could easily be extracted from the full-width-at-half-maximum (FWHM) and a clear distinction between concentrations is also evident at the falling edge. This provides three possible regions on the derivative plot that could be correlated to fluorescence intensity or concentration: the rising edge, peak, and falling edge. The OLED-based platform was benchmarked against the RAPID ELISA laboratory test for the detection of HPV16 E7 viral biomarkers (HPV16 E7 specific IgG antibodies). For this experiment, a random selection of 15 known samples, positive for HPV16 E7 IgG antibodies (case) and 15 healthy controls were selected. Figure 31 shows the OLED-based system response expressed as the detection time (DT) and the RAPID ELISA response (RLU) expressed as antibody (Ab)-to-GST ratio. Both indicate a clear separation between the case (HPV16 E7 positive patients) and controls (HPV16 E7 negative patients).

The OLED-based platform demonstrated 100% sensitivity for the detection of HPV16 E7 IgG antibodies. No negative samples were falsely identified as positive in this experiment.

4.5.6 Mechanically Actuated Multiplex Detection of HPV16 E2 and E7 IgG Antibodies in Human Plasma

To demonstrate the utility of the developed assay and OLED-based platform for multiplexed detection of biomarkers, recombinant HPV16 E2 and E7, BSA protein were immobilized on the same glass slide in a 1 x 3 array. The multi-antigenic slides were measured in the FlexDx platform by pushing the slides into the reader. Each site was sequentially aligned to the single-site reader using predefined notches. The design of an automated sequential-read multi-antigenic platform is the focus of subsequent chapters in this dissertation. The signal intensity measured from known HPV16 E7 and E2 positive patient plasma, indicated an elevated serum antibody levels to HPV16 E2, and E7 compared to the healthy controls. Table 6 reports the sensitivity and specificity for any Early (E2 and/or E7) protein. The overall

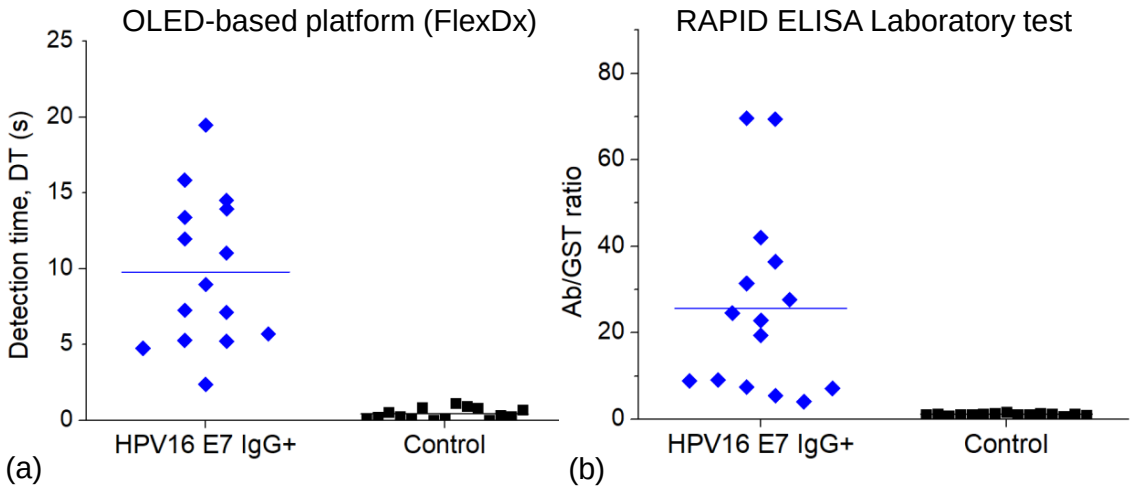

Figure 31: (a) OLED-based Platform Applied Toward the Detection of Biomarkers in Patient Plasma Samples. A Clear Separation Between Case and Controls is Observed. (b) Standard Laboratory Microplate-based RAPID ELISA Performance ($p < 3.6x10^{-6}$ in both systems).

sensitivity and specificity reported here is based on 29 randomly selected HPV16+ plasma samples and 39 controls comparing OLED POC platform (FlexDx), RAPID ELISA, and customer specific target values. The cutoff value for positive serology was determined using the mean of the response of the controls + 3 standard deviation according to the IUPAC definition.

Table 6: OLED-based, RAPID ELISA, and Target Sensitivity and Specificity for Any Early (E2, E6, E7) Protein in Patient Plasma.

Figure of merit	Sensitivity, SEN (%)	Specificity, SPC (%)
RAPID ELISA	83*	95*
FlexDx	58	95
Target†	50	80

* or better

†This research has been funded in part by the National Cancer Institute Cancer Detection, Diagnosis, and Treatment Technologies for Global Health [grant number CA211415]: "Rapid Point-of-Care Detection of HPV-associated Malignancies". The SEN and SPC target should account for local resources and skill level of health workers. Between day coefficient of variability should be $\leqslant$ 20%.

4.6 Summary

In this chapter, the utility of OLEDs as an excitation source for POC diagnosis of HPV has been demonstrated. The assay platform draws inspiration from microarray and RAPID ELISA techniques to develop a low-cost pre-screening tool for cervical cancer in resource-constrained settings (RCS). The radiant energy emitted by the organic light emitting diodes (OLEDs) used in this work, is capable of generating an excited state in fluorescent molecules. Recent advancements in flexible display technology based on organic electronics, therefore, presents a viable path toward

integrating a low-cost biorecognition assay with a highly sensitive and inexpensive fluorescence-based reader platform. An effective design strategy for low-cost fluorescence systems is to maximize the in-coupling of the excitation light toward the sample, minimize the excitation light reaching the detector, while maximizing the out-coupling of the emitted fluorescence, to increase the SNR. This approach ensures that the use of complicated transfer optics is minimized, enabling the use of small pixel size OLED arrays not only for high throughput applications, but also for multispectral analysis. This chapter detailed a design approach that uses interference filters for higher performance, compared to cross-polarizers previously reported in the literature. By using interference filters and charge-integration-based readout electronics, the developed system (FlexDx) has a 1000-fold lower noise floor than a system based on cross-polarizers with a lock-in amplifier. The developed system eliminates the use of transfer optics hence reducing cost, with the goal of designing a rugged and robust field-deployable platform for RCS. The limit-of-detection for IgG in human plasma is in the pg/mL range which approaches the performance standard central laboratory diagnostic instrumentation. Since UV and OLEDs across the visible light region have been demonstrated, it is not hard to imagine that high volume production of OLEDs would open new avenues for integrated high-throughput sensor platforms suitable for wearable applications, and for multiplexed multispectral analysis. The detection of serologic biomarkers (antibodies) for human papillomavirus (HPV) has been demonstrated. A high-risk HPV infection has been linked to cervical cancer, hence this effort has focused on the detection of HPV16 E2 and E7 IgG antibodies. The sensitivity and specificity of the platform compared to a standard laboratory-based ELISA, thus it is capable of providing clinical-level sensitivity for the detection of tumor-specific circulating IgG antibodies. For practical applications, the platform will be used as a pre-screening tool in RCS, to assist healthcare providers in decision making regard-

ing referral or follow-up. In this work, the limited shelf-life of OLEDs due to gradual degradation (even when pulsed), encapsulation, and cost currently limited the application of OLEDs for a variety of applications. The device degradation mechanism characteristics need to be better understood and compensated for in manufacturing and applications. For example, apart from the gradual decrease in intensity as the emissive layer degrades due to current induced, localized joule heating, there could be a slight spectral shift associated with the degradation. For most applications, a spectral shift of a few nanometers may not be noticeable, however, for narrow bandpass interference filter-based fluorescence applications, a spectral shift could drastically affect the overall system performance. Enhanced fluorescence light out-coupling, high optical isolation, direct deposition of thin film interference filters, and integrated microfluidics, although feasible, present a significant engineering challenge that is worth undertaking.

Chapter 5

FLUORESCENCE-BASED MULTIPLEXED ARRAY DETECTION PLATFORM DESIGN AND CHARACTERIZATION

5.1 Introduction

In Chapter 4, the use of organic light emitting diodes (OLEDs) was reported. The OLEDs were adapted from flat panel display technology, and used as the excitation source in a single-plex detection system. The detection of antibodies to human papillomavirus (HPV16) E7 protein was demonstrated using expensive interference filters. Compared to single-plex systems, low-cost, multiplexed diagnostic platforms are useful for disease diagnosis, making it possible for simultaneous detection of multiple analytes from a single patient sample volume. The detection of more than one biomarker is usually required to fully understand and diagnose a particular disease. Multiplexed systems have the potential to reduce cost per test, increase speed, and minimize both false positives and negatives.

This effort details a compact, multiplexed fluorescence detection platform. The design and assembly of a 2 x 2 array platform is presented, using inexpensive high-Q interference filters and readout electronics. The system leverages time integration of the output signal to improve accuracy by providing quantitative results. The platform is suitable for low-cost applications as the optoelectronic and optomechanic parts are designed from inexpensive off-the-shelf components, making it amenable to mass manufacturing. Visual colorimetric methods are still the dominant means of signal readout in most lateral flow assays. Labels used in a typical colorimetric assay are compared to fluorescent labels with the aim of highlighting the benefits

and properly quantifying the advantages of fluorescence without compounding the interpretation with assay dependencies including assay efficiency, repeatability, and reproducibility. By estimating the number of colored latex microspheres required for test line visibility Mansfield (2015) in a lateral flow assay, a comparison of similarly sized fluorescent latex microspheres is made. The LOD of the fluorescence-based approach is quantified, and the performance of the low-cost system is benchmarked against central laboratory fluorescence detection instrumentation. The platform is designed to read LFA test strips with 2 to 3 orders of magnitude enhancement in sensitivity over visual or reflected-light colorimetric readouts, hence it is capable of detecting biomarkers with clinical-level-sensitivity in a point-of-care fluorescence-based configuration.

This chapter focuses on the development of a low-cost, multiplexed fluorescence detection platform that has a high sensitivity and wide dynamic range. The system features inexpensive 3 mm x 3 mm interference filters with a high stop-band rejection, sharp transition edges, and greater than 90% transmission in the passband. In addition to the filters, the signal-to-noise ratio is improved by leveraging time for accuracy using a charge-integration-based readout. The fluorescence sensing platform provides a sensitivity to photon flux of $\sim$1x10^4 photons/mm^{2}sec and has the potential for 2 to 3 orders of magnitude improvement in sensitivity over standard colorimetric detection that uses colored latex microspheres. This effort also details the design, development, and characterization of the low-cost fluorescence detection platform and demonstrates 100% and 97.96% reduction in cross-talk probability and filter cost, respectively. This is achieved by reducing filter dimensions and ensuring appropriate channel isolation in a 2 x 2 array configuration. Practical considerations with low-cost interference filter system design, analysis, and system performance are also discussed. The performance of the platform is compared to that of a standard

laboratory array scanner. The study also demonstrates the multiplexed detection of antibodies to human papillomavirus (HPV16) E7 protein, as a potential biomarker for early cervical cancer detection in human plasma. This is performed by an automated readout sequence compared to the manual multiplexed detection demonstrated in Chapter 4.

First, the principle of operation, materials, and techniques used in the development of the inexpensive interference filter-based fluorescence system design and fabrication is presented. The characterization, experimental results, and system performance are discussed in subsequent sections. Initial tests performed to evaluate the system performance and discuss the characterization results, including cross-talk as a function of concentration is detailed. Finally, this chapter concludes with a discussion on the application of the system in disease diagnosis by demonstrating the detection of antibodies to HPV16 E7 protein, as a potential biomarker for early cervical cancer detection in human plasma. The techniques developed in this chapter are extended to higher density arrays presented in Chapter 7.

5.1.1 Materials and Methods

Previously, many groups have reported the use of interference filters in the design of compact fluorescence detection systems Thrush *et al.* (2003); Dandin *et al.* (2007); Banerjee *et al.* (2010a). However, some of the major challenges with such systems are the tight process control required in fabrication, difficulty in integration, and the prohibitive cost of interference filters Banerjee *et al.* (2010a). Furthermore, low-cost systems do not favor the use of laser excitation sources, PMTs, CCD, or CMOS based camera systems, mostly due to form factor and cost constraints. Other low cost options like gel/absorption filters, cross polarizers are not capable of providing the excitation source rejection required for high sensitivity and a low limit

of detection (see Chapter 4). Here, the design, construction, assembly, and testing of a prototype 4-site (2 x 2) fluorescence detection platform is detailed. The architecture borrows inspiration from typical laboratory-based fluorescence measurement devices like the epi-fluorescence microscope, array scanners, spectrophotometers, and spectrofluorometers. Common to these instruments is an optical path, which usually includes an excitation light source, focusing optics, filters, a photo detector, electronic readout, and signal processing circuits. A transillumination detection architecture with bottom-side illumination was adopted, eliminating expensive focusing optics, substituting laser/tungsten-halogen sources for light emitting diodes (LEDs), and using photodiodes in place of PMTs, CCD or CMOS cameras, thus ensuring a reduction in overall instrument cost and size.

5.1.2 Principle of Operation

A functional diagram for the prototype sensing platform is shown in Figure 32.

The system is divided into 5 modules detailed below. The excitation module (M1) comprises an 11.5 mm pitched 2 x 2 array of inorganic light emitting diodes (LEDs) that have a peak emission $\lambda = 520$ nm (SunLED, XZM2DG45S). The LEDs are mounted on a printed circuit board (PCB) as shown in Figure 33 (b). The LED broadband spectrum is filtered using a low-cost 3 mm x 3 mm excitation (520/40 nm) interference filter (Chroma Technology Corp.) mounted directly on each LED in the array. Filter mounting and assembly is discussed in Section 5.2.1. The LEDs function as excitation sources, which are sequentially turned on for each position in the array (designated hereafter as sites/channels A0, A1, A2, and A3) to interrogate a fluorescence biorecognition site or test line/spot in the sample chamber module (M2). The sample chamber is capable of holding glass microscope slides with or without mounted nitrocellulose membranes. The emission and signal readout mod-

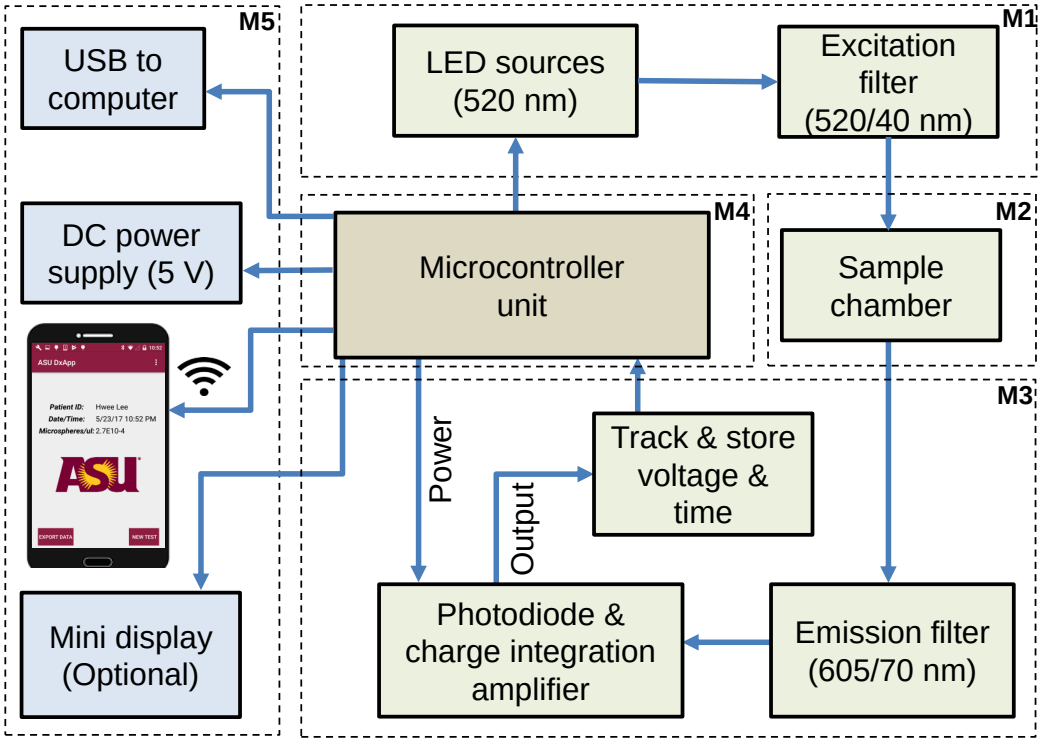

Figure 32: Functional Block Diagram of the System. The Platform Includes: an Excitation Module (M1) Consisting of LEDs (520 nm Center) and Excitation Filters (520/40 nm); a Sample Chamber Module (M2, that Accommodates a Microscope slide, Nitrocellulose Membrane, or Cassette; an Emission and Signal Readout Module (M3), Consisting of Emission Filters (605/70 nm), Photodiodes, and Charge Integration Readout Electronics; a Microcontroller Module (M4), at the Heart of Sequence Control, Power, and Data Processing; a Display and Connectivity Module (M5) Which Includes an Optional Mini Display that Prompts and Presents Results to the User. A Smart-phone with a User Interface Establishes Data Connectivity Via Bluetooth, Shows Device Status, and Displays Results with the Capability of Uploading the Information for Cloud-based Processing and Interpretation by a Primary Care Physician.

ule (M3) captures the weak fluorescence signal re-emitted at a longer wavelength (Stokes shift). The emitted fluorescence passes through an emission filter (Chroma Technologies, 605/70 nm) and is detected using coaxially aligned photodiodes (Advanced Photonix Incorporated, Camarillo, CA, USA, PDB-C139, responsivity, R(λ) of $\sim$0.2 to 0.3 A/W from 550 to 650 nm and a 59° viewing angle). The photodiodes are connected in photovoltaic mode as part of a low-noise charge-integration amplifier readout (LMC6041IN, National Semiconductor). The readout circuit is shown in Figure 33 (a), with a dedicated charge integrator, LED, photodiode, and filters for each channel.

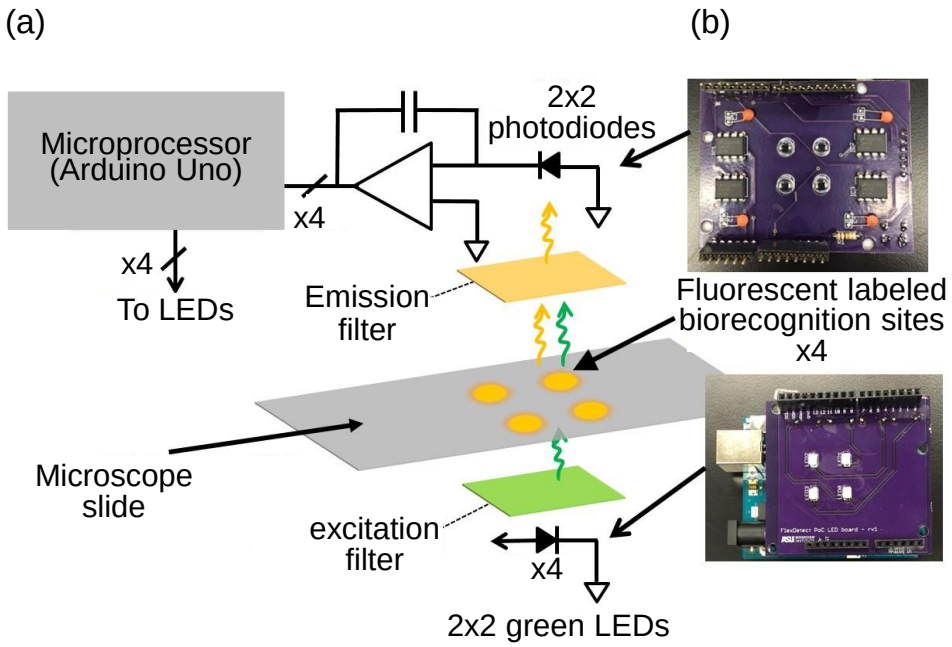

Figure 33: Schematic, Prototype Board, in a 2 x 2 Array Fluorescence Detection Platform. (a) Circuit Schematic Showing Charge-integration Amplifier Readout Circuit, 2 x 2 Biorecognition Sites on a Microscope Slide and LEDs Used as the Excitation Source (b) Printed Circuit Board (PCB) Showing 2 x 2 Photodiode and Amplifiers as well as the 2 x 2 LEDs Soldered.

Figure 34 (a) depicts the optomechanical design structure that houses the 25 mm filters shown in Figure 34 (b), apertures and isolation structures for each LED and photodiode for each channel in the array. The optomechanical structure provides a slot for a microscope slide, on which the biorecognition elements have been immobilized. Figure 34 (c) shows the 3 mm x 3 mm filters deposited on a 6 inch substrate and diced to size while Figure 34 (d) shows the assembled 2 x 2 system with a tray in front to insert the microscope slide.

The magnitude of the current generated by the photodiode, I, is proportional to the fluorescence power or intensity reaching the photodiode Guilbault (1990); Banerjee *et al.* (2010a); Sze (2007); Thrush (2004) and could be written as

$$I = KI_0(\lambda)[1 - e^{-\epsilon(\lambda)lc}] \tag{5.1}$$

where, c, is the molar concentration; l, is the optical path length through the sample; $\epsilon(\lambda)$ is the extinction coefficient or molar absorptivity of the fluorophore; $I_0(\lambda)$, is the excitation source (LED) intensity; K, is a lumped constant that depends on photodiode responsivity, $R(\lambda)$; collection efficiency of the system, η_{LCE}; excitation, $T_X(\lambda)$ and emission, $T_M(\lambda)$ filter transmission, and fluorophore quantum yield ($QY_{fl}(\lambda)$). Optical spectra are shown in Figure 36 (e). The photodiode responsivity $R(\lambda)$, is plotted on the secondary axis. The output of the system is a fluorophore concentration-dependent voltage ramp which is inversely correlated with the slope of the voltage-time profile and written as

$$V_{out} = \frac{1}{C}\int_0^T [KI_0(\lambda)((1 - exp(-\epsilon(\lambda)lc)) + I_B]dt \tag{5.2}$$

where I_B represents total noise current (I_{dark}+I_{leak}+I_{noise}). Equation 5.2 models sensor output voltage as a function of system parameters, photodiode output current and time. This equation is useful for predicting the output voltage profile over time

and determining system performance during the design stage. Details of the derivation and an example predicting the system response has been presented previously in Chapter 3. By leveraging time for accuracy, this technique ensures high sensitivity, as it can detect weak fluorescence signals above the noise floor. Furthermore, this readout method enables inexpensive electronic processing as high speed circuits

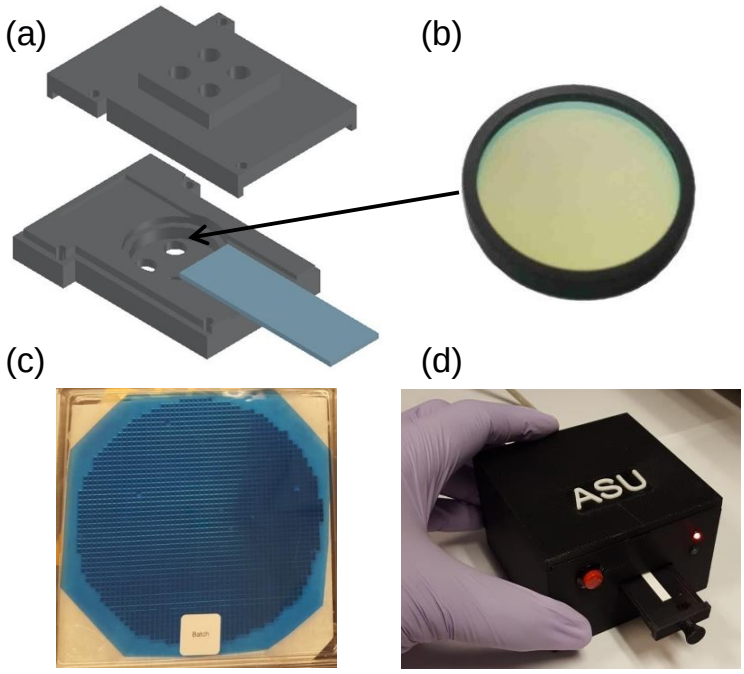

Figure 34: CAD drawing of Optomechanical Assembly and Filters in a 2 x 2 Array Fluorescence Detection Platform. (a) 3D Printed Optomechanical Assembly Showing Apertures for Excitation Sources, Holders for Filters, Slot for Microscope Slide, and Aperture to Fit Photodiodes on the Top Piece (Emission Filter Slot on Reverse Side) (b) 25 mm Filter Typically Used in Fluorescence Microscopy; Arrow Points to 25.3 mm Diameter Slot in 3D Printed Assembly Shown (c) 6 Inch Filter Dielectric Stack Deposited on a 1 mm Thick Substrate and Diced to ∼3 x 3 mm (Not to Scale) (d) Fully Assembled System. Houses the Stacked Microcontroller Board, PCBs, and 3D Printed Assembly Packaged Fitted in the Opaque 3D Printed Enclosure. Access Tray Open in Front to Show Insertion of a Sample.

and/or high accuracy analog-to-digital converters are not required since the system averages the measured signal over a relatively long time period (30 to 60 sec). At the center of the system, providing sequencing and control is the microcontroller module (M4) implemented with an Arduino Uno, that monitors, acquires, and digitizes the amplifier output voltage, recording time taken for the output voltage to rise to the voltage rail of the amplifier (ramp-time, RT). As discussed in previous chapters, the RT is inversely correlated with the sample concentration as a higher fluorophore concentration implies more light, a steeper slope, and thus, a smaller RT. The detection time (DT) as the ramp time difference between a negative control or reference sample and a sample under test. Detection time is directly correlated with sample concentration or fluorescence intensity. A completely miniaturized configuration that would be paired with a smart-phone via Bluetooth communication is therefore achievable. User instructions and data would be issued, transmitted, and saved on the smart-phone or remotely in the cloud. The microcontroller module was programmed to control the ON and OFF sequence of the precisely aligned LED-photodiode pairs. Each LED-photodiode pair is sequentially turned on, and the time taken to reach a predefined threshold voltage is recorded and stored. The display and data connectivity module (M5) comprises an OLED display (optional) and a smart-phone or computer that prompts the user, analyzes the data, and displays/reports the results of a test. The optomechanical housing for the system was printed at 100% density on a Stratasys Dimension 3D printer using acrylonitrile butadiene styrene (ABS) plastic. An exploded view drawing is shown in Figure 35 (all units in mm).

5.2 Experimental Procedure

5.2.1 Low-cost Interference Filters

The fluorescence-based systems detailed in Chapters 3 and 4 used relatively expensive 25 mm filters ($650 excitation and emission set) in a single-site configuration. To reduce the cost of the array platform and efficiently increase the array density the use of smaller dimension filters was adopted. Working in conjunction with Chroma Technologies, the filter quality ∼OD 6 in the stop-band, substrate requirements, and cost, led to the production of the 3 mm x 3 mm filters discussed in this chapter. The 3 mm x 3 mm filters were mounted directly on the LEDs and photodiodes using optically clear UV curing adhesive, (NOA63, Norland Prodcuts Inc., NJ, USA) as shown in Figure 36 (a) and (c), respectively. The top surface of LEDs and photodiode was

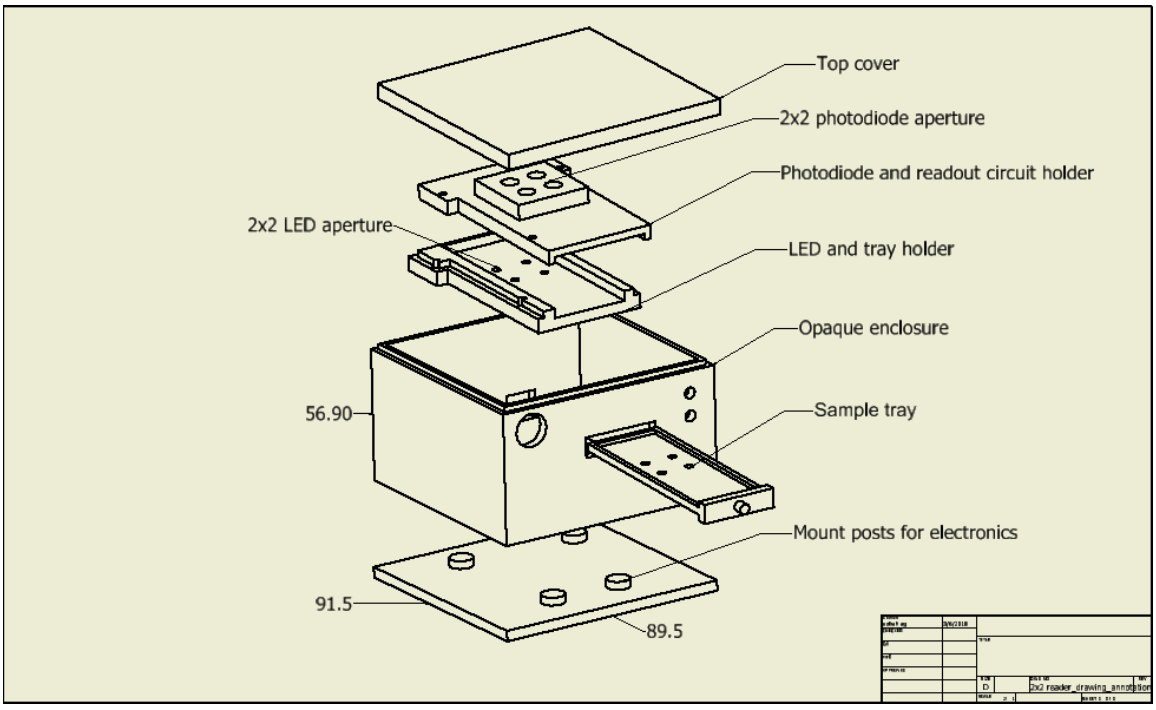

Figure 35: Exploded View Drawing of the 3D Printed Optomechanical Components and Housing.

coated with epoxy, and the 3 mm x 3 mm filters were centered using a mask and forceps. The assembly was then exposed to UV light using a hand-held UV lamp (Spectroline EN-180, Spectronics Corp. NY, USA) for 5 minutes. The side walls of the assembly were then coated with an opaque paint to block light leakage through the sides of the photodiode and filter substrate.

Additionally, a 0.5 mm margin was coated around the top surface of the filters to block leakage light through the notches and imperfections as a result of the dicing process. The assembly was left to air-dry under ambient conditions for 24 hours. A 2 x 2 aperture array configuration fitted with 25 mm filters was also fabricated, and the configuration is shown in Figure 36 (b) and (d). Apertures were created in the 3D-printed structures for each site, and a filter slot was incorporated into the design. The performance of the 25 mm system was compared to the 3 x 3 mm filter system by measuring the intensity of the response from known fluorophore concentrations and by cross-talk characterization. Previously, cost-prohibitive interference filters (25 mm diameter) used in Filter Cubes for fluorescence microscopes, would render the cost of optoelectronic platforms like ours impractical, especially for the deployment of high-performance diagnostic devices, in low and middle-income countries (LMICs). Compact and integrated fluorescence-based systems are limited by the optical noise/background mostly dominated by excitation light leakage reaching the detector. This is further aggravated by the fact that it is desirable to have the excitation light source in close proximity with the sample and with the detector Thrush *et al.* (2003). The low-cost 2 x 2 array platform addresses this issue. In the 25 mm 4-site system reported here as well as the single site system previously reported in earlier chapters, the 25 mm diameter filter set (excitation and emission) costs $625, whereas the 3 x 3 mm individual filter set on each channel costs $3.18 and thus, a total of $12.72 for all four channels (for a production quantity of 1,000 pieces). The

cost of these filters at production quantities greater than 100,000 is less than $1 each.

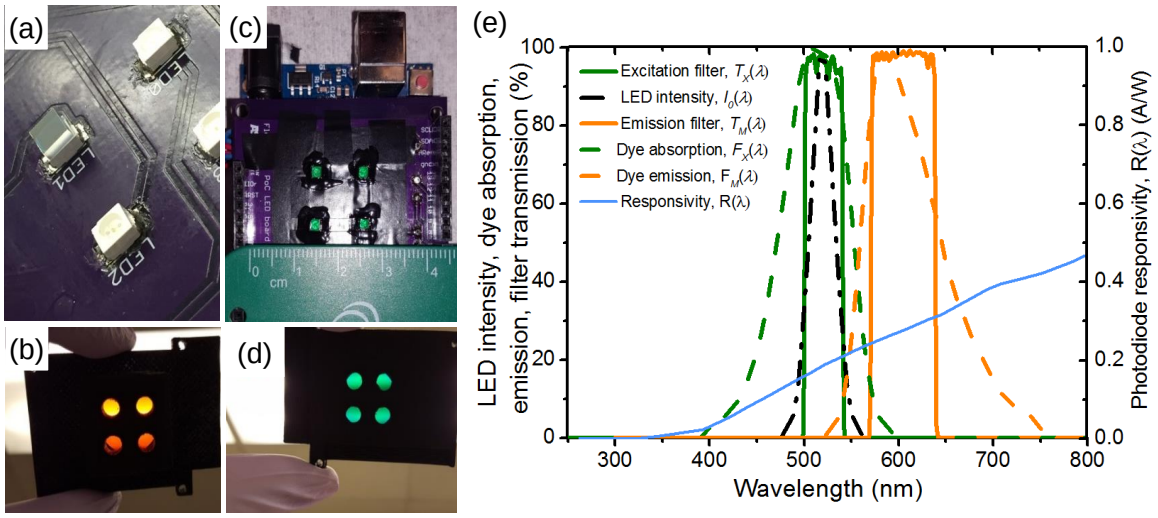

Figure 36: Low-cost Filter Assembly, Alignment on LEDs, Apertures, and Optical Design of a 2 x 2 Array Fluorescence Detection Platform. (A) 3 mm x 3 mm 520/40 nm Green Excitation Filter Mounted on an LED and Cured with a Clear UV Curing Adhesive (Top Left, Marked LED1) (B) 2 x 2 Aperture Array in a 3D-printed Optical Isolation for Orange Emission Filters (a Single 25 mm Diameter Filter Ring on Reverse Side) (C) 3 mm x 3 mm, 520/40 nm Green Excitation Filter Mounted on LED, Cured with UV Adhesive and the Walls Coated with an Opaque Paint (D) 2 x 2 Aperture Array in a 3D-printed Optical Isolation for Green Excitation Filters (25 mm Diameter Filter Ring on Reverse Side) (E) LED Intensity (Left Dash Dot), Fluorophore Absorption Spectra (Left Dashed) and Fluorophore Emission (Right Dashed), Excitation (Left Solid) and Emission Filter (Right Solid) Transmission Spectra. The Filters Were Chosen to Match the Excitation Light Source, Peak Excitation and Emission Spectrum of the Fluorophore. The Fluorophore Was Chosen to Match the Led Peak Emission. The Photodiode Responsivity, $R(\lambda)$ is Plotted on the Secondary Axis.

This represents a significant reduction in filter cost by 97.96% without compromising device performance.

5.2.2 Multiplexed Platform Characterization

Nile red fluorescent microspheres (1 μm diameter, product no. F-8819, lot no. 1154194, specified absorption/emission peak/center wavelength 535/575 nm, molar absorption coefficient, ϵ, 37859 M^{-1} cm^{-1}, relative quantum yield, QY_{fl}, 0.19) were purchased from Life Technologies, CA, USA. These fluorescent particles were designed by entrapping Nile red fluorophores in latex spheres. The microspheres were intentionally chosen as the dye has a good match for the excitation spectrum of the LEDs. The filters described above in Section 5.2.1, were also designed to match the absorption and emission spectra of the fluorophore. The filter set ensures the dye is excited at peak absorption and that peak emissions are collected, while significantly rejecting excitation light. To reduce the excitation light reaching the detector, an orange emission filter with sharp transition edges was used as shown in Figure 36 (e).

To characterize the 2 x 2 platform, samples of spotted fluorophores were prepared. Microscope slides were pre-treated with 2% 3-Aminopropyl-ethoxysilane (APTES) purchased from Sigma Aldrich, and prepared by dissolving 12 mL of 99.5% APTES in 600 mL of acetone. The slides were submerged in APTES solution for 15 mins, rinsed 5x in acetone, followed by a deionized (DI) water rinse, and then blow-dried with compressed air. The microspheres were diluted in DI water (Milli-Q system, Millipore, MA), immobilized, and dried on the pre-treated microscope slides (VWR Microscope slides, 75 mm x 25 mm x 1 mm). To prevent agglomeration, the Nile red microspheres were first sonicated for 5 minutes before use. A log dilution series was prepared, and test samples were spotted (N=5) using a silicone-well template cut-out for precise and repeatable location of test spots in the 2 x 2 array. Four 2.3

mm diameter holes, with an 11.5 mm pitch (same as LED and photodiode pitch) were laser cut (Universal Laser Cutter, VLS 6.60) in a 3 mm thick Silicone Isolator sheet (GraceBio, OR). Silicone sheets were brought in contact with the surface of the APTES coated glass slides, and fluorophore dilutions were pipetted into wells minimizing sample spreading on the glass slide and preventing misalignment of the samples in the optical path. Five slides for each dilution (1:10 to $1:10^6$) were prepared and spotted at 37°C on a hot plate (Torrey Pines Scientific, CA) to accelerate sample drying.

To estimate the LOD of the 2 x 2 platform, fluorescent samples (N=3) were prepared by logarithmically varying the concentration over 7 orders of magnitude to determine the dose response. Half-log and log-dilutions were then prepared (N=10), to add more points to the dose response curve and estimate the LOD at low concentrations. The 0.5 μm fluorescent microspheres (Millipore, F-Y050), are supplied as a suspension in water, sodium azide (NaN_3), PBS and Tween20. Corresponding blank samples were prepared (N=10) using diluted samples of 2mM NaN3, and PBST in DI water to account for the solvent. The confidence level was determined by the point on the response curve where the analyte concentration was reliably different than the blank with a high level of confidence (k=6). A five-parameter logistic fit was applied to fit the data points. The system photon sensitivity, optical signal-to-noise (SNR), and cross-talk were evaluated as presented in Section 5.3.2 and Section 5.3.3.

5.2.3 Detection of Antibodies to HPV16 E7 Protein in Human Plasma

Glass microscope slides (VWR International) were treated with 2% aminosilane (Pierce) for 15 minutes at room temperature, rinsed with acetone, DI water, dried with compressed air, and inspected for imperfections. All proteins (E7, BSA, and IgG) were diluted in DI water to 25 ug/mL. HPV16 E7 Protein was spotted on two

of four sites on the aminosilane-treated slides at room temperature. A template was used to ensure that the sites were aligned to the optical path (channels) in the 2 x 2 array platform. For controls, 5 μL of BSA (negative control, 25 μg/mL) and 5 μL of whole human IgG protein (positive control) were spotted on the other two sites on the aminosilane-treated slides at room temperature. Slides were stored at 4°C overnight and blocked with 5% milk-PBST for one hour at room temperature. Plasma samples were diluted 1:1 in 5% milk-PBST, incubated on the slides for one hour at room temperature and washed with PBST (0.2% Tween in 1XPBS). Two labeling methods were used as the secondary capture antibody conjugate to detect the presence of human IgG antibodies specific for HPV E7 proteins: Dylight 549-conjugated AffiniPure goat anti-human IgG (Jackson ImmunoResearch Laboratories, Inc.) and 1 μm Nile red microspheres-conjugated AffiniPure goat anti-human IgG. Slides were incubated with secondary antibodies diluted 1:50 for one hour at room temperature in the dark, rinsed 3X with PBST (0.2% Tween in 1XPBS), DI water, dried with compressed air, and analyzed with the 2 x 2 array platform.

5.3 Results and Discussion

5.3.1 Performance Characterization: Analytical Sensitivity and Limit of Detection (LLOD)

To evaluate the performance of the multiplexed fluorescence 2 x 2 array platform, microscope slides prepared as described above in Section 5.2.2 were inserted into the sample chamber and analyzed. To ensure that performance of each channel was identical, the 2 x 2 array was characterized with all four sites containing the same concentration per microscope slide (N=5), for the entire dilution series. The results were then compared with a top-of-the-line laboratory array scanner. The rep-

resentative images shown in Figure 37 (a) were acquired using microarray scanner, (PowerScanner, Tecan), typically used in the analysis of high-density DNA and protein microarrays. The samples were scanned (PMT gain = 50%; green laser power = 50%) and the images analyzed and quantified with Array-Pro Analyzer software. The

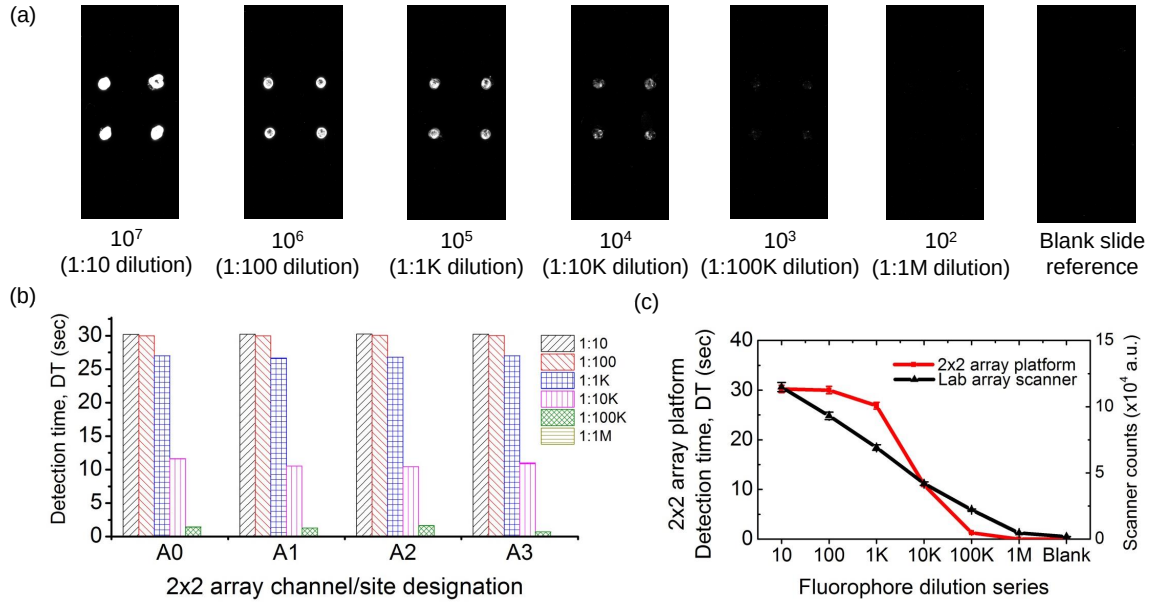

Figure 37: A Comparison of the Low-cost 2 x 2 Array Platform and a Top-of-the-line Laboratory Array Scanner. (A) Representative Laboratory Array Scanner Images of Nile Red Fluorescent Microspheres Spotted with a Silicone Well. Below Each Image is the Estimated Number of Microspheres on Each Spot and the Dilution (in Parenthesis) (B) Detection Time (DT) Response to the Fluorophore Dilution Series from 1:10 to 1:1M, Measured by the 2 x 2 Array Platform. Each Set of Bars Show All Four Sites/Channels (A0, A1, A2 and A3) and Their Responses (C) Comparison of the Responses of Laboratory Array Scanner and the 2 x 2 Array Fluorescence Detection Platform. Dilution Series: 1:10, 1:100, $1{:}10^3$, $1{:}10^4$, $1{:}10^5$ and $1{:}10^6$ Are Denoted as 10, 100, 1k, 10k, 100k, and 1M; Corresponding to 10^7, 10^6, 10^5, 10^4, 10^3, and 10^2 Microspheres Respectively.

system response/signal intensity expressed as a detection time (DT) for each channel for all concentrations is compared as shown in Figure 37 (b), with a blank slide used as the reference. The detection time was obtained as described previously in Section 5.1.2. Integration time for the reference was 32 sec per channel. All channels (A0 to A3) produced identical performance for each set of slides and slight variations were primarily due to spotting variability, accounting for 500 msec maximum deviation (not visible on the scale of the plot) in Figure 37 (b). The counts (a.u.) from the array scanner and the detection time, DT (sec), from the low cost 2 x 2 array platform are compared in Figure 37 (c). Results indicate that the low-cost platform has a nonlinear response at higher concentrations and that the performance is within an order of magnitude of the laboratory microarray scanner. The difference between the POC and conventional laboratory instrument response result from the fact that the laboratory array scanner has extensive signal acquisition and processing tools that enables "auto-gain", such that the system adaptively adjusts the gain in the saturation regions and normalizes the result to an internal standard. System parameters, including the gain-capacitor size (integration time), voltage range, overall noise, and background in the optical path, play an important role in the performance of the array platform. The low-cost 2 x 2 array fluorescence detection platform can reliably detect $2x10^4$ 0.5 μm diameter fluorescent microspheres on a glass substrate with a signal-to-noise (SNR) ratio of 2:1 at a 99.73% confidence level. The LOD was determined as the concentration corresponding to the mean plus six standard deviations. Instrument errors (a few tens of milliseconds), errors due to pipetting, and variations in glass slides are included in the relative standard error as computed and shown in Figure 37 (c). Applying a simple and low-cost integration technique, the 2 x 2 array platform achieves high sensitivity by separating out the low-intensity or weak fluorescence signal over an established, relatively higher background intensity.

To determine the LOD for the platform, a representative dose response curve obtained from log and half-log dilutions of 0.5 μm microspheres is shown in Figure 38. Here we used 0.5 μm diameter fluorescent microspheres since 0.5 μm colorimetric microspheres are widely used in colorimetric applications in visual and instrumented lateral flow assay Mansfield (2015); Mak *et al.* (2016) (see Section 5.3.5).

A five-parameter logistic fit has been applied here and the red horizontal dashed line indicates the mean of responses of the blank measures plus 6 standard deviations.

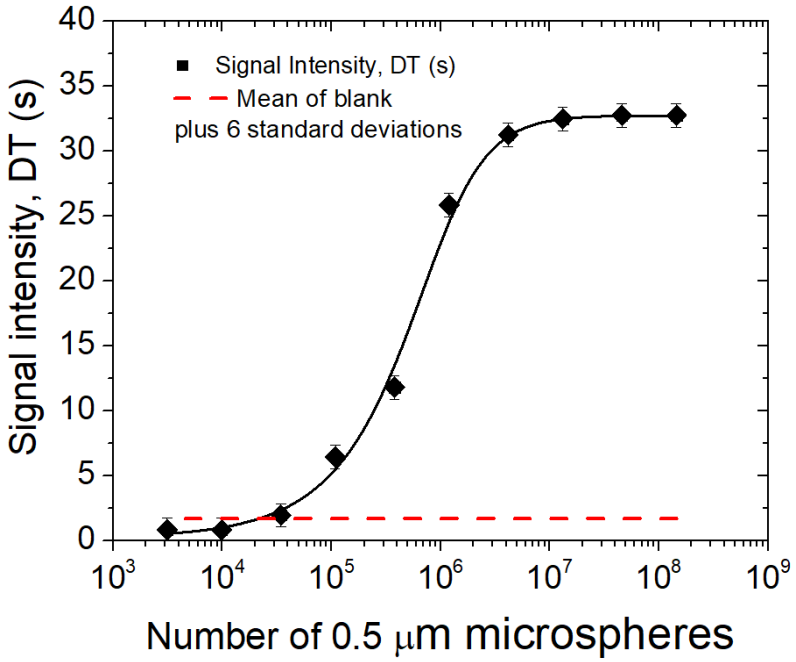

Figure 38: Representative Dose Response Curve for the 2 x 2 Array Platform. Microsphere Concentration Varied in Log and Half-log Steps from 3.13x10^3 to 4.59x10^7 Microspheres (10 Replicates). The Response from Sample Concentrations Less than 1x10^4 Microspheres are not Distinguishable from the Blank Measures. Repeated Measures of the Blank are Indicated (with 6 Standard Deviations) on the Error Bars. The LOD Is Calculated as the Concentration Corresponding 6σ above the Mean of the Blank Responses (LOD 2.1x10^4 at 99.73% Confidence).

The LOD is extracted from the corresponding concentration (LOD = 2.1x10^4 microspheres with 99.73% confidence level). To benchmark the LOD of the system against a lab scale array scanner (Tecan), we applied the same method described above. The LOD was determined to be 2.2x10^3 microspheres at a 99.73% confidence level. The LOD of the 2 x 2 array platform is within an order of magnitude of a central analytical lab device. Previously, we have determined the LOD by visual inspection of the response curve and conservatively selected the LOD. Other methods to calculate LOD has been used widely in literature as discussed in Chapter 2. Particularly the LOD is calculated using the equation: $LOD = \kappa\sigma/SEN$ where the sensitivity, $SEN = dr/dc$ (the slope of the linear dynamic range of the sensor response, i.e. the change in response, dr, due to a small change in concentration, dc; κ has a value of 3 or 6 and σ is the standard deviation. Because the slope changes from one region to the sigmoidal dose response curve, the calculated LOD based on this technique depends on the region of the curve chosen.

5.3.2 Photon Sensitivity and Optical Signal-to-noise Ratio

Photon sensitivity was determined by measuring power density of the lowest detectable sample concentration. The readout circuit was replaced by an optical power meter (Newport, 1830-C) fitted with a calibrated photodiode (818-SL). A power density value of 27.5 pW/cm^2 was measured (after correcting for background and ambient light). The photon flux (photons/m^2sec), was calculated by dividing the power density by the available photon energy (Joules or Wsec) due to fluorescence emissions (taking into account necessary unit conversions and background noise). The system is sensitive to a photon flux of $\sim$1x10^4 photons/mm^{2}sec at a signal to noise ratio of 2:1. The SNR is defined as the ratio of the emitted fluorescence power (F) to the total noise power level (N). The SNR decreases from 1000:1 at the highest concentration to

an SNR of 1:1 at 1:10^5 dilution. The relatively weak optical signals from fluorophores make SNR analysis very important. As with any fluorescence sensing platform, the amount of fluorescence signal is usually measured alongside undesired sources of light, which contribute to the noise or background level. These include: excitation source (LED) leakage light through the filters (imperfect absorption edges from tiny variations in thin film layer depositions and shift in absorption edge as angle of incidence varies), ambient light leakage and stray light within the enclosure, background and autofluorescence, and electronic contributions such as fluorescence noise (shot noise) and dark current in the photodiode/readout circuit.

5.3.3 Cross-talk Characterization

Cross-talk is caused by light leakage in the system housing, off-axis excitation light transmission through the filters due to oblique incidence, and scattering in the sample chamber. The high performance of interference filters are limited to normal incidence, and undesirable off-axis light at oblique angles will go through the filters with almost no attenuation. This is due to the fact that there is a significant shift in the absorption edge as the incidence angle is varied Chediak *et al.* (2004). The fluorescence detection systems discussed in previous chapters used 25 mm filter sets. Although the light collection area is larger and alignment is easier, the 3 mm x 3 mm filters perform equally well in terms of the LOD and even better as the cross-talk is eliminated by reducing the filter size and using aperture stops integrated into the optomechanical design. To perform the cross-talk measurements, the LED at site A0 was used as the reference excitation source, the readout circuit for the other channels were sequentially turned on and ramp time was recorded. Here, we compute the cross-talk probability (CP) as the difference between the ramp times for the active readout channel (A_i) and the reference excitation channel (A_0) divided by the ramp

time of the reference excitation channel as shown in Equation 5.3,

$$CP = \left[1 - \frac{(A_i - A_0)}{A_0}\right] * 100\% \tag{5.3}$$

where A_i denotes the channel in the 2 x 2 array for i = 0, 1, 2, 3. Two configurations were analyzed: one with a single 25 mm filter positioned over all four channels and the other with the individual 3 mm x 3 mm filter positioned on each channel. The data in Figure 39 shows a concentration dependence of the cross-talk which decreases as analyte concentration decreases in the 25 mm system (a) - (g).

Figure 39 (h) shows the 2 x 2 array platform with zero cross-talk detected even at the highest concentration. This ensures that the measured responses are an accurate representation of the sample under test. Furthermore, with zero cross-talk on each channel, it is worth investigating the implementation of a parallel processing system as long as a near perfect isolation is achieved in the system housing design. Parallel array processing, also decreases the time from sample-to-answer in a multiplexed system. To this end, the cross-talk present at each detection site/channel due to adjacent fluorescent labels is characterized. Selecting an appropriate opaque materials and limiting the aperture size are key factors to reducing cross-talk. One method to reduce cross-talk is to ensure normal incidence or limit off-axis light by constricting the aperture size or by increasing separation between detection sites (array pitch). The latter is not desirable as it leads to larger and more expensive filters for single filter systems and lower array density. The cross-talk is eliminated with the 3 x 3 mm filters.

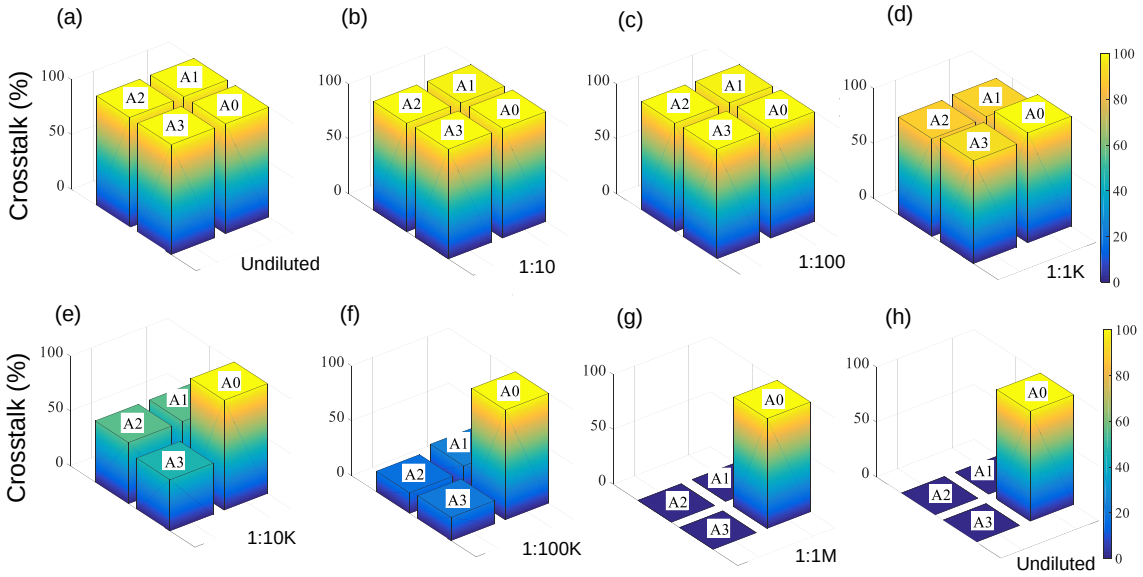

Figure 39: Cross-talk Comparison in 25 mm and 3 mm x 3 mm Filter Systems as a Function of Fluorophore Concentration Spotted on Site A0 Only. (a) to (g) Show Concentration Dependent Cross-talk in the 25 mm System, Obtained from 10 μL Samples of Nile Red Microspheres Spotted at Concentrations Ranging from the Stock Concentration (Undiluted, 10^8 Microspheres/mL) to 10^2 Microspheres/mL (1:1M Dilution) on Site A0. Dilutions are Indicated below Each Plot. The Signal at Adjacent Blank/Negative Channels is Measured by Exciting Channel A0 but Sequentially Turning on the Readout Circuit at Channels A1, A2, and A3. (h) Shows Zero Cross-talk in the 3 x 3 mm System Even with the Highest Concentration (Undiluted) on Channel A0. 10 μL of Stock Concentration was Spotted on a Microscope Slide at Site A0 and No Detectable Signal on Any Reference Channel was Observed; Compare (a).

5.3.4 Fluorescence Immunoassay for the Detection of Antibodies to HPV16 E7 Protein in Human Plasma

The Center for Disease Control and Prevention and the World Health Organization (World Cancer Report) indicates that HPV is the most common sexually transmitted infection (STI) with HPV16 and 18 strains of the virus being responsible for more than 70% of all cervical cancer cases. HPV is an infectious disease with almost 70% of the global burden occurring in developing countries. It is the fourth most common cause of cancer deaths in women accounting for 266,000 deaths worldwide in 2012. Although preventable, vaccines are not a treatment for pre-existing infections. Screening in the developed world is currently performed by cytology requiring access to central laboratory facilities. To deliver clinical-level sensitivity at the point-of-need, a multiplexed, high-sensitivity platform is required, especially for early detection. In this section, the utility of the 2 x 2 array platform for detection of antibodies specific to HPV16 E7 protein in patient plasma is demonstrated. Herein, fluorescent microspheres are used with an aim to translating the assay developed in Chapter 4, to a nitrocellulose-based lateral flow assay format (see Chapter 7). The microsphere conjugation protocol is included in the Appendix A. HPV16 E7 protein/antigen, was printed on APTES functionalized glass. Human HPV16 E7 specific IgG Abs from patient sera (primary antibody) was incubated with the immobilized protein. HPV16 E7-specific IgG antibodies in patient plasma samples were detected using a goat anti-human IgG-fluorescent microsphere conjugate. Goat anti-human IgG antibody was conjugated to the 1 μm fluorescent microspheres and DyLight549 (secondary antibody conjugate) and incubated with the captured E7-specific plasma antibodies. The secondary antibody conjugate was used as the fluorescent detector label/probe. The goat anti-human IgG antibody binds specifically to the constant

region of human IgG antibodies. Thus, during the patient sample incubation, E7-specific IgG antibodies in the plasma will bind to the E7 antigen printed on the substrate. Other IgG antibodies present in the sample will be washed away during the wash steps so that during the secondary antibody incubation, the E7-specific IgG antibodies bound to E7 antigen are labeled with the goat anti-human IgG antibodies conjugated to fluorescent microspheres. Results are shown in Figure 40 (a) - (d). The measured responses using the 25 mm filter system is shown in Figure 40 (a) and (b), and the 3 mm x 3 mm system in Figure 40 (c) - (d), with the Nile red and DyLight549 labels, respectively. Triplicate slides were incubated with selected plasma samples from 2 patients, one with known antibodies to the HPV16 E7 protein and one negative, respectively. These samples were probed with DyLight549 and microsphere conjugates respectively, and tested on the 25 mm and 3 mm x 3 mm filter systems. The signal intensity for the microsphere conjugate was relatively higher than the Dylight conjugate, although the microsphere conjugates indicate a significantly higher background level due to non-specific binding (NSB) of the microspheres to the glass substrate and non-specific reaction in the negative control plasma sample. The performance of both systems are comparable in detecting both labels. This further supports the hypothesis that reducing the filter dimensions will not only reduce cost, but also improve the overall performance of the platform. Hand-spotting and non-specific adsorption are the most likely causes of variability indicated by the error bars. To resolve these problems, we recently procured a pressure-time dispensing unit even as we continue to explore effective blocking strategies to reduce NSB and intrinsic fluorescence of substrates.

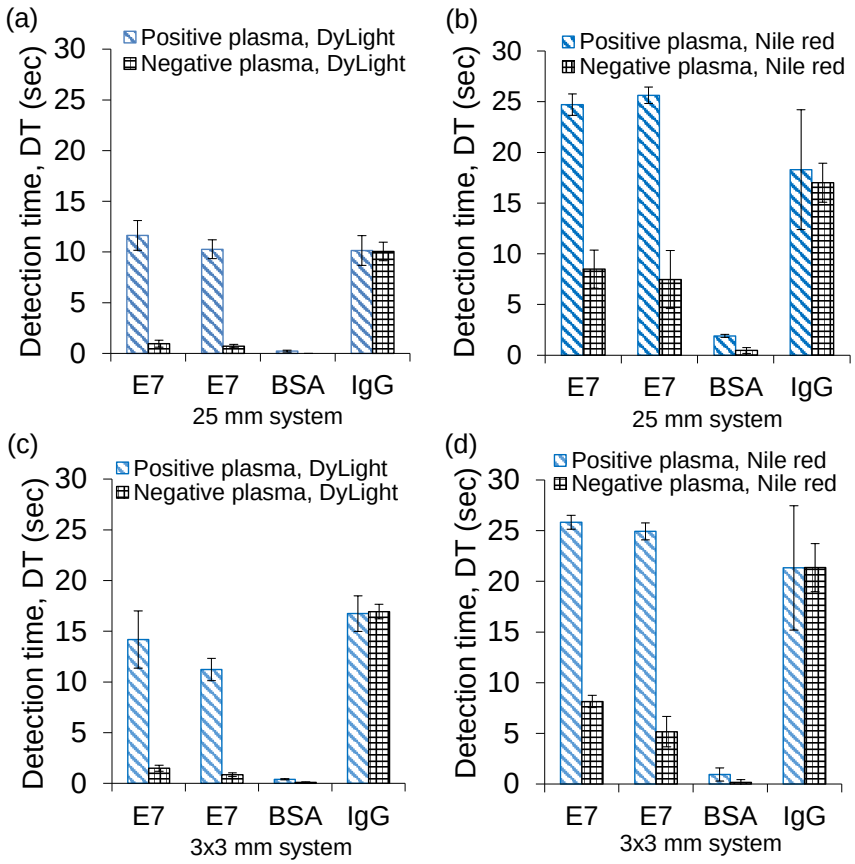

Figure 40: Low-cost Array Platform Applied in the Detection of Antibodies to HPV16 E7 Protein, Using Two Secondary Labels. Patient Plasma Positive for Antibodies to HPV16 E7 and a Negative Control Plasma Were Used. (a) Positive and Negative Patient Plasma Probed with DyLight549 and Analyzed with 25 mm Filter System (b) Positive and Negative Patient Plasma Probed with Nile Red Microspheres and Analyzed with 25 mm Filter System (c) Positive and Negative Patient Plasma, Probed with DyLight549 and Analyzed with 3 mm x 3 mm Filter System (d) Positive and Negative Patient Plasma Probed with Nile Red Microspheres and Analyzed with 3 mm x 3 mm Filter System.

5.3.5 Predicted Sensitivity Gains Using the Fluorescent Biorecognition Platform in Lateral Flow Immunoassay Tests.

In this Section, the potential improvement of colorimetric assays using the low-cost 2 x 2 array fluorescence platform is evaluated by directly testing the system with colored and fluorescent labels on nitrocellulose strips and comparing the results. A more detailed comparison is presented in Chapter 6. This approach compares labels used in a typical colorimetric assay to a fluorescent label with the aim of highlighting the benefits and properly quantifying the advantages of fluorescence without compounding the interpretation with assay dependencies including assay efficiency, repeatability and reproducibility. A very common label used in colorimetry is 0.5 μm diameter blue colored polystyrene/latex microspheres. To match the size of the colored latex microspheres, 0.5 μm diameter fluorescent polystyrene microspheres (F1-Y 050, Merck Millipore) was used. Many lateral flow assays use 0.3 μm to 0.5 μm diameter microspheres to ensure good mobility in porous membrane structures with average pore size of 8 to 15 μm Wong and Tse (2009); Mansfield (2015). Nitrocellulose sheets (HF18004XSS, Merck Millipore) were laser cut to 5 mm x 50 mm strips. The strips were mounted on microscope slides with a transparent adhesive and aligned to the optical path using a pre-printed template. For this study, the single site/channel fluorescence detection system to accommodate the rectangular nitrocellulose strips. A circular aperture (5 mm diameter) was used to precisely align the LED-photodiode pair. Filters were mounted on the LEDs and photodiodes as described previously in Section 5.2.1. A dilution series of the blue latex microspheres (K1 050 Blue, Merck Millipore) was prepared by diluting 10 μL of the stock (10^{10} microspheres) from 1:10 to 1:100k (10^5 microspheres) at which point the blue color was no longer visible to the eye as shown in Figure 41 (a). A similar dilution series of fluorescent polystyrene

microspheres (F1-Y 050, Merck Millipore) was also prepared but this time diluting 10 μL of the stock concentration (10^9 microspheres) down to 1:1M (10^3 microspheres).

The 0.5 μm diameter blue polystyrene/latex microspheres and fluorescent polystyrene microspheres were pipetted on nitrocellulose strips mounted on glass slides (N=5). The blue latex microspheres become invisible to the naked eye when the number of microspheres is below 10^9. The low-cost platform can reliably detect 5x10^5 0.5 μm diameter fluorescent microspheres at a 99.73% confidence level on a nitrocellulose

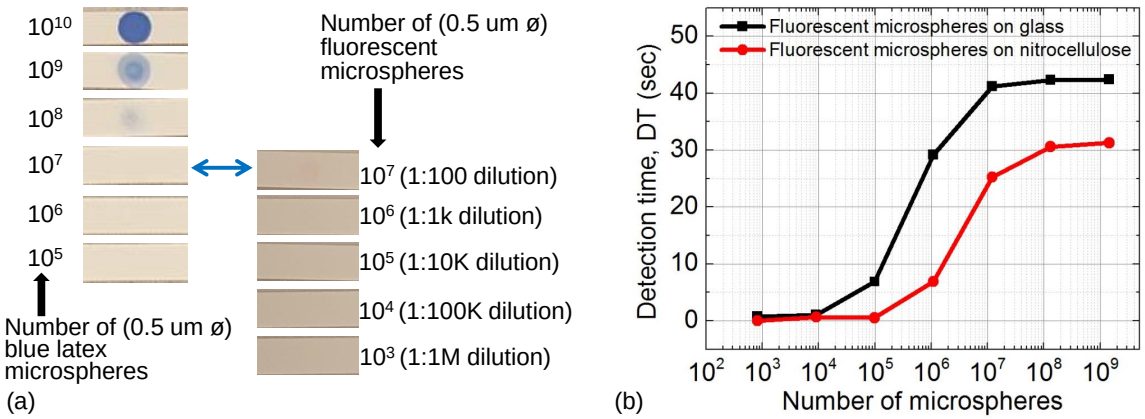

Figure 41: Potential Improvement of Colorimetric Assays by Using Fluorescent Labels. (a) Blue Polystyrene/Latex Colorimetry Microspheres and Fluorescent Latex Microspheres Spotted on Nitrocellulose. 10 μL of Dilutions Were Spotted, and the Number of Microspheres at Each Dilution is Shown. (b) Detection Time for Fluorescent Latex Dilutions Spotted on Nitrocellulose and Glass Analyzed by the Low-cost Array Platform. The Platform Can Reliably Detect 5x10^5 0.5 μm Microspheres on Nitrocellulose Membranes. This Represents 2 to 3 Orders of Magnitude Decrease in the Number of Microspheres Detected, When Compared to the Number of Colored Latex Microspheres Required for a Visible (Positive) Test Line. It is Predicted That Actual Assay Variables Could Limit This Number to 2 Orders of Magnitude.

substrate as shown in Figure 41(b). Here, a direct comparison to standard colorimetry is disucssed. To reliably determine if a test is positive in visual colorimetric assays, a test line, 5 mm length, 0.5 mm width, and 10 μm depth requires 3x10^8 colored microspheres (0.5 μm diameter) on a white nitrocellulose membrane Mansfield (2015). The ability to detect 5x10^5 0.5 μm diameter microspheres represents a 2 to 3 orders of magnitude improvement (over standard latex colorimetry microspheres) in the number of microspheres that can be detected, or the number of biorecognition elements that need to be present in the analyte/patient sample. Hence, better sensitivity can be achieved using the fluorescence platform. However, it is conservatively estimated, that signal losses due to assay efficiency, non-specific binding, and losses due to intrinsic background fluorescence may limit this improvement to 2 orders of magnitude. Generally, there is an observed attenuation of fluorescence emissions with polymeric substrates like nitrocellulose and thus an overall decrease in the measured signal compared to microscope slides as shown in Figure 41(b). An early signal cutoff at low concentrations was also observed with nitrocellulose.

5.4 Summary

A low-cost multiplexed (2 x 2 array) and highly sensitive fluorescence platform has been presented with 2 to 3 orders of magnitude improvement over colorimetry-based assays. The performance of the array platform is enabled by high quality, inexpensive 3 mm x 3 mm interference filters, and charge integration readout electronics. The limit of detection of the 2 x 2 array platform was determined to be 2.1x10^4 and 5x10^5 0.5 μm microspheres on glass and nitrocellulose substrates, respectively. These numbers are within an order of magnitude relative to the performance of a top-of-the-line clinical laboratory fluorescence array scanner. Although the throughput and array density of the developed platform is limited by the physical constraints in the discrete

component layout and assembly, this system fits well with the form factor, performance, and cost requirements for compact hand-held devices in resource-constrained settings. Such devices become especially useful for personal health monitoring and mobile or decentralized applications in resource-limited areas. We are working toward implementing the multiplexed platform in field trials, for screening patients and detecting antibodies to HPV16 and 18 proteins. The system has been engineered and adapted to meet the demands of detecting multiple analytes from a single patient sample at the point-of-need.

In this chapter, significant improvements to the system discussed previously in Chapters 3 and 4 have been presented. A new protocol for assembling diced filters has been developed and the filter and overall system performance was benchmarked against the standard 25 mm filters frequently used in laboratory instrumentation. The customized filters are equivalent in performance, to the 25 mm filters with the added advantage of a significant reduction in cost from $635 (pair of 25 mm filters) to $12.72 (four 3 x 3 mm filters pairs, production quantity of 1000 pieces). These relatively inexpensive filters cost less than $1 for production quantities upwards of 100,000. Several attempts by other researchers toward inexpensive implementation of filtering technologies suffer from poor sensitivity especially for early detection applications at the point-of-care. Particularly, the use of gel filters, absorption filters and cross polarizers, do not meet the performance requirements in order to take advantage of the fluorescence technique. High performance fluorescence-based diagnostic devices require high performance filtering technologies. This is where interference filters come into play. Other researchers and developers can take advantage of this filter design for their respective platforms as against trading performance for lower cost by using less efficient filtering technologies. The fluorescence system development reported in previous chapters of this dissertation was based on 25 mm filter designs. In Chapter 7

the development of higher array density platforms (2x8 and 4x4) is reported based on the results in this chapter. The 3 mm x 3 mm filters have an equivalent performance in terms of the limit of detection (LOD) compared to 25 mm filters. However, the new reported "decentralized" filter design in this dissertation lowers cross-talk (useful in parallel processing) and offers a path toward lower cost per test required for applications intended for translation in low and medium income countries.

Chapter 6

CONSIDERATIONS FOR LOW-COST READER DESIGN - ARCHITECTURE AND CONFIGURATION

6.1 Introduction

The use of colored labels for lateral flow and vertical flow assays enables a visual readout. These devices have become commonplace in the detection of biomarkers used for the diagnosis of infectious diseases, heart disease, and cancers, as well as other applications in food safety, environmental testing, and water analysis. Particularly, lateral flow assays including the gold standard urine-based pregnancy test, are very popular and have had great success mostly due to the ability to visually read results of the test Mak *et al.* (2016). Researchers, developers, and manufacturers have continued to make improvements to enhance the overall performance, ease of use, and interpretation of the results from lateral flow assays. Presently, advanced home-use pregnancy tests like the Clearblue® digital pregnancy test (Swiss Precision Diagnostics), presents the results to the user in words, or estimates the number of weeks a woman is pregnant, eliminating the subjective interpretation associated with faint lines in a typical lateral flow test. The development of advanced lateral flow tests targets improvements in the sensitivity and limit-of-detection (LOD) O'Farrell (2013), especially for applications in early disease diagnosis, vaccine coverage screening, and infectious disease outbreak control. As discussed in previous chapters of this dissertation, a viable approach towards improving sensitivity and LOD is to substitute colorimetric labels for fluorescent labels, coupled with instrumented optical detection. However, it is imperative that the optoelectronic detection system be min-

imal, simple, and inexpensive, especially for POC applications in low-resource settings or low-and-middle income countries (LMIC). Furthermore, beyond just digitizing the results, the optical detection system should be capable of delivering reliable results comparable in performance to existing central laboratory diagnostic procedures, to justify the additional complexity added to the simple lateral flow assay.

In Chapters 3, 4, and 5, the design, optical analysis, and application of the transmission/transillumination mode (T-mode) fluorescence architecture was presented. Particularly, the application was for the detection of biomarkers for human papillomavirus (HPV) infection, toward the diagnosis of cervical cancer. This chapter compares, the performance characteristics of two configurations of the developed low-cost, quantitative, and miniaturized label detection platform; the T-mode and the coplanar mode (C-mode) architectures based on the optoelectronic configuration shown in Figure 42 (a) and (b).

To compare both configurations, the sensitivity is estimated from the slope of the linear region of the system response (linear dynamic range), while the LOD was calculated from repeated measures of the blank plus 6 standard deviations for a high level of confidence. Both configurations are capable of delivering clinical/central laboratory sensitivity and LOD. In this study, a detailed characterization, analysis, and comparison of the T-mode and C-mode POC platform is presented. Furthermore, we compare the performance of both platforms to a central laboratory-scale microplate reader. The sensitivity and LOD of the POC platform was measured by characterizing several fluorophores. The platform was determined to be capable of delivering the same LOD as a well-plate reader.

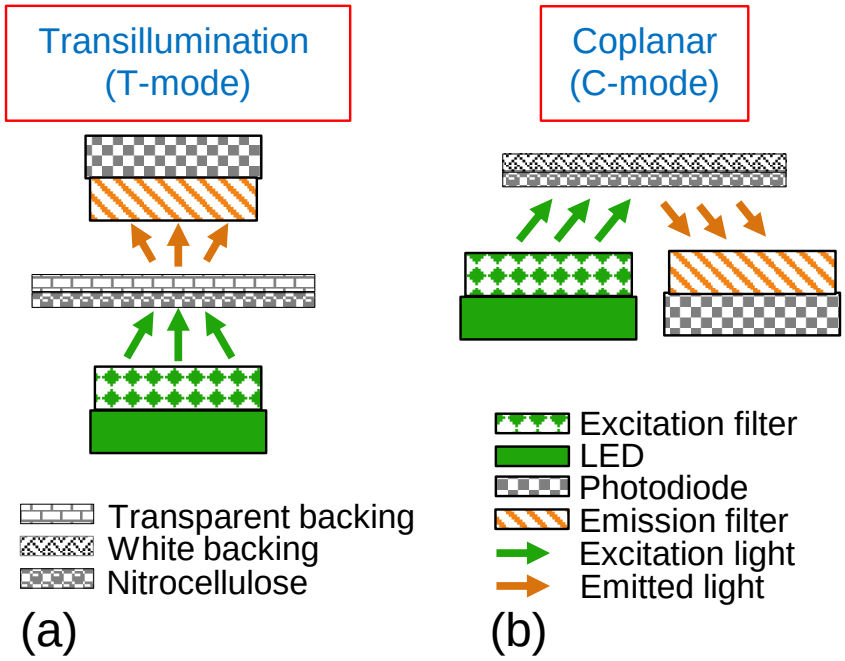

Figure 42: Reader Platform Architecture. (a) Transillumination (T-mode) (b) Coplanar Architecture (C-mode).

6.2 Experimental Procedure

6.2.1 Optoelectronic Design: Transillumination (T-mode) and Coplanar (C-mode) Architecture

To reduce the complexity and minimize the cost of instrumented detection platforms, innovative designs are required. A viable and effective approach is to minimize or eliminate the use of focusing optics which add to the complexity, cost, and instrument size. Complexity and bulkiness present a significant limitation especially for field-deployable applications in LMICs and low-resource setting. To this end, we implement an optoelectronic setup comprising an interference filter-based system coupled with a charge integration readout. The interference filters provide the required selectivity, capturing the emitted fluorescence while suppressing the excitation

light (LED) reaching the photodiode-based integrating amplifier detector. It is worth noting that integrated layouts using organic optoelectronics have been reported in literature Lefèvre *et al.* (2015). A schematic representation of the transmission (T-mode) and coplanar (C-mode) architectures is shown in Figure 42 (a) and (b). These architectures draw inspiration from those found in bioanalytical instruments that employ focusing and transfer optics. However the design constraints in this architecture require minimizing complexity and cost of the optoelectronic design, while maximizing performance, in order to achieve sensitivity and LOD comparable to central laboratory analytical devices. In the T-mode architecture, the analytical membrane (nitrocellulose) is sandwiched between a constant current driven LED and a photodiode connected to a capacitive charge integration amplifier as discussed in previous chapters and illustrated in Figure 42 (a), whereas, in the C-mode architecture, the LED and photodiode are on the same plane as shown in Figure 42 (b). The integrating amplifier, photodiode, and LED assembly on a printed circuit board is shown in Figure 43 (a). The nitrocellulose is vertically aligned with the photodiode to maximize fluorescence light collection.

Figure 43 (b) shows the assembled system and the inset shows an illuminated clear-backed membrane (top) and a white-backed membrane (bottom). The signal intensity measured by both configurations is proportional to the photodiode generated current. The concentration-dependent voltage output shown in Figure 44 is characterized by the slope of the voltage-time response (S). When used for fluorescence detection, a biorecognition event is indicated by an increase in the slope (S_F) with concentration above the reference (S_{REF}). When used to measure absorbance (colorimetry), the deviation of the slope (S_A) from the reference is proportional to optical density of the sample.

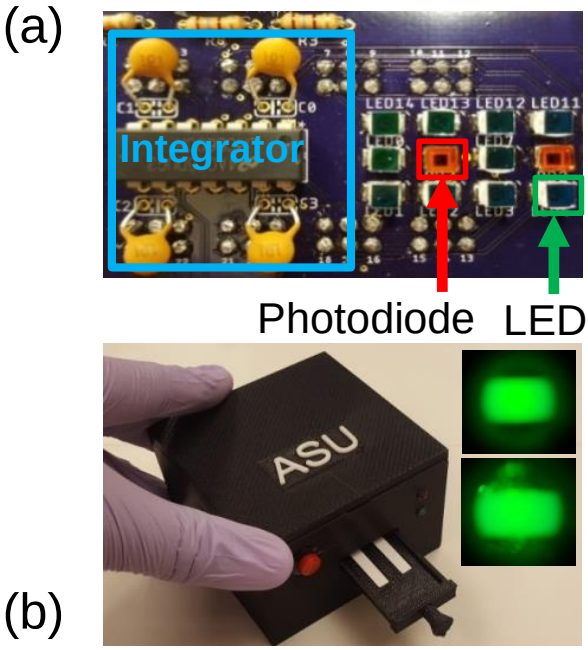

Figure 43: (a) Coplanar Architecture Showing a Low-noise Charge-integration Amplifier (LMC660AI, Texas Instruments), Photodiodes (PDB-C154SM, Luna Optoelectronics) and LEDs (XZM2DG45S, SunLED) with Filters Mounted. (b) The Reader Housing with Sample Tray Open. Excitation Light Through Clear/Transparent-backed Membrane (Top Right), Higher Scattering is Observed with White-backed Membrane.

6.2.2 Membrane Effects

The acceptance of nitrocellulose as the gold-standard analytical membrane is due to its low production cost, protein binding affinity, control of its porous microstructure, simplicity, and ease of use. Usually, the membrane is produced by casting onto a thin plastic film. The membrane needs to be backed to provide mechanical support for handling and prevent contamination from adhesives. The opacity of nitrocellulose represents a significant challenge for detector configurations that involve

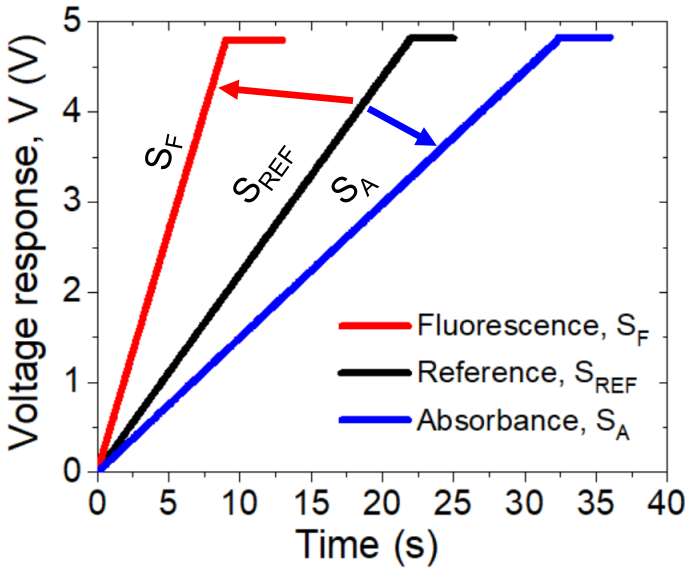

Figure 44: Concentration Dependent System Output Voltage Response for Fluorescence and Absorbance.

detecting light from within the microstructure of the membrane. Furthermore, the transparency of the backing material also impacts the amount of light that can be transmitted and reflected/scattered. Typically, the industry standard is to use a white polyester or polystyrene backing material, however a few products with a clear backing are also available. In this work, a clear-backed material is used in the T-mode architecture to increase the light penetration depth into the membrane and a white-backed membrane for the C-mode, such that the white backing provides multiple light paths exciting the label immobilized in the membrane. Figure 42 (a) and (b) delineates the two types of backing material considered. A more detailed analysis of membrane and backing type effects in lateral flow assay development is also presented in Chapter 7.

6.2.3 Labels, Reagents, and Sample Preparation

A logarithmic dilution series (ranging from 1:10 to 1:1,000,000 in deionized water) was prepared for all labels; 1 μm Nile Red fluorescent microspheres (catalog no. F-8819, ThermoFisher Scientific, CA, USA), 1 μm and 0.5 μm fluorescent functionalized microspheres (catalog nos. 80380140-F1-Y 100 and 80380534-F1-Y 050, respectively, Merck Millipore, Cedex, France), DyLight^{TM}549-TFP ester and Cyanine Cy^{TM}3 (catalog nos. 005-500-003 and 109-165-003, respectively, Jackson ImmunoResearch Laboratories Inc., CA, USA), and dye funtionalized colorimetry microspheres (catalog no. 39544001-K1-050 blue, Merck Millipore, Pithiviers, France). Sample references were obtained by preparing reference buffers, sodium azide (NaN_3), phosphate buffered saline (1X PBS) and sodium chloride (NaCl) to represent the preservatives, buffers, and stabilizers in which the labels are typically suspended by manufacturers. The microspheres were sonicated before use and the molecular dyes were vortexed according to the manufacturers recommendations. The optoelectronic components used in the design of the POC platform have been discussed in other chapters.

6.2.4 Fluorescence and Absorbance Scans With Microplate Reader

A multi-mode microplate reader (SpectraMax®M5, Molecular Devices) was used to measure and analyze fluorescence and absorbance scans as well as single wavelength readings. The data presented here for the microplate reader was acquired using the minimum recommended volume (100 μL). This corresponds to 10X the volume used for characterizing the POC device. The results were normalized accordingly. Each label dilution was pipetted into a microplate (N=3). Appropriate reference buffers were prepared as described in Section 6.2.3, and were used to obtain accurate cuvette and microplate references for blank normalization and pathlength correction.

For example, a 2 mM solution of NaN_3 in 1X PBS was prepared and diluted to obtain a cuvette reference and microplate blank references for the 1 μm Nile red microspheres. The cuvette reference was used to correct for pathlength differences in the microplate samples and the microplate references were used to normalize the fluorescence (relative fluorescence units, RFU) and the absorbance (optical density, OD). Single wavelength measurements were obtained under medium photomultiplier tube (PMT) gain settings and spectrum scans were performed in autogain mode.

6.2.5 Fluorescence and Absorbance Measurements on the POC Platform

The label dilutions were immobilized by pipetting 10 μL of each dilution on nitrocellulose membranes (N=3). The clear-backed nitrocellulose sheets (HF07504XSS, Millipore) and white-backed cards (FF80HP, GE Healthcare) were cut to 25 mm x 5 mm strips, mounted on glass slides, and read by inserting the slides into the POC device.

6.3 Results and Discussion

6.3.1 Effect of Reader Architecture on Fluorescence Intensity

In this section, we present a comparison between the T-mode and C-mode architectures using two labels, molecular dye (Cyanine Cy3) and 0.5 μm fluorescent microspheres (F1-Y050) on nitrocellulose membranes with clear and white backing respectively. The dose response of both architectures is shown in Figure 45.

The collected fluorescence signal for both Cy3 and F1-Y050 was determined to be higher in the T-mode architecture than the C-mode, leading to an order of magnitude lower LOD than the C-mode architecture. The T-mode ensures that more light is collected as the detector is positioned directly on top of the clear-backed nitrocel-

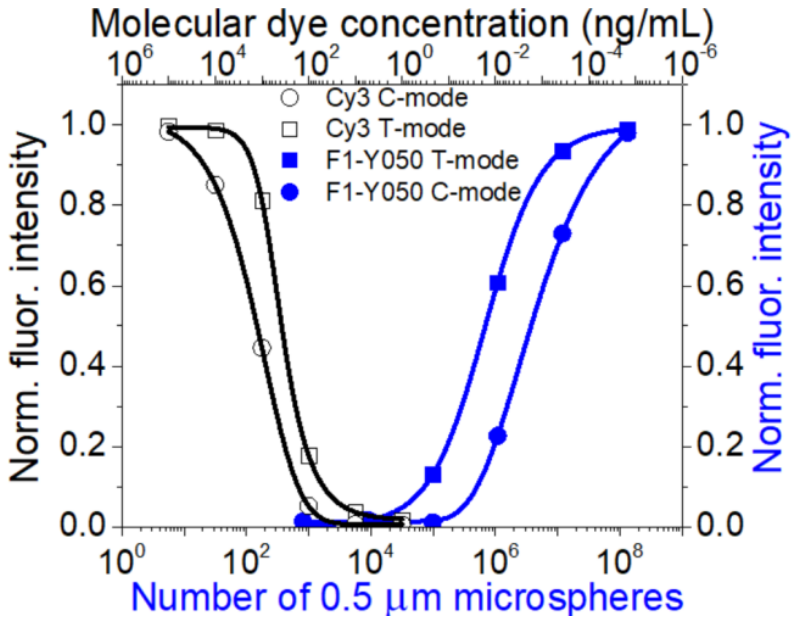

Figure 45: Normalized (Norm.) Fluorescence (Fluor.) Intensity as a Function of Fluorophore Concentration (a) 0.5 μm Microspheres (Right and Bottom Axes) and Cy3 Molecular Dye (Left and Top Axes); Transillumination (T-mode) and Coplanar (C-mode) Architecture Responses are Shown for Both Fluorophores.

lulose membranes in which the fluorophores are immobilized, representing an actual binding event. However, in the C-mode, the isotropic emissions of the fluorophores are collected via a smaller viewing angle, since the photodiode and LED are on the same plane. Potential improvements to the C-mode includes capitalizing on the lower background noise, since the excitation light is not aimed directly at the detector. For our platform, we could therefore increase the gain of the charge integration amplifier by using a smaller capacitor and hence integrate for a longer time. Additionally, no significant difference was observed when the white-backed membrane (only) was used in both the C-mode and T-mode architectures for fluorescence detection. We propose that the losses due to transmission in the white backing material (when used in the the T-mode), is offset by the losses due to incomplete collection of isotropic emissions

of the fluorophores in the C-mode.

6.3.2 Effect of Brightness and Spectra Mismatch

A very important parameter in fluorophore selection is the brightness, which is related to the fluorophore quantum yield, cross-section for absorption, and the collection efficiency of the optical system. In other words, it is the number of photons per second emitted by a fluorophore and observed by a detection system. The observed fluorescence intensity is proportional to the fluorophore brightness and excitation light intensity. Furthermore, exciting the fluorophores at the peak absorption and collecting fluorescence at the peak emission wavelength is critical for the overall system performance. The relative brightness of 5 fluorophores can be inferred from the relative fluorescence intensity (RFU) measured using the microplate reader as shown in Figure 46.

The effect of fluorophore brightness and matching is observed in developed platform as illustrated in Figure 47 (a) and (b). In Figure 47 (a), 1 μm microspheres (Nile red and F1-Y100) are compared. The steeper slope (higher sensitivity) observed for the Nile red fluorophore is a result of the higher brightness and matching for optical system as shown in Figure 47 (b). In Figure 47 (b), the fluorescence spectra scan of both fluorophores at 1:1000 dilution ($\sim$20,000 microspheres) indicates a higher relative fluorescence intensity (peak A compared to B) for Nile red and F1-Y100 respectively. Furthermore, most of peak emission of the Nile red fluorophores is captured by the emission filter, compared to F1-Y100. This culminates into a lower detection limit using the Nile red fluorophores, rather than F1-Y100, although they are the same size microspheres.

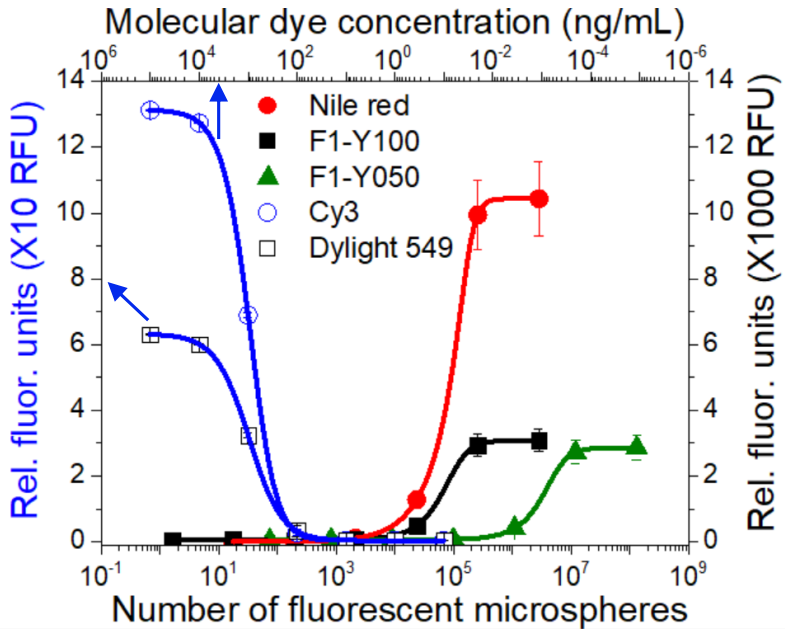

Figure 46: Fluorescence Intensity Measurements in Relative (Rel.) Fluorescence (Fluor.) Units (RFU) of Different Molecular Dyes (Left, Top Axes) and Dye Encapsulated Microspheres (Right, Bottom Axes).

6.3.3 Application of Reader Platform for Colorimetric Detection

The developed POC platform provides an inexpensive path to improving the performance of many lateral flow assays in use today, even those that use colorimetric labels like colored microspheres and gold nanoparticles (AuNP). The translation from visual to an instrumented readout enables quantitative results and enhances the lower limit of detection. Figure 48 depicts the absorbance response to varying concentrations of blue colorimetry microspheres (K1 050) at 520 nm and maximum optical density (OD).

The OD was measured using the microplate reader and is shown on the right Y-axis. No significant difference was observed between the response of the T-mode and C-mode architectures when used to detect blue colorimetry microspheres, with

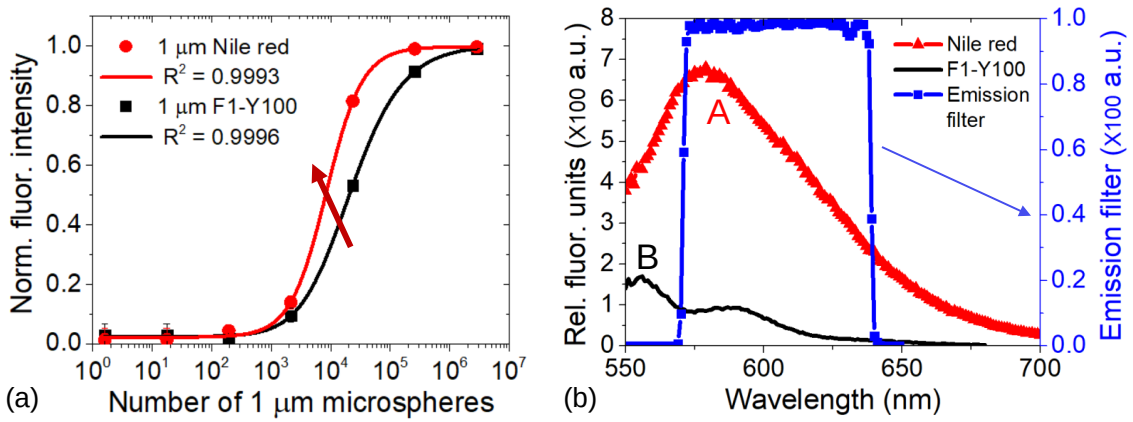

Figure 47: (a) Effect of Spectra Mismatch and Brightness for the Same Size Microspheres with Different Encapsulated Dyes. Higher Intensity and Sensitivity (Slope) for the Better Matched Nile Red Microspheres (b) Spectra Scans Showing Slight Peak Mismatch With Respect to the Excitation Filter (Secondary Axis) in Relative (Rel.) Fluorescence Units (RFU); Lower Sensitivity and LOD for the F1-Y050 Microspheres.

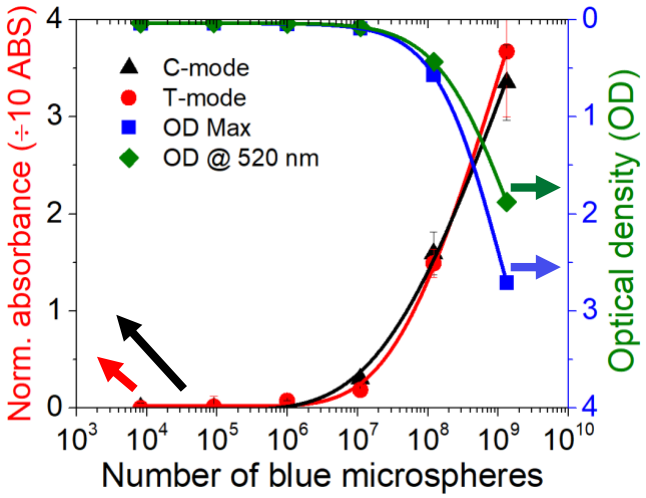

Figure 48: (a) Normalized (Norm.) Absorbance (ABS) Measurements Comparing the POC Transillumination (T-mode) and Coplanar (C-mode) Architectures and Optical Density Measured With Central Laboratory Microplate Reader (Secondary Axis).

clear and white-backed nitrocellulose respectively. A comparison of the response between 0.5 μm fluorescent microspheres and 0.5 μm colored microspheres is shown in Figure 49 (a). The LOD was determined to be 2 x 10^7 and 2 x 10^4 microspheres for the colored and fluorescent microspheres respectively. This represents a 3 orders of magnitude lower detection limit using fluorophores rather than chromophores. The higher slope of the fluorophore response in the linear range is indicative of a higher sensitivity over the colorimetric readout. Absorbance scans of the K1 050 dilution series is shown in Figure 49 (b) (top). Figure 49 (b) (bottom) shows the K1 050 dilution indicating that it becomes visually impossible to see microsphere concentrations less than 10^7 microspheres.

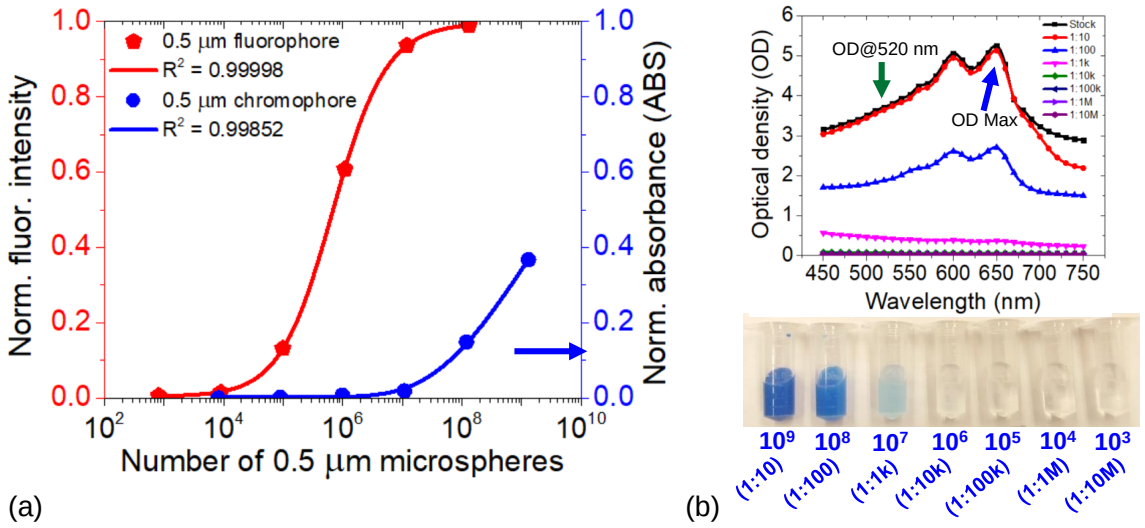

Figure 49: (a) Response From Equal Sized Fluorescence and Colorimetry Microspheres, 3 Orders of Magnitude Lower LOD With Fluorescence (b) Absorbance Scans at Different Concentrations for Blue Latex Microspheres; Maximum Optical Density (at 650 nm) and OD at 520 nm Shown.

Currently, many colorimetry applications are capable of detection in the ng/mL range. The use of fluorescent labels (molecular dyes, microspheres, Qdots, europium)

have the potential to decrease the detection limit to the pg/mL range Bahadır and Sezgintürk (2016).

6.4 Summary

In this study, a low-cost fluorescence and colorimetry label detection platform for point-of-care (POC) applications was developed. The platform is designed to deliver clinical-level diagnostic sensitivity. It improves the performance of the traditional lateral flow assay (LFA), decreasing the detection limit by 3 orders of magnitude and enabling quantitative detection of analytes. In this work, the fluorescence detection platforms were characterized. This chapter also detailed the effects of label selection on the overall system performance. The effects of optoelectronic configuration, brightness, and spectral matching are presented. Finally, the utility of the developed platform for colorimetric detection was demonstrated and its performance compared to a standard central laboratory microplate reader. The limit-of-detection (LOD) for the point-of-care platform was determined to be the same as the microplate reader, detecting 2 x 10^4 0.5 μm microspheres without the use of focusing or transfer optics. There is significant value in being able to use the same reader/detector to probe multiple label types including gold nanoparticles, colored latex microspheres, and fluorescent labels without any changes to the instrument configuration. This chapter detailed the development of an inexpensive fluorescence and colorimetry platform for improving the detection limit of lateral flow assays and providing a quantitative readout. The utility of the transillumination (T-mode) and coplanar (C-mode) architectures for fluorescence and colorimetry applications has been investigated. The configuration of choice depends on the specific application. Although the C-mode performs less than the T-mode by an order of magnitude in fluorescence applications, it is useful for a more compact design, for example, in wearable applications. The

T-mode platform provides 3 orders of magnitude improvement in detection limit for fluorescence compared to colorimetry. No significant difference was observed between the performance of the T-mode and C-mode architecture for colorimetric detection. Although the human eye has a wide dynamic range, the resolution is poor. Hence improvements to lateral flow assay devices with instrument-based readers has huge significance especially for biomarkers that are minimally expressed or applications where high sensitivity and low LOD is desired.

Chapter 7

TECHNICAL ASPECTS AND CHALLENGES OF FLUORESCENCE LATERAL FLOW ASSAY DEVELOPMENT FOR MULTIPLEXED POINT-OF-CARE APPLICATIONS

7.1 Introduction

In Chapter 5, the design and characterization of a multiplexed (2 x 2), low-cost, high-sensitivity fluorescence detection platform is presented. To meet the demand for a multiplexed platform for detecting circulating oncogenic biomarkers for human papillomavirus (HPV), this chapter details the design and development of a 4 x 2 (8-site) and 4 x 4 (16-site) multiplexed fluorescence detection platform (DxArray). The glass-based HPV16 E7 IgG antibody detection assay presented in Chapter 4 is adapted to a nitrocellulose-based lateral flow assay (LFA) format. This chapter focuses on the unique requirements and challenges for fluorescence-based LFA development on paper-based solid supports (nitrocellulose).

The lateral flow assay (LFA) market is predicted to reach ∼10 billion dollars in 2020 O'Farrell (2013) at a compound annual growth rate (CAGR) of 7%. Despite the success of the colorimetric LFA devices, researchers and developers have long identified potential challenges and limitations of LFA technology. Generally, LFAs have lower performance (sensitivity, specificity, and reproducibility) compared to gold-standard central laboratory techniques like the enzyme-linked immunosorbent assay (ELISA) or DNA amplification by polymerase chain reaction (PCR). The limitations of LFAs, poses a significant challenge for their deployment and application especially for infectious disease diagnosis for early detection and for the management of diseases

where biomarkers are minimally expressed.

A promising approach for improving the sensitivity of LFAs is the substitution of colorimetry labels with fluorescent labels. Compared to similar technologies including nucleic acid lateral flow assay (NALF) and micro paper analytical devices (μPAD), LFA holds great promise for applications in resource-poor settings, providing clinical-level diagnostic performance. Although fluorescence has been widely deployed in many laboratory-based bioanalytical applications, a significant challenge is to translate central laboratory fluorescence-based techniques to relatively inexpensive tests for point-of-care (POC) applications. Such tests should allow minimally trained users to detect low concentration of multiple targets/analytes in human samples (plasma, serum, or whole blood) in resource constrained settings.

Currently, the gold standard in LFAs is the use of colorimetric labels. In applications for early detection, there is significant value in being able to detect low concentrations of species/analytes in a sample matrix. For infectious disease applications, enhanced performance LFAs are required O'Farrell (2013); O'Farrell (2015b). Such platforms should be inexpensive, compact, robust, and have the required sensitivity to detect clinically significant concentrations. Furthermore, advanced lateral flow devices need to incorporate efficient instrumentation along with high performance biomarkers and labels (Linares *et al.*, 2012) to improve sensitivity and limit-of-detection (LOD), user-centric designs are needed for ease of use, and enhanced accuracy in the interpretation of the results is needed, as opposed to traditional visual inspection (Mak *et al.*, 2016).

Compared to LFAs (paper-based microfluidics), a significant challenge with most microfluidic technologies is the difficulty in translating excellent science from the laboratory bench-top to the field. For example, the dependence of many microfluidic systems on an external source of pressure or vacuum limits their applications

to a standard laboratory setting. There are only a few commercialized non-paper-based autonomous microfluidic devices for point-of-care applications such as the Alere Triage device. Many researchers and developers struggle with shelf-life and stability of the surface characteristics required for capillary flow, hence it is very difficult to implement and commercialize field-deployable, stable, and user-friendly microfluidic devices (van Amerongen *et al.*, 2018). For these reasons, we adopt paper-based microfluidics using nitrocellulose, enabling fluid routing by capillary action, and taking advantage of the existing infrastructure that is a result of almost 40 years of industrial manufacturing and processing.

Lateral flow assays have long been identified as a viable option for POC settings because they are rapid, easy to use, and meet the requirement of long shelf-life even when stored at ambient temperature for prolonged periods of time (Posthuma-Trumpie *et al.*, 2009). However, poor sensitivity even with commercially available reader systems is a significant issue. There are not many compact, low-cost, and highly sensitive fluorescence-based LFA detection systems on the market. This is partly due to the challenges associated with miniaturization, e.g., implementing high-quality interference filter required for high performance in fluorescence-based detection systems.

This chapter details the development of fluorescence-based detection platform for use with LFAs in detecting infectious diseases. Our platform enhances the standard visual (colorimetric) LFA by integrating interference filters and charge integration readout electronics while taking advantage of the selectivity of fluorescence and the sensitivity and antigen(Ag)-antibody(Ab) interactions. For the development of field-deployable and high sensitivity fluorescence-based LFAs, specific attention needs to be paid to certain areas of development. We report on considerations for reader platform development, fluorophore selection, and size effects, as well as membrane

selection and flow rate, porosity/pore size effects.

First, the development of a multiplexed biomarker detection platform, using a decentralized filter design is presented. The customized filter dimension (3 mm x 3 mm) used in the development of a 2 x 2 array in Chapter 5 is extended towards the development of a 4 x 2 and 4 x 4 array platform. In our previous configuration, protein capture spots were immobilized on glass slides and each spot was read by physically moving the glass slide using alignment marks in order to measure each spot. We enhance the degrees of freedom in the spatial arrangement of the channels, simplify the operation, and reduce the logistical constraints with the use of the platform. The higher density array platform automatically reads up to 16 sites sequentially. Herein, the systematic development of a low-cost IgG, Epstein Barr nuclear antigen-1 (EBNA-1), and human papillomavirus (HPV) assay on nitrocellulose membranes are reported. We hypothesized that the porous 3D microstructure of nitrocellulose provides more binding sites for the capture agent compared to a 2D planar glass substrate and that the increased binding sites will lead to improved assay performance regardless of the optical limitations of nitrocellulose.

7.2 Experimental Procedure

7.2.1 High-density Fluorescence Detection Array Platform (4 x 2 and 4 x 4 Channels) Design and Assembly

The system assembly presented in Chapter 5, Section 5.1.2 and 5.2.1, is extended and adapted in this chapter to fabricate a 4 x 2 and 4 x 4 array of fluorescence detection sites in a compact configuration (DxArray). The decentralized filter design enables individual detection sites with dedicated low-cost LEDs, excitation, photodiodes (PD), emission filters, and amplifiers, with a flexible spatial configuration. The

circuit design schematic and double-sided board layout were implemented using Eagle PCB design software (Autodesk). A representative schematic and board layout of the LED-board and photodiode-amplifier (PD-board) is shown in Figure 50 (a) - (d). The system was designed to detect biorecognition sites on nitrocellulose membranes used in lateral flow assays. Figure 50 (a) and (b) depicts the circuit schematic and board layout of the excitation/LED-board. Based on cross-talk studies, physical constraints of discrete component assembly, and 3D printing limitations, the prototype configuration was designed with a 6 mm pitch in the lateral direction (x-direction indicated) or along the length of a test strip. The linear arrays were designed at 9 mm pitch (in the y-direction) chosen to fit with a the pitch of a standard microplate reader. The inorganic light emitting diodes (LEDs) have a peak emission $\lambda = 520$ nm (SunLED, XZM2DG45S). The LEDs are mounted on a printed circuit board (PCB) as shown in Figure 51 (a), (b), and (g). The LED spectrum is filtered using a low-cost 3 mm x 3 mm excitation (520/40 nm) interference filter (Chroma Technology Corp.) mounted directly on each LED. To ensure efficient control of the LED intensity, a constant current driver (TLC5947 24-channel, 12-bit pulse width modulated (PWM) LED driver, Texas Instruments, Dallas, USA) was used to drive the LEDs from an Adafruit LED driver breakout board (NY, USA). The constant current driver shown in Figure 51 (c) allows some flexibility with the supply voltage fluctuations, such that the LED intensity is held constant (assuming constant temperature). The breakout board was operated from a 9 V source and configured for 15 mA maximum output current (set using a single 3.3 kΩ resistor, 30 mA capability, based on TLC5947). Each LED channel is individually adjustable using 4096 PWM steps.

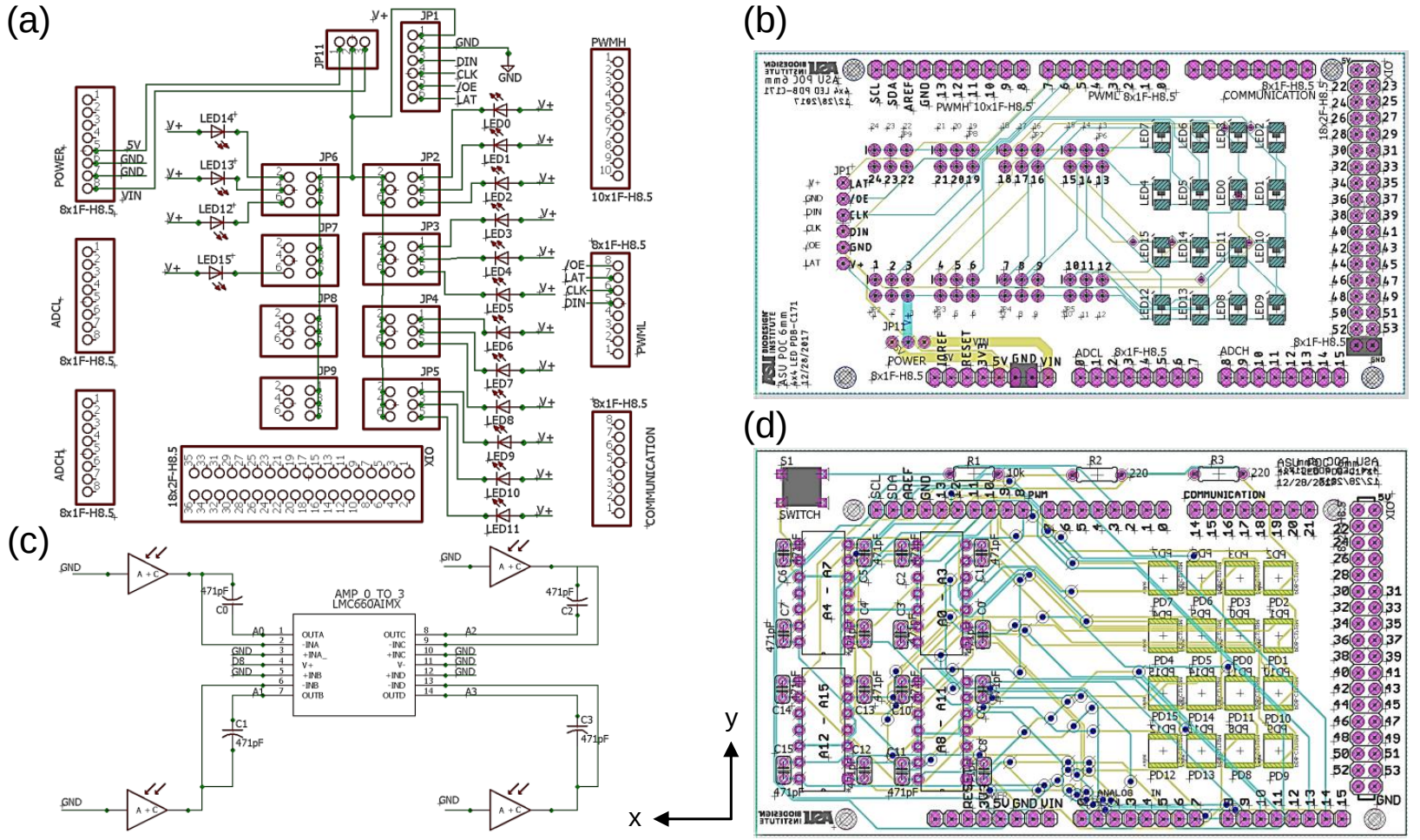

Figure 50: Multiplexed Detection Array (Dxarray) - Schematic and PCB Layout (a) Front - 4 x 4 LED-board Schematic Showing 16 LEDs, Arduino Mega Header Pins, TLC5947 LED Driver Header Pins, and Power Jumper Pins (b) Front - 4 x 4 Led-board Layout Showing LED Pads and Wiring (c) Photodiode (PD) and Integrating Amplifier Schematic (d) Front - 4 x 4 Photodiodes, (PD)-board Layout Showing PD Pads, Amplifier Pins, and Wiring.

Figure 50 (c) and (d) shows representative schematic and layout of the photodiodes and charge integrating amplifiers (PD-board). The photodiodes are connected in photovoltaic mode as part of a low-noise charge-integration amplifier readout (LMC660), so that dark current becomes negligible. Photodiode (TEMD5020X01, Vishay Semiconductors, Inc., PA, USA) were pitch-matched to the LED board described previously and mounted on the PD-board as shown in Figure 51 (d), (e), and (h). Compared to the through-hole, photodiode used previously in this dissertation (PDB-C139, 59° viewing angle, 2.03 mm^2 active area, responsivity, R(λ) of ~0.2 to 0.3 A/W from 550 to 650 nm), the viewing angle and active area of the surface mount device (SMD) photodiode used here is 130° and 4.4 mm^2, respectively. The responsivity, R(λ) is ~0.4 to 0.6 A/W from 550 to 650 nm. The integrating amplifiers (LMC660 quad amplifiers, Texas Instruments, Dallas, TX, USA) and 1000 pF capacitors are shown on the reverse side of the PD-board in Figure 51 (f). The PD-board is stacked on the LED-board using headers that match the microcontroller (Aruduino Mega 2560) at the bottom of the assembly (Figure 51 (m) and (n)). The optomechanical structure in Figure 51 (k) is sandwiched between both boards. The optomechanical structure isolates each channel (LED and PD) and provides a means for inserting samples via a tray while eliminating any external ambient light entering the detector. The internal optomechanical structures and housing were designed using AutoCAD and printed with a Stratasys Dimension 1200es^{TM} 3D printer (Eden Prairie, MN, USA).

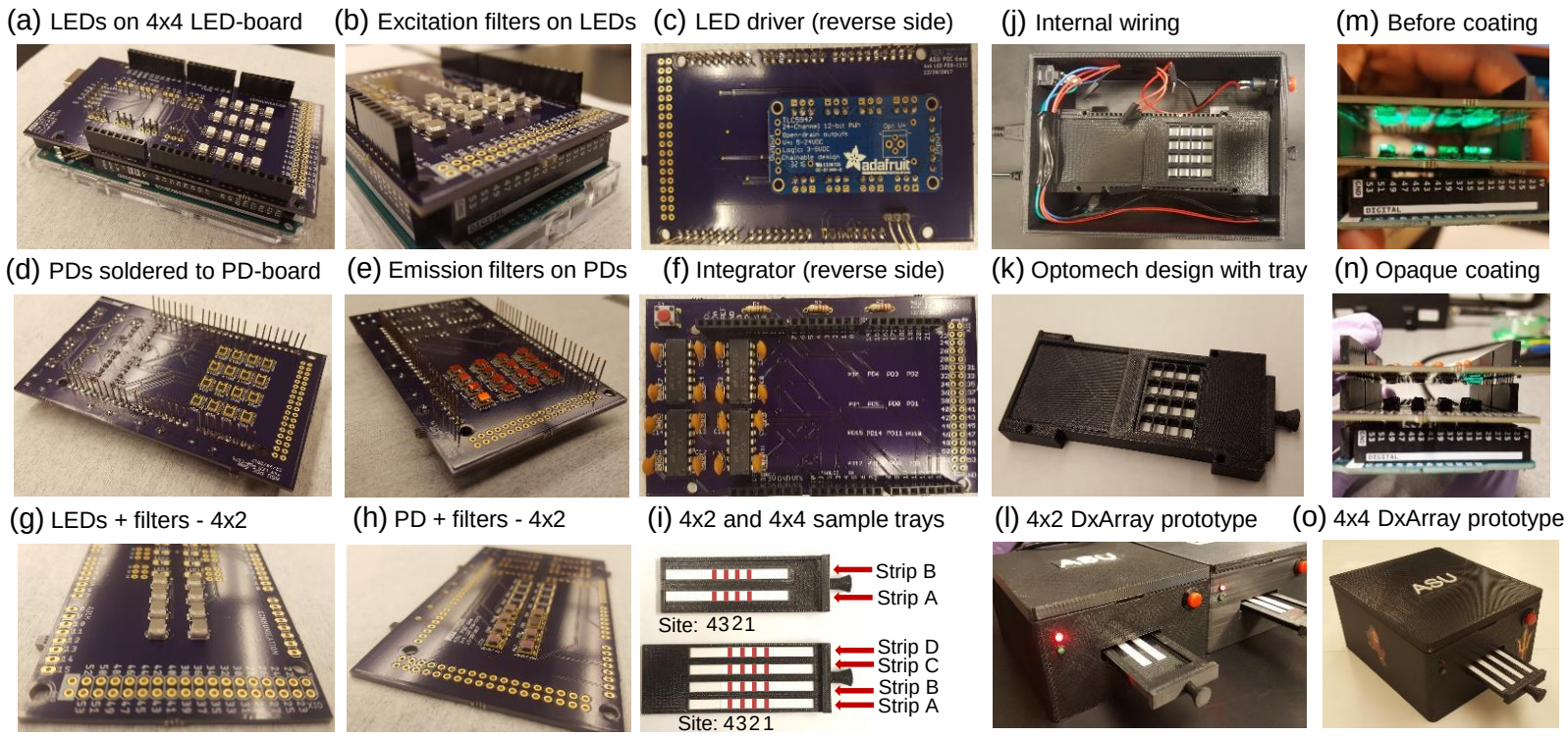

Figure 51: Fabrication and Assembly of the DxArray. (a) Front - 4 x 4 LED-board (b) Excitation Filters on LEDs, Cured with UV Epoxy (c) Back - LED-board Showing LED Constant Current 12-bit 24-channel PWM Driver (d) Front - 4 x 4 Photodiodes (PD)-board (e) Emission Filters on Photodiodes, Cured with UV Epoxy (f) Back - PD-board, Integrator Amplifiers, Resistors for Front Panel LED, Reset Switch (g) LEDs on 4 x 2 LED-board (h) Photodiodes on 4 x 2 PD-board (i) Sample Trays (j) Internal Wiring, Power Switch, Run Switch, Power and USB Cable, (k) Internal Optomechanical Isolation and Apperture Structure (l) Assembled 4 x 2 DxArray Prototype (m) LEDs and PD Activated Without Opaque Coating of Filters (n) After Opaque Coating of LEDs and PDs (o) Assembled 4 x 4 DxArray Prototype.

The 3 mm x 3 mm filters were mounted directly on the LEDs and photodiodes using optically clear (∼100% from 350 to 3000 nm) UV curing adhesive, (NOA63, Norland Prodcuts Inc., NJ, USA) and cured using a 6 W Spectroline® E-series UV lamp for 15 min. The filters were then coated with an opaque paint to provide optical isolation and prevent light leakage out or through the sides of the filter substrate (Figure 51 (m) and (n)) and the imperfections on the edges (kerf) as a result of the dicing process. Under normal operation, the LEDs and corresponding detector site were sequentially turned to measure the emitted fluorescence intensity from a sample. Each site is designated hereafter as sites/channels A1 to A4, B1 to B4, C1 to C4, and D1 to D4 on the 4 x 2 and 4 x 4 platform as depicted in Figure 51 (i). The fully assembled and functional 4 x 2 and 4 x 4 DxArray is shown in Figure 51 (l) and (o), respectively.

Two units of the 4 x 4 DxArray were assembled at the same time and tested. To ensure zero drop-off for any channel, each channel was set to an integration period of ∼30 s, by adjusting the LED intensity using the PWM driver. A representative response to blank nitrocellulose strips for the 4 x 4 channel reader is shown in Figure 52 (a) and (b). The units were allowed to warm up for 30 min once powered up. A blank reference nitrocellulose membrane was read on all 16 channels on both units, 15 times to study the stability and repeatability of the DxArray. The minimum and maximum standard deviation were 35 and 700 ms, respectively, on any channel across both systems under test. This indicates negligible instrument variations (high repeatability/precision) when the units are powered and run over many cycles. The resolution is only limited by the 10-bit ADC in the microcontroller platform. For an integration period of 30 s, it takes a total time of 8 min to cycle sequentially through all 16-channels.

Finer control of each channel could be achieved, in an attempt to balance all the

channels. However, this was unnecessary to ensure functionality of all channels on both units. The reasons for the slight differences in ramp time, RT (s) observed between channels in Figure 52 (a) and (b) will be discussed through the rest of this chapter. Particularly, optical variability in nitrocellulose membranes is discussed in Section 7.5.2. Figure 52 (c) and (d) shows the signal intensity in terms of the slope of the voltage-time output response of the integrating amplifier. The slope is directly correlated to signal intensity, whereas RT is inversely correlated to intensity. All the channels were stable and produced a repeatable response, indicating that the

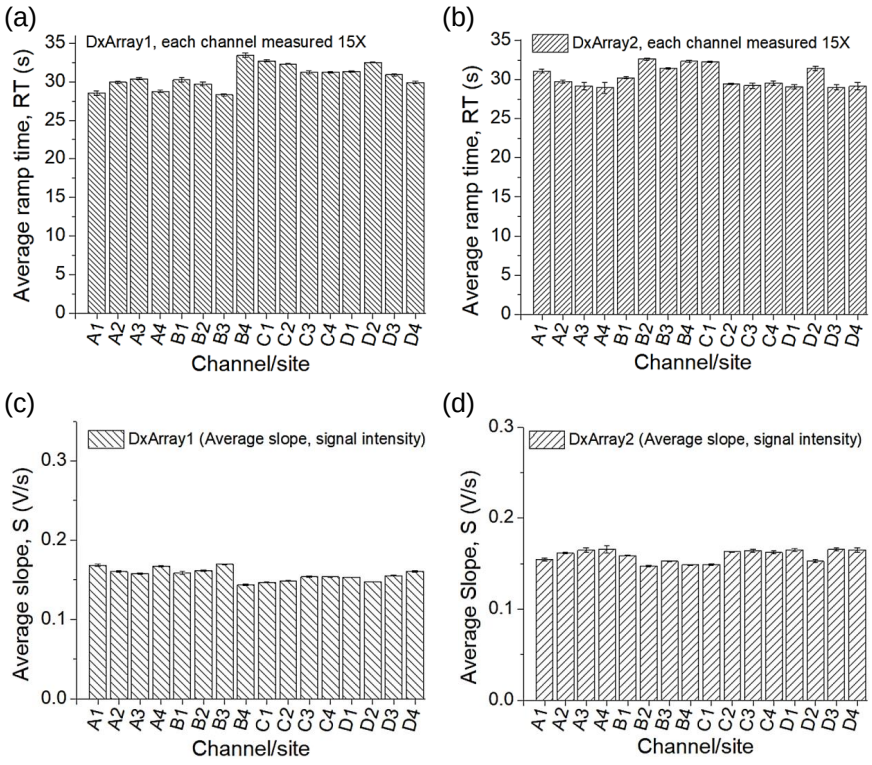

Figure 52: Representative Response Showing the Ramp Time, RT (s) and Signal Intensity (Slope), S (V/s) of the Output Voltage Profile of All 16 Channels After Channel on Two 4 x 4 DxArray Units. The DxArray Units Were Cycled 15 Times With a Blank Nitrocellulose Membrane Inserted.

DxArray could be used to measure small changes in fluorophore concentration at a high sensitivity for the development of a quantitative assay readout. The slope metric is discussed and used extensively in the development of the normalized fluorescence intensity (NFI) algorithm presented in Section 7.5.3.

7.2.2 Membrane and Fluorophore Selection

The opacity of nitrocellulose due to scattering limits light measurements compared to the use of a transparent solid support. However, the many benefits of nitrocellulose make it a useful platform for low-cost fluorescence-based LFA development. The existing industry production infrastructure, advanced processing tools developed over the years, its self-driven capillary properties, protein compatibility, biodegradability, and low-cost ensure that nitrocellulose will continue to be the material of choice in LFA in the foreseeable future. Fluorophore selection involves a careful consideration including: the flow properties in nitrocellulose to limit non-specific binding; brightness to enable measurable fluorescence emissions; cost and a reliable supply source to prevent wasted laborious and time-consuming development; photostability and conjugation stability and consistency, for a reliable and reproducible performance. Fluorophores evaluated in the dissertation include those listed in Table 1 and used in Chapters 3 through 6. Dye entrapped polystyrene microspheres were observed to have better flow properties in nitrocellulose and provided the needed radiant intensity or brightness to provide the required SNR, sensitivity, and LOD. A preliminary evaluation was performed to determine a suitable membrane and fluorophore for LFA development. The flow rate and pore size of the membrane as well as the flow characteristics, and brightness of the fluorophore was used as a metric to down-select from a variety of options. To demonstrate the viability of fluorescent microspheres for LFA, 0.5 μm microspheres (Merck Millipore, France) were selected for use with nitrocellulose mem-

brane, HF07504XSS (Millipore, USA), in line with the industry accepted hypothesis that the pore size of the membrane should be 10X or more than the diameter of the microspheres used in a LFA to achieve an optimal flow rate Bangs Laboratories (2013). This hypothesis was tested in this chapter. The 0.5 μm microspheres and all fluorophore used in this work were conjugated to AffiniPure Goat anti-human IgG (Jackson ImmunoResearch Laboratories Inc., PA) using the manufacturers recommended protocol, for carboxyl functionalized microspheres. (Protocol details are presented in Appendix A). A more detailed treatment of membrane and fluorophores selection is presented in Section 7.3.1.

7.2.3 Membrane Cutting

Impregnation/protein immobilization on the nitrocellulose membranes was done by dispensing and drying overnight in a desiccator under vacuum. Clear backed Nitrocellulose membranes (30 cm x25 cm) sheets were cut to 50 mm x5 mm strips using a CNC Universal® laser cutter VLS 6.60 (Universal Laser Systems, Inc., AZ, USA) at and a state-of-the-art Industry standard diagnostic test strip cutter, Matrix 2360 programmable shear (Kinematic Automation Inc., CA, USA). The 60 W laser cutter was set to 34.5% power, 90% speed, 0.2 mm z-axis, and thickness set to 0.18 mm. Initial assay development was performed with laser-cut strips. Membranes were cut along the preferred flow direction Pelton (2009), which is usually along the length of the membrane sheet or roll. Laser cutting nitrocellulose and paper-based membranes have been widely reported by several research groups developing lateral flow, paper-based, μPAD, 2D and 3D paper networks Fridley *et al.* (2014); Li and Macdonald (2016b); Fu *et al.* (2011); Lee *et al.* (2016), and is useful for rapid prototyping. The benefit of laser cutting compared to diagnostic strip cutters is the ability to create exotic shapes and dimensions cut out of low-cost membranes.

Diagnostic cutters are designed to cut rectangular strips from pre-laminated cards, unbacked, or membrane rolls. The strips used in most diagnostic test are 3 to 6 mm wide. Diagnostic test strip cutters are designed to fit an assembly line for a high throughput in manufacturing, dispensing, strip, and cassette assembly. In this work, we observed that laser cut nitrocellulose has significantly higher autofluorescence background and higher intra and inter strip background variability, compared to mechanically cut strips. This is a significant problem for fluorescence-based assay development for high-sensitivity, especially if the laser cut area is in the detection zone of the assay. In contrast, these effects are not noticeable or inconsequential with visual or instrumented colorimetric applications. The effects of laser cutting are discussed in Section 7.5.2.

7.2.4 Test and Control Line Dispensing Protocols

Using a multipurpose fluid dispenser (Ultimus V and EV3 robot, Nordson EFD, USA), dispensing conditions for the antigens was determined. To prevent line broadening due to dispensed volume excess, a dispense pressure, 30 psi; vacuum pressure, 0.1 mmH_2O, 32 gauge stainless steel tip, and a 7 ms valve-on time was used to obtain 0.1 μL per spot. The spots were 1 mm pitch across the membrane width and 0.5 mm pitch along the lateral dimension of the strip, so that the spots bled into one another forming a scalloped microarray of antigen spots. The number of passes (0.1 μL x 10) was used to vary the dispensed volume as needed.

Proof-of-concept Lateral Flow Assay Development - IgG, EBNA, and HPV

The use and development of glass-based microfluidics and polymers including PDMS, PMMA, and Topas have been well documented in the literature . Modifying and functionalizing planar surfaces has also been explored extensively . However, nitrocellulose-

based microfluidics is well established and compatible with the demands and requirements for field-deployable diagnostic devices, especially in LMICs as discussed in Chapter 2. Some attractive features of nitrocellulose compared to glass include easy disposal of nitrocellulose and the added benefit of routing fluid by capillary action without any external pressure source. It was also hypothesized that a nitrocellulose membrane-based lateral flow assay will enable a lower detection limit, compared to a 2-dimensional planar glass substrate, due to the increased specific surface area in the 3-dimensional nitrocellulose membrane. To adapt the glass-based HPV assay discussed in Chapter 4 to a nitrocellulose membrane based lateral flow assay format, the lateral flow assay development was conducted in three phases, using 0.5 μm diameter polystyrene fluorescent microspheres (F1-Y050, Merck Millipore, France) and 75 s/4 cm nitrocellulose membrane (HF07504XSS, Millipore, USA).

IgG Titration on Nitrocellulose

First, a preliminary demonstration of the fluorescence detection of IgG antibodies on a nitrocellulose membrane was used to study the effect of fluorophore dilution and the dispensed/immobilized protein concentration. A titration of the microsphere-conjugate (secondary) and the immobilized whole human IgG (IgG assay) was conducted to determine the optimal concentration of immobilized protein and secondary. The immobilized whole human IgG recombinant protein concentration was 250 μg/mL, 25 μg/mL, 2.5 μg/mL, and 0.25 μg/mL, corresponding to 1.25 μg, 125 ng, 12.5 ng, and 1.25 ng of hIgG, respectively. The immobilized hIgG was incubated with different goat anti-human IgG-F1-Y050 microsphere conjugate concentrations, 1:100, 1:500, 1:1k, 1:5k, and 1:10k, corresponding to $58\text{x}10^6$, $11.6\text{x}10^6$, $5.8\text{x}10^6$, $1.16\text{x}10^6$, and $0.58\text{x}10^6$ microspheres, respectively. All recombinant protein dilutions were in phosphate buffered saline (PBS). Microsphere-conjugate dilutions were prepared in

BlockAid^{TM}Blocking Solution (Life Technologies, CA, USA) and 0.2% PBST, to minimize non-specific binding and agglomeration of the microspheres. For example, the 1:100 dilution was first prepared in BlockAid, then 2:1 of 1:100 dilution in 0.2% PBST. Microspheres were also sonicated before use. Samples were processed in triplicates for a total sample size, n=60.

Laser cut strips were mounted (centralized) on microscope slides, 75 mm x 25 mm x 1 mm (VWR International, Radnor, PA, USA) using a solvent resistant adhesive. The membranes were rinsed by by immersion in Di water (5X) and dried on a hotplate at 37°C, 19% relative humidity for 2 hours. 5 μL of the whole human IgG recombinant protein (hIgG), was dispensed using a 5x2 array of 0.1 μL spots to delineate the test (hIgG) and control lines (matching BSA concentrations). The process was repeated 4X for a total dispensed volume of 5 μL per line, with a 5 min pause between passes for the lines to dry. The test and control lines were dispensed at 6 mm pitch to match with the location of the fluorescence detection site and in line with previously reported crosstalk studies. The dispensed capture antigen was incubated for 16 - 18 hours in a vacuum desiccator at room temperature (22 - 23°C). Assays were performed by manually aspirating and applying reagents to the upstream end of the strips allow the reagents to flow through the nitrocellulose membrane and across the test and control lines by capillary action. The strips were pre-wet and conditioned by first applying 60 μL of PBST (2% tween in 1XPBS). For each strip, 60 μL of diluted secondary (microsphere-anti-human IgG conjugate) was applied and allowed to flow through the membrane for 20 min. The membranes were washed by aspirating and applying 200 μL of PBST in 4 steps (50 μL each). DI water was used to rinse the membranes by applying 100 μL in 2 steps (50 μL each). The assay was performed in an opaque staining tray to limit sample evaporation and ambient light effects. The test strips were allowed to drain completely into the wicking pad before drying on

a hotplate, at 37°C for 20 min. The fluorescence intensity was quantified using the ramp time difference and ratio between the test (IgG) and control (BSA) sites.

Epstein-Barr Virus Nuclear Antigen-1 (EBNA-1) Assay on Nitrocellulose

Next, the optimal conditions, dilutions, and concentrations determined from the IgG assay were used to develop a fluorescence-based assay to detect antibodies to Epstein-Barr Nuclear Antigen-1 (EBNA-1) in patient plasma. The goal was to study the effects of plasma dilution on signal intensity, immobilized protein concentration, and non-specific binding in a lateral flow assay format. According to the CDC, Epstein-Barr virus (human herpesvirus 4) infects humans only and over 90% of adults have been infected and show elevated antibody levels that persist for years. There is no vaccine for the disease and patients usually get better on their own. Studying plasma effects in a LFA using EBNA enabled access to a high volume of patient plasma or serum required during assay development. The relative ease of obtaining plasma samples positive for anti-EBNA-1 IgG antibodies (compared to HPV+ plasma samples) enabled its use in troubleshooting. Recombinant EBNA-1 protein (Advanced Biotechnologies Inc.) was dispensed in 3 passes and immobilized using 3 μL of 25 μg/mL and 3 μL of 50 μg/mL, for a total protein of 75 ng and 150 ng, respectively on the test line position of the strip, 6 mm further downstream than the BSA control line. A third line (positive control IgG) was added at 6 mm pitch from the EBNA test line. The multi-line (3 line) multiplexed test was used to study serum, microsphere, and membrane effects. A titration of EBNA-1 seropositive plasma dilutions (1:10, 1:50, 1:100, 1:200, 1:500, 1:1k, 1:5k, and 1:10k) in PBS was performed. The protocol is similar to the IgG titration protocol except for a few additions. After pre-conditioning the strip with 60 μL PBST, 75 μL of diluted plasma samples was added and allowed to flow through for 25 min, followed by a 200 μL PBST wash in

4 steps (50 μL each). The rest of the protocol was continued as discussed previously. Compared to the IgG protocol (no plasma), a sequential multi-step assay using patient plasma positive for EBNA-1 IgG antibodies was performed by applying reagents at the upstream end of the strips and allowing flow by capillary action through the strips, from the upstream to downstream end. A wicking pad was attached downstream to collect waste reagents and maintain the required capillary pull. Samples were processed in triplicates. The performance of the EBNA assay on nitrocellulose was compared to a glass-based assay and a laboratory-based chemiluminescence assay for EBNA.

Human Papillomavirus (HPV16 E7) Assay on Nitrocellulose

Finally, the knowledge, experience, and protocols developed in the IgG and EBNA assay was applied to toward the development of a fluorescence-based HPV16 E7 lateral flow assay. The target analyte is HPV16 E7 specific IgG antibodies in human plasma. Purified HPV16 E7 recombinant protein (produced at the Anderson Lab, Biodesign Institute, Arizona State University) was dispensed at 50 ng/mL in three 1 μL passes (150 ng of protein). BSA and IgG were used positive and negative control lines, respectively. The assay protocol is similar to the EBNA-1 assay protocol above except that patient plasma positive for HPV16 E7 IgG antibodies was titrated (1:10, 1:100, 1:1k, and 1:10k) and a negative patient control samples was used. Positive (case) and negative (control) plasma samples were processed in triplicates. The immunochromatographic reaction is initiated by the addition of patient plasma to the pre-functionalized lateral flow strips. When specimens containing high-risk HPV antibodies are present, the HPV antibodies bind to the immobilized recombinant protein on the nitrocellulose membrane (solid support). The membrane is washed with PBST to remove non-specific material that may have bound all over the strip.

A fluorophore-anti-human IgG antibody conjugate (secondary antibodies) is then used to detect the bound HPV antibodies followed by a PBST was to remove non-specifically bound secondary-fluorophore conjugates. The secondary antibodies are bound in proportion to the concentration of the circulating biomarkers. Fluorescence was measured using the DxArray platform which correlates with the amount of HPV IgG antibodies present. The performance of the HPV16 E7 assay on nitrocellulose was compared to the glass-based assay developed in Chapter 4 and a laboratory-based chemiluminescence assay for HPV16 E7.

7.2.5 Plasma Samples

De-identified pooled normal human plasma samples for the EBNA and HPV assay development were obtained from Blood Centers of the Pacific (San Francisco, CA, USA). Commercially available pooled normal donor whole blood samples were obtained from Innovative Research (Phoenix, AZ, USA). Plasma separation was performed by centrifugation at 1200xg for 10 min. The extracted plasma sample was aliquoted (200 μL) and stored at -20°C and used in the study of microsphere diameter and flow rate effects (no hemolysis was observed). The plasma samples (HPV+ and healthy controls) used in this work were previously tested for HPV16 E7 DNA by PCR in a previous study, the Human Oral Papillomavirus Transmission in Partners over Time (HOTSPOT) study Anderson *et al.* (2015c). The study design, enrollment, and serologic responses to HPV16 has been previously detailed and reported D'Souza *et al.* (2014). (Clinical Trials number: NCT01342978). Written informed consent was obtained from all subjects in accordance with Arizona State University institutional review board approval. All experimental protocols were approved and were carried out in accordance with the relevant guidelines under the Arizona State University institutional review board. All of the methods involving human subjects were car-

ried out in accordance with the relevant guidelines previously stated Anderson *et al.* (2015c).

7.3 Effect of Membrane Flow Rate and Microsphere Diameter in Fluorescence LFA Development

The membrane flow rate directly impacts the assay performance by influencing the reaction rate of the species in a lateral flow assay membrane. The reaction rate decreases as the square of the flow rate. The flow rate is determined by the surface characteristics and the porosity of the membrane. The membrane porosity also influences the specific surface area available for capture agent immobilization. The fluorescent microsphere diameter plays a significant role in the flow of the detector reagent. Size limitations, surface properties, brightness, and degree of agglomeration are important parameters to consider in microsphere selection. This section focuses on the effect of microsphere diameter and membrane pore size on lateral flow assay performance. The microsphere diameter determines fluorescence intensity, larger microspheres are brighter but present a significant challenge in flow dynamics. It is, therefore, necessary to investigate the entire experimental space of varying membrane pore sizes for lateral flow and fluorescent microsphere diameter.

7.3.1 Membrane and Microsphere Selection

Table 7, lists some commercially available transparent-backed lateral flow membranes. The HF series membranes (Millipore-Sigma, MA, USA) and the Unisart series (Sartorious, NY, USA) cover the entire space of commercially available membrane flow rates, ranging from 75 s/4cm to 180 s/4cm. Generally, membranes used in lateral flow assays have pore sizes between 8 to 15 μm Wong and Tse (2009). A more representative metric for the sponge-like polymeric structure is the capillary

flow/wicking rate or capillary rise time that characterizes lateral flow membranes. The industry standard is to measure capillary flow times with water for 4 cm distance on a 10-mm wide membrane strip.

Table 7: Commercially Available Clear-backed Nitrocellulose for Lateral Flow Assays

Catalogue No.	Lot No.	Flow rate*	Av. flow rate†	Thickness‡
HF07504XSS	R6MA20904C	75	67 to 83	224 to 246
HF09004XSS	R7DA99876C	90	81 to 99	224 to 246
HF12004XSS	R7JA45494C	120	108 to 132	224 to 246
HF13504XSS	R7HA32496C	135	121 to 149	224 to 246
HF18004XSS	R7EA17860C	180	162 to 198	224 to 246
Unisart CN95	1800683	89.9	83.3 to 96.4	242.6 to 248
Unisart CN110	1605203	110.6	105.4 to 115.8	191.9 to 196.9
Unisart CN140	1800393	121.6	115.6 to 127.6	235.8 to 240.6

*Nominal capillary flow rate (s/4 cm). Capillary flow test performed at 50±5% RH and 21±1.5°C
†Average (master roll) capillary flow rate (s/4 cm)
‡Average (master roll) composite thickness (μm)

It is worth noting that nitrocellulose-based lateral flow membranes are significantly different than nitrocellulose membranes used in filtration, blotting, and vertical flow or flow-through devices; these tend to have a sub-micron pore size and hydrophobic surface characteristics. A more comprehensive discussion of the role of analytical membranes in lateral flow assays was presented in Chapter 2, Section 2.6.3. Carboxyl functionalized, monodispersed polystyrene dye entrapped fluorescent microspheres, F1-Y010, F1-Y030, F1-Y050, F1-Y080, and F1-Y100 (Merck Millipore, France) corresponding to 0.1, 0.3, 0.5, 0.8, and 1 μm diameter, respectively was used to investigate the effect of microsphere diameter in fluorescent microsphere-based lateral flow assay.

The fluorophores were characterized by preparing logarithmic dilutions in DI water and corresponding/matching reference buffers were used to quantify the fluorescence response using a dilution factor from stock down to 1:10M. The microspheres were sonicated for 5 min before use to reduce the tendency for agglomeration, ensuring that the microspheres are monodispersed. 10 μL of each dilution was spotted HF07504XSS (N=3) and the normalized fluorescence intensity was obtained. The sigmoidal titration curve was fitted with a 5 parameter logistic (5PL) fit and iso-response points were identified and used to characterized the microsphere diameter and membrane pore size effect. Epstein-Barr nuclear antigen-1 assay was used as a model assay with BSA and IgG as negative and positive control, respectively. The BSA negative control, EBNA-1 recombinant protein (test), and whole human IgG recombinant protein (positive control) lines were spotted in 3 passes using a concentration of 50 μg/mL for a total of 150 ng of protein. The upstream BSA and a blank (no protein) line further downstream was used to monitor the nonspecific binding in the membrane as a function of pore and microsphere size. The carboxyl functionalized microspheres were conjugated to goat anti-human IgG antibodies according to the manufacturers recommended protocol.

7.3.2 Nitrocellulose-based Multiplexed Assays - The Effect of Upstream-downstream Test Line Position

Multiplexed LFA has the potential to improve diagnostic accuracy, precision, enable decision making by physicians, lower diagnostic costs, and expand the application of LFA in general Li and Macdonald (2016b,a). For example, the diverse array of oncogenic HPV types presents a significant engineering challenge for low-cost high-throughput/multiplexed systems to measure serologic responses across multiple types and oncogenic proteins. The standard single rectangular strip multiplexed lateral flow

assay design suffers from a number of challenges Cogan (2017b). For a single strip, there is a non-linear decrease in the flow rate of the fluid as the fluid front makes its way downstream. Therefore, the kinetics of the binding reaction varies with position on the strip. Assuming an infinite supply of analyte and detector reagents, test lines of the same capture agent concentration located further downstream are more likely to generate a higher signal intensity compared to those located upstream Mansfield (2015); Cogan (2017a). To account for this effect, the capture reagent concentration dispensed needs to be adjusted accordingly (concentration compensation), along with the detector reagent concentration. Using the IgG assay described in Section 7.2.4, multiple (3) lines of equal IgG recombinant protein concentration was studied to quantify the effect of upstream-downstream position, as a function of membrane flow rate and secondary label concentration. Recombinant IgG (75 ng) was dispensed at 6 mm pitch on nitrocellulose membranes with flow rate varying from 75 s/4cm to 180 s/4cm (Millipore HF-series). Goat-antihuman IgG-microsphere conjugate (0.5 μm) (secondary-conjugate) concentration, 1:5, 1:20, 1:50, 1:100, and 1:500) corresponding to 5.28x10^8, 2.64x10^8, 1.32x10^8, 5.76x10^7, 2.88x10^7, and 1.44x10^7, respectively, prepared in a sequential dilution.

7.3.3 Membrane/Polymer Transmission Measurement

In Chapter 6, the use of transparent-backed nitrocellulose for transmission mode detection and white-backed nitrocellulose for coplanar mode detection was discussed. The transmission mode detection was found to be more sensitive. The scattering characteristics of nitrocellulose limits the excitation light penetration and the emitted fluorescence collection efficiency. Furthermore, the opacity of the industry standard polyester backing versus a transparent backing material shows poor light transmission. The transmission of membranes listed in Table 7 was measured between 350 to 850 nm,

dry and wet with DI and 1XPBS. The transmission of stand-alone industry standard white and optically clear backing polymers (Lohmann, CA, USA) was measured from 350 to 850 nm.

7.3.4 Membrane Autofluorescence

Many of the gold standard techniques, materials, and methods used in the design and development of visual colorimetric assays and paper-based microfluidics are not compatible with fluorescence-based lateral flow assay development. Autofluorescence of plant-based, organic and inorganic materials synthesized with additives that show significant autofluorescence are commonplace in most fabrication processes. This leads to contamination and increased background in many polymeric membranes. Care and consideration in material selection for use in fluorescence applications is a critical process and autofluorescence usually manifests in limiting the dynamic range of the overall system. For example, paper patterning using photoresist and wax Martinez *et al.* (2008) may be detrimental for fluorescence-based devices and limit the detection sensitivity for applications requiring the detection of extremely low analyte concentrations. Several reports using cotton, fabric, and paper in the development of colorimetric assays do not have to bother about the high intrinsic autofluorescence and variability that becomes immediately apparent in fluorescence applications. Membranes were inspected for autofluorescence using an epi-fluorescence microscope (Eclipse LV100, Nikon Instruments Inc., NY, USA).

7.4 Results and Discussion

7.4.1 Secondary-fluorophore Conjugate and Immobilized Whole Human IgG (hIgG) Protein Titration

Figure 53 (a) and (b) depicts a representative plot of the titration of immobilized whole human IgG on and nitrocellulose and the titration of the secondary-fluorophore conjugate. This experiment was used to determine the concentration range of recombinant protein to dispense on the test, negative, and positive control lines in the EBNA-1 and HPV assay.

The detected fluorescence intensity decreased with decreasing protein concentration and secondary concentration. Recombinant protein concentration, 25 μg/mL and 50 μg/mL (three 1μL dispense passes for a total of 75 ng and 150 ng, respectively, of immobilized recombinant protein) was chosen as the signal intensity saturated be-

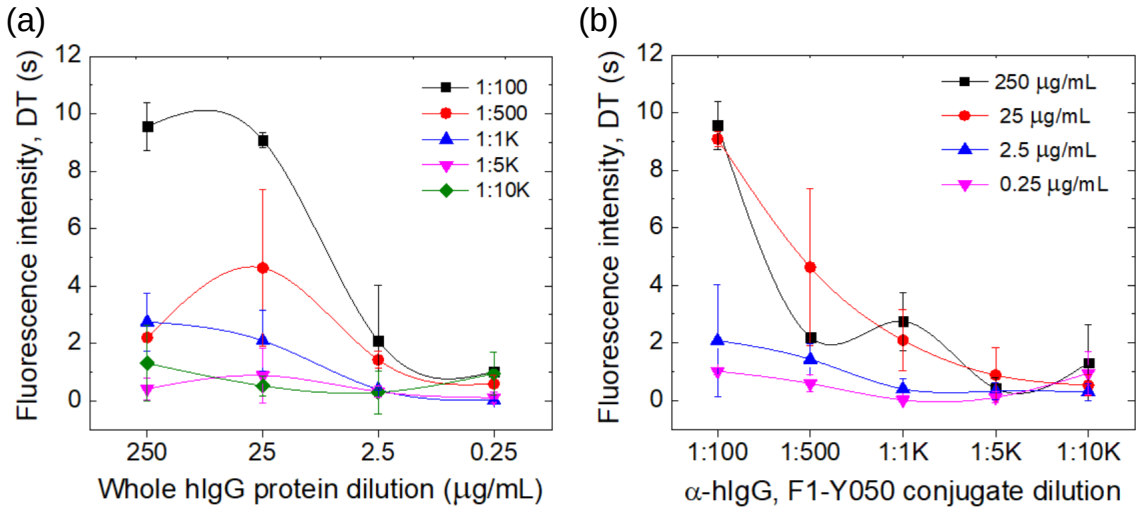

Figure 53: (a) Signal Intensity (Detection Time, DT) as a Function of α-hIgG-F1-Y050 Conjugate Concentration (b) Signal Intensity, (Detection Time, DT) as a Function of Whole Human IgG Recombinant Protein Concentration.

tween 25 μg/mL and 250 μg/mL. Secondary-fluorophore conjugate dilution, 1:100 was selected for assay development (40 μL of 1:100 dilution in BlockAid, mixed with 20 μL of 0.2% Tween in 1X PBS). The corresponding number of microspheres, $57.6\text{x}10^6$, was estimated using the unconjugated stock concentration ($1.45\text{x}10^{11}$ 0.5 μm diameter microspheres/mL). For context, colorimetric LFAs that use 0.5 μm blue latex microspheres require $1.45\text{x}10^{10}$ microspheres stored on a conjugate pad and concentrations less than $1\text{x}10^8$ are not visible by the naked eye.

7.4.2 Effect of Upstream-downstream Test Line Position on Single-strip Multiplexed Test

Figure 54 (a) shows the experimental space investigated with membranes of variable flow rate and at different secondary-conjugate concentrations (Figure 54 (b)). Figure 54 (a) (below) depicts the test line setup for equal concentrations of dispensed recombinant IgG protein (75 ng). IgG was used for this study as it has been observed to bind effectively to nitrocellulose and is extensively used as a positive control in serology. BSA was used as a reference/negative control.

The BSA line intensity was used to estimate the degree of non-specific binding (NSB) as a function of membrane flow rate and conjugate concentration. An expected decrease in NSB is observed as conjugate concentration decreases, flattening out at 1:100 ($\sim$57.6 million microspheres). An intensity dispersion is observed as conjugate concentration is increased to 1:5 ($\sim$529 million microspheres). The measured background or BSA intensity is a function of the intrinsic membrane background and is related to the pore size and distribution dependent extinction (scattering plus absorption) of each membrane type. The flat intensity profile at lower concentrations is indicative of indistinguishable conjugate concentrations due to NSB as the probability of agglomeration and pore clogging reduces with the number of microspheres.

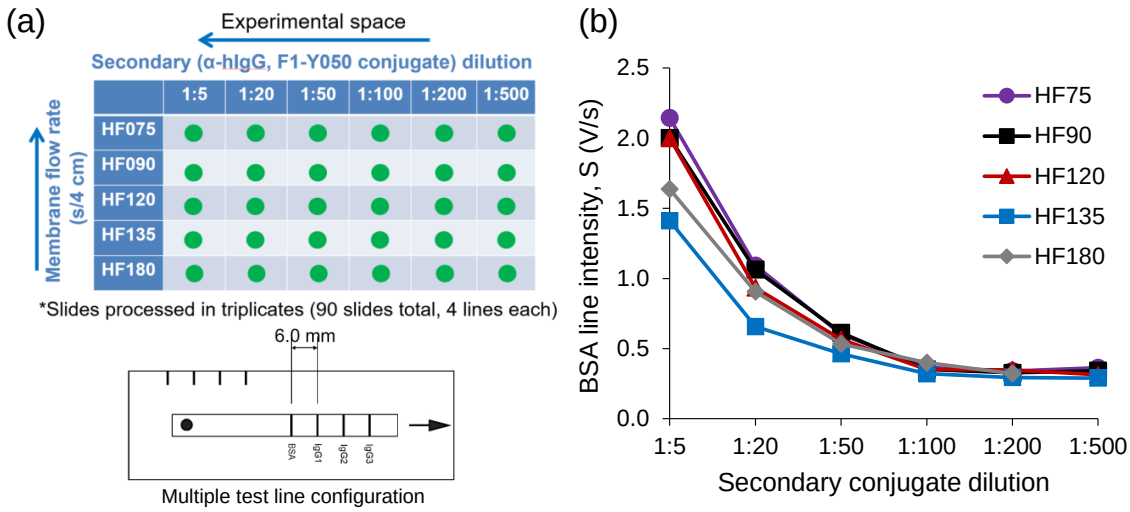

Figure 54: (a) Experimental Space to Study to Effect of Upstream-downstream Test Line Position Using Varying Membrane Flow Rate and Fluorescent Label Conjugate Concentration (b) Signal Intensity, S (V/S) for the BSA Control Line; Indicative of Non-specific Binding as a Function of Fluorophore Concentration in Different Membrane Types.

Therefore, an optimal concentration that minimizes NSB while maximizing SNR was selected (1:100). A more detailed treatment of membrane effects is presented in Section 7.5.4. Figure 55 (a) is a representative fluorescence image of three at concentration (1:5, 1:50, and 1:500), the BSA line is not shown (however no different in intensity than other areas of the strip away from the IgG test lines). The image was acquired using a Nikon LV100 microscope with a smartphone camera attached to a TV lens adapter to increase the field of view. Figure 55 (b) to (d) shows the relative fluorescence intensity (average across membrane types) of the BSA and three IgG lines (IgG1, IgG2, and IgG3) indicated as spectrum A1, A2, A3, and A4, respectively. The spectra was acquired using a thermo-electrically cooled CCD fiber optic fluorescence spectrometer (QEPro, Ocean Optics, FL, USA).

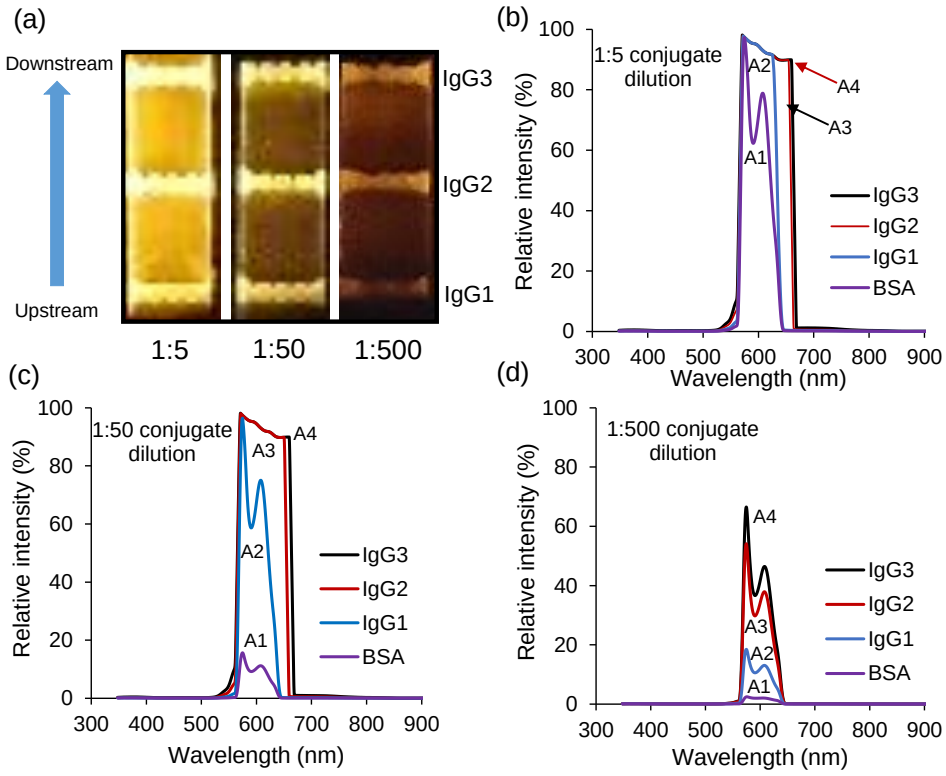

Figure 55: (a) Representative Fluorescence Images of Multiple Lines of Equal IgG Recombinant Protein Concentration Dispensed on a Rectangular Nitrocellulose Membrane (50 mm x 5 mm), 6 mm Pitch and at Logarithmically Varied Fluorophore Concentration (1:5, 1:50, and 1:500) (b) to (d) Average Relative Fluorescence Intensity of BSA and IgG Test Lines at 1:5, 1:50, and 1:500 Microsphere-conjugate Concentration Across Membrane Types. Spectra Was Measured with a Fiber Optic High-sensitivity Fluorescence Spectrometer.

Appropriate filters (520/40 nm excitation and 605/70 emission filters were used in all measurements and the fiber was connected to the epi-fluorescence microscope using a SMA905 and TV lens adapter. A decrease in the concentration dependent background NSB and fluorescence intensity from the test lines is observed with decreasing conjugate concentration. The CCD detector is saturated under normal settings (5 s

integration time, true boxcar width = 5, with a 200 μm fiber) for IgG lines 2 (A3) and 3 (A4) at 1:5 and 1:50 conjugate concentration. The true emission spectra of the microspheres (F1-Y050, Merck, France) and the effect of line position (upstream versus downstream) is shown in Figure 55 (d). It is advantageous to have the farthest line on a strip located at least 10 mm away from the wicking/absorption pad as the fluidic resistance at the interface increases when the wick is fully wetted.

This may lead to an accumulation of microspheres downstream in the absence of a wash buffer excess. Figure 56 (a) to (f) depicts the effect of varying concentration, membrane flow rate, and test line position. Overall, the IgG3 line (farthest downstream) was shown to generated the highest signal intensity as long as the secondary-conjugate was in excess (at higher concentration, 1:10 to 1:100) as shown in Figure 56 (a) to (d). As the conjugate concentration decreases, the overall signal intensity decreases. The available (limited) conjugate gets taken up by the first and second test lines (IgG1 and IgG2). The slowest flow rate membrane (HF18004XSS) had the highest sensitivity to test line position and thus would require significant concentration compensation to be used in a multiplexed quantitative test. The slower flow rate membranes (HF07504XSS and HF09004XSS) are least sensitive to test line position, although the fast flow rate may negatively impact reaction time required for signal development. For the development of quantitative fluorescence LFA, the small differences in signal intensity observed significantly impacts the results or interpretation, albeit many visual and instrumented colorimetric applications are not sensitive to such changes.

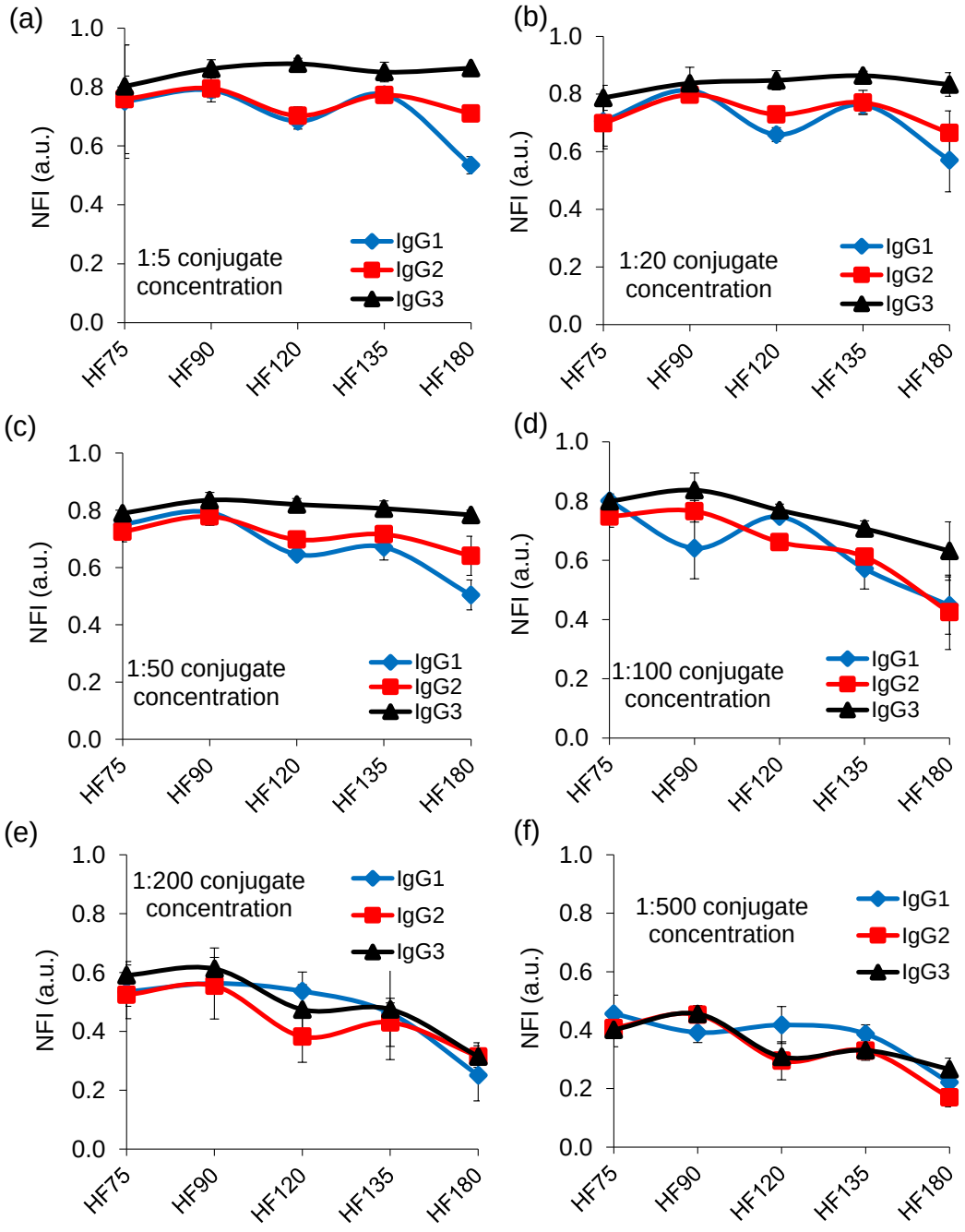

Figure 56: Normalized Fluorescence Intensity (NFI) as a Function of Membrane Type and Test Line Upstream-downstream Position. (a) Intensity Changes with Secondary Microsphere Conjugate Concentration (a) 1:5 (b) 1:20 (c) 1:50 (d) 1:100 (e) 1:200 (f) 1:500. N=3 at Each Dilution and for Each Membrane; Total n=90

7.4.3 *EBNA-1 Assay and Plasma Dilution on Glass and Nitrocellulose*

The objective of this experiment was to develop a multi-step HPV lateral flow assay using EBNA-1 as a model assay, with patient plasma. First, the anti-EBNA-1 IgG assay was performed on glass and nitrocellulose. 150 ng of recombinant EBNA-1 protein was immobilized on glass and 75 ng on nitrocellulose. Patient plasma positive for anti-EBNA-1 antibodies was diluted from 1:1 to 1:10k and tested with the glass-based samples. Figure 57 (a) and (b) shows the measured fluorescence intensity from glass and nitrocellulose-based assays.

The inset of Figure 57 (a), indicates that the EBNA-1 IgG antibodies are barely detectable even at high serum dilutions. The limited surface binding area and mass

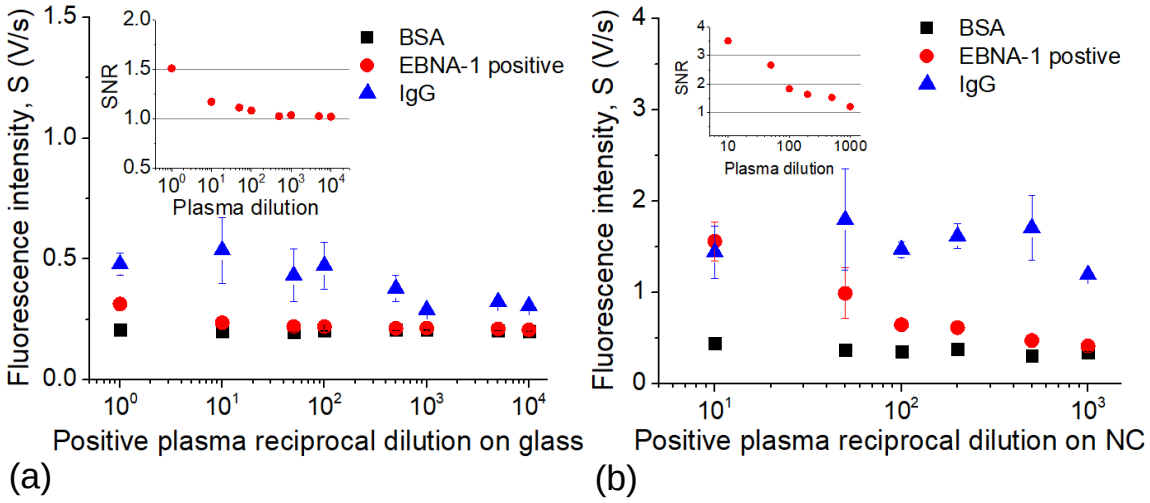

Figure 57: Signal Intensity, S (V/S) as a Function of Reciprocal Dilution of Patient Plasma. (a) Anti-EBNA-1 IgG Positive Plasma Dilution from 1:1 to 1:10k on Glass. Immobilized Recombinant IgG and BSA Positive and Negative Control, Respectively at 75 ng, EBNA-1 at 150 ng (b) Anti-EBNA-1 IgG Positive Plasma Dilution from 1:10 to 1:1k on Nitrocellulose. Immobilized Recombinant IgG and BSA Positive and Negative Control, Respectively at 75 ng, EBNA-1 at 75 ng.

transport limitations significantly impacts the performance of the assay on glass. The recombinant protein (EBNA-1) was dispensed directly on APTES coated slides and incubated at 4°C for 16 - 18 hours. It is possible that covalent adsorption could improve the performance of assays on 2D planar surfaces, however a 3D porous membrane offers several orders of magnitude increase in the available binding area for protein immobilization. This effect is evident in Figure 57 (b) which depicts the measured fluorescence intensity from assays on nitrocellulose. As an initial test, a titration of anti-EBNA-1 IgG positive patient plasma from 1:10 to 1:1k was performed on the pre-functionalized nitrocellulose samples. The inset indicates 2 orders of magnitude improvement using nitrocellulose over glass, with half the amount of protein immobilized (75 ng) compared to glass (150 ng). To improve the performance of the assay on nitrocellulose, the immobilized recombinant protein concentration was increase to 150 ng. Figure 58 depicts the fluorescence intensity measured against the reciprocal plasma dilution on the x-axis.

Positive (anti-EBNA-1 IgG positive) and negative (anti-EBNA-1 IgG negative) patient plasma was diluted and tested on pre-functionalized nitrocellulose membranes. Membranes were functionalized by dispensing capture proteins on the negative control (BSA), test line (EBNA-1) and positive control (IgG). Figure 58 (a) shows the titration of EBNA-1 IgG positive patient plasma, effective decreasing the analyte concentration in the sample. The generated fluorescence signal intensity decreased with plasma dilution for the positive plasma. The corresponding increase in the positive control signal intensity (IgG) is indicative of a secondary-conjugate excess, taken up by the IgG line, as more conjugate becomes available with decreasing analyte concentration in the sample. We conservatively estimate that the positive plasma titers out between 1:500 and 1:1000 dilution as indicated by the SNR shown in the inset. This represents a 3 orders of magnitude improvement over assays performed on glass. A

slightly elevated intensity of the negative plasma compared to BSA (Figure 58 (b)) is indicative of non-specific binding in plasma. Surface treatment and drying conditions significantly affect capture protein adhesion/immobilization to nitrocellulose EMD Millipore (2013). However, passive adhesion presents a fast and easy immobilization strategy, especially in nitrocellulose-based LFA development. In this study, protein immobilization was investigated by applying different drying conditions after protein dispensing. Nitrocellulose samples with dispensed recombinant protein were stored at ambient (23°C, 19% RH), on a hot plate at 37°C, air-dryer at 37°C, and vacuum desiccator at ambient (23°C, 19% RH), for 16-18 hours. After troubleshooting and optimizing the microsphere concentration, running buffer volume, washing conditions,

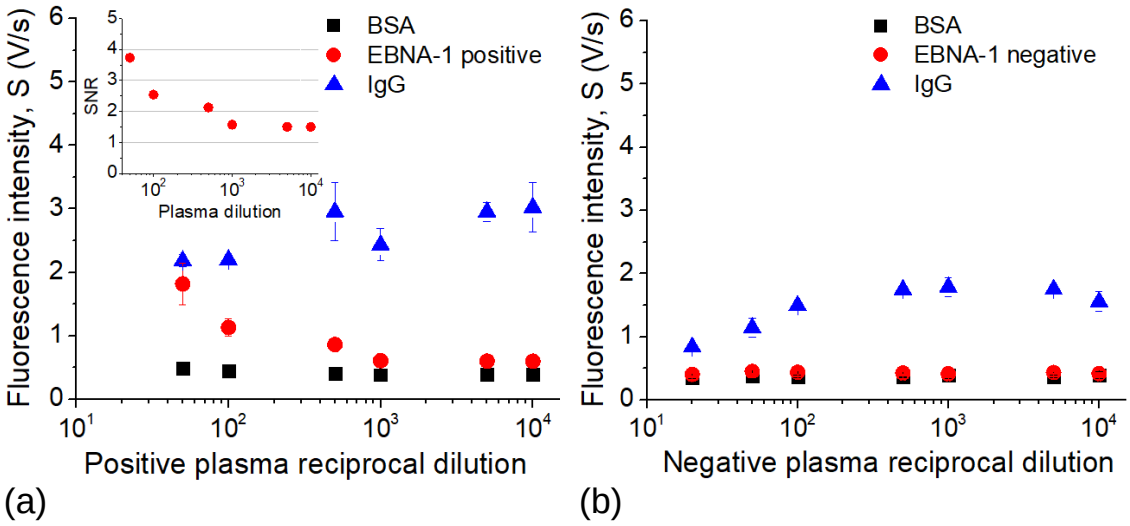

Figure 58: Signal Intensity, S (V/S) as a Function of Reciprocal Dilution of Patient Plasma. (a) Anti-EBNA-1 IgG Positive Plasma Dilution from 1:50 to 1:10k. Inset Shows SNR. Immobilized Recombinant IgG and BSA Positive and Negative Control, Respectively at 150 ng, EBNA-1 at 150 ng (B) Anti-EBNA-1 IgG Negative Plasma Dilution from 1:10 to 1:10k. Immobilized Recombinant IgG at 75 ng, BSA at 150 ng, and EBNA-1 at 150 ng (N=3 at Each Dilution).

serum dilution, non-specific binding, it was determined that drying the dispensed recombinant protein on nitrocellulose in a vacuum desiccator gave the most reliable and consistent result of all the drying processes investigated.

7.4.4 HPV16 E7 Assay and Plasma Dilution on Nitrocellulose

Here, the knowledge and techniques developed and reported in Chapter 4 and those discussed in this chapter towards the development of an IgG and EBNA-1 assay on nitrocellulose was extended and applied towards the development of a nitrocellulose-based anti-HPV16 E7 IgG assay. Figure 59 depicts the fluorescence intensity generated by a titration of known patient plasma positive and negative for anti-HPV16 E7 antibodies. The case (HPV16 E7 positive) and control (healthy spouse) samples were obtained as described in Section 7.2.5.

Plasma dilutions, 1:10 to 1:5k was tested on a nitrocellulose membranes as described previously. As expected, the fluorescence intensity decreased with decreasing analyte concentration. The corresponding increase in IgG positive control signal is a result of more secondary conjugate available at the downstream end of the strip as analyte concentration was decreased in the dilution series. Figure 60 (a) and (b) compares the signal intensity obtained from the DxArray platform using nitrocellulose and a chemiluminescence-based laboratory microplate ELISA. The inset of Figure 60 (a) shows the signal-to-noise ratio calculated as a signal-to-BSA ratio for the case. The DxArray is capable of detecting a 1:1000 plasma dilution which represents an order of magnitude improvement over the glass-based assay reported in Chapter 4. The non-zero intensity on the negative BSA control line due to NSB (microspheres getting trapped or bound within the pores of the NC membrane). Furthermore, the non-zero intensity observed with the negative anti-HPV16 E7 IgG plasma is likely due to cross-reactivity, interferants, and NSB in membrane due to agglomeration and

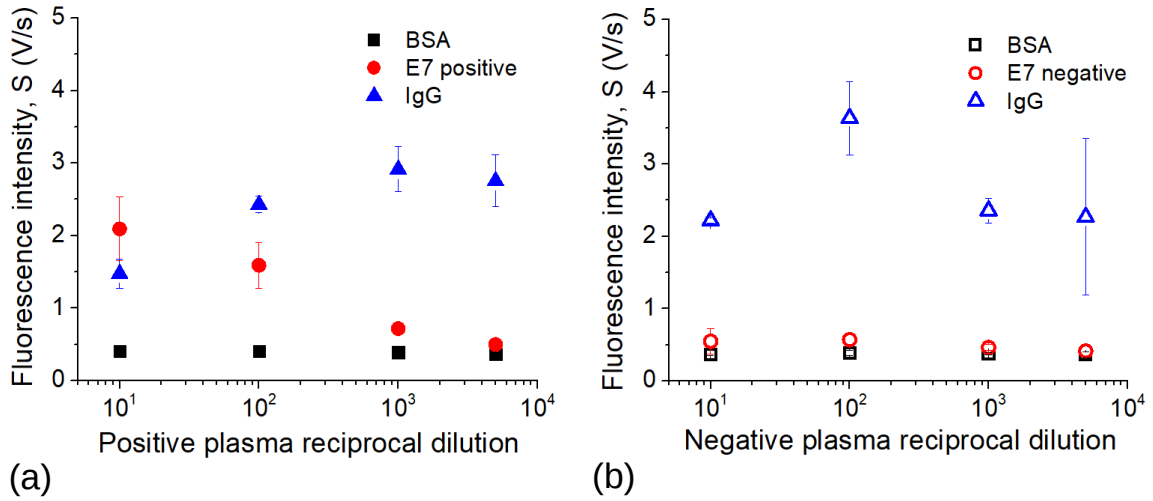

Figure 59: Fluorescence Intensity, S (V/s) as Function of Plasma Dilution for Nitrocellulose-based HPV Assay. (a) Anti-HPV16 E7 IgG Positive Plasma Diluted From 1:10 to 1:5k. (b) Anti-HPV16 E7 IgG Negative Plasma Diluted From 1:10 to 1:5k. Immobilized Recombinant IgG at 150 ng, BSA at 150 ng, and Purified Recombinant HPV16 E7 at 150 ng (N=3 at Each Dilution).

pore/microsphere size effect.

The inset of Figure 60 (b) shows that the chemiluminescence based test is capable of detection analytes in plasma dilutions less than 1:10,000. This is as a result of the low background/NSB associated with the control compared to the POC platform. The ELISA process embodies several wash steps and efficient protein immobilization to the walls of the microplate wells, uses larger reagent volumes, and self-amplifying chemiluminescence reaction. Table 8 compares some performance and protocol parameters of the glass-based HPV assay developed in Chapter 4, the nitrocellulose-based HPV assay developed in this chapter, and a laboratory ELISA evaluated using the same patient plasma. There is significant room for improvement in the performance of the platform and significant gains could be made by optimizing the fluorescence and nitrocellulose-based assay components as detailed in the conclusions of the disserta-

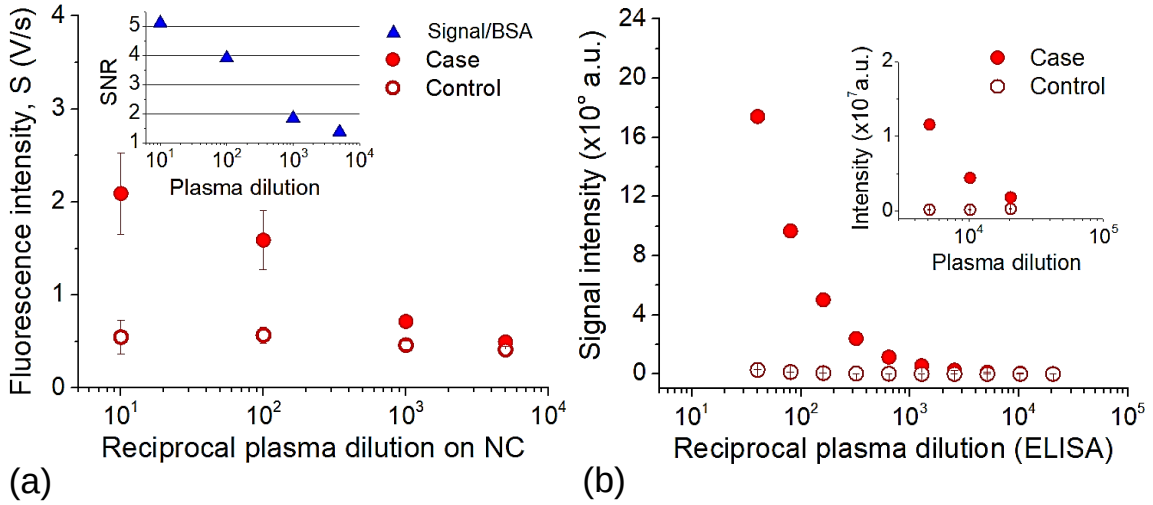

Figure 60: (a) Fluorescence Intensity Generated From a Titration of Patient Plasma Positive (Case) and Negative (Control) for Anti-HPV16 E7 Antibodies, The Inset Shows the Signal-to-BSA Ratio (SNR). (b) The Same Plasma Samples Analyzed by a Standard Laboratory Microplate Chemiluminescence ELISA.

tion (see Chapter 8). Overall, the result of translating the HPV test from a glass to nitrocellulose-based format indicates that the developed platform is a viable tool with potential applications toward rapidly screening patient populations especially in LMICs to risk stratify patients and support clinical decisions made by physicians.

7.5 Practical Considerations for Fluorescence Lateral Flow Assay Development

Many of the industry norms have been driven by the design and development of rapid diagnostic tests, which mostly use color indicators that are visible to the naked eye, that can be captured by a camera, or measured with minimal instrumentation. However, there are significant challenges to the development of fluorescence-based quantitative assays including, the opacity and autofluorescence of nitrocellulose, non-specific binding, poor sensitivity, and lack of repeatability and reproducibility. This section discusses some of these issues.

Table 8: Comparison Between HPV Assay on Glass, Nitrocellulose, and ELISA.

Parameter	HPV assay on glass	HPV assay on NC*	ELISA†
Capture immobilization	Passive (APTES)	Passive	Covalent
Dispenser	By hand	Ultimus V	Multiple options-
Protein concentration	3 μL of 50 ug/mL (150 ng)	3 μL of 50 ug/mL (150 ng)	-
Plasma volume	150 μL	<2 μL	150 μL
Blocking	5% milk, 1 hour	None	E. coli lysate
Plasma incubation time	1 hr	25 min	1 hour
Number/vol. of wash	Buffer excess (BE)	3, 500 μL	BE
Actual assay time	3 hours	1 hour	2 hours
Titre/LOD	1:100	1:1k	<1:10k
Dynamic range	1 log	2 logs	2-3 logs

*NC = nitrocellulose; BE = buffer excess
†Rapid antigenic In-sutu Protein Display ELISA

7.5.1 Membrane and Backing Material Transmission

The optical properties of solid support materials used for assays plays a significant role in device performance. The ubiquity glass and other optically similar polymers (e.g., polystyrene) in laboratory applications is mainly driven by their low-cost and transparency. Particularly, the optical properties of the polyester backing material used to provide mechanical support for nitrocellulose membranes directly impacts optical measurements on nitrocellulose membranes. Figure 61 (a) compares the transmission of NC mounted on an opaque backing, and optically clear/transparent

backing and improvements in transmission when the membranes are wet compared to when dry.

Besides the attractive benefits of paper including low-cost and immunochromatographic characteristics, sensitive detection from nitrocellulose could be challenging Kim and Herr (2013) due to the optically opaque characteristics as shown in Figure 61 (a). The ideal membrane or microfluidic device should have stable capillary characteristics, a 3D surface for binding, allow light penetration to excite fluorophores, and enable the efficient collection of emitted fluorescence light. Figure 61 (b) shows the transmission of industry standard backing materials. The white backed materials are most frequently used, especially in in colorimetry applications. The use of a clear

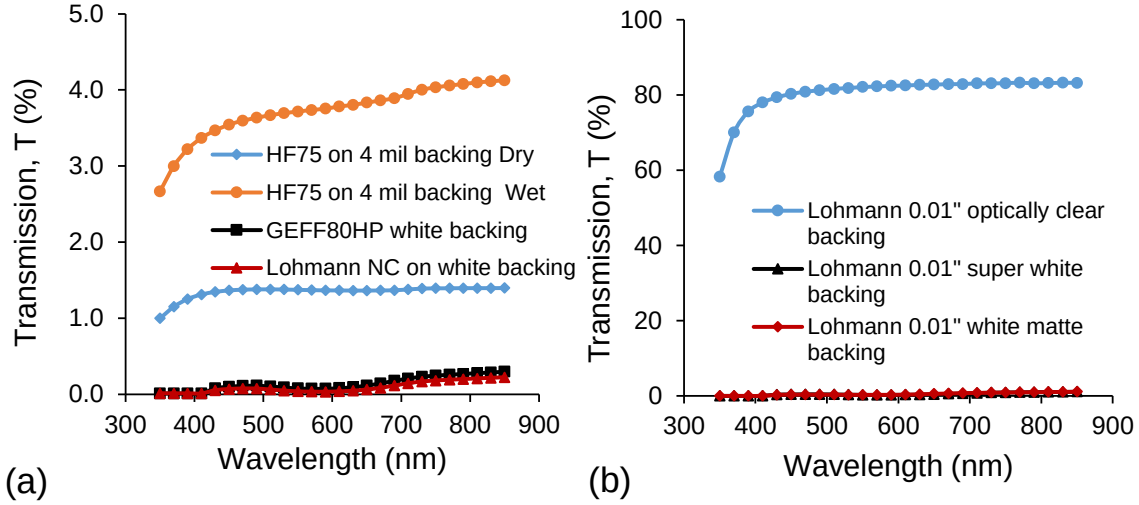

Figure 61: Transmittance of Nitrocellulose and Backing Materials (a) Transmittance of a Typical 130-150 μm Thick Nitrocellulose Membranes on a Clear 4 mil Backing (HF07504XSS, Millipore). Dry and Wet (DI and PBS) Membrane Transmittance Measured. White Backed Membranes (GEFF80HP, GE Healthcare) and White Backed Nitrocellulose (Lohmann Inc.), Backing Thickness is 10 mil. (b) Transmittance of Stand-alone 10 mil Thick Backing Polyester Material (Clear and White).

backing material enables excitation light coupling into the nitrocellulose.

7.5.2 Autofluorescence, Background Variability, Non-specific Binding and Quantitative Tests

Autofluorescence in paper-based membranes is higher at shorter wavelengths and decreases toward longer wavelength. For this reason there has been significant effort toward developing fluorophores in the red to near IR regions of the electromagnetic spectrum Swanson and D'Andrea (2013) to improve analytical sensitivity. However, such developments have not limited the development of fluorophores in the near UV and blue range, especially Europium (III) and quantum dots excited at shorter wavelength light (300-400 nm). The wide Stokes shift and relatively long decay time allows for time-gated applications (detect fluorescence signal during decay after the excitation light has been turned off). Autofluorescence decay lifetime (10^9) is comparable to the lifetime of many organic dyes and usually shorter than the fluorescence lifetime of quantum dots and Europium-based labels (a few μs to ms). All other factors being constant, time-gated applications may enable systems with higher performance. However, for low-cost applications the potential gain is limited to finding efficient non-absorbing materials at short wavelength as well as portable and efficient light sources.

Intra and inter lot variations in nitrocellulose membrane properties ($\sim$5 to 10%) are related to the production process and the tight control required to produce reliable and reproducible sheets and rolls Wong and Tse (2009); Nargang *et al.* (2016), with uniform thickness and composite structure. The mean optical background varies for different membrane types as shown in Figure 62 (a). This variation is due to small differences in porosity (leading to tunable flow rate) and extinction due to intentional production related variations in microstructure.

The variability in nitrocellulose could be further impacted by the membrane cutting technique used during assembly and manufacturing. While such effects may not be significant for visual-based colorimetric or qualitative fluorescence applications, we observed higher variability in membranes cut with a laser cutter and a bright autofluorescent edge due to the heat dissipated in the cutting process, compared to mechanically cut strips as shown in Figure 62 (b) and (d).

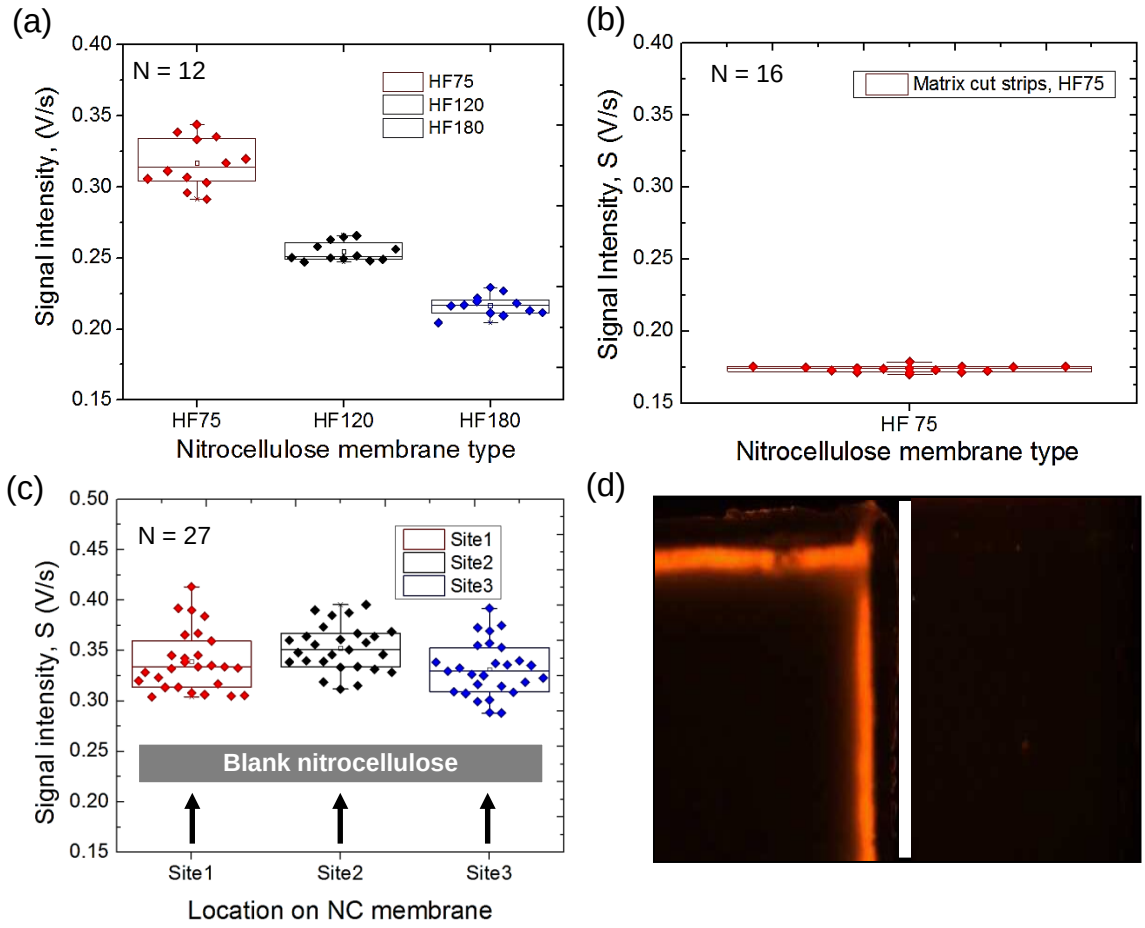

Figure 62: (a) Optical Background Variability in Nitrocellulose Membrane Types (Different Flow Rate) (b) Effect of Cutting Technique on Optical Background (c) Intra and Inter Strip Optical Background Variability (d) Representative Images of Laser Cut (Left) and Mechanically Cut (Matrix 2560) Nitrocellulose Membranes (Right).

For quantitative fluorescence applications, the uniqueness of each nitrocellulose membrane as observed by the intra and inter membrane variability (Figure 62 (c)) has to be accounted for. The variability in the measured optical background is due to the unique distribution of the membrane structure that directly affects transmission and bulk autofluorescence through the membrane cross-section. Overall, it is our observation that both low transmittance and autofluorescence affects light out-coupling from the membrane and dominates inter and intra strip variability, hence limiting sensitivity. In Section 7.5.3 an algorithm that accounts for membrane uniqueness and non-specific binding using a ratio-metric measurement is presented.

7.5.3 Development of the Normalized Fluorescence Intensity (NFI) Algorithm

The intrinsic variability in each reaction zone on a nitrocellulose strip necessitates the need for an algorithm that would take into account the unique or individual differences of each membrane and each line on each strip for quantitative measurements. The goal of this section is to develop an algorithm that computes the measured fluorescence intensity from a lateral flow strip and translates it into a a specific fluorophore/analyte concentration, normalizing the result to the intrinsic and processing induced variability. The normalized fluorescence intensity (NFI) algorithm accounts for potential sources of error due to membrane uniqueness and non-specific binding. The NFI technique implements "ratioing" in that it divides the sample signal intensity by the background and subtracts the non-specific binding (NSB), thus removing the bias effects caused by the instrument, alignment, and the assay specific processes. Hence, the reported intensity obtained is solely due to the sample/analyte under test. This technique improves the accuracy of the detection platform. As presented in Chapters 3 and 4, the fluorescence intensity from a sample is directly proportional to the slope of the voltage-time output of the detector and is computed as,

$$S = \frac{(V_{threshold-max} - V_{threshold-min})}{(t_{threshold-max} - t_{threshold-min}).} \tag{7.1}$$

By measuring the optical background and fluorescence intensity of each reaction zone on a membranes before and after an assay, respectively, we can write that,

$$NFI = \frac{(S_T/S_{Tref}) - (S_C/S_{Cref})}{(S_T/S_{Tref})} \tag{7.2}$$

where, S_T, is the fluorescence signal intensity measured from a test line after assay; S_{Tref}, is the optical background measured from the test line before assay; S_C, is the fluorescence signal intensity measured from a control line after assay; S_{Cref}, is the optical background measured from the control line before assay. Empirically, it was observed that the flow of microspheres through a nitrocellulose membrane guarantees that the measured fluorescence at any point on the membrane is higher than or at least equal to the optical intensity before the test. The latter is a rare occurrence as the use of microsphere concentrations that enable a measurable fluorescence response, ensures that non-specific binding (NSB) occurs in the membrane pores and surfaces. In a closed cassette configuration the intensity ratios before and after the test could be used as a check for valid or incorrectly performed (invalid) tests. Hence, if $(S_T/S_{Tref}) \geq 1$ and $(S_C/S_{Cref}) \geq 1$, such that $(S_T/S_{Tref}) - (S_C/S_{Cref}) \geq 0$, the NFI is computed, analyzed, and reported, else the result is inconclusive or the test is declared invalid.

Two extreme cases can be observed with the NFI algorithm:

Case 1: Low non-specific binding (NSB), weak testline signal (S_C is low and S_T is low), i.e., $S_C \longrightarrow S_{Cref}$ and $S_T \longrightarrow S_{Tref}$, so that, $S_C/S_{Cref} \longrightarrow 1$ and $S_T/S_{Tref} \longrightarrow 1$. In this case, the numerator in the NFI equation $\longrightarrow 0$ and hence, NFI is Minimum (NFI $\longrightarrow 0$).

Case 2: Low non-specific binding (NSB), high test line intensity (S_C is low and S_T

is high), i.e., $S_C \longrightarrow S_{Cref}$ and $S_T \longrightarrow \infty$, so that, $S_C/S_{Cref} \longrightarrow 1$ and $S_T/S_{Tref} \longrightarrow \infty$. In this case, the numerator in the NFI equation $\longrightarrow S_T/S_{Tref}$ and hence, NFI is Maximum (NFI $\longrightarrow$ 1).

The second term in the numerator of Equation 7.2, accounts for the non-specific binding observed in fluorescence lateral flow assays and the ratios account for the uniqueness of each strip, allowing measurements to be compared with higher accuracy, especially when small differences or trends are under observation.

7.5.4 Effect of Membrane Flow Rate and Microsphere Diameter in Fluorescence LFA Development

This section explores the effect of fluorescent microsphere diameter and membrane flow rate (determined by pore size/porosity) on a multiplexed fluorescence lateral flow assay targeting EBNA-1 IgG antibodies in commercially obtained plasma extracted from whole blood samples (see Section 7.2.5). The samples were analyzed with different size microsphere-goat anti-human IgG conjugate.

Microsphere Characteristics

Figure 63 depicts the fluorescence intensity measured from a dilution series of different microsphere sizes (0.185, 0.328, 0.506, 0.899, and 1.009 μm diameter, Merck Milliopore, France). The sizes investigate here covers the size range typically used in lateral flow assays. The fluorescence intensity response to a logarithmic dilution series was characterized using nitrocellulose (HF07504XSS) as the substrate.

A 5-parameter logistic fit (5PL) Gottschalk and Dunn (2005); Findlay and Dillard (2007) was applied to the normalized fluorescence intensity (NFI) response for each microsphere size using OriginPro 8.5.1 (OriginLab Corp., MA, USA). The fitting parameters are presented in Table 9 and could be used to infer the concentration of

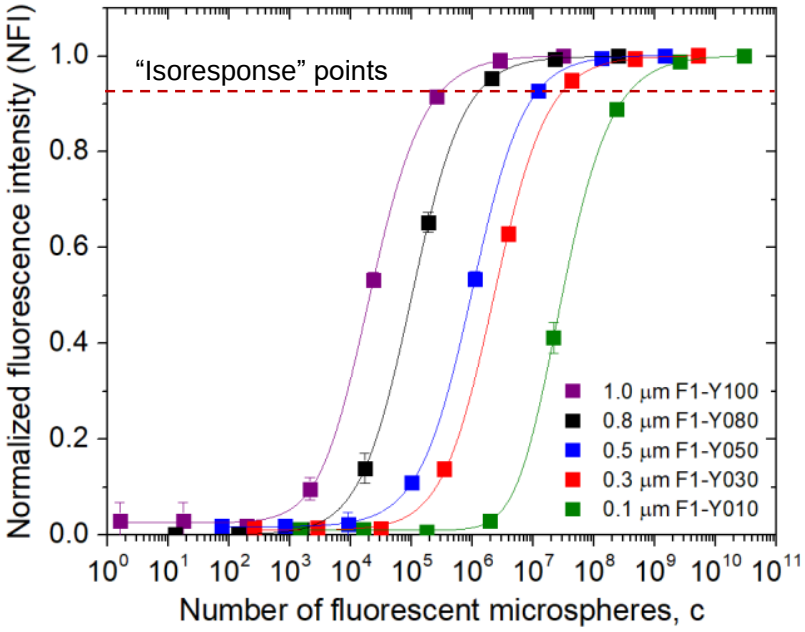

Figure 63: Normalized Fluorescence Intensity as a Function of Concentration (Number of Fluorescent Microspheres) for Different Microsphere Sizes (0.185, 0.328, 0.506, 0.899, and 1.009 μm Diameter).

an unknown sample, using Equations 7.3 and 7.4,

$$NFI = NFI_{max} + \left[\frac{NFI_{min} - NFI_{max}}{\left(1 + \left(\frac{c_0}{c}\right)^h\right)^s}\right], \tag{7.3}$$

$$c = c_0\left[\left(\frac{NFI - NFI_{max}}{NFI_{min} - NFI_{max}}\right)^{-1/s} - 1\right]^{1/h}, \tag{7.4}$$

where, NFI, is the measured fluorescence intensity from an unknown sample; NFI_{min} and NFI_{max} are the minimum and maximum fluorescence intensity over the concentration range; c_0 is the concentration corresponding to half the maximum NFI; c, is the unknown concentration; h, is the hill slope or sensitivity; and s, is the

asymmetry factor.

Table 9: Calibration Curve Fitting Using a Five Parameter Logistic (5PL) Fit.

Microsphere	†NFI_{min}	NFI_{max}	c_0	h	s	R^2
F1-Y100	$2.6x10^{-2}$	1.00	$1.10x10^4$	0.89	1.58	0.99976
F1-Y080	$5.5x10^{-4}$	0.99	$9.07x10^4$	0.99	1.08	1.00000
F1-Y050	$1.7x10^{-2}$	1.00	$1.03x10^6$	1.01	0.97	0.99996
F1-Y030	$1.0x10^{-2}$	1.00	$1.84x10^6$	0.96	1.17	0.99983
F1-Y010	$1.0x10^{-2}$	1.00	$8.88x10^6$	0.91	2.54	0.99998

†Normalized fluorescence intensity (NFI)

As expected, the fluorescence intensity increased with microsphere diameter. The parallel response in the linear dynamic range of the sigmoidal curves is indicative of the entrapped fluorophore characteristics. The calculated fitting constants could be used to determine the concentration based on arbitrary measured normalized fluorescence intensity. In a clinical study, reference or negative and positive calibrator samples could be used to determine the test outcome implementing a cutoff (CO) or the results of the assays could be quantified by comparing the NFI generated in each assay with those of calibration curves.

Microsphere and Membrane Pore Size Effect

The challenge is finding an optimum microsphere size and membrane flow rate for a given application, since the measured fluorescence intensity and NSB is a function of microsphere diameter, pore size and the reaction rate decreases as the square of the membrane flow rate. To isolate the effect of microsphere diameter on the measured

fluorescence intensity, an "isoresponse" point was chosen for all microspheres based on previous studies as shown in Figure 63. The concentration corresponding to the isoresponse point for each fluorophore was then used to probe EBNA-1 functionalized nitrocellulose membranes (HF075, HF090, HF120, HF135, HF180, CN95, CN110, and CN140); see Table 7 and experimental details in Section 7.3. The concentration chosen using the isoresponse points should be sufficiently high enough to supply the demands of the number of test lines in the sample and low enough to minimize agglomeration and NSB. The goal is to infuse an effective fluorophore concentration that elicits the same fluorescence intensity, in order to study size effects by fluorescence detection. The ratiometric analysis enables this study as it accounts for the different optical background observed with different membrane types. The nitrocellulose membranes were functionalized with BSA (150 ng, negative control), EBNA-1 (150 ng, test), and IgG (150 ng, positive control), upstream to downstream in the sequence listed. A 4^{th} line after the IgG was used as a blank line (no protein) in conjunction with the BSA line to track the NSB as a function of membrane type and fluorophore size. Membranes were processed in replicates (N=4) for each membrane type (N=8), and at each fluorophore size (N=5). All samples were tested on the 4 x 2 DxArray platform (total n=160). Membranes were measured before the test to obtain the optical background and estimate the NSB changes as a result of the fluorescence microspheres flowing through the membranes. Blank line estimates the microsphere retention as a function of membrane type and microsphere size. Figure 64 (a) - (c) and (d) - (f), depicts the response from the BSA line and blank line (no protein) before and after the assay was performed. The relative position of the BSA line, EBNA-1, IgG, and blank line reference (upstream to downstream) as well as the direction of fluid flow is indicated in Figure 65 (b).

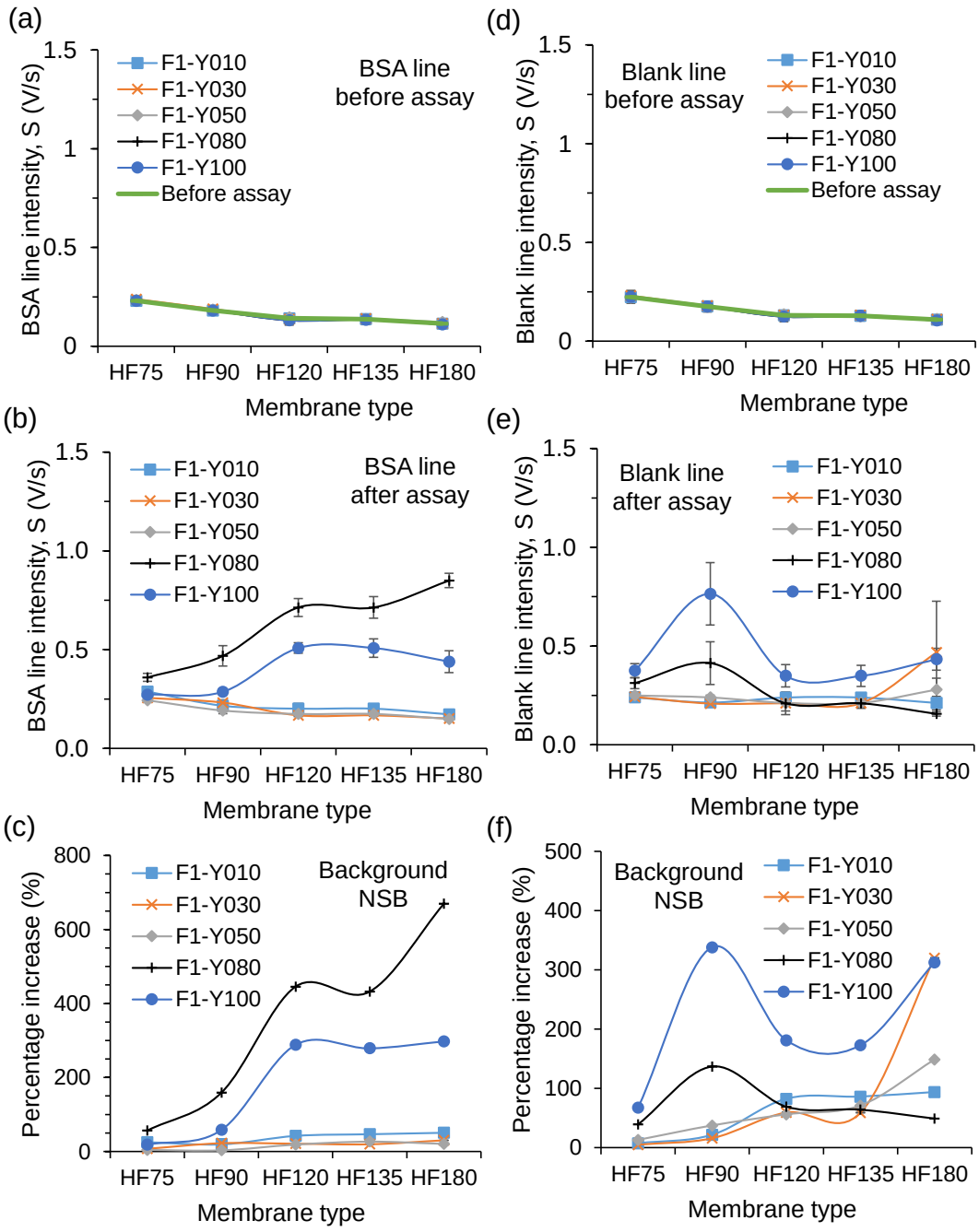

Figure 64: Effect of Fluorescent Microsphere Diameter and Membrane Flow Rate (Pore Size) on Non-specific Binding (NSB). (a) BSA Line Before the Assay (b) BSA Line After the Assay (c) Percentage Increase in Background for the BSA Line (d) Blank Line Before the Assay (b) Blank Line After the Assay (c) Percentage Increase in Background for the Blank Line.

Overall, the NSB increased with increasing microsphere size and decreasing pore size or flow rate. The gains made by a decreased optical background (Figure 64 (a) - (d)) and longer reaction time in slower flow rate membranes, as well as higher intensity due to microsphere size, may be masked by the increased NSB. For example, using 1 μm microspheres, the background NSB on the BSA line increased with decreasing pore size, by 18% in HF75, to 300% in HF180, compared to the BSA line before the assay as shown in Figure 64 (c). Figure 65 (a) summarizes the result and compares

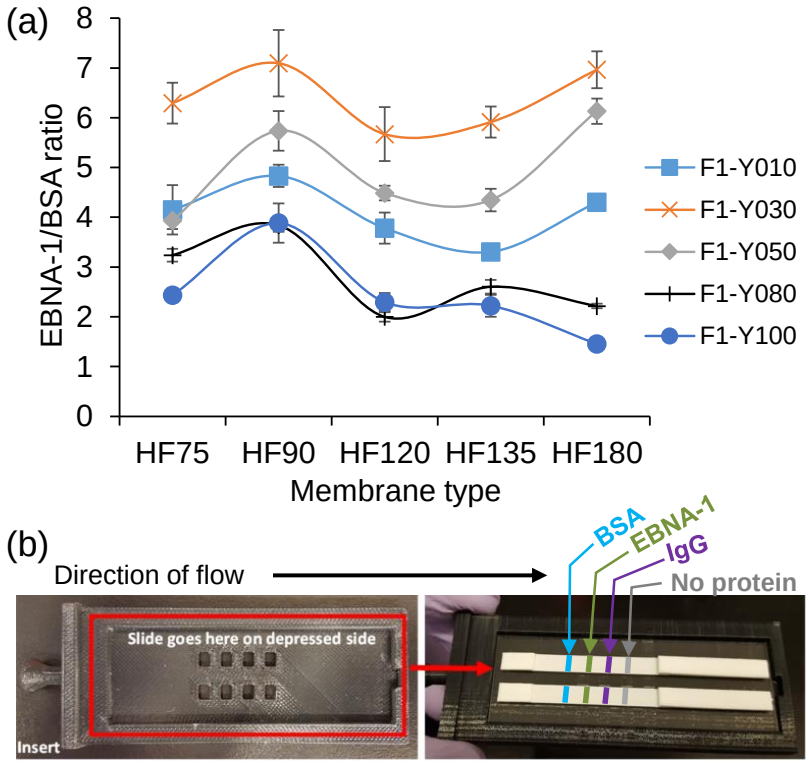

Figure 65: (a) EBNA-1 Test Line Intensity to BSA Line Ratio as a Function of Membrane Flow Rate (Decreasing to the Right) and Microsphere Diameter. (b) Image Showing Relative Test Line Position of BSA, EBNA-1, IgG and Blank Line, Measured Using the 4 x 4 Array Platform. The Lines Were at 6 mm Pitch. N=4 for Each Membrane Types and at Each Microsphere Size.

the performance of the membranes and fluorophores using an SNR metric expressed as the EBNA-1 line intensity to BSA line intensity ratio.

The anomalous behavior and large standard error mean (SEM) observed with larger microspheres size as indicated by the BSA and blank line, is evidence of inconsistent flow characteristics and hence would lead to unreliable results from test-to-test. The 0.3 μm microspheres (F1-Y030) generated the highest SNR across all membrane types. The result in Figure 65 (a) also suggests the use of HF090 or HF180.

7.5.5 Fluorescent Microsphere Stability

A significant advantage of fluorescent microspheres in lateral flow assays is the brightness. However, it is also important that the microspheres have a long shelf life, do not require any special storage, and are stable over the signal acquisition time (for the DxArray platform, signal acquisition time is between 25 to 60 s). Figure 66 (a) shows the fluorescence intensity generated by different dilutions of fluorescent microsphere (F1-Y050) upon continuous LED excitation for 5 minutes. No significant drift in intensity was observed during this time, indicating that the fluorophores entrapped in the microsphere are resistant to photobleaching. Figure 66 (b) shows EBNA-1 LFA strips re-measured 6 months after the initial assay was performed. The strips were stored at ambient temperature and relative humidity (23°C and 70% RH, respectively) for six months. The result indicates that the fluorophores are stable and do not require cold chain shipping or storage.

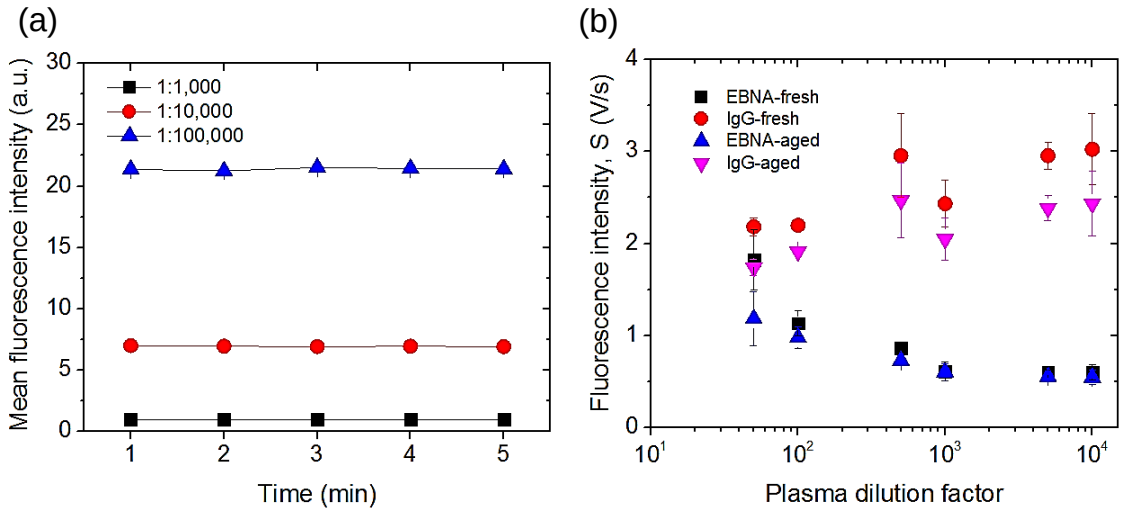

Figure 66: (a) Photostability of Microsphere Dilutions Interrogated With a 1.3 mW Excitation Source for 5 min (b) EBNA-1 Assay Strips Remeasured 6 Months After Assay was Performed (Aged) and Compared to the Generated Intensity Measured at the Time of the Assay (Fresh). Samples Were Stored at Ambient Conditions (23°C, 70% Relative Humidity).

7.6 Summary

This chapter presented a practical perspective on fluorescence lateral flow assay development, highlighting specific considerations for design and development of a multiplexed biomarker detection platform. Nitrocellulose is the gold-standard membrane in many rapid diagnostic tests, especially visual-based colorimetry tests. The excellent flow characteristics, low-cost, and protein affinity make it an attractive option for fluorescence-based assay. However, the design of fluorescence-based assays on nitrocellulose takes considerable effort, to overcome the lack of sensitivity, repeatability, reproducibility, and quantitative output that characterizes lateral flow assays in general. This work addresses these challenges, herein, we reported a successful translation of glass-based HPV assay to a nitrocellulose-based platform. To the best

of our knowledge this is the first highly-sensitive fluorescence-based HPV lateral flow assay for circulating cancer biomarkers, using patient plasma. The volume of plasma and the LOD was significantly reduced from 150 μL on a glass based assay format to <2 μL in a nitrocellulose-based LFA format. The LOD for known patient plasma positive for HPV16 E7 IgG antibodies was improved. The lateral flow assay can detect the biomarker at a plasma dilution of 1:1k compared to the glass-based assay discussed in Chapter 4 (titer at 1:100). This indicates that the 3D microstructure of nitrocellulose provides more binding sites compared to a 2D planar glass substrate. The assay time was also reduced from ∼3 hours to less than 1 hour. The brightness of dye-entrapped carboxyl functionalized calibrated latex/polystyrene microspheres used in this study, relative to molecular dye enables detection through a relatively opaque nitrocellulose membrane. A 0.4 μm diameter microsphere could contain up to 30,000 molecular dyes (O'Farrell, 2013). We conjugated goat anti-human IgG via covalent attachments to the carboxyl functionalized surface for this development. The effect of fluorescent microsphere diameter and membrane flow rate (porosity/pore size) was investigated using commercially available transparent-backed nitrocellulose membranes and tested using a fabricated 4 x 4 and 4 x 2 multiplexed fluorescence detection platform (DxArray) in a transillumination-mode configuration. The data generated using fluorescent microspheres with diameter ranging from 0.1 to 1 μm and membrane flow rate ranging from 75 to 180 s/4cm covers the parameter space useful for fluorescence-based lateral flow assay and serves as a useful reference guide for fluorescence lateral flow assay researchers and developers. Currently, significant effort is being invested towards the development of an autonomous assay processing unit, post-sample input (whole blood) to enhance the assay precision, limiting operator-dependent variability. The difficulty of implementing multi-step assays where some reagents cannot mix before interacting with the capture antigens poses a significant

engineering problem. The complexity of the assay processing unit, is directly related to the number of steps in the assay. Research efforts to decrease assay steps without sacrificing performance are worth investigating.

Chapter 8

CONCLUSION AND PROPOSED FUTURE RESEARCH

8.1 Summary of This Work

This work has explored the design and development of a high sensitivity, low-cost, robust, and scalable multiplexed fluorescence-based detection platform for biomarkers in plasma and ultimately, in whole blood. The target application investigated is the detection of circulating oncogenic biomarkers for cervical cancer diagnosis in resource constrained settings. The design approach adopted has been directly driven by the constraints of this development.

Chapter 3 presented a new approach for fluorescence-based detection that enables the development of portable, inexpensive, and high sensitivity platform. The system design draws inspiration from standard laboratory diagnostic instrumentation, however, it does not use of focusing or transfer optics and bulky excitation sources and detectors for a rugged and robust low-cost design that fits the target product and application profile - low and middle-income countries (LMICs). The optoelectronic parameters that determine the performance of this new approach comprising light-emitting diode (LED), photodiode-based charge integration readout electronics, and interference filters was presented. The benefit of charge integration averaging current generated from weak fluorescence emissions over a noisy background, thus improving accuracy. The radiant emissions from a fluorophore is converted to a voltage time space that does not require high speed electronics but trades off time for accuracy, producing a quantitative concentration-dependent voltage output. It was postulated that the ramp time (RT) and detection time (DT) metric would be sufficient to dis-

criminate fluorophore concentrations for quantitative applications in disease diagnosis and personal health monitoring. A theoretical model to predict the performance characteristics of the system was developed and found to agree with empirical data. The limit-of-detection (LOD) of the system was estimated as ∼200 1 μm Nile red fluorescent microspheres. This showed that the developed system could be used for high sensitivity biomarker detection applications.

Chapter 4 explored the use of organic light emitting diodes (OLEDs) as an excitation source for low-cost biorecognition technologies. A brief review of the applications of flexible display optoelectronics for biochemical analysis and the potential applications and benefits in point-of-care (POC) technologies was highlighted. The pixel size, planar structure, and flexible form factor of OLEDs, organic and a-Si photodiodes, provides a viable pathway for an integrated source-filter-detector system with microfluidics and lab-on-chip technologies in a high-density multiplexed fluorescence detection array. To show proof-of-concept, this chapter detailed the adaptation of protein and DNA microarray technologies to a low-cost microscope glass-slide based platform for potential use as a pre-screening tool for circulating cervical cancer biomarkers in LMICs. The OLED-based platform (FlexDx) has 3 orders of magnitude lower optical noise floor (using interference filters) compared to other cross-polarizer and absorption filter-based systems reported in the literature. This significantly lowers the noise floor enabled a 10pg/mL detection limit for anti-human IgG-Dylight 549 conjugate using charge integration readout electronics. The detection of high-risk HPV (hrHPV) specific IgG antibodies was demonstrated and compared to a standard laboratory microplate ELISA. It was determined that the low-cost OLED-based biorecognition system approaches the performance of laboratory-based instrumentation and is capable of detecting low concentration biomarkers at clinically significant concentrations.

Chapters 5 and 6 presented the design, development, and characterization of a high sensitivity multiplexed (2x2 array) fluorescence detection array. Multiplexed POC devices provide robust clinical information, high throughput, saves time and improves accuracy. Design considerations including the optoelectronic configuration, fluorophore selection, and substrate effects was considered and analyzed. A low cost filter architecture and implementation was demonstrated. High quality interference filters are required to maximize the benefit of selectivity and increased SNR afforded by fluorescence techniques. However these filters are prohibitively expensive and difficult to integrate in low-cost and miniaturized applications. Attempts by other researchers in the literature to implement low-cost filtering technologies (cross polarizers, absorption filters) has led to devices that are no better in sensitivity than many absorbance or reflection based detection techniques. To tackle these challenges, this dissertation details the development a filter mounting, assembly, and encapsulation technique and reported the integration and deployment of high-quality optical interference filters for low-cost applications. The filters have an OD6 rejection in the stop band and greater than 90% transmission in the pass-band, with near perfectly vertical rising and falling edges. A significant reduction (98%) in filter cost was achieved by reducing the filter dimensions to 3 mm x3 mm, allowing for a decentralized multi-site design approach that increases array density. The reported technique can be easily adapted for mass production at low-cost, and is useful to the diagnostic device research, development, and manufacturing community. Optomechanical aperture, isolation, and enclosure design techniques have been developed for crosstalk elimination in an array configuration. This development demonstrated a 100% crosstalk reduction in a multiplexed configuration with zero channel dropout. A transillumination (T-mode) and coplanar mode (C-mode) excitation-detection configuration was developed and extensively characterized. The utility of either low-cost platform for

detecting colorimetric and fluorescent labels was investigated and demonstrated successfully with no changes to the device configuration. It was observed that overall, fluorescent labels improved performance by 2-3 orders of magnitude (LOD), over colorimetric labels. We have shown improvements in the LOD of the state-of-the-art colorimetric and visual based rapid diagnostic systems by 2-3 orders of magnitude. The system was also benchmarked against laboratory scale instrumentation. Compared to standard absorbance techniques, the platform improves the LOD by 2-3 orders of magnitude and is well within an order of magnitude of typical central laboratory fluorescence microarray scanner. The developed platform is rugged, robust, and suitable for early disease detection in POC settings, especially for cervical cancer linked to a variety of high risk virus types and oncogenic proteins in humans. The system is agnostic to specific biomarkers and thus could also be applied toward any bioanalytical procedure that requires high performance fluorescence detection at low-cost.

Chapters 7 detailed the extension of the array design techniques used for the 2x2 fluorescence array architecture Chapters 5 towards the detection of a higher density arrays (4x2 and 4x4) for multiplexed applications. The glass-based assay for detecting anti-HPV16 E7 IgG antibodies presented in Chapters 4, is adapted to a nitrocellulose-based format. Nitrocellulose has several attractive characteristics including low-cost, self-capillary fluid routing, protein affinity, and a 3D microstructure that increases the number of available binding sites, compared to 2D planar substrates (plain microscope slide). Specific challenges in the design and development of nitrocellulose-based fluorescence lateral flow assays (LFA) have been highlighted. Some of these challenges (high extinction of nitrocellulose, autofluorescence background, membrane variability) are not immediately apparent in colorimetry-based lateral flow assay application. The 4x2 and 4x4 platform (DxArray) is built entirely

from off-the-shelf components as described in previous chapters to fit with an array of nitrocellulose strips. Fluorescent recognition samples are excited in the reaction zones/test lines on membranes using green LEDs and the orange emission is detected with photodiodes connected in a transimpedance amplifier configuration. A microcontroller platform with 10 bit ADC is capable of delivering the required resolution. The current generated is converted to a concentration dependent voltage ramp, yielding a quantitative readout in a voltage-time space. An algorithm for the fluorescence signal interpretation was developed to account for inter and intra-strip variations in membranes, alignment variability and non-specific binding (NSB) in nitrocellulose membranes, increasing the accuracy of the reported fluorescence intensity for quantitative measurements. This chapter also presented assay development protocols on nitrocellulose membranes. Using the detection of anti-human IgG and anti-EBNA-1 IgG antibodies, a nitrocellulose-based assay protocol was establish and then extended for the detection of anti-HPV16 E7 antibodies in patient plasma. By monitoring the HPV antigen-specific immune responses, antibodies to the virus (e.g., anti-HPV16 E7) are captured using purified HPV proteins immobilized on test lines of a nitrocellulose membrane and detected with goat anti-human IgG-fluorescent microsphere conjugate. The platform was capable of detecting anti-EBNA-1 IgG and anti-HPV16 E7 IgG antibodies at 3 and 1 orders of magnitude lower than a glass-based assays. This represents a significant improvement over the previously demonstrated glass-based assays indicating that nitrocellulose could enable higher sensitivity and lower limit of detection, regardless of the optical constraints associated with its use. We also report a significant reduction in the assay time from $\sim$3 hours to less than 1 hour, and a reduction in patient sample volume from 150 μL to less than 2 μL. Considerations and the effects of microsphere diameter and membrane flow rate as well as the effect of relative test line positions (upstream-downstream) was investigated.

It was observed that NSB increased in slower flow rate membranes (smaller pore size) and with larger microsphere size thus limiting the overall signal-to-noise ratio. Optimum membrane flow rate and microsphere sizes could be inferred from the generated data with the goal of maximizing the signal to noise ratio. The developed multiplexed HPV-DxArray platform will be applied toward simultaneous detection of up to 12 human papillomavirus (HPV)-specific IgG serologic biomarkers. A pilot study and field trials will be performed under the National Cancer Institute (NCI) Cancer Detection grant and in collaboration with researchers at the All India Institute of Medical Science (AIIMS), India. We are in the process of scaling production of the detection platform and assay technology transfer toward field trials in two phases: (a) testing blood samples from 100 women with high grade dysplasia and ICC at AIIMS. The results from this training set will provide useful feedback for fine-tuning (b) screening 13,000 women in rural areas. The platform is useful as a pre-screening tool to risk-stratify patients at risk of developing cervical cancer and aid physicians in decision making. Some challenges in using circulating antibodies as biomarkers for cervical cancer include the difficulty associated with *in vitro* culture of HPV, protein purification, and separation. Furthermore, not all patients infected with HPV show an antibody response. Significant research effort is underway at Dr. Karen S. Anderson's laboratory, aimed at understanding and developing a biomarker panel for several HPV types. This dissertation addressed many of the practical challenges associated with implementing a low-cost fluorescence-based detection platform that is easily integrated with resource constrained or resource limited environments.

Finally, details of this development enables fundamental and comprehensive understanding of the design constraints for low-cost fluorescence-based lateral flow devices, especially for resource-limited settings and could serve as a useful guide for further development and improvements to the developed platform.

8.2 Proposed Research Plans and Suggested Improvements

We envision a fully field-deployable platform to screen women for cervical cancer biomarkers in resource limited settings. It is desired that the assay platform accepts whole blood as input from a finger stick, independently analyzes the sample with minimal user/operator interference, continuously provides updates to a user interface (touchscreen/smartphone app) via Bluetooth or wifi, has repeatable and reproducible assay performance with detection limits in the pg/mL range or lower, sample-to-answer time less than 30 min and actual assay run-time less than 20 min, high specificity and sensitivity, CLIA waivable, and overall compatibility with the ASSURED criteria.

Some specific suggested tasks and ideas towards improving the current platform, productization, and translation of the overall platform technology to field-use include but are not limited to the following:

- Find a suitable covalent coupler/linker for reliably and reproducibly immobilizing recombinant protein to a solid support (nitrocellulose), with emphasis on protein conformation and orientation.

- Automate the assay and integrate the assay with the reader to monitor the assay progress, with accurate timing that allows the strips to be measured and monitored at different points in the assay process. Reading the strips when wet, will improve the excitation source in coupling and fluorescence out-coupling toward the detector from the nitrocellulose membrane. However this process needs to be sequenced for repeatability. The overall platform performance will benefit from the implementing a low-cost mechanical/automated assay processing unit to minimize user dependent assay steps that are best implemented in a laboratory. Based on the designed fluorescence detection platform in this dis-

sertation, it is preferable that the assay processing unit is design to process a disposable cassette/consumable that is compatible with the detector optoelectronics and optomechanics. The pre-functionalized cassette processed in the assay unit should be detachable and measureable in the DxArray. The assay unit must also eliminate biofouling, contaminations, and ensure a safe collection and disposal of processed patient sample (blood/plasma/serum) and any biohazardous waste generated in the process.

- Optimization of membrane thickness to maximize signal visibility while maintaining good control of bed volume (binding capacity), tensile strength, width of printed protein lines. GE Healthcare is open to working with us on this, provided the minimum order quantity (MOQ) is satisfied. Furthermore, may be worth investigating a hybrid lateral flow assay with transparent custom membranes/solid support that is compatible with the standard LFA assembly process in the region of test and control lines. Previously we investigate the use of hydrophilic teflon, silica microspheres, and sol gels without success.

- Migrate from the manual (by hand) opaque encapsulation to a simple, semi-automated, reproducible, and scalable filter opaque coating/encapsulation method, that ensures uniform coverage and hence uniform channel performance.

- The effect of ambient temperature and relative humidity (RH), as well as other sources of variation and bias (altitude, vibrations, etc.) should be studied. Preliminary study of temperature effects on the DxArray shows a reversible temperature dependence. Assay kinetics and reaction rate are temperature depended, hence the development of a temperature control environment designed around the platform will be useful. For example, a system to raise the temperature by 2-3 degrees above ambient while the test is being performed. This will

require that the instrument software calibration has a function that accounts for temperature, depending on the temperature that the assay was performed.

- The addition of a low-cost plastic lens or light guide structures to the C-mode architecture may improve the performance of the C-mode architecture, perhaps by an order of magnitude or more, making it equivalent or better than the T-mode in terms of performance. It may be possible to include optical feedback for intensity control in the C-mode without significantly affecting the spatial distribution of the array as in the T-mode. This will be easier to implement in a coplanar configuration, using one photodiode as a reference for multiple adjacent sites. It will be beneficial to transition all off-the-shelf components to surface mount packaging and using guards on amplifier inputs, minimizing the use of vias on the PD-board to minimize the effects of stray capacitance that may contribute to channel variations.

- Lateral flow microarrays are gaining more attention in research and industry. It may be useful to investigate the use of spot arrays toward multiplexing to overcome the challenges of multiplexing using lines perpendicular to the direction of flow. Flow and reaction rate kinetics could be severely impacted by the standard rectangular strip design in multiplexed tests. This may require modifications to the reader architecture as scanning based readers are more compatible with the lateral flow microarray design. The use of a photodiode array on-chip rather than individual photodiodes to implement a "scanning" detection mode platform may help. One could imagine taking advantage of the intensity changes as a function of position of each pixel and the changes in intensity based on the offset in a pooled antigen array (lateral flow microarray). An IC based linear sensor array, for example the TSL1401CL manufactured by

AMS was used for the development of a colorimetric reader by Pilavaki and Demosthenous (2017). It is a 128x1 linear sensor array with each pixel having a 2524.3 square micrometer active area and 8 μm spacing between pixels. It has a responsivity of $\sim$0.7 to 0.75 at 575 to 600 nm, built in charge integrator for each pixel with adjustable integration period to change the analog output voltage and avoid saturation or dynamically do so to combat crosstalk. Issues with crosstalk will present a significant engineering challenge that will be worth pursuing, using fabrication techniques and signal processing. This sensor is manufactured in a 9.4 mm x 3 mm package, operates up to 8 MHz, and costs \$4.31 at order quantities greater that 500. Technological advances in organic and inorganic electronics will enable more options for fluorescence lateral flow detection.

- Inclusion of an internal reference standard for instrument calibration and to implement standardization by MESF computations.

- Translating all 3D printed optomechanical parts of the system into injection molded unit will enhance aesthetics and performance. Importantly, the array pitch could be reduced by 1 to 2 mm.

- Determine the performance of the system and compare to others by using mouse monoclonal anti-HPV16 E7 antibodies (Sant Cruz Biotech), e.g., the work by Prof. Demirci's group at Standford Inan *et al.* (2017). Procure the anti-human papillomavirus type 16 serum (1st International Standard) calibrator standards from the National Institute for Biological Standards and Control (NIBSC), to reliably quantify the DxArray platform performance, and for use in quantitative test dwevelopment.

- The use of the derivative as a metric for detected fluorescence intensity may shorten the sample measurement time in an array configuration. Furthermore, the analysis of the systems response by examining the derivative of the output as presented in Chapter 4, indicates that there may be no added benefit to integrating beyond a few seconds into the ramp. Parallel processing may also be possible with efficient designs of isolation structures in injection molded parts.

At the early stages of this effort, it was hypothesized that longer integration time enables charge collection over a longer time period and thus a better discrimination or detection of low concentrations of analyte or low fluorescence emissions from a sample under test. In the developed fluorescence-detection platform, there are 3 knobs to increase the ramp/integration period of the system.

1. Decreasing the LED intensity - increases the integration period or reduces the background, allowing longer integration time, but the desired fluorescence emission intensity is directly proportional to excitation light intensity.

2. Increasing the capacitor size - increases the integration time, however the gain of the amplifier is impacted, thus the sensitivity of the entire system

3. Reducing the leakage light reaching the detector - The blank level/background is dominated by excitation light reaching the detector through the filters. For a given substrate (glass or paper), with a fixed integrating capacitor size and LED intensity, filter combinations that decrease the background by several orders of magnitude, while decreasing the desired fluorescence by a small factor is desired. Further rejection of excitation light reaching the detector could be achieved using angle-independent hybrid-filter structures (gel and fluorescence) optimized for a chosen fluorophore.

Clearly, archiving longer integration time, is best implemented by reducing the leakage light reaching the detector. In this dissertation, the use of an additional low-cost gel emission filter significantly decreased the excitation light reaching the detector while allowing emitted fluorescence through. Further investigation into more efficient low-cost filter combinations/additions to the current setup, will increase the SNR of the system.

Ahmad, A. L., S. C. Low, S. R. A. Shukor and A. Ismail, "Investigating membrane morphology and quantity of immobilized protein for the development of lateral flow immunoassay", Journal of Immunoassay and Immunochemistry **33**, 1, 48–58 (2012).

Anderson, K. S., D. W. Cramer, S. Sibani, G. Wallstrom, J. Wong, J. Park, J. Qiu, A. Vitonis and J. Labaer, "Autoantibody signature for the serologic detection of ovarian cancer", Journal of proteome research **14**, 1 (2015a).

Anderson, K. S., K. R. Dahlstrom, J. N. Cheng, R. Alam, G. Li, Q. Wei, N. D. Gross, D. Chowell, M. Posner and E. M. Sturgis, "Hpv16 antibodies as risk factors for oropharyngeal cancer and their association with tumor hpv and smoking status", Oral Oncology **51**, 7, 662–667 (2015b).

Anderson, K. S., J. E. Gerber, G. D'souza, S. I. Pai, J. N. Cheng, R. Alam, S. Kesiraju, D. Chowell, N. D. Gross, R. Haddad, M. L. Gillison and M. Posner, "Biologic predictors of serologic responses to hpv in oropharyngeal cancer: The hotspot study", Oral Oncology **51**, 8, 751–758 (2015c).

Anderson, K. S., N. Ramachandran, J. Wong, J. V. Raphael, E. Hainsworth, G. Demirkan, D. Cramer, D. Aronzon, F. S. Hodi, L. Harris, T. Logvinenko and J. Labaer, "Application of protein microarrays for multiplexed detection of antibodies to tumor antigens in breast cancer", Journal of proteome research **7**, 4 (2008).

Anderson, K. S., S. Sibani, G. Wallstrom, J. Qiu, E. A. Mendoza, J. Raphael, E. Hainsworth, W. R. Montor, J. Wong, J. G. Park, N. Lokko, T. Logvinenko, N. Ramachandran, A. K. Godwin, J. Marks, P. Engstrom and J. Labaer, "Protein microarray signature of autoantibody biomarkers for the early detection of breast cancer", Journal of proteome research **10**, 1 (2011a).

Anderson, K. S., J. Wong, G. D'Souza, A. B. Riemer, J. Lorch, R. Haddad, S. I. Pai, J. Longtine, M. Mcclean, J. Labaer, K. T. Kelsey and M. Posner, "Serum antibodies to the hpv16 proteome as biomarkers for head and neck cancer", British Journal of Cancer **104**, 12 (2011b).

Anderson, K. S., J. Wong, A. Vitonis, C. P. Crum, P. M. Sluss, J. Labaer and D. Cramer, "p53 autoantibodies as potential detection and prognostic biomarkers in serous ovarian cancer", Cancer epidemiology, biomarkers & prevention : a publication of the American Association for Cancer Research, cosponsored by the American Society of Preventive Oncology **19**, 3 (2010).

Armbruster, D. A. and T. Pry, "Limit of blank, limit of detection and limit of quantitation", The Clinical biochemist. Reviews **29 Sup** (2008).

Atila Biosystems, "Isothermal HPV diagnostic kits", URL `https://www.atilabiosystems.com/` (2018).

Bahadır, E. B. and M. K. Sezgintürk, "Lateral flow assays: Principles, designs and labels", Trends in Analytical Chemistry **82**, C, 286–306 (2016).

Banerjee, A., Y. Shuai, R. Dixit, I. Papautsky and D. Klotzkin, "Concentration dependence of fluorescence signal in a microfluidic fluorescence detector", Journal of Luminescence **130**, 6, 1095 – 1100 (2010a).

Banerjee, A., Y. Shuai, R. Dixit, I. Papautsky and D. Klotzkin, "Concentration dependence of fluorescence signal in a microfluidic fluorescence detector", Journal of Luminescence **130**, 6, 1095 – 1100, URL `http://www.sciencedirect.com/science/article/pii/S0022231310000414` (2010b).

Bangs Laboratories, I., "Lateral flow tests technote 303", Technical note Rev. 003, Bangs Laboratories, Inc., URL `https://www.bangslabs.com/sites/default/files/imce/docs/TechNote%20103%20Web.pdf` (2013).

Barnett, J. M., P. Wraith, J. Kiely, R. Persad, K. Hurley, P. Hawkins and R. Luxton, "An inexpensive, fast and sensitive quantitative lateral flow magneto-immunoassay for total prostate specific antigen", Biosensors **4**, 3, 204–220, URL `https://doaj.org/article/377949c190ef486696ff319b7b7cf044` (2014).

Brown, G. O., "Henry darcy and the making of a law", Water Resources Research **38**, 7, 11–1–11–12 (2002).

Bruus, H., *Theoretical microfluidics, 4th ed* (Oxford University Press, 2008).

Bui, D. A. and P. C. Hauser, "Analytical devices based on light-emitting diodes – a review of the state-of-the-art", Analytica Chimica Acta **853**, 46 – 58, URL `http://www.sciencedirect.com/science/article/pii/S0003267014011702` (2015).

Cai, Y., R. Shinar, Z. Zhou and J. Shinar, "Multianalyte sensor array based on an organic light emitting diode platform", Sensors & Actuators: B. Chemical **134**, 2, 727–735 (2008).

Camou, S., M. Kitamura, J.-P. Gouy, H. Fujita, Y. Arakawa and T. Fujii, "Organic light emitting device as a fluorescence spectroscopy's light source : one step towards the lab-on-a-chip device", vol. 4833, pp. 4833 – 4833 – 8 (2003), URL `https://doi.org/10.1117/12.474296`.

Cardoso, S., D. C. Leitao, T. M. Dias, J. Valadeiro, M. D. Silva, A. Chicharo, V. Silverio, J. Gaspar and P. P. Freitas, "Challenges and trends in magnetic sensor integration with microfluidics for biomedical applications", Journal of Physics D: Applied Physics **50**, 21 (2017).

Cepheid, "Xpert® hpv reliable detection of high-risk hpv dna with genotyping of hpv 16 and 18/45", (2017).

Chard, T., "Review: Pregnancy tests: A review", Human Reproduction **7**, 5, 701–710 (1992).

Chediak, J., Z. Luo, J. Seo, N. Cheung, L. P. Lee and T. D. Sands, "Heterogeneous integration of cds filters with gan {LEDs} for fluorescence detection microsystems", Sensors and Actuators A: Physical **111**, 1, 1 – 7, URL http://www.sciencedirect.com/science/article/pii/S0924424703005272, micromechanics section of Sensors and Actuators, based on contributions revised from the Technical Digest of the 16th {IEEE} International conference on Micro Electro mechanical Systems (MEMS 2003) (2004).

Chin, C., V. Linder and S. Sia, "Lab-on-a-chip devices for global health: Past studies and future opportunities", Lab On A Chip **7**, 1, 41–57 (2007).

Cho, E. J. and F. V. Bright, "Optical sensor array and integrated light source", Analytical Chemistry **73**, 14, 3289–3293, URL https://doi.org/10.1021/ac010051u, pMID: 11476227 (2001).

Choudhury, B., R. Shinar and J. Shinar, "Glucose biosensors based on organic light-emitting devices structurally integrated with a luminescent sensing element", Journal of Applied Physics **96**, 5, 2949–2954, URL https://doi.org/10.1063/1.1778477 (2004).

Cogan, M., "Part 2: Where are all the multiplexed LFI's?", Online, URL https://www.dcndx.com/part-2-arent-multiplexed-lateral-flow-tests/ (2017a).

Cogan, M., "Where are all the multiplexed LFI's?", Online (2017b).

Connolly, R. and R. O. Kennedy, "Magnetic lateral flow immunoassay test strip development – considerations for proof of concept evaluation", Methods **116**, 132 – 140, URL http://www.sciencedirect.com/science/article/pii/S1046202317300713, antibodies –Analytical Masterpieces Production and Applications (2017).

Crawford, G. P., *Flexible Flat Panel Display Technology*, chap. 1, pp. 1–9 (Wiley-Blackwell, 2005), URL https://onlinelibrary.wiley.com/doi/abs/10.1002/0470870508.ch1.

Cretich, M., F. Damin and M. Chiari, "Protein microarray technology: how far off is routine diagnostics?", The Analyst **139**, 3, 528–542 (2013).

Cunningham, A. J., *Introduction to bioanalytical sensors*, Techniques in analytical chemistry series (Wiley, New York, 1998).

Dandin, M., P. Abshire and E. Smela, "Optical filtering technologies for integrated fluorescence sensors", Lab Chip **7**, 955–977 (2007).

Department of Health and Human Services, "Clia program; simplifying clia regulations relating to accreditation, exemption of laboratories under a state licensure program, proficiency testing, and inspection", Federal Register Vol. 63, No. 93, URL https://www.gpo.gov/fdsys/pkg/FR-1998-05-14/pdf/98-12752.pdf#page=1 (1998).

DeRose, P. C., E. A. Early and G. W. Kramer, "Qualification of a fluorescence spectrometer for measuring true fluorescence spectra", Review of Scientific Instruments **78**, 3, 033107, URL https://doi.org/10.1063/1.2715952 (2007).

Deshpande, R., O. Pawar and A. Kute, "Advancement in the technology of organic light emitting diodes", International Conference on Innovations in Information, Embedded and Communication Systems (ICIIECS) pp. 1–5 (2017).

D'Souza, G., N. D. Gross, S. I. Pai, R. Haddad, K. S. Anderson, S. Rajan, J. Gerber, M. L. Gillison and M. R. Posner, "Oral human papillomavirus (hpv) infection in hpv-positive patients with oropharyngeal cancer and their partners", Journal of Clinical Oncology **32**, 23, 2408–2415, URL https://doi.org/10.1200/JCO.2014.55.1341, pMID: 24778397 (2014).

Eeshita, M., F. Fadzai, B. Rana, S. Joseph and S. Ruth, "Tunable near uv microcavity oled arrays: Characterization and analytical applications", Advanced Functional Materials **25**, 8, 1226–1232, URL https://onlinelibrary.wiley.com/doi/abs/10.1002/adfm.201403313 (2015).

EMD Millipore, "Rapid lateral flow test strips. considerations for product development", Rev. C Lit. No. TB500EN00EM, EMD Millipore, Billerica, MA., URL https://www.emdmillipore.com/Web-US-Site/en_CA/-/USD/ShowDocument-Pronet?id=201306.12550 (2013).

Ewaisha, R., I. Meshay, J. Resnik, B. A. Katchman and K. S. Anderson, "Programmable protein arrays for immunoprofiling hpv associated cancers", PROTEOMICS **16**, 8, 1215–1224 (2016).

Ewaisha, R., G. Panicker, P. Maranian, E. R. Unger and K. S. Anderson, "Serum immune profiling for early detection of cervical disease", Theranostics **7**, 16 (2017).

Ferlay, J., I. Soerjomataram, R. Dikshit, S. Eser, C. Mathers, M. Rebelo, D. M. Parkin, D. Forman and F. Bray, "Cancer incidence and mortality worldwide: Sources, methods and major patterns in globocan 2012", International Journal of Cancer **136**, 5, E359–E386 (2015).

Findlay, J. and R. Dillard, "Appropriate calibration curve fitting in ligand binding assays", The AAPS Journal **9o**, 2, E260–E267 (2007).

Finger, I., S. Phillips, E. Mobley, R. Tucker and H. Hess, "Absolute brightness of fluorescent microspheres", Lab Chip **9**, 476–478 (2009).

Fleming, W., R. Buck, R. Miracle, D. Morrow, L. Dietz and S. Myrick, "Optical reader systems and lateral flow assays", URL https://patents.google.com/patent/US20150010992A1/en (2014).

Foubert, A., N. V. Beloglazova and S. D. Saeger, "Comparative study of colloidal gold and quantum dots as labels for multiplex screening tests for multi-mycotoxin detection", Analytica Chimica Acta **955**, 48 – 57, URL http://www.sciencedirect.com/science/article/pii/S0003267016313903 (2017).

Fridley, G., C. Holstein, S. Oza and P. Yager, "The evolution of nitrocellulose as a material for bioassays", MRS Bulletin **38**, 4, 326–330, URL `http://search.proquest.com/docview/1326322475/` (2013).

Fridley, G. E., H. Le and P. Yager, "Highly sensitive immunoassay based on controlled rehydration of patterned reagents in a 2-dimensional paper network", Analytical Chemistry **86**, 13, 6447–6453, URL `https://doi.org/10.1021/ac500872j`, pMID: 24882058 (2014).

Fu, E., S. Ramsey, P. Kauffman, B. Lutz and P. Yager, "Transport in two-dimensional paper networks", Microfluidics and Nanofluidics **10**, 1, 29–35 (2011).

Gaigalas, A., L. Wang, A. Schwartz, G. E. Marti and J. Vogt, Robert F., "Quantitating fluorescence intensity from fluorophore: assignment of mesf values.(molecules of equivalent soluble fluorophore)", Journal of Research of the National Institute of Standards and Technology **110**, 2 (2005).

Gallerano, D., E. Wollmann, C. Lupinek, T. Schlederer, D. Ebner, C. Harwanegg, K. Niespodziana, K. Schmetterer, W. Pickl, E. Puchhammer-Stckl, E. Sibanda and R. Valenta, "Hiv microarray for the mapping and characterization of hiv-specific antibody responses", Lab on a Chip **15**, 6, 1574–1589 (2015).

Gottschalk, P. G. and J. R. Dunn, "The five-parameter logistic: A characterization and comparison with the four-parameter logistic", Analytical Biochemistry **343**, 1, 54–65 (2005).

Gubala, V., L. F. Harris, A. J. Ricco, M. X. Tan and D. E. Williams, "Point of care diagnostics: status and future", Analytical chemistry **84**, 2 (2012).

Guilbault, G. G., *Practical Fluorescence, 2nd Ed.* (Marcel Dekker, Inc, Madison Avenue, New York, 1990).

Hofmann, O., D. D. C. Bradley, A. J. deMello and J. C. deMello, *Lab-on-a-Chip Devices with Organic Semiconductor-Based Optical Detection*, pp. 97–140 (Springer Berlin Heidelberg, Berlin, Heidelberg, 2008).

Hofmann, O., X. Wang, J. C. deMello, D. D. C. Bradley and A. J. deMello, "Towards microalbuminuria determination on a disposable diagnostic microchip with integrated fluorescence detection based on thin-film organic light emitting diodes", Lab on a Chip **5**, 8, 863–868 (2005).

Holstein, C., A. Chevalier, S. Bennett, C. Anderson, K. Keniston, C. Olsen, B. Li, B. Bales, D. Moore, E. Fu, D. Baker and P. Yager, "Immobilizing affinity proteins to nitrocellulose: a toolbox for paper-based assay developers", Analytical and Bioanalytical Chemistry **408**, 5, 1335–1346 (2016).

Hu, J., J. R. Choi, S. Wang, Y. Gong, S. Feng, B. Pingguan-Murphy, T. J. Lu and F. Xu, "Multiple test zones for improved detection performance in lateral flow assays", Sensors and Actuators B: Chemical **243**, 484 – 488, URL `http://www.sciencedirect.com/science/article/pii/S0925400516319700` (2017).

Hu, J., L. Wang, F. Li, Y. L. Han, M. Lin, T. J. Lu and F. Xu, "Oligonucleotide-linked gold nanoparticle aggregates for enhanced sensitivity in lateral flow assays", Lab Chip **13**, 4352–4357, URL http://dx.doi.org/10.1039/C3LC50672J (2013).

Hu, J., S. Wang, L. Wang, F. Li, B. Pingguan-Murphy, T. J. Lu and F. Xu, "Advances in paper-based point-of-care diagnostics", Biosensors and Bioelectronics **54**, 585 – 597, URL http://www.sciencedirect.com/science/article/pii/S095656631300777X (2014).

Huang, X., Z. P. Aguilar, H. Xu, W. Lai and Y. Xiong, "Membrane-based lateral flow immunochromatographic strip with nanoparticles as reporters for detection: A review", Biosensors and Bioelectronics **75**, 166 – 180, URL http://www.sciencedirect.com/science/article/pii/S0956566315303584 (2016).

ICH Harmonised Tripartite Guideline, "Validation of analytical procedures: Text and methodology q2(r1)", Online, URL https://www.ich.org/fileadmin/Public_Web_Site/ICH_Products/Guidelines/Quality/Q2_R1/Step4/Q2_R1__Guideline.pdf (2005).

Inan, H., S. Wang, F. Inci, M. Baday, R. Zangar, S. Kesiraju, K. S. Anderson, B. T. Cunningham and U. Demirci, "Isolation, detection, and quantification of cancer biomarkers in hpv-associated malignancies", Scientific Reports **7**, 1, 3322, URL https://doi.org/10.1038/s41598-017-02672-6 (2017).

Jacinto, M. J., J. R. C. Trabuco, B. V. Vu, G. Garvey, M. Khodadady, A. M. Azevedo, M. R. Aires-Barros, L. Chang, K. Kourentzi, D. Litvinov and R. C. Willson, "Enhancement of lateral flow assay performance by electromagnetic relocation of reporter particles.(research article)(report)", PLoS ONE **13**, 1 (2018).

Jaione Tirapu-Azpiroz, M. E. F. W. F. L. C. P. W. B. R. L. O. M. E. M. B. S., Ademir Ferreira Silva, "Modeling fluid transport in two-dimensional paper networks", Journal of Micro/Nanolithography, MEMS, and MOEMS **17**, 17 – 17 – 10, URL https://doi.org/10.1117/1.JMM.17.2.025003 (2018).

Juntunen, E., T. Myyryläinen, T. Salminen, T. Soukka and K. Pettersson, "Performance of fluorescent europium(iii) nanoparticles and colloidal gold reporters in lateral flow bioaffinity assay", Analytical Biochemistry **428**, 1, 31 – 38, URL http://www.sciencedirect.com/science/article/pii/S0003269712003090 (2012).

Katchman, B. A., R. Barderas, R. Alam, D. Chowell, M. S. Field, L. J. Esserman, G. Wallstrom, J. Labaer, D. W. Cramer, M. A. Hollingsworth and K. S. Anderson, "Proteomic mapping of p53 immunogenicity in pancreatic, ovarian, and breast cancers", PROTEOMICS – Clinical Applications **10**, 7, 720–731 (2016a).

Katchman, B. A., J. T. Smith, U. Obahiagbon, S. Kesiraju, Y.-K. Lee, B. O'Brien, K. Kaftanoglu, J. Blain Christen and K. S. Anderson, "Application of flat panel oled display technology for the point-of-care detection of circulating cancer biomarkers", Scientific Reports **6**, 29057, URL http://dx.doi.org/10.1038/srep29057 (2016b).

Katchman, B. A., J. T. Smith, U. Obahiagbon, S. Kesiraju, Y.-K. Lee, B. O'Brien, K. Kaftanoglu, J. Blain Christen and K. S. Anderson, "Application of flat panel oled display technology for the point-of-care detection of circulating cancer biomarkers", Scientific Reports **6**, 29057, URL http://dx.doi.org/10.1038/srep29057 (2016c).

Khreich, N., P. Lamourette, B. Lagoutte, C. Ronco, X. Franck, C. Créminon and H. Volland, "A fluorescent immunochromatographic test using immunoliposomes for detecting microcystins and nodularins", Analytical and Bioanalytical Chemistry **397**, 5, 1733–1742, URL http://dx.doi.org/10.1007/s00216-009-3348-x (2010).

Kim, D. and A. E. Herr, "Protein immobilization techniques for microfluidic assays", Biomicrofluidics **7**, 4 (2013).

Koetse, M., P. Rensing, G. van Heck, N. Meulendijks, P. Kruijt, E. Enting, F. Wieringa and H. Schoo, "Optical sensor platforms by modular assembly of organic electronic devices", pp. 1–3 (IEEE, 2008).

Kraker, E., A. Haase, B. Lamprecht, G. Jakopic, C. Konrad and S. Köstler, "Integrated organic electronic based optochemical sensors using polarization filters", Applied Physics Letters **92**, 3, 033302, URL https://doi.org/10.1063/1.2837410 (2008).

Krujatz, F., O. Hild, K. Fehse, M. Jahnel, A. Werner and T. Bley, "Exploiting the potential of oled-based photo-organic sensors for biotechnological applications", Chemical Sciences Journal **7**, 134 (2016).

Kumar, A. A., J. W. Hennek, B. S. Smith, S. Kumar, P. Beattie, S. Jain, J. P. Rolland, T. P. Stossel, C. Chunda-Liyoka and G. M. Whitesides, "From the bench to the field in low-cost diagnostics: Two case studies", Angewandte Chemie International Edition **54**, 20, 5836–5853, URL http://dx.doi.org/10.1002/anie.201411741 (2015).

Lakowicz, J. R., *Principles of Fluorescence Spectroscopy* (Springer US, 2006).

Lalkhen, A. G. and A. McCluskey, "Clinical tests: sensitivity and specificity", Continuing Education in Anaesthesia, Critical Care & Pain **8**, 6, 221–223 (2008).

Lee, L. G., E. S. Nordman, M. D. Johnson and M. F. Oldham, "A low-cost, high-performance system for fluorescence lateral flow assays", Biosensors **3**, 4, 360 (2013).

Lee, S., S. Mehta and D. Erickson, "Two-color lateral flow assay for multiplex detection of causative agents behind acute febrile illnesses", Analytical Chemistry **88**, 17, 8359–8363, URL https://doi.org/10.1021/acs.analchem.6b01828, pMID: 27490379 (2016).

Lefevre, F., P. Juneau and R. Izquierdo, "Integration of fluorescence sensors using organic optoelectronic components for microfluidic platform", Sensors and Actuators B: Chemical **221**, 1314 – 1320, URL http://www.sciencedirect.com/science/article/pii/S0925400515301349 (2015).

Lefèvre, F., P. Juneau and R. Izquierdo, "Integration of fluorescence sensors using organic optoelectronic components for microfluidic platform", Sensors and Actuators B: Chemical **221**, 1314 – 1320, URL http://www.sciencedirect.com/science/article/pii/S0925400515301349 (2015).

Li, J. and J. Macdonald, "Multiplex lateral flow detection and binary encoding enables a molecular colorimetric 7-segment display", Lab on a Chip **16**, 2, 242–245 (2016a).

Li, J. and J. Macdonald, "Multiplexed lateral flow biosensors: Technological advances for radically improving point-of-care diagnoses", Biosensors & Bioelectronics **85**, 998–999 (2016b).

Li, X., D. R. Ballerini and W. Shen, "A perspective on paper-based microfluidics: Current status and future trends", Biomicrofluidics **6**, 1, 011301, URL https://doi.org/10.1063/1.3687398 (2012).

Li, Z., Y. Wang, J. Wang, Z. Tang, J. G. Pounds and Y. Lin, "Rapid and sensitive detection of protein biomarker using a portable fluorescence biosensor based on quantum dots and a lateral flow test strip", Analytical Chemistry **82**, 16, 7008–7014, URL http://dx.doi.org/10.1021/ac101405a, pMID: 20704391 (2010).

Life Technologies, "The molecular probes® handbook a guide to fluorescent probes and labeling technologies", Tech. Rep. 11th Edition, Life Technologies (2010).

Linares, E. M., L. T. Kubota, J. Michaelis and S. Thalhammer, "Enhancement of the detection limit for lateral flow immunoassays: Evaluation and comparison of bioconjugates", Journal of Immunological Methods **375**, 1, 264 – 270, URL http://www.sciencedirect.com/science/article/pii/S0022175911003085 (2012).

Liu, R., Y. Cai, P. J. Mok, H. K. Ming, J. Shinar and R. Shinar, "Organic light emitting diode sensing platform: Challenges and solutions", Advanced Functional Materials **21**, 24, 4744–4753, URL https://onlinelibrary.wiley.com/doi/abs/10.1002/adfm.201101536 (2011).

Liu, R., T. Xiao, W. Cui, J. Shinar and R. Shinar, "Multiple approaches for enhancing all-organic electronics photoluminescent sensors: simultaneous oxygen and ph monitoring", Analytica chimica acta **778** (2013).

Mabey, D., R. W. Peeling, A. Ustianowski and M. D. Perkins, "Tropical infectious diseases: Diagnostics for the developing world", Nature Reviews Microbiology **2**, 3 (2004).

Mak, W. C., V. Beni and A. P. Turner, "Lateral-flow technology: From visual to instrumental", TrAC Trends in Analytical Chemistry **79**, 297 – 305, URL http://www.sciencedirect.com/science/article/pii/S0165993615301084, past ,

Present and Future challenges of Biosensors and Bioanalytical tools in Analytical Chemistry: a tribute to Prof Marco Mascini (2016).

Manna, E., T. Xiao, J. Shinar and R. Shinar, "Organic photodetectors in analytical applications", Electronics **4**, 3, 688–722, URL http://www.mdpi.com/2079-9292/4/3/688 (2015).

Mansfield, M. A., "Estapor microspheres in lateral flow assays", Tech. rep., OEM Diagnostics Group, EMD Millipore, Bedford, MA (2015).

Manzano, M., F. Cecchini, M. Fontanot, L. Iacumin, G. Comi and P. Melpignano, "Oled-based dna biochip for campylobacter spp. detection in poultry meat samples", Biosensors and Bioelectronics **66**, 271 – 276, URL http://www.sciencedirect.com/science/article/pii/S0956566314009324 (2015).

Marcello, A., D. Sblattero, C. Cioarec, P. Maiuri and P. Melpignano, "A deep-blue oled-based biochip for protein microarray fluorescence detection", Biosensors and Bioelectronics **46**, 44 – 47, URL http://www.sciencedirect.com/science/article/pii/S0956566313001152 (2013).

Martinez, A. W., S. T. Phillips, E. Carrilho, S. W. Thomas, H. Sindi and G. M. Whitesides, "Simple telemedicine for developing regions: Camera phones and paper-based microfluidic devices for real-time, off-site diagnosis", Analytical Chemistry **80**, 10, 3699–3707, URL https://doi.org/10.1021/ac800112r, pMID: 18407617 (2008).

McNaught, A. D. and A. Wilkinson, "Iupac. compendium of chemical terminology, 2nd ed. (the "gold book")", (1997).

Meng, X., J. Wei, Y. Wang, H. Zhang and Z. Wang, "The role of peptide microarrays in biomedical research", Anal. Methods pp. –, URL http://dx.doi.org/10.1039/C8AY01442F (2018).

Morbioli, G. G., T. Mazzu-Nascimento, A. M. Stockton and E. Carrilho, "Technical aspects and challenges of colorimetric detection with microfluidic paper-based analytical devices (μPADs) - a review", Analytica Chimica Acta **970**, 1–22 (2017).

Motulsky, H., *Intuitive Biostatistics*, no. ISBN: 9780190643560 (Oxford University Press, 2017), fourth edition edn.

Mueller, G., *Electroluminescence I*, Semiconductors and semimetals, v. 64 (Academic, San Diego ; London, 2000).

Nakamura, K., T. Tanaka and K. Takeo, "Characterization of protein binding to a nitrocellulose membrane", SEIBUTSU BUTSURI KAGAKU **33**, 6, 293–303 (1989).

Nargang, T. M., M. Runck, D. Helmer and B. E. Rapp, "Functionalization of paper using photobleaching: A fast and convenient method for creating paper-based assays with colorimetric and fluorescent readout", Engineering in Life Sciences **16**, 6, 525–531 (2016).

Natoli, M. E., R. A. Schwarz, M. Bond, C. E. Majors, B. A. Rohrman, C. A. Smith and R. R. Richards-Kortum, *Advances in Point-of-Care Diagnostics for Infectious Disease*, pp. 1–21 (Springer International Publishing, Cham, 2018), URL https://doi.org/10.1007/978-3-319-66647-1_1.

Ngom, B., Y. Guo, X. Wang and D. Bi, "Development and application of lateral flow test strip technology for detection of infectious agents and chemical contaminants: a review", Analytical and Bioanalytical Chemistry **397**, 3, 1113–1135 (2010).

Nikam, M., R. Singh and S. Bhise, "Article: Organic light emitting diodes: Future of displays", IJCA Proceedings on International Conference on Advances in Communication and Computing Technologies 2012 **3**, 3, 31–34, URL https://www.ijcaonline.org/proceedings/icacact/number3/7985-1021, full text available (2012).

Novus Biologicals, "Novus spectra viewer", Accessed online September 25, 2018, URL https://www.novusbio.com/spectraviewer (2018).

O' Brien, B., Y. K. Lee, M. Marrs, J. Smith, M. Strnad, E. Forsythe and D. Morton, "70.2l: Late-news paper : 14.7" active matrix pholed displays on temporary bonded pen substrates with low temperature igzo tfts", SID Symposium Digest of Technical Papers **44**, 1, 447–450 (2013).

Obahiagbon, U., K. S. Anderson and M. Blain Christen Jennifer, "Flexible displays for medical applications", (2019).

Obahiagbon, U., D. Kullman, J. T. Smith, B. A. Katchman, H. Arafa, K. S. Anderson and J. B. Christen, "Characterization of a compact and highly sensitive fluorescence-based detection system for point-of-care applications", in "2016 IEEE Healthcare Innovation Point-Of-Care Technologies Conference (HI-POCT)", pp. 117–120 (2016).

Obahiagbon, U., J. T. Smith, M. Zhu, B. A. Katchman, H. Arafa, K. S. Anderson and J. M. Blain Christen, "A compact, low-cost, quantitative and multiplexed fluorescence detection platform for point-of-care applications", Biosensors and Bioelectronics URL http://www.sciencedirect.com/science/article/pii/S0956566318302562 (2018).

O'Farrell, B., "Chapter 2.4 - lateral flow immunoassay systems: Evolution from the current state of the art to the next generation of highly sensitive, quantitative rapid assays", in "The Immunoassay Handbook (Fourth Edition)", edited by D. Wild, pp. 89 – 107 (Elsevier, Oxford, 2013), fourth edition edn., URL https://www.sciencedirect.com/science/article/pii/B9780080970370000075.

O'Farrell, B., "Lateral flow technology for field-based applications-basics and advanced developments", Topics in Companion Animal Medicine **30**, 4, 139 – 147, URL http://www.sciencedirect.com/science/article/pii/S1938973615000938 (2015a).

O'Farrell, B., "Lateral flow technology for field-based applications—basics and advanced developments", Topics in Companion Animal Medicine **30**, 4, 139 – 147, URL http://www.sciencedirect.com/science/article/pii/S1938973615000938 (2015b).

Oncescu, V., D. O'dell and D. Erickson, "Smartphone based health accessory for colorimetric detection of biomarkers in sweat and saliva", Lab on a Chip **13**, 16, 3232–3238 (2013).

Osborn, J. L., B. Lutz, E. Fu, P. Kauffman, D. Y. Stevens and P. Yager, "Microfluidics without pumps: reinventing the t-sensor and h-filter in paper networks", Lab on a chip **10**, 20 (2010).

Pais, A., A. Banerjee, D. Klotzkin and I. Papautsky, "High-sensitivity, disposable lab-on-a-chip with thin-film organic electronics for fluorescence detection", Lab Chip **8**, 794–800 (2008a).

Pais, A., A. Banerjee, D. Klotzkin and I. Papautsky, "High-sensitivity, disposable lab-on-a-chip with thin-film organic electronics for fluorescence detection", Lab Chip **8**, 794–800, URL http://dx.doi.org/10.1039/B715143H (2008b).

Peeling, R. and D. Mabey, "Point-of-care tests for diagnosing infections in the developing world", Clinical Microbiology and Infection **16**, 8, 1062 – 1069, URL http://www.sciencedirect.com/science/article/pii/S1198743X14641951 (2010).

Pelton, R., "Bioactive paper provides a low-cost platform for diagnostics", TrAC Trends in Analytical Chemistry **28**, 8, 925 – 942, URL http://www.sciencedirect.com/science/article/pii/S0165993609001307 (2009).

Peterson, D. S., "Solid supports for micro analytical systems", Lab on a Chip **5**, 2, 132–139 (2005).

Pierre, A. and A. C. Arias, "Solution-processed image sensors on flexible substrates", Flexible and Printed Electronics **1**, 4, 043001, URL http://stacks.iop.org/2058-8585/1/i=4/a=043001 (2016).

Pilavaki, E. and A. Demosthenous, "Optimized lateral flow immunoassay reader for the detection of infectious diseases in developing countries", Sensors **17**, 11, URL http://www.mdpi.com/1424-8220/17/11/2673 (2017).

Posthuma-Trumpie, G. A., J. Korf and A. van Amerongen, "Lateral flow (immuno)assay: its strengths, weaknesses, opportunities and threats. a literature survey", Analytical and Bioanalytical Chemistry **393**, 2, 569–582, URL https://doi.org/10.1007/s00216-008-2287-2 (2009).

Prabowo, B. A., Y.-F. Chang, Y.-Y. Lee, L.-C. Su, C.-J. Yu, Y.-H. Lin, C. Chou, N.-F. Chiu, H.-C. Lai and K.-C. Liu, "Application of an oled integrated with bef and giant birefringent optical (gbo) film in a spr biosensor", Sensors & Actuators: B. Chemical **198**, 424–430 (2014).

Qin, Z., W. C. W. Chan, D. R. Boulware, T. Akkin, E. K. Butler and J. C. Bischof, "Significantly improved analytical sensitivity of lateral flow immunoassays by using thermal contrast", Angewandte Chemie International Edition **51**, 18, 4358–4361, URL https://onlinelibrary.wiley.com/doi/abs/10.1002/anie.201200997 (2012).

Qu, H., Y. Zhang, B. Qu, H. Kong, G. Qin, S. Liu, J. Cheng, Q. Wang and Y. Zhao, "Rapid lateral-flow immunoassay for the quantum dot-based detection of puerarin", Biosensors and Bioelectronics **81**, 358 – 362, URL http://www.sciencedirect.com/science/article/pii/S0956566316302020 (2016).

Ramachandran, N., K. S. Anderson, J. V. Raphael, E. Hainsworth, S. Sibani, W. R. Montor, M. Pacek, J. Wong, M. Eljanne, M. G. Sanda, Y. Hu, T. Logvinenko and J. Labaer, "Tracking humoral responses using self assembling protein microarrays", PROTEOMICS – Clinical Applications **2**, 10-11, 1518–1527 (2008a).

Ramachandran, N., E. Hainsworth, B. Bhullar, S. Eisenstein, B. Rosen, A. Y. Lau, J. C. Walter and J. Labaer, "Self-assembling protein microarrays", Science (New York, N.Y.) **305**, 5680 (2004).

Ramachandran, N., J. V. Raphael, E. Hainsworth, G. Demirkan, M. G. Fuentes, A. Rolfs, Y. Hu and J. Labaer, "Next-generation high-density self-assembling functional protein arrays", Nature Methods **5**, 6 (2008b).

Raupp, G. B., S. M. O'Rourke, C. Moyer, B. P. O'Brien, S. K. Ageno, D. E. Loy, E. J. Bawolek, D. R. Allee, S. M. Venugopal, J. Kaminski, D. Bottesch, J. Dailey, K. Long, M. Marrs, N. R. Munizza, H. Haverinen and N. Colaneri, "Low-temperature amorphous-silicon backplane technology development for flexible displays in a manufacturing pilot-line environment", Journal of the Society for Information Display **15**, 7 (2007).

Reck, M., F. Stahl, J. G. Walter, M. Hollas, D. Melzner and T. Scheper, "Optimization of a microarray sandwich-elisa against hinf-γ on a modified nitrocellulose membrane", Biotechnology Progress **23**, 6, 1498–1505, URL https://onlinelibrary.wiley.com/doi/abs/10.1021/bp070179i (2008).

Roche Molecular Systems, Inc., "cobas® hpv test", URL https://www.accessdata.fda.gov/cdrh_docs/pdf10/p100020s017c.pdf, doc Rev. 12.0 (2015).

Roda, A., *Chemiluminescence and bioluminescence past, present and future* (Royal Society of Chemistry, Cambridg, U.K., 2011).

Roda, A., E. Michelini, M. Zangheri, M. Di Fusco, D. Calabria and P. Simoni, "Smartphone-based biosensors: A critical review and perspectives", Trends in Analytical Chemistry **79**, 317–325 (2016).

Ryu, G., J. Huang, O. Hofmann, C. A. Walshe, J. Y. Y. Sze, G. D. McClean, A. Mosley, S. J. Rattle, J. C. deMello, A. J. deMello and D. D. C. Bradley, "Highly sensitive fluorescence detection system for microfluidic lab-on-a-chip", Lab Chip **11**, 1664–1670, URL http://dx.doi.org/10.1039/C0LC00586J (2011a).

Ryu, G., J. Huang, O. Hofmann, C. A. Walshe, J. Y. Y. Sze, G. D. McClean, A. Mosley, S. J. Rattle, J. C. deMello, A. J. deMello and D. D. C. Bradley, "Highly sensitive fluorescence detection system for microfluidic lab-on-a-chip", Lab Chip **11**, 1664–1670, URL http://dx.doi.org/10.1039/C0LC00586J (2011b).

Sajid, M., A.-N. Kawde and M. Daud, "Designs, formats and applications of lateral flow assay: A literature review", Journal of Saudi Chemical Society **19**, 6, 689–705 (2015).

Savin, M., C.-M. Mihailescu, I. Matei, D. Stan, C. A. Moldovan, M. Ion and I. Baciu, "A quantum dot-based lateral flow immunoassay for the sensitive detection of human heart fatty acid binding protein (hfabp) in human serum", Talanta **178**, 910–915 (2018).

Scheeline, A., "Cell phone spectrometry: Science in your pocket?", Trends in Analytical Chemistry **85**, 20–25 (2016).

Schwartz, A., A. K. Gaigalas, L. Wang, G. E. Marti, R. F. Vogt and E. Fernandez-Repollet, "Formalization of the mesf unit of fluorescence intensity", Cytometry Part B: Clinical Cytometry **57**, 1, 1–6 (2004).

Schwartz, A., L. Wang and E. Early, "Quantitating fluorescence intensity from fluorophore: The definition of mesf assignment", Journal of Research of the National Institute of Standards and Technology **107**, 1, URL http://search.proquest.com/docview/214785478/ (2002).

Shinar, J. and R. Shinar, "Organic light-emitting devices (oleds) and oled-based chemical and biological sensors: an overview", Journal of Physics D: Applied Physics **41**, 13, 133001, URL http://stacks.iop.org/0022-3727/41/i=13/a=133001 (2008).

Shu, Z., F. Kemper, E. Beckert, R. Eberhardt and A. Tunnermann, "Highly sensitive on-chip fluorescence sensor with integrated fully solution processed organic light sources and detectors", RSC Adv. **7**, 26384–26391, URL http://dx.doi.org/10.1039/C7RA03841K (2017).

Smith, J., B. Katchman, D. Kullman, U. Obahiagbon, Y. Lee, B. OBrien, G. Raupp, K. Anderson and J. Christen, "Application of flexible oled display technology to point-of-care medical diagnostic testing", IEEE/OSA Journal of Display Technology **12**, 3, 273–280 (2016a).

Smith, J. T., B. A. Katchman, D. E. Kullman, U. Obahiagbon, Y.-K. Lee, B. P. O'Brien, G. B. Raupp, K. S. Anderson and J. Blain Christen, "Application of flexible oled display technology to point-of-care medical diagnostic testing", Journal of Display Technology **12**, 3, 273–280 (2016b).

Song, X. and M. Knotts, "Time-resolved luminescent lateral flow assay technology", Analytica Chimica Acta **626**, 2, 186–192 (2008).

Swanson, C. and A. D'Andrea, "Lateral flow assay with near-infrared dye for multiplex detection", Clinical Chemistry **59**, 4, 641–8, URL http://search.proquest.com/docview/1430985425/ (2013).

Swinehart, D., "The beer-lambert law", Journal of Chemical Education **39**, 7, 333–335 (1962).

Sze, S. M., *Physics of semiconductor devices, 3rd Ed.* (Wiley Interscience, Hoboken, New Jersey, 2007).

Tam, H. L., W. H. Choi and F. Zhu, "Organic optical sensor based on monolithic integration of organic electronic devices", Electronics **4**, 3, 623–632, URL https://doaj.org/article/7d0af3291c5d479faeaf2570b06257f6 (2015).

Tan, Y. H., M. Liu, B. Nolting, J. G. Go, J. Gervay-Hague and G.-Y. Liu, "A nanoengineering approach for investigation and regulation of protein immobilization", ACS nano **2**, 11 (2008).

Tang, R., H. Yang, J. R. Choi, Y. Gong, J. Hu, S. Feng, B. Pingguan-Murphy, Q. Mei and F. Xu, "Improved sensitivity of lateral flow assay using paper-based sample concentration technique", Talanta **152**, 269 – 276, URL http://www.sciencedirect.com/science/article/pii/S0039914016300868 (2016).

Thermo Fisher Scientific, "Fluospheres^{TM}carboxylate-modified microspheres, 0.2 μm, europium luminescent (365/610), 0.5% solids", URL https://www.thermofisher.com/order/catalog/product/F20881?SID=srch-srp-F20881 (2009).

ThermoFisher Scientific, "Fluorescence spectraviewer", Accessed online September 9, 2018, URL https://www.thermofisher.com/us/en/home/life-science/cell-analysis/labeling-chemistry/fluorescence-spectraviewer.html (2018).

Thrush, E., O. Levi, W. Ha, K. Wang, S. J. Smith and J. S. H. Jr., "Integrated biofluorescence sensor", Journal of Chromatography A **1013**, 1013, 103 – 110, 16th International Symposium on Microscale Separations and Analysis. Part I (2003).

Thrush, E. P., *Integrated fluorescence sensor*, Ph.D. thesis, Standford University (2004).

Tobjörk, D. and R. Österbacka, "Paper electronics", Advanced Materials **23**, 17, 1935–1961 (2011).

Tonkinson, J. L., "Nitrocellulose: A tried and true polymer finds utility as a postgenomic substrate", Frontiers in Bioscience **7**, 1 (2002).

Tovey, E. R. and B. A. Baldo, "Protein binding to nitrocellulose, nylon and pvdf membranes in immunoassays and electroblotting", Journal of Biochemical and Biophysical Methods **19**, 2, 169–183 (1989).

Tylkowski, B. and I. Tsibranska, "Overview of main techniques used for membrane characterization", Journal of Chemical Technology and Metallurgy **50,**, 1, 3–12, URL https://pdfs.semanticscholar.org/500b/ed86fb934acd3e388de2d04e14f33416b158.pdf (2015).

Valeur, B., *Molecular fluorescence : principles and applications* (Wiley-VCH, Weinheim, 2002).

van Amerongen, A., J. Veen, H. A. Arends and M. Koets, "Chapter 7 - lateral flow immunoassays", in "Handbook of Immunoassay Technologies", edited by S. K. Vashist and J. H. Luong, pp. 157 – 182 (Academic Press, 2018), URL https://www.sciencedirect.com/science/article/pii/B9780128117620000074.

Venkatraman, V. and A. J. Steckl, "Integrated {OLED} as excitation light source in fluorescent lateral flow immunoassays", Biosensors and Bioelectronics **74**, 150 – 155, URL http://www.sciencedirect.com/science/article/pii/S0956566315302165 (2015a).

Venkatraman, V. and A. J. Steckl, "Integrated oled as excitation light source in fluorescent lateral flow immunoassays", Biosensors and Bioelectronics **74**, 150 – 155, URL http://www.sciencedirect.com/science/article/pii/S0956566315302165 (2015b).

Venkatraman, V. and A. J. Steckl, "Quantitative detection in lateral flow immunoassay using integrated organic optoelectronics", Sensors Journal, IEEE **17**, 24, 8343–8349 (2017).

Wang, J., F. Cao, S. He, Y. Xia, X. Liu, W. Jiang, Y. Yu, H. Zhang and W. Chen, "Fret on lateral flow test strip to enhance sensitivity for detecting cancer biomarker", Talanta **176**, 444 – 449, URL http://www.sciencedirect.com/science/article/pii/S0039914017308184 (2018).

Wang, J., D. Johannsmann, M. Hollas and V. Thom, "Visualization of capture line protein binding in nitrocellulose diagnostic membranes", Desalination **199**, 1, 232–233 (2006).

Wang, L., A. Gaigalas, F. Abbasi and G. Marti, "Quantitating fluorescence intensity from fluorophores: Practical use of mesf values", Journal of Research of the National Institute of Standards and Technology **107**, 4, URL http://search.proquest.com/docview/214792989/ (2002).

Wang, L. and R. A. Hoffman, "Standardization, calibration, and control in flow cytometry", Current Protocols in Cytometry **79**, 1, 1.3.1–1.3.27, URL https://currentprotocols.onlinelibrary.wiley.com/doi/abs/10.1002/cpcy.14 (2017).

Washburn, E. W., "The dynamics of capillary flow", Phys. Rev. **17**, 273–283, URL https://link.aps.org/doi/10.1103/PhysRev.17.273 (1921).

Wild, D., ed., *The Immunoassay Handbook, 3rd ed* (Elservier, 2005).

Williams, G., C. Backhouse and H. Aziz, "Integration of organic light emitting diodes and organic photodetectors for lab-on-a-chip bio-detection systems", Electronics **3**, 1, 43–75, URL http://www.mdpi.com/2079-9292/3/1/43 (2014).

Wong, R. C. and H. Y. Tse, eds., *Lateral flow immunoassay* (Springer, 2009).

World Health Organization, "Who list of prequalified in vitro diagnostic products", URL http://www.who.int/diagnostics_laboratory/evaluations/180912_prequalified_product_list.pdf?ua=1 (2018a).

World Health Organization, "Who prequalification of in vitro diagnostics public report. product: carehpv^{TM} test", URL http://www.who.int/diagnostics_laboratory/evaluations/pq-list/180713_pqpr_pqdx_0085_028_00_carehpv_with_labelling.pdf?ua=1 (2018b).

Wu, G. and M. Zaman, "Low-cost tools for diagnosing and monitoring hiv infection in low-resource settings", Bulletin of The World Health Organization **90**, 12, 914–920, URL http://search.proquest.com/docview/1315606338/ (2012).

Wu, R., S. Zhou, T. Chen, J. Li, H. Shen, Y. Chai and L. S. Li, "Quantitative and rapid detection of c-reactive protein using quantum dot-based lateral flow test strip", Analytica Chimica Acta **1008**, 1–7 (2018).

Yeh, P., N. Yeh, C.-H. Lee and T.-J. Ding, "Applications of leds in optical sensors and chemical sensing device for detection of biochemicals, heavy metals, and environmental nutrients", Renewable and Sustainable Energy Reviews **75**, 461 – 468, URL http://www.sciencedirect.com/science/article/pii/S1364032116307584 (2017).

Yetisen, A. K., M. S. Akram and C. R. Lowe, "Paper-based microfluidic point-of-care diagnostic devices", Lab Chip **13**, 2210–2251 (2013a).

Yetisen, A. K., M. S. Akram and C. R. Lowe, "Paper-based microfluidic point-of-care diagnostic devices", Lab Chip **13**, 2210–2251 (2013b).

Yun Shuai, A., D. Banerjee, I. Klotzkin and I. Papautsky, "On-chip fluorescence detection using organic thin film devices for a disposable lab-on-a-chip", University/Government/Industry Micro/Nano Symposium, 2008. UGIM 2008. 17th Biennial pp. 169–172 (2008).

APPENDIX A

CONJUGATION PROTOCOL

To conjugate 1 μm Nile red fluorescent Microspheres to AffiniPure Goat Anti-Human IgG, 10-25 mg of AffiniPure Goat Anti-Human IgG protein was dissolved in 2.5 mL of 2-ethanesulfonic acid (MES) buffer in a plastic centrifuge tube. A 2% aqueous suspension of carboxylate-modified Nile red microspheres (200 μL) was added and incubated at room temperature for 15 minutes. 2 mg of 1-ethyl-3-(3-dimethylaminopropyl)-carbodiimide (EDAC) (Molecular Probes E2247) was added and the reaction mixture was vortexed. The pH was adjusted to 6.5$\pm$0.2 with 0.1 M NaOH. The reaction mixture was incubated on a rocker at room temperature for two hours. Glycine (550 μL of 1 M) was added to quench the reaction. The carboxyl modified polystyrene microspheres are covalently conjugated to goat anti-human IgG antibodies via 1-Ethyl-3-(3-dimethylaminopropyl) carbodiimide (EDC) cross-linking. EDC covalently binds to the carboxyl groups on the microspheres and primary amine groups of proteins. The glycine is used to quench the reaction by occupying any remaining active carboxyl-EDC sites. Glycine is used because it is a rather inert amino acid having only a hydrogen as the R-group. To wash the IgG-conjugated microspheres, the mixture was centrifuged at 5000xg for 20 minutes to separate protein-labeled microsphere particles from unreacted protein. The supernatant was aspirated and pellet resuspended in 3 mL of 50 mM PBS by gentle vortex. After a 3x wash, IgG-conjugated microspheres were re-suspended in 250 μL of 50 mM PBS with 1% BSA and 2 mM sodium azide.

The carboxyl modified polystyrene microspheres are conjugated to goat anti-human IgG antibodies via 1-Ethyl-3-(3-dimethylaminopropyl) carbodiimide (EDC) cross-linking. EDC covalently binds to the carboxyl groups on the microspheres and primary amine groups of proteins. The glycine is used to quench the reaction by occupying any remaining active carboxyl-EDC sites. Glycine is used because it is a rather inert amino acid having only a hydrogen as the R-group.

APPENDIX B

THREE-DIMENSIONAL IMMOBILIZATION SURFACES

Solid Support in Lateral Flow Assays: Challenges and Limitations

The ideal solid support membrane should have high transparency/translucency, low scattering, low autofluorescence, wettability and flow (pore size, 8 – 20 μm), large surface-area-to-volume ratio (SAV), high protein affinity and compatibility, low cost, and should be suitable for high volume production. However, significant manufacturing and processing effort is required to overcome a lot of these challenges and satisfy the requirements for an ideal membrane. The difficulty in finding a suitable replacement for nitrocellulose is depicted in the development and poor acceptance of Fusion5 Wong and Tse (2009). Several membranes were investigated in this work, including: glass, PDMS, nitrocellulose, sol gels, immunodyne ABC, Fusion5, silica microspheres, filter paper, parchment paper, cotton, etc. For commercialization and deployment, it is advantageous to take advantage of already existing infrastructure in developing solid support surfaces.

Some challenges in developing 3D surfaces for immobilizing capture agents in fluorescence-based assays include the preparation and optical background (scattering, reflection, and autofluorescence) associated with the chosen solid support. Furthermore, the development of quantitative tests relies on the repeatability and reproducibility of the assay. The lack of strip-to-strip reproducibility has dogged the reputation of lateral flow assay (LFA) format in general. Much of this lack of reproducibility comes from the materials used in the assays. Manufacturing technology and process control have improved over the past 20 years and have allowed lateral flow immunoassays technologies to flourish. Prior to that, LFA membranes were difficult to reproduce on a consistent lot-to-lot basis.

Plain Silica Microspheres

The opacity, variable wicking characteristics, intrinsic background, autofluorescence, and poor stability associated with potential solid support materials limit the performance of fluorescence-based immunoassays. To investigate the use of plain non-functionalized silica microspheres as a potential solid support material to improve SAV, silica microspheres (0.5 μm and 5 μm) were purchased from Bangs Laboratories (Fishers, IN, USA). Silica microspheres potentially offers a customizable platform with transparency of glass, enhanced surface area for immobilization, binding and well-known conjugation chemistry, low-autofluorescence, and hydrophilicity. However, in this work we observed a high background from plain microspheres associated with light scattering and reflections leading to filter leakage as depicted in Figure 67. We hypothesize that the observed high background is associated with scattering and reflection/refraction since no significant autofluorescence was observed in the microspheres or the extracted supernatant under a fluorescence microscope in the blue, green, and red region. It may be beneficial to have the fluorophore trapped in a microfluidic construct with height constrained channels as detailed in Peterson (2005). Adjustments to the operating region of the low-cost fluorescence detector platform may be necessary.

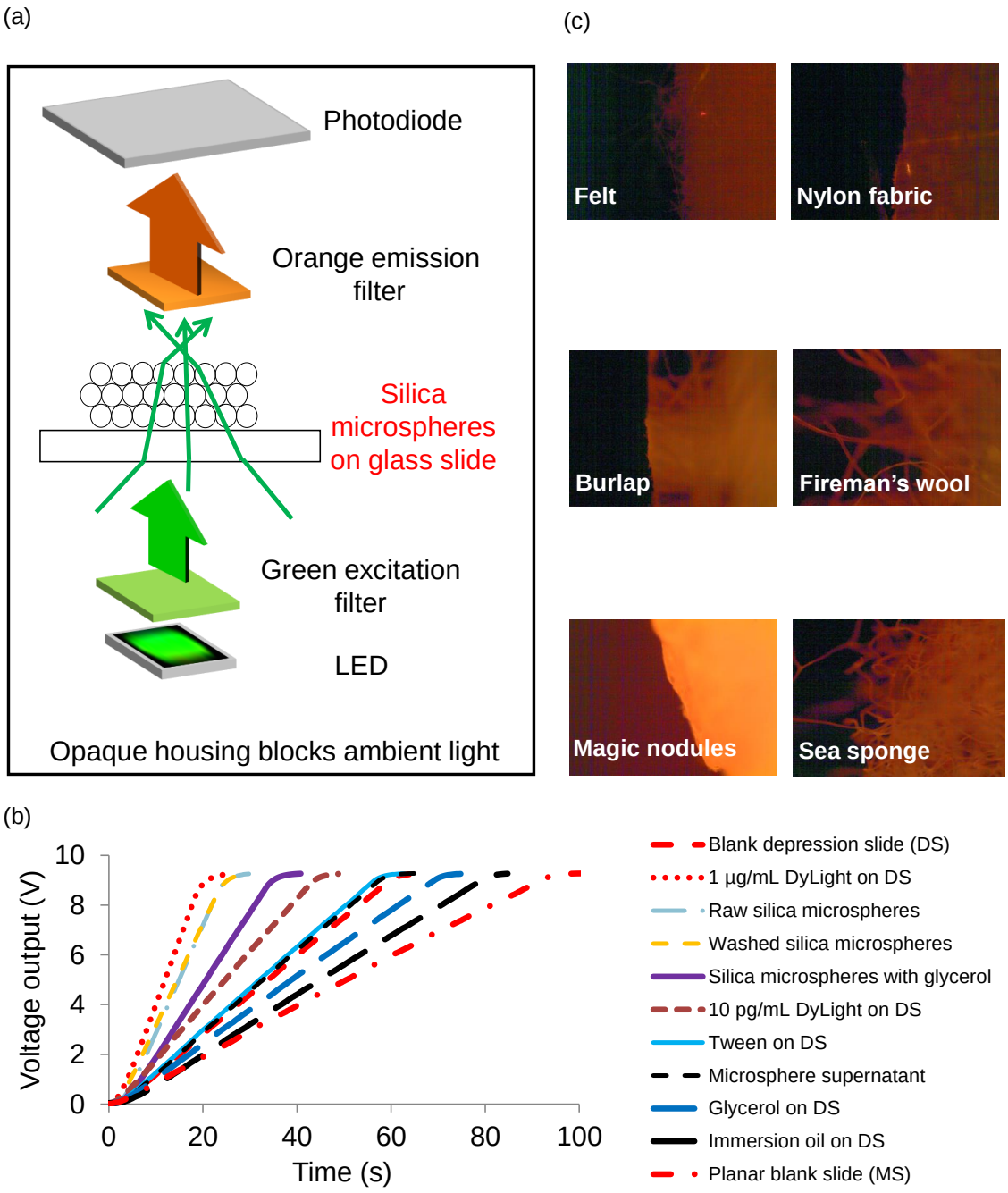

Figure 67: Plain Silica Microspheres. (a) Silica Microspheres Immobilized on Planar Glass Microscope Slide (MS) (b) Background (Voltage-time Response) for Silica Microspheres, Depression Slides (DS), Immersion Oil, Glycerol, Supernatant, and Tween 20; High and Low DyLight 549 Concentrations Measured for Reference and Concavity (Depression) Slides Were Used to Constrain the Index Matching Oils (c) Autofluorescence of Common Low-cost Fabric.

Sol gel (3D Printed Glass)

A piezo-printer was used to dispense Tetraethoxysilane (TEOS) in picoliter droplets (16.6 pL) over multiple passes. The substrate (microscope slide) was heated up to 125°C before dispensing (Figure 68). The TEOS was mixed with ethanol, water and HCl (as catalyst) in a ratio 2.1%: 2.1%: 1.05%: 0.03%, respectively, and dispensed immediately (reactive ink) or hydrolyzed for 3 hours (hydrolysis ink). Grain and pore sizes depend on mixture and reaction time. 1-propanol and methanol was also investigate as potential solvents. However, ethanol (EtOH) was most stable and adhesion was improved by printing at higher temperature coupled with a post-anneal step. Autofluorescence increased with high printing and anneal temperature. Fluorescence images were acquired using a fluorescence microscope at 10X magnification (Nikon Eclipse LV 100); Excitation Filter: 545/25 nm; Emission Filter: 605/70 nm, Dichroic mirror: 540 nm. Significant delamination was observed in the TEOS films during the assay process and led to decreased signal intensity in an IgG assay. The TEOS film and glass surface were treated with APTES and 5 μL of 100 μg/mL whole human IgG was immobilized. The anti-human IgG-DyLight 549 conjugate concentration was varied from 13 μg/mL to 130 pg/mL. The ideal solid support material should be consistent before, during, and after the assay process and should be resistant to buffers. Fluorophores bound to "loose" sol gel supports may have been washed off in the final rinse stages leading to an overall decrease in output signal. The TEOS printing was done in collaboration with Dr. Owen Hildreth's research group at Arizona State University (ASU).

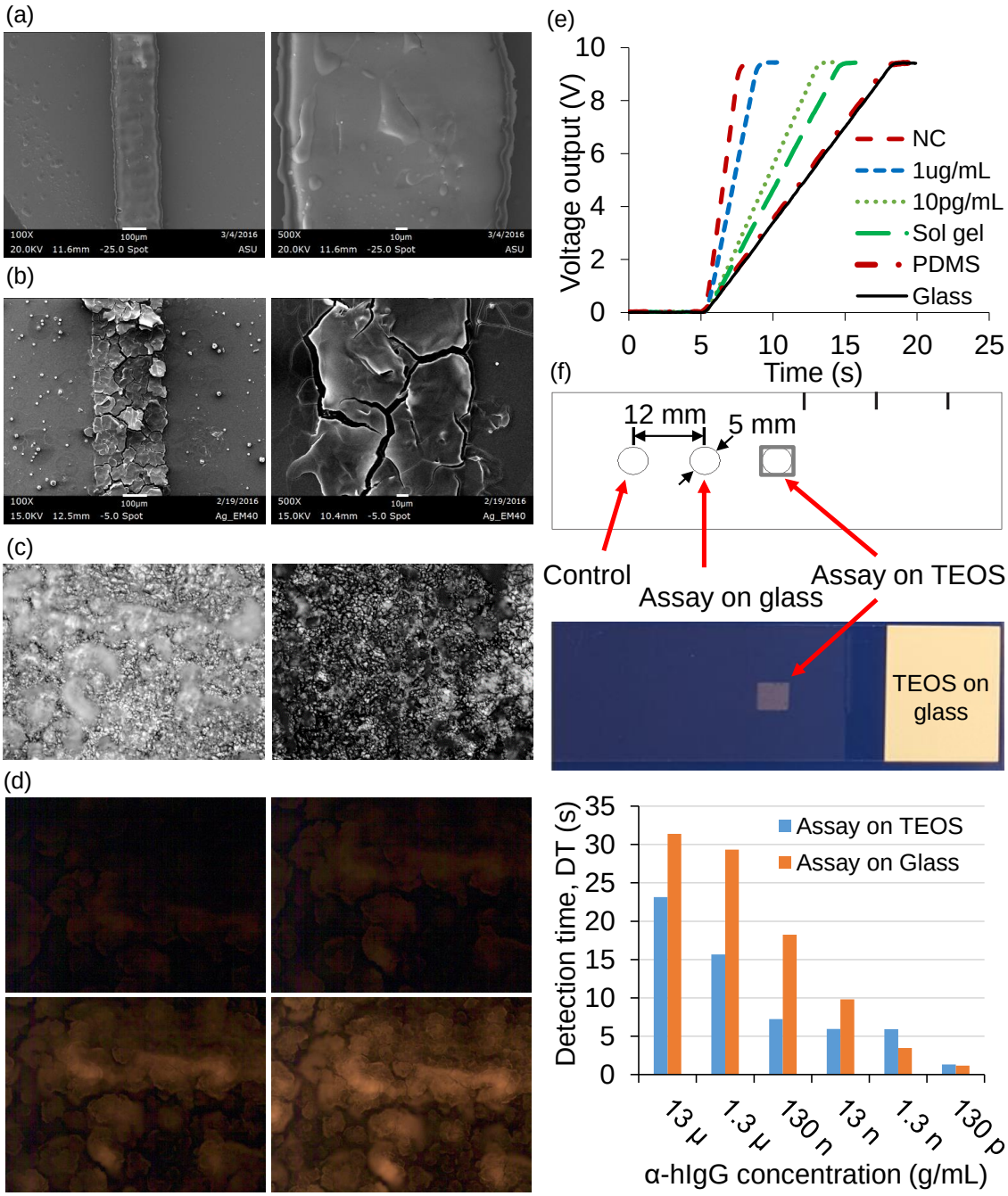

Figure 68: Printed Sol Gel Ink (Tetraethoxysilane, TEOS). (a) SEM Images (100X Left, 500X Right) of Reactive Ink (TEOS in Ethanol, Dispensed at 125°C) Substrate Temperature (b) SEM Images (100X Left, 500X Right) of 3 Hour Hydrolysis Ink (TEOS in Ethanol, Dispensed at 125°C Substrate Temperature) (c) Bright Field (Left) and Dark Field (Right) Microscope Images of Hydrolyzed TEOS (10X) (d) Autofluorescence of Printed TEOS as a Function of Temperature; Before Heat Treatment (Top Left), 150°C (Top Right), 250°C (Bottom Left), 350°C (Bottom Right). (e) Solid Support Background Compared to a Low and High DyLight549 Concentration (f) Assay Performed on TEOS Compared to Assay on Glass.

APPENDIX C

CO-AUTHOR PERMISSIONS

Jennifer M. Blain Christen (Ph.D.) and Karen S. Anderson (M.D., Ph.D.) supervised the work, revised, and edited all publications related to this work. All co-authors have granted their permissions to adapt parts of the following publications for inclusion in this dissertation.

- **U. Obahiagbon**, J. T. Smith, M. Zhu, B. A. Katchman, H. Arafa, K. S. Anderson, and J. M. Blain Christen, "A Compact, Low-cost, Quantitative and Multiplexed Fluorescence Detection Platform for Point-of-Care Applications", Biosensors and Bioelectronics, 2018, (ISSN 0956-5663, IF=8.173) https://doi.org/10.1016/j.bios.2018.04.002

- **U. Obahiagbon** et al., "Characterization of a compact and highly sensitive fluorescence-based detection system for point-of-care applications", 2016 IEEE Healthcare Innovation Point-Of-Care Technologies Conference (HI-POCT), Cancun, 2016, pp. 117-120, doi: 10.1109/HIC.2016.7797711 (1st place student paper presentation competition)

- B. A. Katchman, J. T. Smith, **U. Obahiagbon**, S. Kesiraju, Y. K. Lee, B. O'Brien, K. Kaftanoglu, J. Blain Christen, K. S. Anderson, "Application of at panel OLED display technology for the point-of-care detection of circulating cancer biomarkers", Scientific Reports 6, 29057, 2016, doi: 10.1038/srep29057 (ISSN 2045-2322, IF=4.609)

- J. T. Smith, B. A. Katchman, D. Kullman, **U. Obahiagbon**, Y. Lee, B. O'Brien, K. P. Madabhushi, V. Surampudi, G. B. Raupp, K. S. Anderson, and J. Blain Christen, "Application of flat panel display technology to point-of-care medical diagnostic testing", J. Disp. Technol. 2015

APPENDIX D

LIST OF PUBLICATIONS

Publications Related to Dissertation Research

- **U. Obahiagbon**, J. T. Smith, M. Zhu, B. A. Katchman, H. Arafa, K. S. Anderson, and J. M. Blain Christen, "A Compact, Low-cost, Quantitative and Multiplexed Fluorescence Detection Platform for Point-of-Care Applications", Biosensors and Bioelectronics, 2018, (ISSN 0956-5663, IF=8.173) https://doi.org/10.1016/j.bios.2018.04.002

- **U. Obahiagbon** and J. M. Blain Christen, "Considerations for Low-Cost Reader Designs and Label Selection for Lateral Flow Assays", 2018 IEEE Biomedical Circuits and Systems Conference (BIOCAS), Cleveland, OH, October, 2018.

- **U. Obahiagbon**, K. S. Anderson, and J. M. Blain Christen, "Flexible Displays for Medical Applications", in Flexible Flat Panel Displays, 2nd edition, G. P. Crawford, D. R. Cairns eds., Wiley, ISBN 978-1-118-75111-4, 2019 (submitted, under review)

- M. Zhu, C. Hou, **U. Obahiagbon**, K. S. Anderson, and J. Blain Christen, "Characterizing Antibody-Microsphere Conjugates for Fluorescence-based Lateral Flow Immunoassays", 2018 IEEE Life Sciences Conference (LSC), Montreal, Canada, 2018 (Accepted paper)

- C. Hou, M. Zhu, **U. Obahiagbon**, K. S. Anderson, and J. Blain Christen, "Assay Development for Fluorescence-based Lateral Flow Immunoassay", 2018 IEEE Life Sciences Conference (LSC), Montreal, Canada, 2018 (Accepted paper)

- M. Zhu, **U. Obahiagbon**, K. S. Anderson, J. Blain Christen, "Highly Sensitive Fluorescence-Based Lateral Flow Platform for Point-Of-Care Detection of Biomarkers in Plasma", 2017 IEEE Healthcare Innovation Point-Of-Care Technologies Conference (HI-POCT), Bethesda, MD, 2017, doi: 10.1109/HIC.2017.8227631

- J. T. Smith, **U. Obahiagbon**, R. Ewaisha, M. Zhu, et al., "Future Strategies for Managing Congestion in Heart Failure Patients Using Cardiac Biomarker-Guided Self-Testing", J Clin. Exp. Cardiolog. 8: 548, 2017, doi: 10.4172/2155-9880.1000548

- **U. Obahiagbon**, et al., "Live demonstration: A highly sensitive and quantitative fluorescence sensing platform, for disease diagnosis", 2017 IEEE International Symposium on Circuits and Systems (ISCAS), Baltimore, MD, 2017, doi: 10.1109/ISCAS.2017.8050723

- **U. Obahiagbon** et al., "Characterization of a compact and highly sensitive fluorescence-based detection system for point-of-care applications", 2016 IEEE Healthcare Innovation Point-Of-Care Technologies Conference (HI-POCT), Cancun, 2016, pp. 117-120, doi: 10.1109/HIC.2016.7797711 (1st place student paper presentation competition)

- J. Smith, **U. Obahiagbon**, R. Ewaisha, B. Katchman, K. Kaftanoglu, H. Arafa, D. Kullman, K. Anderson, and J. Blain Christen, "Low-Cost, Disposable Fluorescence-Based Biorecognition System Architecture for Multiplexed Point-of-Care Molecular Diagnostics", in the IEEE -NIH 2016 Special Topics Conference on Healthcare, doi: 10.1109/HIC.2016.7797720

- B. A. Katchman, J. T. Smith, **U. Obahiagbon**, S. Kesiraju, Y. K. Lee, B. O'Brien, K. Kaftanoglu, J. Blain Christen, K. S. Anderson, "Application of at panel OLED display technology for the point-of-care detection of circulating cancer biomarkers", Scientific Reports 6, 29057, 2016, doi: 10.1038/srep29057 (ISSN 2045-2322, IF=4.609)

- J. T. Smith, B. A. Katchman, D. Kullman, **U. Obahiagbon**, Y. Lee, B. O'Brien, K. P. Madabhushi, V. Surampudi, G. B. Raupp, K. S. Anderson, and J. Blain Christen, "Application of flat panel display technology to point-of-care medical diagnostic testing", J. Disp. Technol. 2015

Publications unrelated to Dissertation Research

- H. Arafa, **U. Obahiagbon**, D. Kullman, F. Dominguez, A. Magee, J. Blain Christen, "Characterization and Application of a Discrete Quartz Extended-Gate ISFET for the Assessment of Tumor Cell Viability", in the IEEE -NIH 2016 Special Topics Conference on Healthcare, doi: 10.1109/HIC.2016.7797697

- F. Karabacak, **U. Obahiagbon**, U. Ogras, S. Ozev and J. B. Christen, "Making unreliable Chem-FET sensors smart via soft calibration", ISQED, Santa Clara, CA, 2016, pp. 456-461, doi: 10.1109/ISQED.2016.7479243